SHEAR WAVE VELOCITY OF SOILS BY

THE SPECTRAL ANALYSIS OF SURFACE WAVES (SASW) METHOD

Seyed Mohammad Ali Zomorodian, B.SC., Eng., M.Sc.

A Thesis
submitted to School of Graduate Studies
Under the supervision of

Dr. Vinod K. Garga, P.Eng.
and
Dr. M. Osama Al-Hunaidi

in partial fulfillment of the requirements for degree of

Doctor of Philosophy in Civil Engineering

Department of Civil Engineering
University of Ottawa
Ottawa, Ontario
Canada K1N 6N5

July 1996

The Doctor of Philosophy in Civil Engineering is a joint program between Carleton University and the University of Ottawa, which is administered by the Ottawa-Carleton Institute for Civil Engineering

ISBN 0-612-16479-9

Canada

UNIVERSITÉ D'OTTAWA
UNIVERSITY OF OTTAWA

IN THE NAME OF GOD

DEDICATED TO MY FAMILY

ACKNOWLEDGMENTS

The author expresses appreciation to his research supervisors, Dr. Vinod K. Garga and Dr. Osama Al-Hunaidi, for their advice and guidance throughout this study. The author is also thankful to Dr. D. Lau, Dr. H. Tanaka, Dr. K.T. Law, Dr. E. Evgin and Dr. B.H. Fellenius for serving as members on various examination committees during this study.

The support of the National Research Council of Canada (NRC) for providing field testing equipment is gratefully acknowledged.

Moreover, the financial assistance provided by Ministry of Culture and Higher Education of Islamic Republic of Iran to pursue this study is highly appreciated.

The author would like to thank his parents and parents-in-law for their constant encouragement and moral support during the period of this study.

Finally, it is the author's wife, Manijeh Khalaf, whose encouragement made this programme a success. The patience of the author's sons, Mehdi, and Alireza and the author's daughter, Zahrasadat, who have been waiting to see their father's post-student life, would be acknowledged.

ABSTRACT

Spectral analysis of surface waves (SASW) method is an in-situ seismic method used for determining the thickness and elastic properties of soil and pavement. The SASW method is fast and economical to perform since no boreholes are required. The method is suitable for sites where the use of large equipment is difficult or where sublayer conditions make it difficult to perform other seismic tests. The SASW method is also ideal for preliminary field investigations to be conducted prior to more detailed site investigation, and for quality control and monitoring of ground improvement.

The SASW method is based on the theory of surface waves (generalized Rayleigh waves) dispersion in a multi-layered medium. According to this theory, surface waves of different frequencies or wavelengths travel at different velocities in layered media, a phenomenon known as dispersion. In simple terms, dispersion occurs as a result of the fact that as the wavelength of surface waves increases, their penetration depth into the layered medium also increases. The propagation velocity of surface waves at a particular wavelength, reflects the properties of the layers in which the wave propagates.

The SASW method involves the generation and measurement of surface waves by impacting the surface of the soil and detection of these waves at the surface at several points. The captured signals are transformed to the frequency domain using the Fast Fourier Transform (FFT) to determine the cross-power spectrum and the coherence function. The phase angle of the cross-power spectrum is then used to calculate the phase velocity at each frequency and consequently obtain the dispersion curve of the site. The coherence function is used to judge the quality of data. Then inversion of Rayleigh wave dispersion curve provides information on the variation of shear wave velocity with depth.

The stiffness profile of the site is backcalculated (or backfigured) by matching the dispersion curve obtained from SASW field tests with a theoretical dispersion obtained using a theoretical model. Layer properties in the theoretical model are varied iteratively until satisfactory agreement is obtained between the theoretical and experimental curves. The theoretical stiffness profile is then taken to represent the actual profile. The above backcalculation procedure is based on the assumption of single mode propagation (using the first mode). The participation of each mode varies depending on soil stratification as well as frequency. Under some conditions, however, several modes can propagate at the same time with each mode having its own phase velocity. Consequently, under this condition, existing backcalculation procedures yield inaccurate results.

The purpose of this research was to improve the SASW method by incorporating multi-mode propagation in the backcalculation procedure.

In order to facilitate the investigation carried out in this study, two computer programs were developed to simulate SASW tests (and also Steady-State surface wave tests) and to calculate theoretical dispersion curves. The program for calculating theoretical dispersion curves was based on the root-searching procedure used in existing backcalculation methods. The computer programs developed in this study were used in a case study to demonstrate difficulties encountered by existing methods in dealing with multi-mode situations.

It was shown that: (i) wavelength filtering criteria used by existing methods yield inconsistent (i.e. erroneous) dispersion curves when more than one propagation mode participate in the wave field, and (ii) backcalculation procedures based on root-searching can not identify predominant propagation modes and hence fail to yield accurate results in the case of multi-mode propagation. Two developments were made in the present study to overcome the above difficulties.

First, a new wavelength filtering criterion was adopted. In this criterion, the dispersion data point for a particular frequency is rejected (i.e. filtered out) if the values of phase velocity obtained from two different receiver-to-receiver spacings are not in close agreement. In this manner, inconsistencies that might result in the dispersion due to multi-mode propagation are avoided.

Second, a new procedure to calculate the theoretical dispersion curve was developed. This procedure is based on the maximum vertical flexibility coefficient (at each frequency) of the theoretical layered model. Unlike root-searching methods, the maximum vertical flexibility coefficient method easily identifies predominant propagation modes. A computer program was developed in this study for backcalculation of SASW data based on the flexibility coefficient method. Least-squares optimization using the down-hill simplex method was also implemented in this program to automate the backcalculation process.

The accuracy of the above proposed procedures was demonstrated using SASW field tests. The shear wave velocity profiles obtained using the procedures developed in this study are in good agreement with those obtained from other in-situ seismic tests.

TABLE OF CONTENTS

APPENDIX: FLOW CHARTS, INPUT AND OUTPUT DATA FILES OF COMPUTER PROGRAMS..... 239

LIST OF TABLES

LIST OF FIGURES

CHAPTER 1

INTRODUCTION

1.1 Statement of the Problem

The shear wave velocity of soil is an important parameter in the design of machine foundations, evaluation of static and dynamic compaction, prediction of liquefaction, and the determination of the elastic modulus of soils.

The shear wave velocity of a soil can be measured in the laboratory using methods, such as the resonant column, cyclic triaxial and cyclic direct simple shear, or in the field using in-situ methods. Factors such as sample disturbance, and change of state of stress lead to non-representative samples which have significant influence on the results from laboratory tests. In addition, only a small volume of soil is tested with laboratory methods. Therefore, it is preferred to measure soil properties by in-situ methods.

Seismic methods are commonly used for in-situ evaluation of shear wave velocity. These methods are based on generating elastic stress waves at one point (source) and detecting

these waves at another point (receiver). Based on the positions of the source and receiver, seismic methods can be categorized into two main groups: borehole methods and surface methods.

In borehole methods, one or more boreholes are utilized. In surface methods, both source and receivers are located at the surface. Thus, surface methods have an economical advantage over borehole methods. An overview of several of the most widely used seismic methods for engineering purposes will be presented in chapter two.

The spectral-analysis-of-surface waves (SASW) method is a seismic technique for determining in-situ elastic moduli and thickness of layered systems, such as soils and pavements. The test is performed from the ground surface and thus requires no boreholes. Measurements are made at strain levels below .001 percent, where elastic properties of soil are essentially independent of strain amplitude as can be seen from Fig. 1.1. The SASW method consists of the generation of surface waves by an impulsive or random-noise load at the surface of soil deposits and the detection of these waves at two points away from the source. The detected signals are transformed to the frequency domain using FFT analysis to obtain the phase difference between receivers as a function of frequency. The phase difference is then used to construct the experimental dispersion curve of the site. The inversion of dispersion curve provides information on the variation of shear wave velocity with depth.

The SASW method has the following advantages: it is nondestructive, it is performed from the surface of the system, the setup and procedure are simple, and it has the potential of being fully automated.

The main disadvantage of the SASW method at this time is the process of inversion of the dispersion curve. The inversion process used until recently is an iterative procedure based on forward modeling of soil layers. In this procedure, the theoretical dispersion curve is matched to the experimental curve obtained in the field which is a

time-consuming process and an experienced operator is needed. Hossian and Drnevich (1989), Addo and Robertson (1992), Yuan and Nazarian (1993) have developed automated techniques based on optimization theory. In these procedures, it is assumed that the first surface wave propagation mode is the predominant one, but this assumption is not true for irregular soil sites due to the predominance of higher modes as shown by Gucunski and Woods (1992). Other disadvantages of the SASW method can be summarized as follows: (i) the test site has to be horizontally stratified, and (ii) in the inversion process, only plane Rayleigh waves are considered, and (iii) generating low frequencies that are needed for testing deep deposits may be difficult.

1.2 Research Objective

The main objective of this research is the development of the SASW method so that it is fully automated and reliable for irregular soil sites. Since the wave field of an irregular soil may consist of more than one surface mode, the phase angle obtained from Fourier analysis will not correspond to one mode. The phase spectrum represents an average of all the participating modes, and consequently, the inversion procedure based on the assumption that the first mode is predominant may not be correct. An inversion procedure that takes this phenomenon into account is needed.

In this study a computer program has been developed for the inversion of multi-mode experimental dispersion curves. In addition, an efficient and stable optimization technique is incorporated in the program.

1.3 Scope of Research

To achieve the above objective, the outline of proposed research is as follows:

1)-To investigate existing methods for computing theoretical Rayleigh wave dispersion curves and to develop a reliable computer program for that purpose.

There are three available methods for computing theoretical Rayleigh wave dispersion curves. The first one evaluates the determinant of the stiffness matrix at each frequency and searches for its roots. The second one evaluates the maximum of the vertical flexibility coefficient in the wave-number domain for each frequency. The third one simulates the SASW test and evaluates relative phase angle spectra for the same spacings used in field tests. Simulation of SASW tests involves the solution of an axisymmetric wave propagation problem in which the source is represented by a disk load on the surface of a layered soil system.

2)-To develop a procedure for the construction of a representative field dispersion curve.

Three filtering criteria were recommended in the past to construct a representative field dispersion curve. These criteria are applied to ensure that the short wavelengths picked up by the receivers are eliminated because their amplitudes might be reduced drastically and consequently they might be dominated by ambient noise. Also, long Rayleigh wavelengths are eliminated because they might not be fully developed or be contaminated by body waves when they arrive at the near receiver. However, these criteria are insufficient to ensure the condition that measured wave field is comprised of one surface mode only as will be discussed in Chapter Four Section 4.4.1.2. A new filter criterion needs to be developed.

3)-To implement the above procedures using actual field tests.

4)-To examine the possibility of incorporating higher modes of Rayleigh waves for irregular soil sites using existing inversion procedures.

In the available inversion procedures, it is assumed that the first surface wave mode is the predominant one, but this assumption is not true in irregular soil layers due to predominance of higher modes. Therefore, the inversion of the experimental dispersion curve should not be governed by the theoretical first Rayleigh mode. Both the maximum

vertical flexibility coefficient method and simulation of SASW tests will be examined for their ability to handle multi-mode dispersion curves.

5)-To automate the dispersion curve matching process and thus minimize the need for subjective experience in the inversion procedures. Automation procedures will have to be efficient and stable.

1.4 Organization of the Thesis

Chapter 2 describes an overview of in situ-methods and the background literature related to the SASW method. Also in Chapter 2, wave propagation in layered media, derivation of three dimensional wave equation, types of waves, parameters affecting shear modulus, determination of stiffness matrix of soil layers, signal analysis and required functions are discussed.

Chapter 3 describes the SASW method in detail in three parts: (i) field collection of data, (ii) construction of field dispersion curve, and (iii) inversion of dispersion curve.

Chapter 4 gives a detailed description of the mathematical modeling of soil layers and the calculation of dispersion curves by the transfer matrix and by the stiffness matrix methods. The results obtained by a computer program developed in this research are presented for a case study.

Chapter 5 gives a detailed description of the development a numerical procedure for simulation of SASW tests. Complete numerical techniques and verification of the method are described in this chapter.

Chapter 6 explains the development of a new method for calculation of the theoretical dispersion curve. The verification and comparison of the new method with existing methods are also described in chapter 6.

Chapter 7 describes different optimization techniques for automatic matching of the theoretical dispersion curve with the experimental one.

Chapter 8 presents the results for several sites that were tested using the new SASW procedures developed in this research.

Chapter 9 presents the conclusions of this research, and provides some recommendations for further research and development.

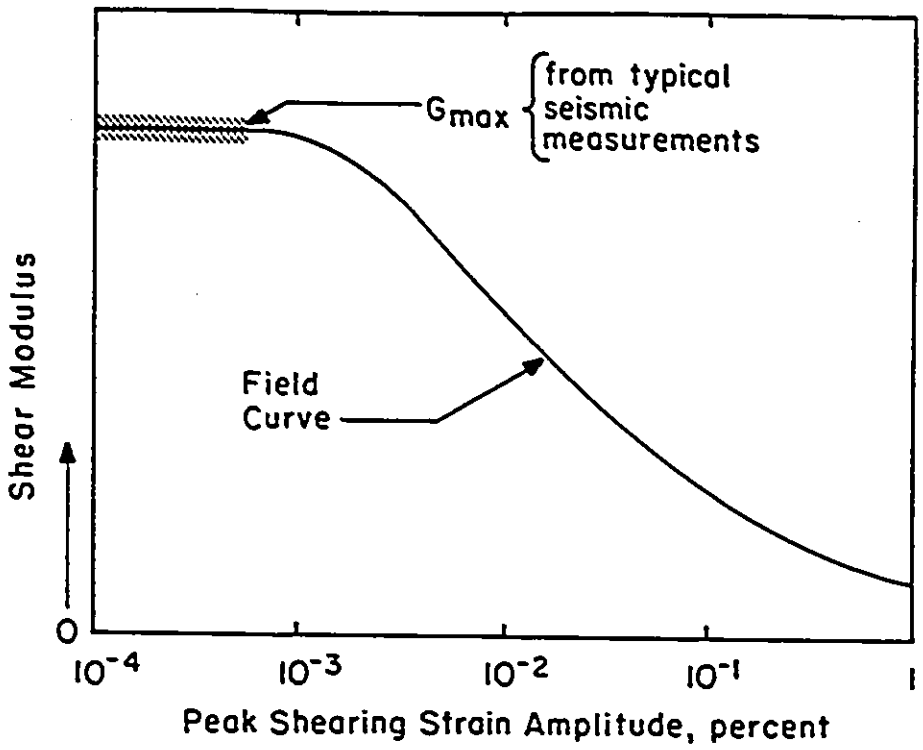

Fig. 1.1-Typical variation of in-situ shear modulus with shearing strain amplitude at the start of cyclic loading (After Stokoe and Hoar, 1977).

CHAPTER 2

LITERATURE REVIEW

2.1 Overview of In-Situ Seismic Methods Used for Engineering Purposes

Compression, shear, and Rayleigh waves are three basic types of seismic (stress) waves which propagate in a layered, elastic half-space. Compression and shear waves are collectively called body waves because these waves propagate within the interior of the layered elastic half space as well as along its surface. Rayleigh waves are often referred to as surface waves because they propagate near the surface of the half space.

Compression and shear wave velocities are most often measured by seismic methods. As mentioned before, the seismic methods available to civil engineers fall into two categories: borehole methods and surface methods.

2.2 Borehole Methods

Borehole methods are used to determine profiles of shear and compression wave velocities and shear and constrained moduli at relatively shallow depths (0 to 60 m). Borehole methods include the crosshole, downhole, uphole, in-hole, bottom-hole, and the seismic cone penetration tests. A schematic illustration of these tests is shown in

Figs. 2.1 and 2.2. Two popular borehole techniques, the crosshole and downhole test methods, are discussed in detail in the following paragraphs.

2.2.1 Crosshole Method

In the crosshole method, the time for compression and shear waves to travel between several points at the same depth within a soil or rock mass is measured. With known travel times and determination of travel distance, wave velocities are calculated.

Fig. 2.3 shows a schematic of one field procedure which is used in practice (Hoar and Stokoe, 1978). This procedure requires a minimum of three or more cased boreholes. These boreholes are drilled and cased to the depth of interest several days before testing. Drilling mud is often used to reduce borehole disturbance from stress relief and squeezing (Shannon and Wilson 1976). Each borehole is logged during drilling to determine soil type and thickness and inclination of layers.

The distance between each of the boreholes in a crossholes test is usually of the order of 3 to 4.6 m. To minimize factors which can effect the measurements such as disturbance, screening and wave interaction effects, the diameter of boreholes is selected as small as feasible. Typically, borehole diameters range from 10.2 to 15.2 cm.

Either aluminum or plastic casing is used, and the casing is grouted in place. Casing with an inner diameter of about 7.6 cm is compatible with seismic equipment. Any borehole deviations from the vertical must be reliably known at all test depths. Standard penetration test (SPT) equipment is employed as a mechanical source. This is accomplished by positioning a drill rig at the location of the source borehole as shown in Fig. 2.3 and advancing a fourth borehole (usually uncased). At each desired test depth for which travel time measurements are to be performed, the drilling operation is stopped.

The SPT equipment is then used to generate vertical impulses in the bottom of the forth borehole. Each impulse generates compression and shear waves in the soil and simultaneously triggers a recording device, an oscilloscope. Three-dimensional geophones (vertical, radial, and transverse) located in the cased boreholes at the same depth as the source are used to monitor the passage of the waves. Each geophone is held tightly in place against the wall of the borehole through the use of some mechanism such as inflatable packers or by pneumatic or hydraulic pistons. After measurements have been performed for all travel paths at a desired depth, the fourth borehole is advanced to the next depth and the test is repeated. This procedure is continued to the final depth. Fig. 2.4 shows a typical travel time record from vertical velocity transducers wedged in three cased boreholes.

The initial wave arrivals at each receiver are identified on the record by P for compression wave and S for the shear wave. Fig. 2.4 shows the determinations of interval travel time for the shear wave. Using interval travel times rather than source-to-receiver travel times has significant advantage in minimizing misinterpretation of a refracted wave as a direct wave.

The velocity of the waves is computed as the ratio of inter-borehole distance at the test depth to the travel time. In soils where stiffness increases with depth, Andreasson (1979) observed that shear waves travel in the deeper and stiffer material and hence travel paths are not necessarily horizontal as assumed in velocity calculations. To reduce the time involved in conventional crosshole testing, and avoid drilling disturbances associated with pre-bored holes, crosshole tests have also been performed with two cone penetration rigs for pushing a receiver and a source (Baldi et al. 1988).

However, tests conducted by Andreasson (1979) concluded that disturbance effects on wave velocities from drilling and pushing relatively large penetrometers are similar. The crosshole test is often considered the most accurate seismic method and is more frequently used as a reference (Larsson and Mulabdic 1991). The most significant

disadvantage of the crosshole method is its higher expense and the time required to install and measure the inclination of the holes.

2.2.2 Downhole Method

In the downhole method, the time for compression and shear waves to travel between a source on the surface and points within a soil or rock mass is measured. With known travel times and travel distance, wave velocities are calculated.

Fig. 2.5 shows a schematic of one field procedure (Hoar and Stokoe, 1978). This procedure requires a minimum of one or more cased boreholes. This borehole is drilled and cased to the maximum depth of interest several days before testing. It is identical to those used as receiver boreholes in the crosshole method. As shown in Fig. 2.5, a 0.6 m cube of concrete is cast-in-place at the location and embedded so that the top of the block is about even with the ground surface. The block should be located about 6 m from the borehole. Two sections of angle iron which extend about 0.3 m out of concrete at a 45 degree angle with the vertical are placed in the block at time of casting.

Body waves are generated in the soil by striking one of the angle irons in the embedded concrete block with a 4.5 kg sledge hammer. Wave arrivals are monitored by a horizontal velocity transducer wedged in the cased borehole at the first measurement depth. This procedure is repeated except that the block is struck in the opposite direction. The test is repeated at about 1.5 to 3 m intervals to the final measurement depth.

The advantages of the downhole test are placement of the source and minimum refraction problems. In addition, this test is relatively inexpensive because only one borehole is required. However, as the depth increases, the path length of the wave increases, and the quality of the signals decreases.

2.3 Surface Methods

In surface methods, both the source and receivers are located at the ground surface. Therefore, these methods are more economical than borehole methods in that no boreholes are required. Common surface methods include the refraction, reflection, steady-state surface wave, and spectral analysis of surface waves. The simplified schemes of each of these tests are shown in Fig. 2.6. The refraction and reflection test methods, are discussed in the following paragraphs and steady-state surface wave, and spectral analysis of surface waves are discussed in chapter four.

2.3.1 Refraction Method

The surface refraction method was the first seismic test to be used in civil engineering. It is a popular way of determining structure features such as depth to bedrock, and has simple data acquisition and analysis procedures.

As shown in Fig. 2.7.a, body waves are generated by an impact source (e.g. explosives or a sledge hammer) on the surface of the material being tested. The test may be performed using either compression or horizontally polarized shear wave which is generated by a vertical and a horizontal impact respectively.

The compression or shear waves which propagate through the medium are detected by receivers placed on the surface at various distances from the source. If the compression waves are being used, the receivers are oriented vertically. In the case of using horizontally polarized shear waves, the receivers are oriented perpendicularly to an imaginary line connecting the source and sensor. Generally, compression waves are used in the refraction method because it has the greatest velocity and will be the first wave which arrives at the receivers. For receiver placed close to the source, the first wave to arrive will be the wave which travels directly from the source to the receiver (path A in Fig. 2.7).

But for some receivers that are located at critical distance from the source, x_c, a wave which travels along path B in Fig. 2.7 will be the first wave to arrive because it travels for a significant time at a higher velocity in the underlying layer. By plotting the time of first arrival at each sensor versus the distance from the source to that receiver, the velocity and thickness of each layer can be calculated using a simple relationship (Fig. 2.8).

The main disadvantage of this method is the inability to detect low velocity layers under high velocity layers. More details of the method can be found in Richard et al. (1970), and Borm, (1977).

2.3.2 Reflection Method

The reflection method is a field test to map geological structures by measuring the arrival times of pulses which have been reflected from interfaces between regions of different impedances. Reflection method is used in geophysics for the exploration of geological formations believed to contain oil and natural gas. The objective of this method is the determination of layer thickness and depth as well as irregularities of layers.

Similar to the refraction method, body waves are generated by impacting a source (e.g., explosives or a sledge hammer) on the surface of the material being tested. Most reflection surveys utilize compression rather than shear waves. The propagated waves through the medium are detected by receivers placed on the surface at known distances from the source. In this method, the goal is to identify the wave arrivals due to reflection from layer boundaries (Fig. 2.9). By plotting the travel time versus offset (distance from the source) as show in Fig. 2.10, thicknesses and velocities of the layer can be determined using values obtained from the curves and simple relationships.

One disadvantage of this method in engineering application is interpretation of the time records which become complicated. The other disadvantage is that multiple reflections from one layer may obscure detection of the primary reflected waves from other layers.

2.4 Wave Propagation in Layered Media

For more than half a century, elastic stress waves have been used for in situ tests for determining soil and pavement properties. These properties are used for site characterization, evaluation of pavement characteristics, design of foundations subjected to dynamic load, etc. Understanding wave propagation in a layered media is necessary for development and application of seismic methods in evaluation of soil properties. Soil media in most instances can be approximated by layered half-space with reasonable accuracy, especially over short distances. With this approximation, the profiles are assumed to be homogeneous and extend to infinity in two horizontal directions while being heterogeneous in vertical direction. This heterogeneity is often modeled by a number of layers with constant properties within each layer. In addition, it is assumed that the material in each layer is elastic and isotropic.

This section reviews background material which is needed for the present study. The review includes wave propagation in layered media, derivation of equations, types of waves, parameters affecting shear modulus, stiffness matrix of soil layer, signal analysis including Fourier transform, discrete Fourier transform, fast Fourier transform, spectral analysis, linear spectrum, auto power spectrum, cross power spectrum, and transfer function.

2.5 Three-Dimensional Wave Equation in Cartesian Coordinates

In the following, the well-known fundamental equations of elastodynamics are summarized. Complete set of equations can be found in the textbooks by Ewing, Jardetzky and Press (1957), Richart, Woods and Hall (1970), Aki and Richards (1980), Ben-Menahem and Singh (1981), Wolf (1985) and others.

The basic wave equations in three-dimensions for body waves in a homogeneous isotropic, elastic half-space can be written in the form of partial differential equations

$$\nabla^2 e = -\frac{\omega^2}{V_p^2} e \qquad [2.1]$$

$$\nabla^2 \{\Omega\} = -\frac{\omega^2}{V_s^2} \{\Omega\} \qquad [2.2]$$

where $\nabla 2$ represents the Laplace operator, e the volumetric strain, ω circular frequency, Ω the rotational-strain vector and V_P and V_S wave velocities. Since the velocity V_P is associated with volumetric strain, it represents the compression or P-wave velocity. Analogously, the velocity V_S is associated with shear deformation and represents the shear or S-wave velocity. The volumetric strain e and the rotation-strain vector {Ω} with the amplitude components Ωx, Ωy, Ωz are defined as

$$e = u_{,x} + v_{,y} + w_{,z} \qquad [2.3]$$

$$\Omega_x = \frac{1}{2}(w_{,y} - v_{,z}) \qquad [2.4a]$$

$$\Omega_y = \frac{1}{2}(u_{,z} - w_{,x}) \qquad [2.4b]$$

$$\Omega_z = \frac{1}{2}(v_{,x} - u_{,y}) \qquad [2.4c]$$

where u, v, w are particle displacements in x, y, z directions, respectively.

The V_P and V_S velocities can be expressed in terms of Lame's constants λ and μ or in terms of the modulus of elasticity E and Poisson's ratio ν, and the mass density ρ

$$V_p = \sqrt{\frac{\lambda + 2\mu}{\rho}} = \sqrt{\frac{E(1-\nu)}{\rho(1+\nu)(1-2\nu)}} \qquad [2.5]$$

$$V_s = \sqrt{\frac{\mu}{\rho}} = \sqrt{\frac{G}{\rho}} \qquad [2.6]$$

where G is the shear modulus, equivalent to Lame's constant μ.

2.6 Types of Waves

2.6.1 Compression (or P) Wave

The solution of Eq. 2.1 can be obtained by substituting the trial function [2.7]. The result is displayed in Fig. 2.11a.

$$e = -\frac{i\omega}{V_p} A_p \exp\left[\frac{i\omega}{V_p}(-l_x x - l_y y - l_z z)\right] \qquad [2.7]$$

It is verified that the trial function (Eq. 2.7) satisfies the wave equation if

$$l_x^2 + l_y^2 + l_z^2 = 1 \qquad [2.8]$$

The three scalars l_X, l_Y, and l_Z may be considered as the direction cosines of a straight line. To interpret the exponential function in Eq. 2.7, it is recalled that harmonic motion is represented as $\exp(+i\omega t)$. An expression of the form $\exp[i\omega(t\text{-}s/Vp)]$ represents a wave propagating in the positive s-direction with velocity Vp . Comparison with Eq. 2.7 leads to

$$s = l_x x + l_y y + l_z z \qquad [2.9]$$

This scalar product shows that the coordinate s is measured along a straight line. It also follows that for a given time t = to, the amplitude of the volumetric strain is constant if s is constant. This is the equation of a plane (Eq. 2.9) normal to the direction of propagation.

The corresponding amplitudes of the displacements can be found from

$$u_p = l_x A_p \exp\left[\frac{i\omega}{V_p}(-l_x x - l_y y - l_z z)\right] \qquad [2.10a]$$

$$v_p = l_y A_p \exp\left[\frac{i\omega}{V_p}(-l_x x - l_y y - l_z z)\right] \qquad [2.10b]$$

$$w_p = l_z A_p \exp\left[\frac{i\omega}{V_p}(-l_x x - l_y y - l_z z)\right] \qquad [2.10a]$$

where Ap is the amplitude of a wave whose displacement vector coincides with direction of propagation. This represents the definition of the dilational or P-wave. The subscript p has been introduced to denote the corresponding displacements in Eq. 2.10. Summarizing, the particle motion of a P-wave with an amplitude Ap takes place along the direction of propagation (determined by the direction cosines l_x, l_y ,l_z) and is constant over the plane perpendicular to it. The velocity of propagation V_p is constant and depends on material properties only.

2.6.2 Shear (or S) Wave

Turning to the other wave equation (Eq. 2.2), a solution analogous to that of Eq. 2.1 is given by

$$\{\Omega\} = -\frac{i\omega}{2V_s}\{C\}\exp\left[\frac{i\omega}{V_s}(-m_x x - m_y y - m_z z)\right] \qquad [2.11]$$

with

$$m_x^2 + m_y^2 + m_z^2 = 1 \qquad [2.12]$$

$$m_x C_x + m_y C_y + m_z C_z = 0 \qquad [2.13]$$

The direction of propagation is specified by the direction cosines m_x, m_y, and m_z (Fig. 2.11b). The velocity equals V_s. As the scalar product vanishes, the vector {C} and thus {Ω} are perpendicular to the direction of propagation.

The corresponding displacement amplitudes are equal to

$$u_s = (m_z C_y - m_y C_z)\exp\left[\frac{i\omega}{V_s}(-m_x x - m_y y - m_z z)\right] \qquad [2.14a]$$

$$v_s = (m_x C_z - m_z C_x)\exp\left[\frac{i\omega}{V_s}(-m_x x - m_y y - m_z z)\right] \qquad [2.14b]$$

$$w_s = (m_y C_x - m_x C_y)\exp\left[\frac{i\omega}{V_s}(-m_x x - m_y y - m_z z)\right] \qquad [2.14c]$$

From Eq. 2.14 it follows that the displacements are proportional to the components of the vector product of {C} and the direction of propagation. This means that the particle motion of this wave lies in a plane perpendicular to the direction of propagation. This is the definition of the distortional or shear (S)-wave. The subscript s denotes the corresponding displacements in Eq. 2.14.

The trial functions selected for e and {Ω} (Eqs. 2.7 and 2.11) do not represent the most general solution of the wave equations; they correspond to plane waves.

In general, the displacement vector of the S-wave can be further decomposed into a horizontal component with an amplitude A_{SH} and into a component with an amplitude A_{SV} lying in the plane which contains the global vertical z-axis and the direction of propagation (Fig. 2.11b).

$$A_{SH} = \frac{C_x}{\sqrt{m_x^2 + m_y^2}} \qquad [2.15a]$$

$$A_{SV} = \frac{m_x C_y - m_y C_x}{\sqrt{m_x^2 + m_y^2}} \qquad [2.15b]$$

A_{SH} and A_{SV} are the amplitudes of the SH- and SV-waves, respectively. The displacements in terms of these amplitudes can be reformulated as

$$u_s = \frac{m_x m_z A_{SV} - m_y A_{SH}}{\sqrt{m_x^2 + m_y^2}} \exp\left[\frac{i\omega}{V_s}(-m_x x - m_y y - m_z z)\right] \qquad [2.16a]$$

$$v_s = \frac{m_y m_z A_{SV} + m_x A_{SH}}{\sqrt{m_x^2 + m_y^2}} \exp\left[\frac{i\omega}{V_s}(-m_x x - m_y y - m_z z)\right] \qquad [2.16b]$$

$$w_s = -\sqrt{m_x^2 + m_y^2} A_{SV} \exp\left[\frac{i\omega}{V_s}(-m_x x - m_y y - m_z z)\right] \qquad [2.16c]$$

These expressions are easily verified using simple geometric considerations.

2.6.3 Surface Waves

In a layered medium, the other two types of waves which can exist are Rayleigh and Love waves. These waves are called surface waves, while P- and S-waves represent body waves. Surface waves propagate near the surface of the layered medium. Rayleigh waves are essentially vertically polarized P-SV waves. For Rayleigh waves the particle motion consists of vertical and horizontal components as shown in Fig. 2.12. The vertical and the horizontal component of the Rayleigh waves in an undamped half-space are 90 degrees out of phase. Particle motion at the surface and at depth (greater than 0.2 λ) follows a retrograde and prograde ellipse, respectively. There is a transition zone in which the horizontal component of particle motion vanishes (see Fig. 2.12).

Since particle motion is predominantly vertical, receivers for detecting and measuring Rayleigh waves are positioned in the vertical direction. Miller and Pursey (1955) found that for the case of a vertically oscillating load on a homogeneous isotropic half-space, approximately 67 percent of energy of the input energy is radiated by Rayleigh waves while shear and compression waves carry 26 and 7 percent of the energy, respectively.

Also the geometrical damping, the decrease of amplitude with distance from the source due to geometry of propagation, is smallest for the Rayleigh wave. At the surface of an elastic half-space, the amplitude of body waves attenuates in proportion to $1/r^2$, where r is the distance from the source; whereas, surface wave amplitude decreases in proportion to $1/\sqrt{r}$. The amplitude of motion decreases rapidly with depth and at a depth of approximately two wavelengths the particle motion becomes negligible.

The propagation velocities of the various waves mentioned above are different. Compression waves propagate faster than shear waves, and Rayleigh waves propagate slightly slower than shear waves. The relation between Poisson's ratio and the P, S, and Rayleigh wave velocities is shown in Fig. 2.13.

In a homogeneous isotropic elastic half-space, the velocity of Rayleigh waves is constant, i.e. it does not vary with frequency (see Fig. 2.14). In a layered medium, however, Rayleigh waves become dispersive (see Fig. 2.15). Dispersion refers to the variation of wave velocity as a function of the frequency of the propagating wave. In layered media, dispersion occurs since Rayleigh waves penetrate to (or sample) various depths of the layered media, depending on their wavelength. High frequency waves, or those with short wavelengths, propagate in shallow layers, i.e. layers near the surface, while long wavelengths penetrate to deeper layers. Consequently, the velocity of the propagating wave depends on the properties of the sampled layers. The velocity of a Rayleigh wave is mainly governed by the properties of the layers through which the bulk of the wave propagates.

Fig. 2.16 represents dispersion curves for the first three Rayleigh wave modes for a soft soil layer underlain by a hard half-space. The first mode begins at R-wave velocity of the half-space for a frequency equal to zero and converges to the Rayleigh wave velocity of the layer as frequency increases. Higher modes do not exist below so called cutoff frequency, the frequency below which the motion ceases to propagate.

Love waves are shear waves that propagate near the surface of a solid medium. Particle motion of wave propagation is contained in a horizontal plane. Love waves are therefore said to be horizontally polarized shear (or SH-) waves. In a formation where shear wave velocity increases with depth, Love wave velocity approaches the S-wave velocity in the surface layer at high frequencies and the S-wave velocity in the deepest layer at sufficiently low frequencies. In Fig. 2.17 all types of waves are shown.

2.7 Shear Modulus and Internal Damping of Soil

The shear modulus and damping in soils are important in the analysis of soil vibration problems such as evaluation of wave propagation and in the solution of problems of soil-

structure interaction. Hardin and Drnevich (1972) have indicated that many parameters affect the shear modulus and damping of soils. The parameters have been grouped into three categories: very important, less important, and relatively unimportant (see Table 2.1). There are five parameters that, in general, are very important. From Table 2.1, e.g., strain amplitude, effective mean principal stress, and void ratio are very important parameters for the shear modulus and damping in all soils, whereas overconsolidation ratio is a less important parameter for cohesive soils, and is unimportant for clean sand. The material damping, which can be different for P- and S-waves, can be described in terms of hysteretic damping ratios ζ_p, and ζ_S respectively. Taking into account material damping by introducing complex material properties the complex shear modulus G^* can be defined as

$$G^* = G(1+2\zeta_s i) \qquad [2.17]$$

For $\zeta_p \neq \zeta_S$, Poisson's ratio ν will also be complex. Complex wave velocities are equal to

$$V_p^* = V_p\sqrt{1+2\zeta_p i} \qquad [2.18]$$

$$V_s^* = V_s\sqrt{1+2\zeta_s i} \qquad [2.19]$$

Generally, the damping ratio increases as the strain increases. The damping ratio of soil can be determined through laboratory tests. In practice, the damping ratio at low-strain levels may be chosen in the range of 1% to 5 % based on the soil classification and viscosity level (Richart and Woods, 1970).

2.8 The Stiffness Matrix Approach in Problems of Soil Structure Interaction

The stiffness matrix approach is similar to the stiffness matrix or displacement method in structural analysis. The stiffness matrix of soil layer, as an extension of the transform matrix (Thomson 1950, Haskell 1953), was derived by Kausel and Roesset (1981), and in slightly different form presented by Wolf and Obernhuber (1982) and Wolf (1985).

The stiffness matrix relates forces and displacements at top and bottom of the layer in the frequency-wave number domain. Simplifying Eqs.2.10, 2.14 by assuming that the directions of propagation of P- and S-wave lie in the same vertical plane (e.g., the x-z plane), i.e. imposing $l_y=m_y=0$ and taking into account material damping lead to

$$u = l_x A_p \exp\left[i\omega\left(-\frac{l_x x}{V_p^*}-\frac{l_z z}{V_p^*}\right)\right]+m_x A_{SV} \exp\left[i\omega\left(-\frac{m_x x}{V_s^*}-\frac{m_z z}{V_s^*}\right)\right] \qquad [2.20a]$$

$$v = A_{SH} \exp\left[i\omega\left(-\frac{m_x x}{V_s^*}-\frac{m_z z}{V_s^*}\right)\right] \qquad [2.20b]$$

$$w = l_x A_p \exp\left[i\omega\left(-\frac{l_x x}{V_p^*}-\frac{l_z z}{V_p^*}\right)\right]-m_x A_{SV} \exp\left[i\omega\left(-\frac{m_x x}{V_s^*}-\frac{m_z z}{V_s^*}\right)\right] \qquad [2.20a]$$

The in-plane displacements with amplitudes u and w depend only on the P- and S-waves. The out-of-plane displacement with amplitude v is caused by the SH-wave and is thus independent of u and w.

Mathematically, the variables x and z of the displacement field can be separated. For both P- and SV-wave traveling in the positive x direction the displacements can be written in the form

$$u(z,x) = u(z)\exp(-ik\alpha x) \qquad [2.21a]$$

$$w(z,x) = w(z)\exp(-ik\alpha x) \qquad [2.21b]$$

where

$$u(z) = l_x\left[A_p \exp(iksz) + B_p \exp(-ksz)\right] - m_x t\left[A_{sv} \exp(ikz) - B_{sv} \exp(-ikz)\right] \quad [2.22a]$$

$$w(z) = l_x s\left[A_p \exp(iksz) - B_p \exp(-ksz)\right] - m_x\left[A_{sv} \exp(ikz) + B_{sv} \exp(-ikz)\right] \quad [2.22b]$$

Here u(z) and w(z) can be interpreted as the amplitudes of the wave traveling in the x-direction.

$$k = \frac{\omega}{c} \quad [2.23]$$

where c and k are the phase velocity and the wave number.

$$c = \frac{V_p^*}{l_x} = \frac{V_s^*}{m_x} \quad [2.24]$$

$$s = -i\sqrt{1 - \frac{1}{l_x^2}} \quad [2.25]$$

and

$$t = -i\sqrt{1 - \frac{1}{m_x^2}} \quad [2.26]$$

The amplitudes A_{SV} and B_{SV} are associated with the SV-wave propagating in the negative and positive z-direction, respectively, while the amplitudes A_p and B_p are associated with P-wave propagating in the negative and positive z-direction, respectively.

The amplitude of the normal stress $\sigma_z(z)$ and the shear stress $\tau_{xz}(z)$ can be expressed as

$$\sigma_z(z) = \lambda^*(u_{,x} + w_{,z}) + 2G^* w_{,z} \quad [2.27a]$$

$$\tau_{xz}(z) = G^*(u_{,z} + w_{,x}) \quad [2.27b]$$

Substituting Eqs. 2.21 and 2.22 in Eq. 2.27 and performing the differentiation with respect to x and z leads to

$$\sigma_z(z) = +ikl_x(1 - t^2)G^*\left[A_p \exp(iksz) + B_p \exp(-iksz)\right] - i2km_x tG^*\left[A_{SV} \exp(ikz) - B_{SV} \exp(-ikz)\right] \quad [2.28a]$$

$$\tau_{xz}(z) = i2kl_s sG^*\left[A_P \exp(iksz) - B_P \exp(-iksz)\right] + ikm_s(1-t^2)G^*\left[A_{SV} \exp(ikz) + B_{SV} \exp(-ikz)\right] \quad [2.28b]$$

The displacement and stress amplitudes at the top u_1, w_1, τ_{xz1}, σ_{z1} and at the bottom of the layer u_2, w_2, τ_{xz2}, σ_{z2} can be calculated from Eqs. 2.22 and 2.28 by introducing z = 0 and = d, respectively, as a function of the amplitudes A_P, A_{SV} of the incident waves and B_P, B_{SV} of the reflected waves. Eliminating these amplitudes results in the transfer matrix shown as Eq. 2.29.

$$\begin{Bmatrix} u_2 \\ w_2 \\ \tau_{xz2} \\ \sigma_{z2} \end{Bmatrix} = \frac{1}{1+t^2} \begin{bmatrix} 2\cos ksd & +i\frac{1-t^2}{s}\sin ksd & +\frac{1}{ksG^*}\sin ksd & \frac{i}{kG^*}\cos ksd \\ +(t^2-1)\cos ktd & +i2t\sin ktd & +\frac{t}{kG^*}\sin ktd & -\frac{i}{kG^*}\cos ktd \\ -i2s\sin ksd & (t^2-1)\cos ksd & \frac{i}{kG^*}\cos ksd & +\frac{s}{kG^*}\sin ksd \\ -i\frac{1-t^2}{t}\sin ktd & +2\cos ktd & -\frac{i}{kG^*}\cos ktd & +\frac{1}{kG^*}\sin ktd \\ -4kG^*s\sin ksd & i2kG^*(1-t^2)\cos ksd & 2\cos ksd & -i2s\sin ksd \\ -kG^*\frac{(1-t^2)^2}{t}\sin ktd & -i2kG^*(1-t^2)\cos ktd & +(t^2-1)\cos ktd & -i\frac{1-t^2}{t}\sin ktd \\ i2kG^*(1-t^2)\cos ksd & -kG^*\frac{(1-t^2)^2}{s}\sin ksd & +i\frac{1-t^2}{s}\sin ksd & (t^2-1)\cos ksd \\ -i2kG^*(1-t^2)\cos ktd & -4kG^*t\sin ktd & +i2t\sin ktd & 2\cos ktd \end{bmatrix} \begin{Bmatrix} u_1 \\ w_1 \\ \tau_{xz1} \\ \sigma_{z1} \end{Bmatrix} \qquad [2.29]$$

The state vector is composed of u, w, τ_{xz}, and σ_z. Imposing the boundary conditions at z = 0, the external load amplitude $P_1 = -\tau_{xz1}$, $R_1 = -\sigma_{z1}$, $P_2 = -\tau_{xz2}$, $R_2 = -\sigma_{z2}$ defined in the global-coordinate system in Eq. 2.29, and performing a partial inversion leads to the dynamic-stiffness matrix of the layer, shown as Eq. 2.30. To achieve symmetry, R_1, R_2, w_1, and w_2 are multiplied by i.

The dynamic stiffness matrix of the half-space is derived by using the same procedure but suppressing the incoming (incident) waves. Therefore Eqs. 2.22 and 2.28 are formulated for z = 0. The condition $A_P = A_{SV} = 0$ is then introduced and finally B_P and B_{SV} are eliminated. This leads to (with $P_0 = -\tau_{xz1}$, $R_0 = -\sigma_{z1}$)

$$\begin{Bmatrix} P_o \\ iR_o \end{Bmatrix} = kG \begin{bmatrix} \frac{is(1+t^2)}{1+st} & 2-\frac{1+t^2}{1+st} \\ 2-\frac{1+t^2}{1+st} & \frac{it(1+t^2)}{1+st} \end{bmatrix} \begin{Bmatrix} u_o \\ iw_o \end{Bmatrix} \quad [2.31]$$

where P_0, R_0, represent external load and u_0, w_0 denote displacement of the free surface of the half space.

Indefinite expression arises in the stiffness matrix in case when k and ω become zero or infinity. Modified stiffness matrices to avoid this situation can be found in Kausel and Roesset (1981) and Wolf (1985).

$$\begin{Bmatrix} P_1 \\ iR_1 \\ P_2 \\ iR_2 \end{Bmatrix} = \frac{(1+t^2)KG^*}{D} \begin{bmatrix} \frac{1}{t}\cos ksd \sin ktd & \frac{3-t^2}{1+t^2}(1-\cos ksd \cos ktd) & -s \sin ksd & \cos ksd \\ +s \sin ksd \cos ktd & +\frac{1+2s^2t^2-t^2}{st(1+t^2)}\sin ksd \sin ktd & -\frac{1}{t}\sin ktd & -\cos ktd \\ \frac{3-t^2}{1+t^2}(1-\cos ksd \cos ktd) & \frac{1}{s}\sin ksd \cos ktd & -\cos ksd & -\frac{1}{s}\sin ksd \\ +\frac{1+2s^2t^2-t^2}{st(1+t^2)}\sin ksd \sin ktd & +t \cos ksd \sin ktd & +\cos ktd & -t \sin ktd \\ -s \sin ksd & -\cos ksd & \frac{1}{t}\cos ksd \sin ktd & \frac{t^2-3}{1+t^2}(1-\cos ksd \cos ktd) \\ -\frac{1}{t}\sin ktd & +\cos ktd & +s \sin ksd \cos ktd & +\frac{t^2-2s^2t^2-1}{st(1+t^2)}\sin ksd \sin ktd \\ \cos ksd & -\frac{1}{s}\sin ksd & +\frac{t^2-3}{1+t^2}(1-\cos ksd \cos ktd) & \frac{1}{s}\sin ksd \cos ktd \\ -\cos ktd & -t \sin ktd & +\frac{t^2-2s^2t^2-1}{st(1+t^2)}\sin ksd \sin ktd & +t \cos ksd \sin ktd \end{bmatrix} \begin{Bmatrix} U_1 \\ iW_1 \\ U_2 \\ iW_2 \end{Bmatrix}$$

[2.30]

where

$$D = 2(1-\cos ksd \cos ktd) + (st + \frac{1}{st})\sin ksd \sin ktd$$

2.9 Signal Analysis

Signal analysis involves the mathematical calculations required to calculate attributes of a wave form and may be described in either time or the frequency domain. Generally, it is preferred to analyse a dynamic system in frequency domain.

Analysis in frequency domain in addition to its computational efficiency possesses several other advantages. By providing a clear representation of the frequency domain content of the forcing function, it enables one to evaluate the potential for it to excite a given structure. For problems involving infinite domains such as those of wave motion in reservoirs of large extent or in unbounded soil media, and in other situations where the physical characteristics of the system are dependent on the vibration frequency, frequency-domain analysis may prove to be more effective than a time-domain analysis. The relationship between time and frequency domain is formulated by Fourier transform equations. The following section presents Fourier transform and its application in SASW.

2.9.1 Fourier Transform

In the analysis of dynamic response of linear structures, Fourier transform can play an important role. Briefly, this transform decomposes an arbitrary function in the time domain into a group of harmonic functions. The Fourier integral transform of a signal is defined as

$$H(f) = \int_{-\infty}^{\infty} h(t) \exp(+i2\pi ft)dt \qquad [2.32]$$

where, H(f) is the frequency domain representation of function h(t). Similarly, the inverse transform can be written as:

$$h(t) = \int_{-\infty}^{\infty} H(f) \exp(-i2\pi ft)df \qquad [2.33]$$

2.9.2 Discrete Fourier Transform

The computation of integrals is not always easy to solve. In most practical cases, therefore, Fourier transform is used in its discrete form, which permits the replacement of the integrals by equivalent numerical computations of areas. The discrete Fourier transform, and its inverse, transform a time series of samples X(nΔt) into a series of frequency domain samples X_d(m Δf), and vice versa, and can be defined as

$$X_d(m\Delta f) = \Delta t \sum_{n=0}^{N-1} X(n\Delta t)\exp(+2\pi mn\Delta f n\Delta t) \qquad [2.34]$$

$$X(n\Delta t) = \Delta f \sum_{n=0}^{N-1} X_d(m\Delta f)\exp(-i2\pi mn\Delta f n\Delta t) \qquad [2.35]$$

where Δt is the time interval between samples, Δf is the increment of frequency between each two discretized points, N is the number of samples considered, n the time sample index, and m the frequency domain sample index.

2.9.3 Fast Fourier Transform

The computations involved in obtaining the discrete Fourier transforms of the functions being convoluted, taking the product of these transforms and evaluating the discrete inverse Fourier transform are no less than those in a direct evaluation of the discrete convolution. However, the development of a special algorithm called fast Fourier transform (FFT) has completely altered this position. The FFT algorithm, which derives its efficiency from exploiting the harmonic property of a discrete transform, cuts down the computations by several orders of magnitude and makes frequency-domain analysis highly efficient. The FFT algorithm requires that the number of samples is a power of 2. Some recently developed algorithms presented by Brigham (1988), allow other bases in operation. A more detailed review of the subject can be found in Churchill and Brown (1987), and its numerical implementation in Ramirez (1985), Press et al. (1992), Brigham (1988), and Hewlett Packard Company (1985).

2.9.4 Spectral Analysis

Spectral analysis is basically a statistical operation in frequency domain on one or two signals. Several types of measurements can be made directly with most of the spectral analyzers that are currently available. The basic requirement is linear spectrum, generally of both an input signal and an output signal. Other functions are defined by using these two spectra or their complex conjugates.

2.9.5 Linear Spectrum

The linear spectrum, denoted by $S_x(f)$, is simply the Fourier transform of the signal. Mathematically, it can be represented as:

$$S_x(f) = \sum_{-\infty}^{\infty} X(t) \exp(+i2\pi ft)dt \qquad [2.36]$$

where $S_x(f)$ and $X(t)$ are the linear spectrum and actual time records, respectively. The spectrum is a complex function, it can be represented either by its real and imaginary parts or by its magnitude and phase. The records of two rectangular signals and corresponding linear spectra are shown in Fig. 2.18. This figure indicates that a short signal provides a broad linear spectrum, and vice versa. The linear spectrum provides both magnitude and absolute phase information for all frequencies within the bandwidth for which the measurement was taken. Since the absolute phase is measured, a trigger is required to synchronize the signal for averaging. Linear spectrum averaging is useful for determining predominant frequencies of dynamic system, or extracting a true signal out of background noise.

2.9.6 Auto Power Spectrum

The auto power spectrum $G_{xx}(f)$ is equal to linear spectrum $S_x(f)$ multiplied by its own complex conjugate $S_x^*(f)$.

$$G_{xx}^{*}(f) = S_x(f)S_x^{*}(f) \qquad [2.37]$$

The magnitude of the auto power spectrum is the magnitude squared of the linear spectrum. However, as the linear spectrum is multiplied by its complex conjugate, $S_X^*(f)$ is a real-valued function. The advantage of the auto power spectrum is that it provides information similar to that of the linear spectrum but does not require a trigger to synchronize the averaging of signals.

2.9.7 Cross Power Spectrum

The cross power spectrum is the Fourier transform of the cross-correlation function between two different signals *X(t)* and *Y(t)*. The cross power spectrum is defined by the following equation:

$$G_{yx} = S_y(f).S_x^{*}(f) \qquad [2.38]$$

where $S_Y(f)$ is the linear spectrum of the output and $S_X^*(f)$ is the complex conjugate of the linear spectrum of the input. The magnitude of $G_{YX}(f)$ is a measure of the mutual power between the two signals, making the cross spectrum an excellent means of identifying predominant frequencies that are present in both the input and output signals.

The phase of $G_{YX}(f)$ is the relative phase between the signals at each frequency in the measurement bandwidth. Since the phase is a relative phase, the cross-spectrum measurement can be made without a synchronizing trigger. The cross spectrum is used primarily to determine the phase relationships between two signals that may be caused by time delays, propagation delays, or varying wave paths between receivers.

2.9.8 Transfer Function

The transfer function H(f), is the ratio of the spectrum of the system's response (output) to the spectrum of the system's excitation (input).

$$H(f)=\frac{S_r(f)}{S_x(f)} \qquad [2.40]$$

Thus, the transfer function is similar to cross spectrum. Both provide the same phase information; the magnitude of the transfer function is normalized by the auto power spectrum of the input $G_{xx}(f)$ relative to the magnitude of the cross spectrum. Consequently, the transfer function of a given system should be constant regardless of the input (if the system does not undergo nonlinear behavior). The transfer function is frequently used to identify natural frequencies and damping coefficients of a dynamic system.

2.9.9 Coherence Function

The coherence function is a practical tool for judging the quality of the observed signals. The coherence function $\gamma^2(f)$ is a measurement made in conjunction with the transfer function. The coherence is a real-valued function that is the ratio of the response (output) power caused by measured input to the total measured response power. Mathematically, the coherence function, $\gamma^2(f)$, is defined as:

$$\gamma^2(f)=\frac{\left[G_{rx}(f).G^*_{rx}(f)\right]}{\left[G_{xx}(f).G_{rr}(f)\right]} \qquad [2.39]$$

The coherence function should be used on averaged signals. If the system is ideal, as shown in Fig. 2.19, the coherence will be equal to unity for all frequencies. However, due to the following reasons, the coherence function may be less than unity:

1-There are multiple input signals in the system that are not being measured.

2-Background noise is present in the measurement.

3-The frequency response function is nonlinear for the system.

4-There are closely spaced resonant peaks that cannot be detected with the given frequency resolution inherent in the digitization of the signal.

5-Waves in frequency range of poor coherence are not adequately excited.

Table 2..1 Parameters Affecting Shear Modulus and Damping for Complete Stress Reversal (Hardin and Drnevich, 1972)

Parameter	Importance to			
	Modulus		Damping	
	Clean sands	Cohesive soils	Clean sands	Cohesive soils
Strain Amplitude	V	V	V	V
Effective Mean Principals Stress	V	V	V	V
Void Ratio	V	V	V	V
Number of Cycles of Loading	R[b]	R	V	V
Degree of Saturation	R	V	L	U
Over consolidation Ratio	R	L	R	L
Effective Strength Envelope	L	L	L	L
Octahedral Shear Stress	L	L	L	L
Frequency of Loading (above 0.1 Hz)	R	R	R	L
Other Time Effects (Thixotropy)	R	L	R	L
Grain Characteristics, Size, Shape, Gradation, Mineralogy	R	R	R	R
Soil Structure	R	R	R	R
Volume Change Due to Shear Strain (for strain less than 0.5 %)	U	R	U	R

a) V means Very Important, L means Less Important, and R means Relatively Unimportant except as it may affect another parameter; U means relative importance is not clearly known at this time.

b) Except for saturated clean sand where the number of cycles of loading is a Less Important Parameter.

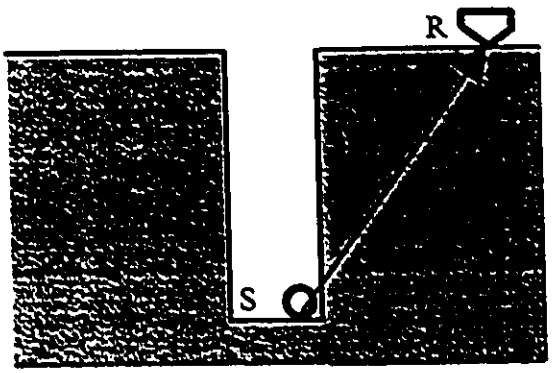

a-Up-Hole

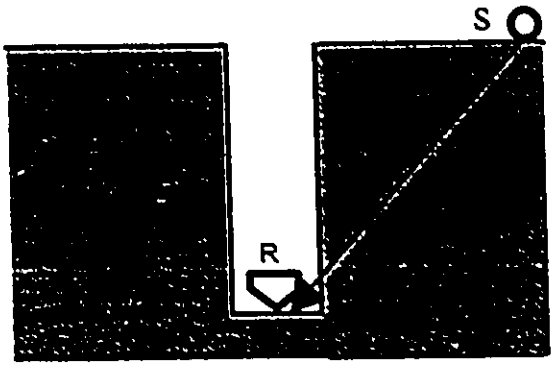

b-Down-Hole

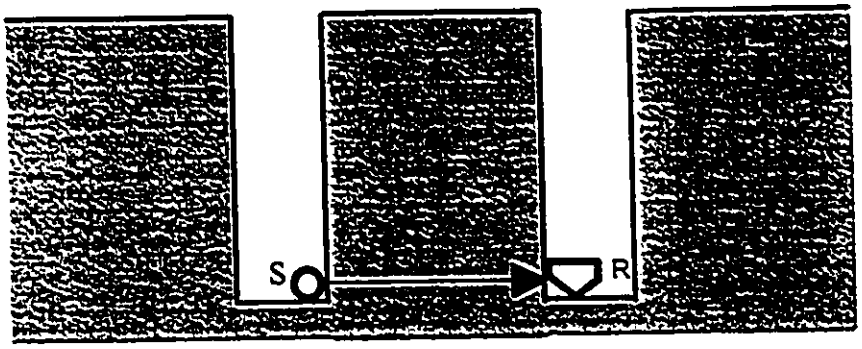

c-Cross-Hole

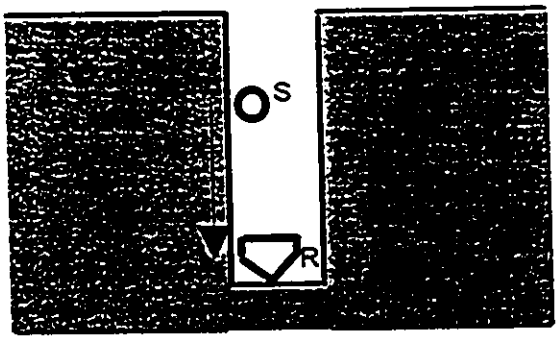

d-In-Hole

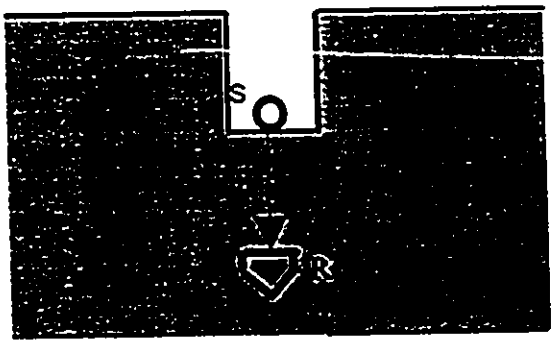

e-Bottom-Hole

R:Receiver
S:Source

Fig. 2.1-Schematic representation of borehole methods (After Hoar, 1982)

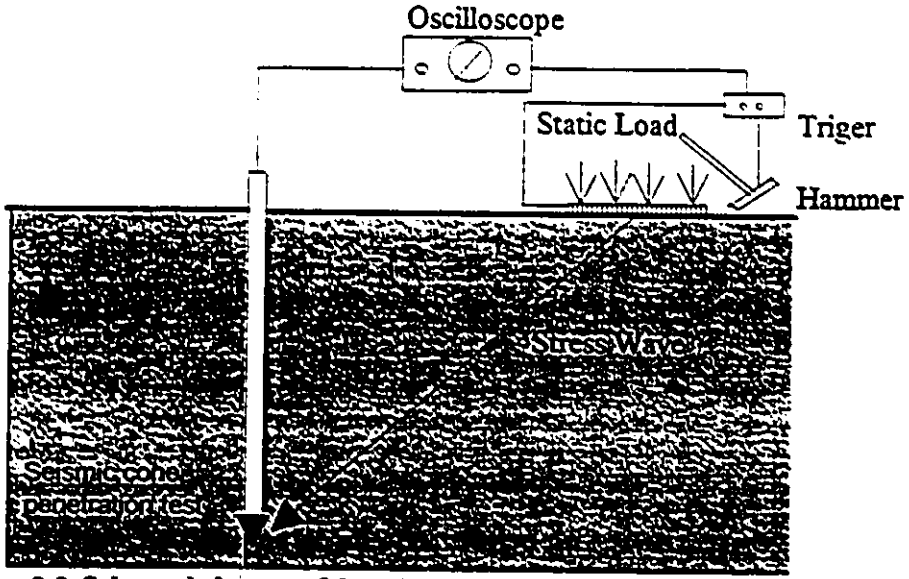

Fig. 2.2-Schematic layout of downhole seismic cone penetration test (After Robertson et al.1986).

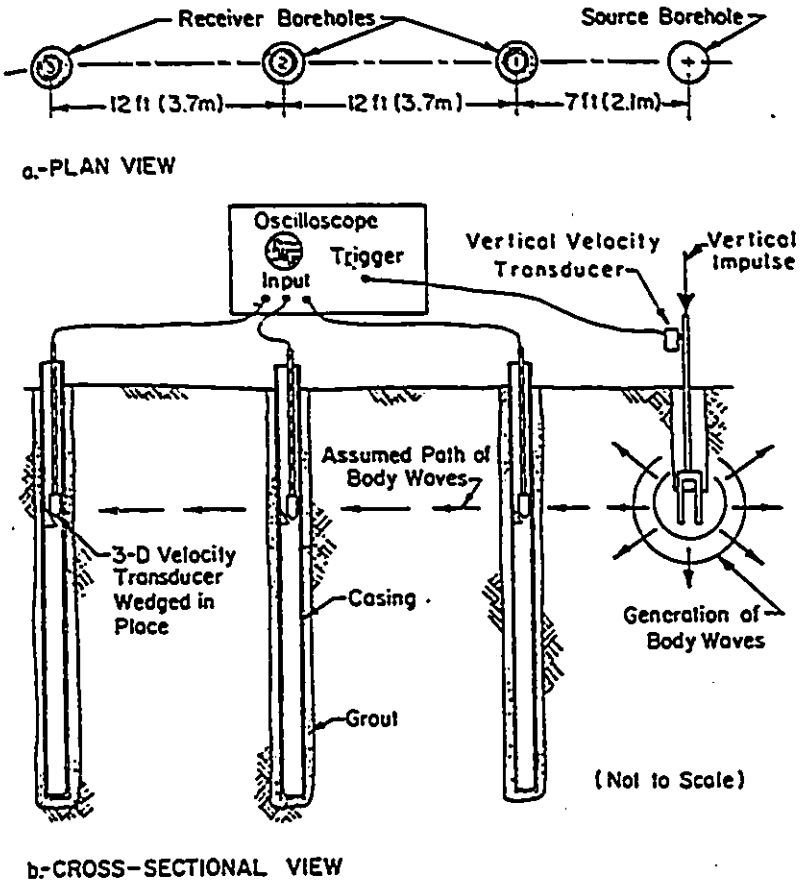

Fig. 2.3-Crosshole seismic method (After Stokoe and Hoar 1978).

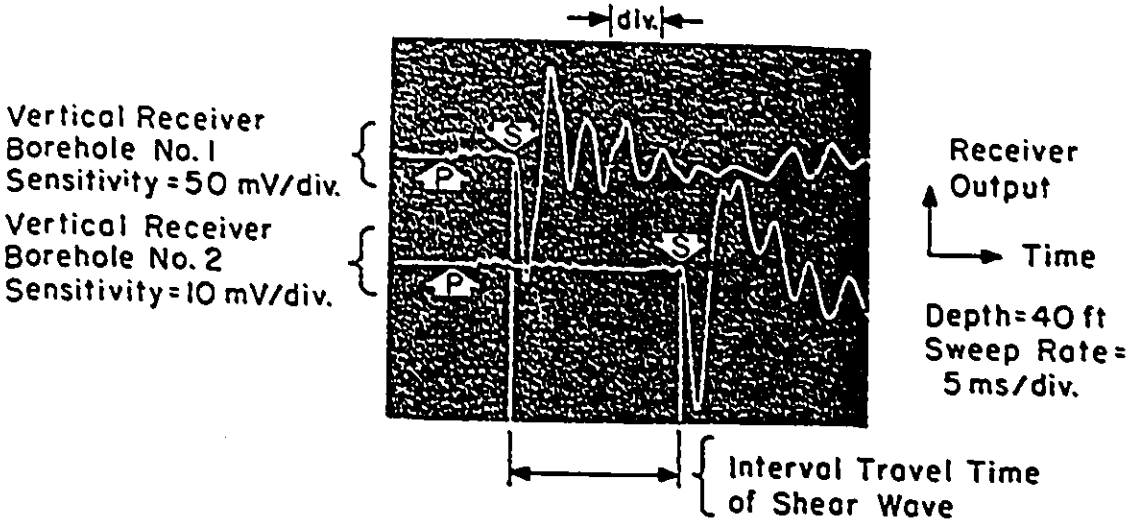

Fig. 2.4-Travel time record using three vertical receivers in the crosshole seismic test (After Stokoe and Hoar 1978).

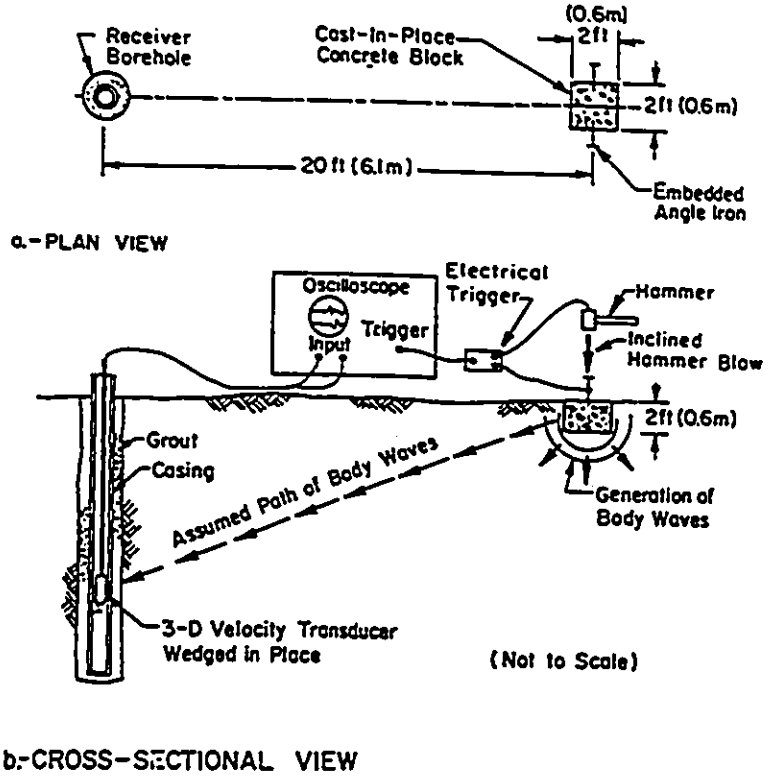

Fig. 2.5-Downhole seismic method (After Stokoe and Hoar 1978).

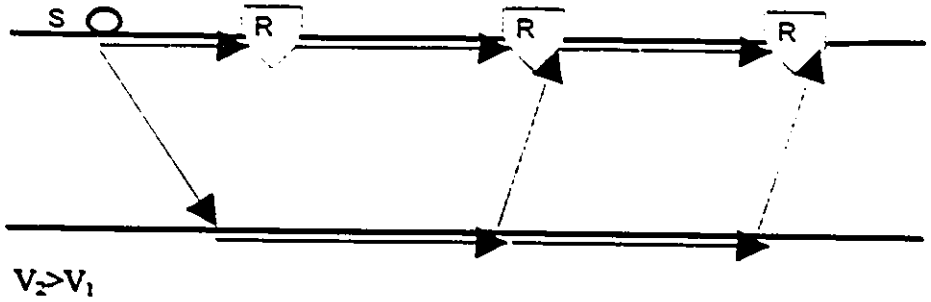

a-Surface Refraction

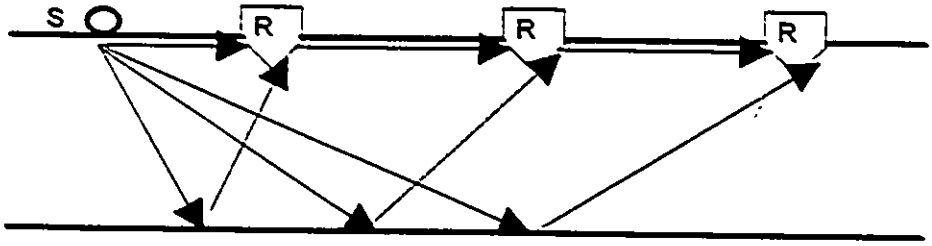

b-Surface Reflection

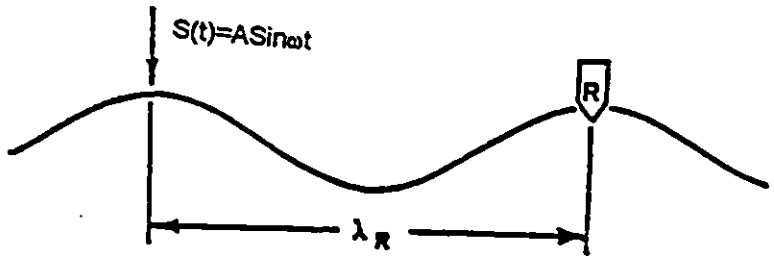

c-Steady-State Rayleigh Wave

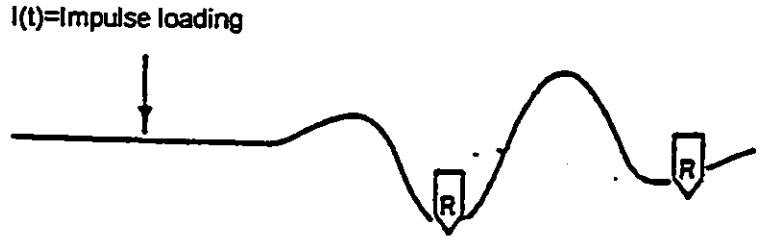

d-Rayleigh Wave Dispersion

Fig. 2.6-Schematic representation of surface seismic method (Nazarian, 1984)

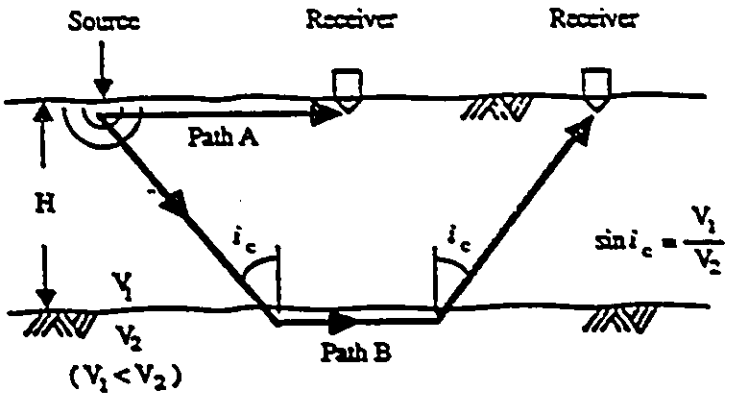

Fig. 2.7-Typical test configuration used in the seismic refraction method (After Richart et al. 1970).

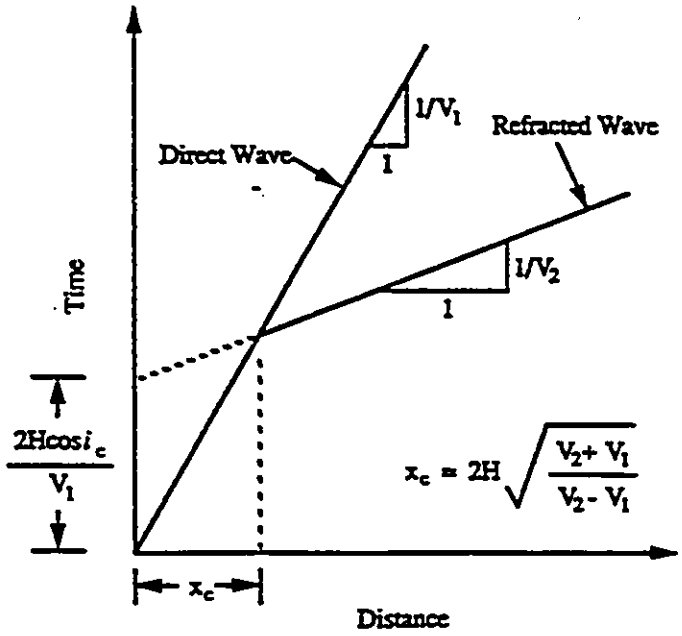

Note: Travel time is based on identifying the initial arrival of the wave type of interest (P or SH wave)

Fig. 2.8-Typical travel time plot from a seismic refraction test at a site composed of two layers (After Richart et al. 1970).

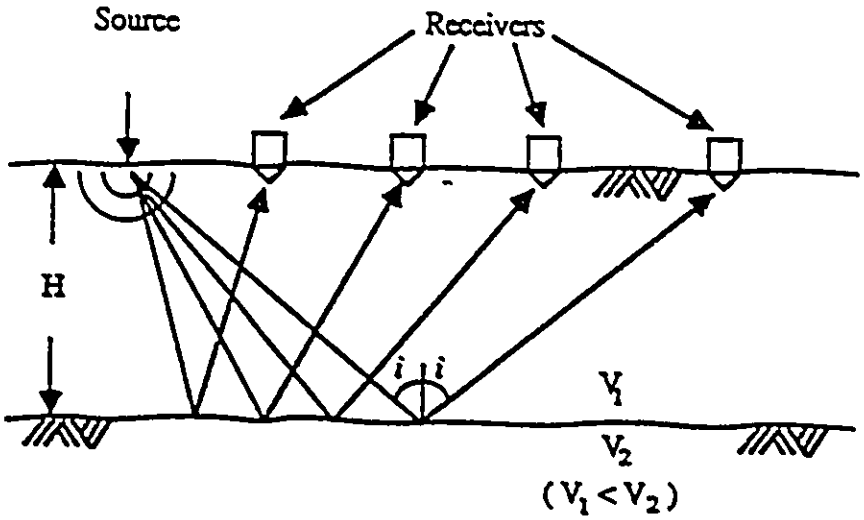

Fig. 2.9-Typical test configuration used in the seismic reflection method (After Richart et al. 1970).

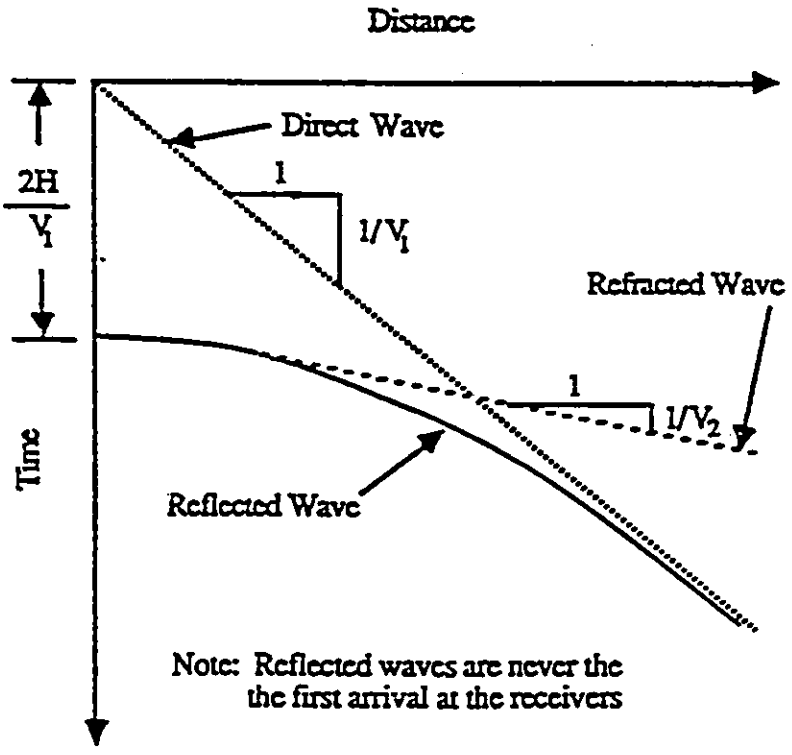

Fig. 2.10-Typical travel time plot from a seismic reflection test at a site composed of two layers (After Richart et al. 1970).

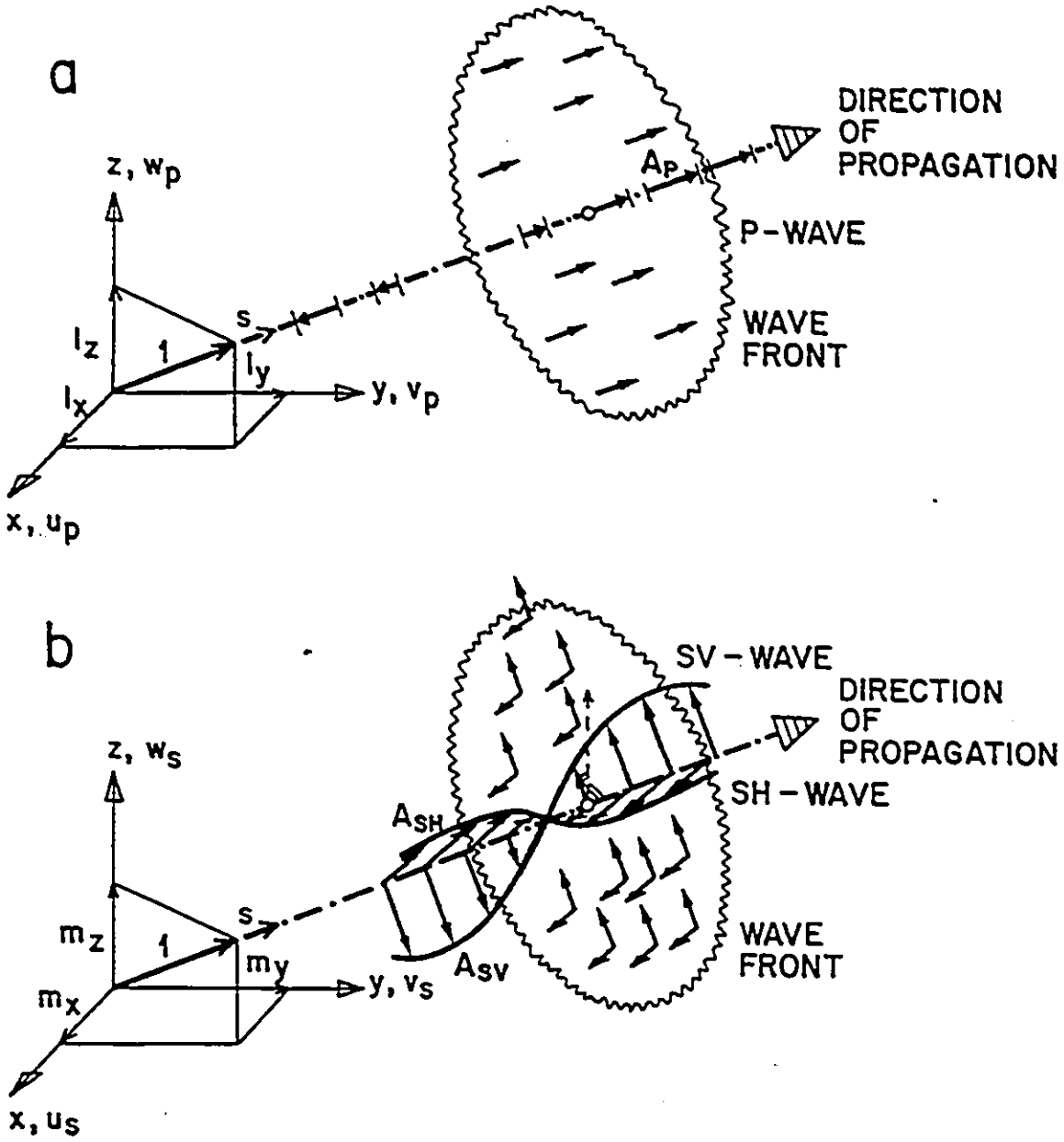

Fig. 2.11-Displacements associated with body waves.(a) P-wave; (b) S-wave (After Wolf, 1985).

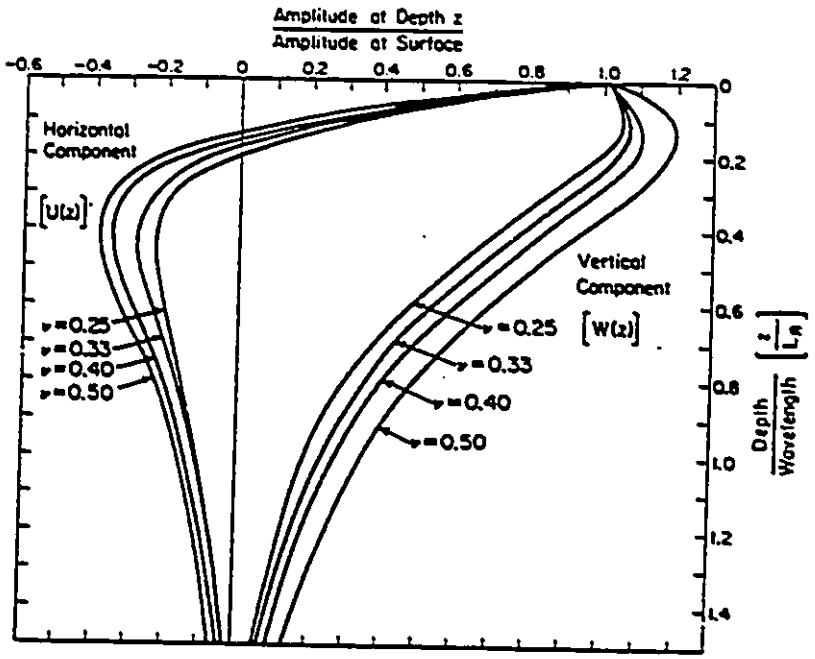

Fig. 2.12a-Amplitude ratio vs. dimensionless depth for Rayleigh wave (After Richart et al. 1970).

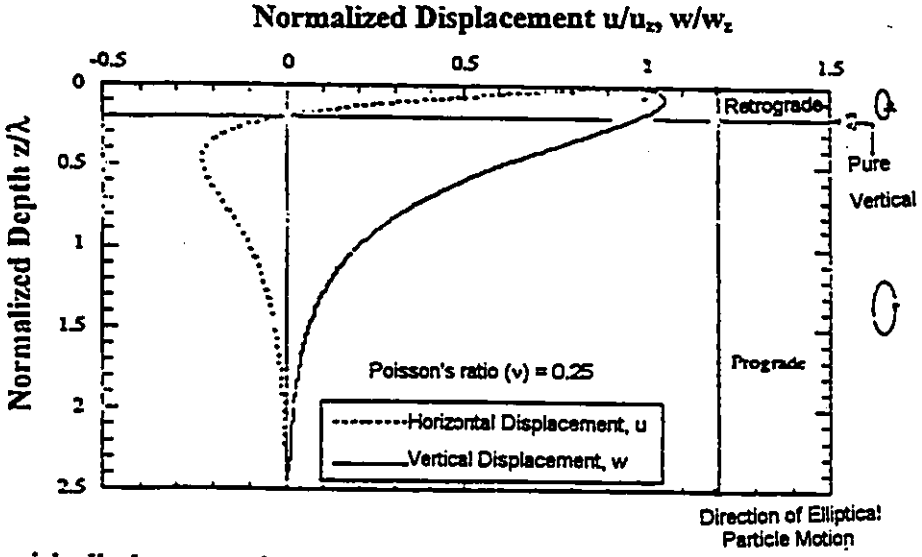

Fig. 2.12b-Particle displacements in a Rayleigh wavefield (After Richart et al. 1970).

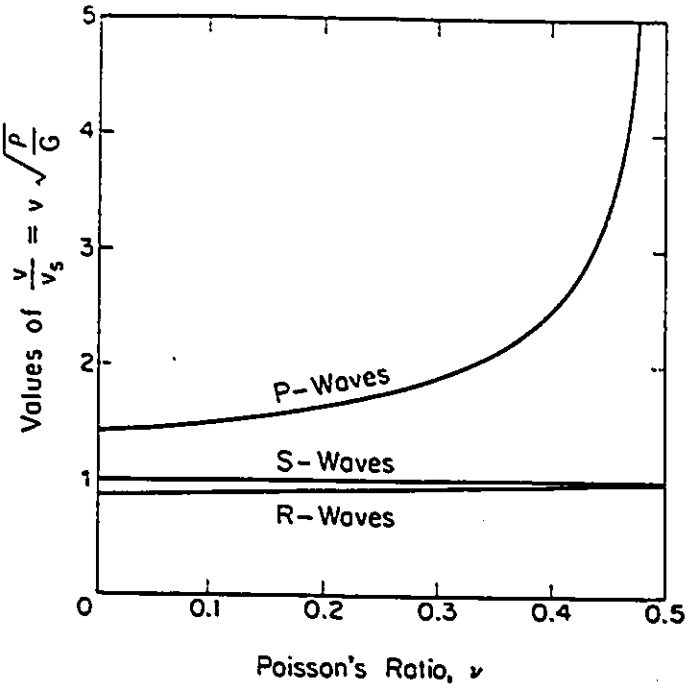

Fig. 2.13-Relation between Poisson's ratio, ν, and velocities of propagation of compression (P), and Rayleigh waves in a semi-infinite elastic medium (from Richart et al. 1970).

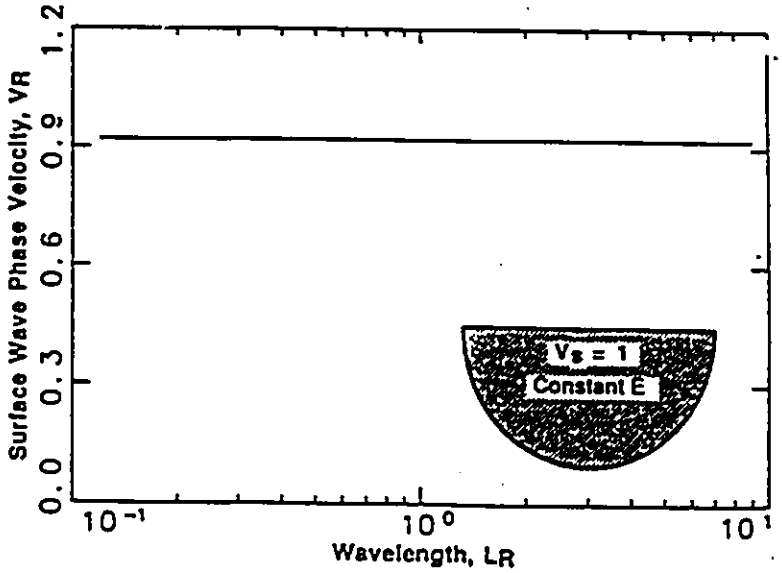

Fig. 2.14-Dispersion Curve for plane Rayleigh waves propagating in a uniform Half-Space (from Rosset et al. 1990).

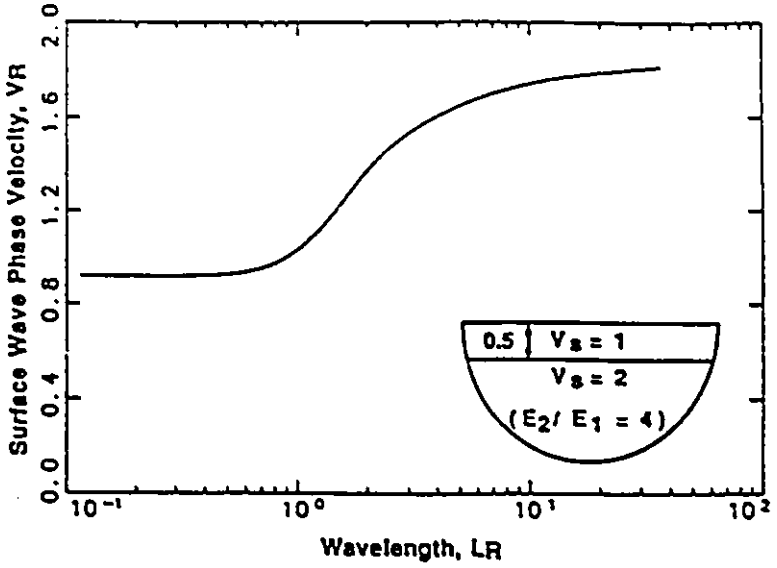

Fig. 2.15-Dispersion Curve for plane Rayleigh waves propagating in a soft layer over a stiff Half-Space (from Roesset et al. 1990).

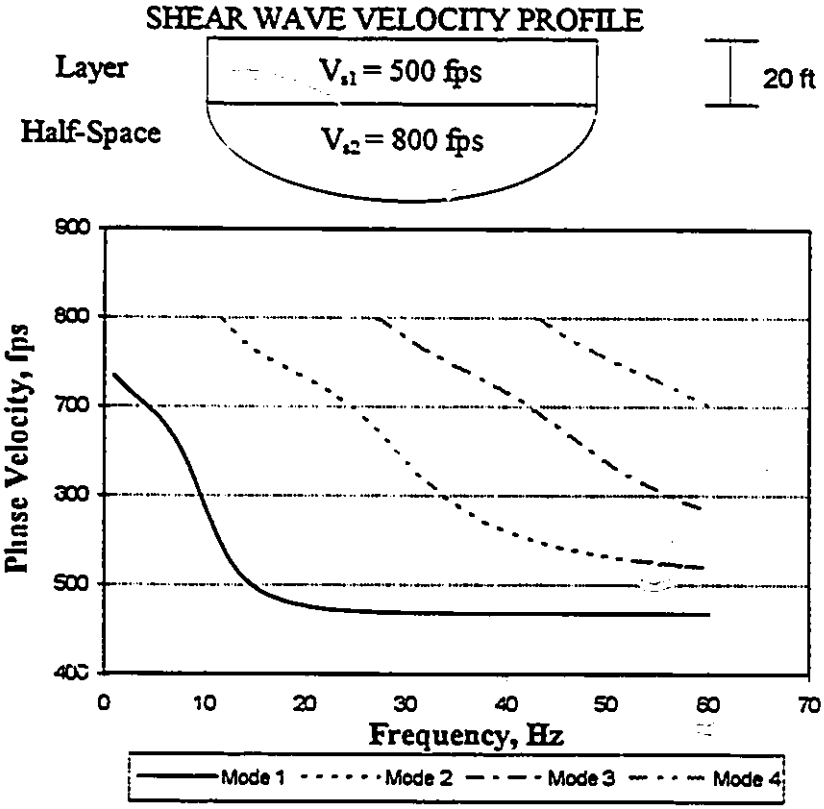

Fig. 2.16-Rayleigh wave dispersion for a layer over a half-space system, n=0.35 (After Gucunski, 1991).

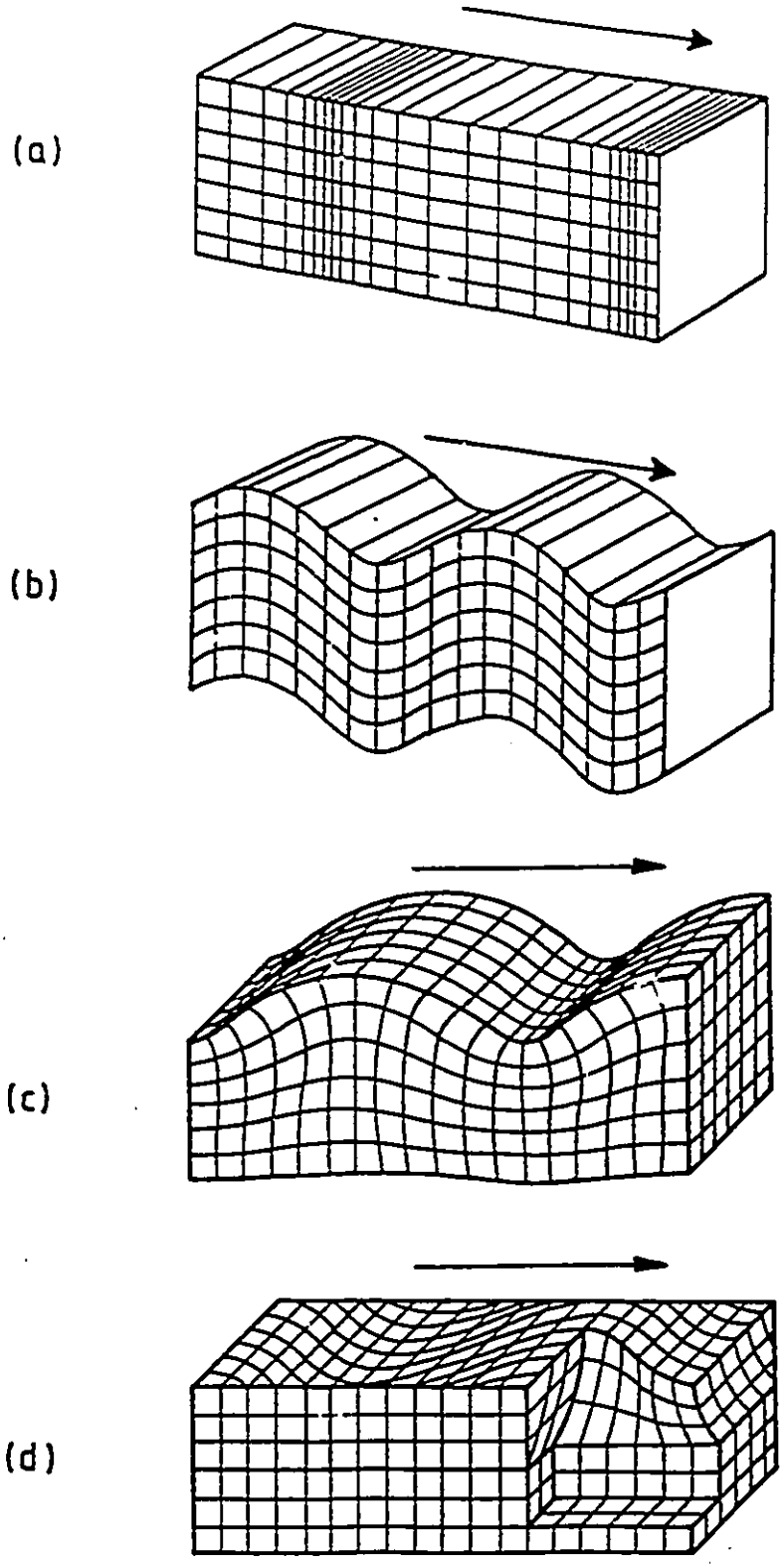

Fig. 2.17-Types of waves in layered soil systems (from Bolt, 1967).

Body waves: (a) compressional wave, (b) shear wave

Surface waves: (c) Rayleigh wave, (d) Love wave.

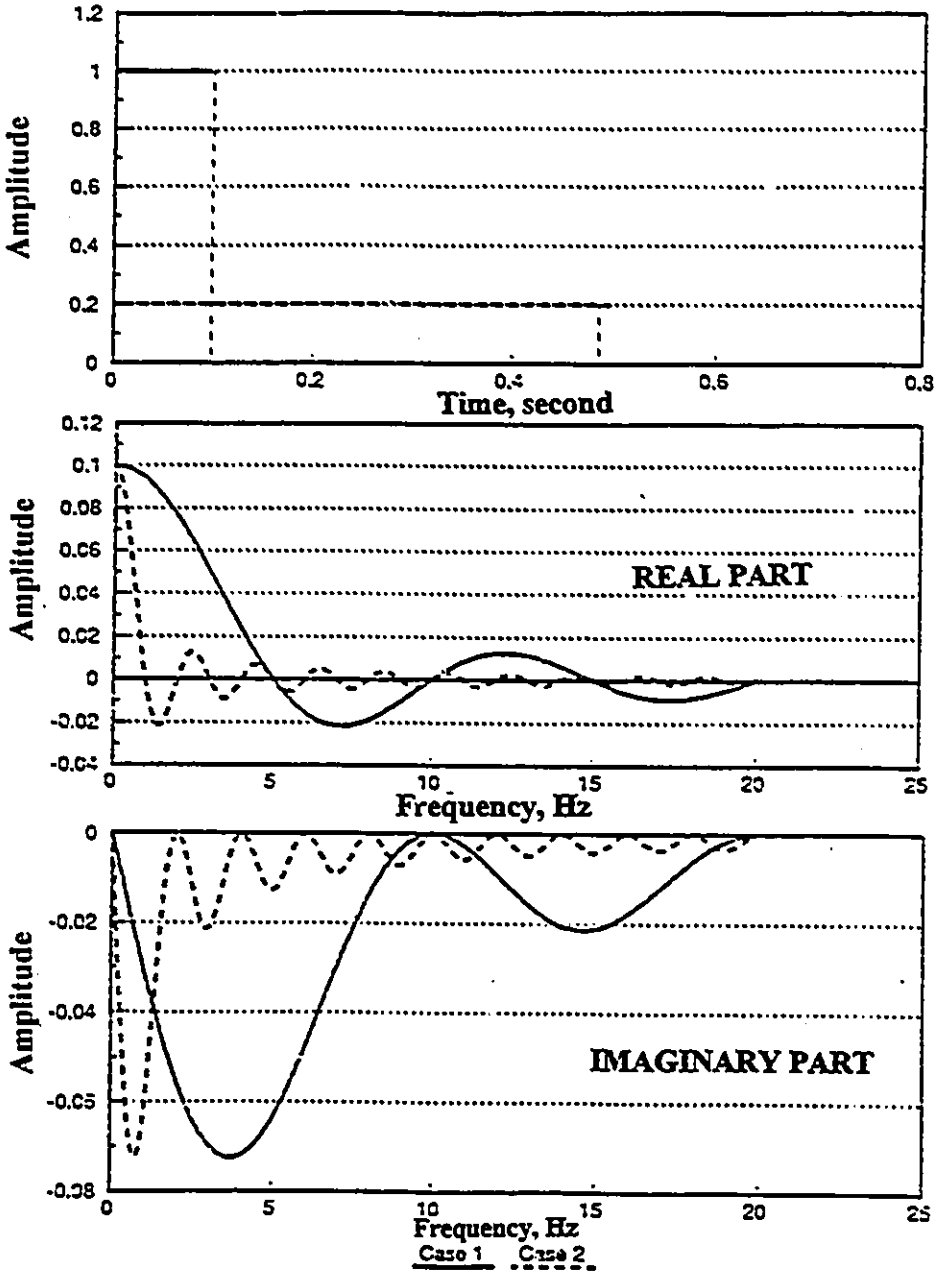

Fig. 2.18-Rectangular time signals and corresponding linear spectra (Gucunski, 1991).

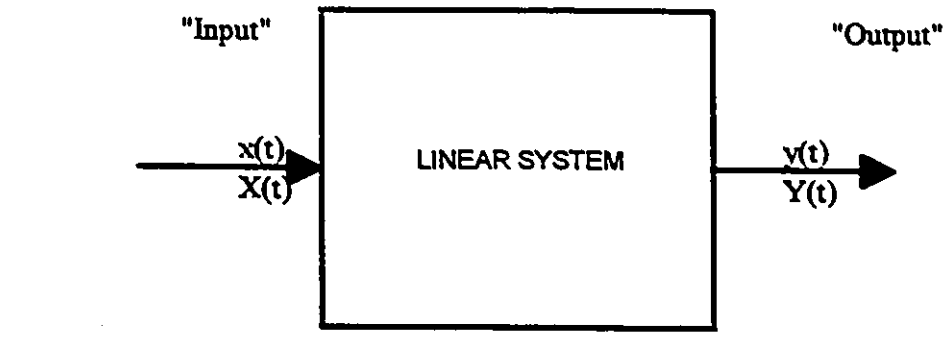

a) Idealized System

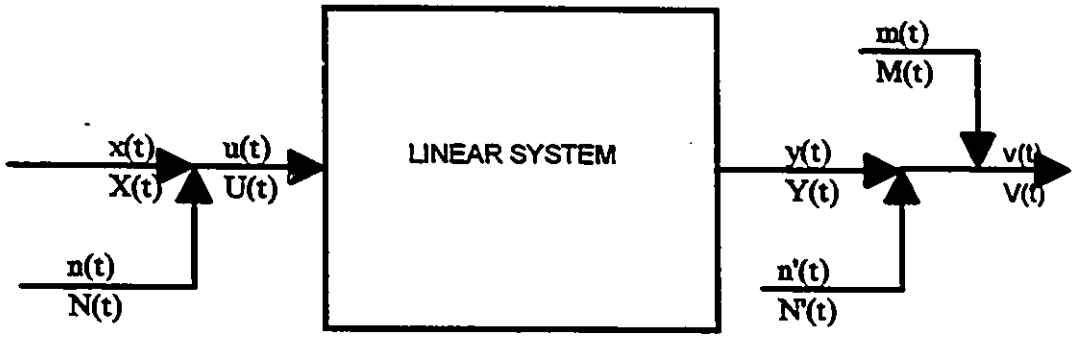

b) Actual System

Note:

x(t) = Input due to Experiment,
y(t) = Output due to Experiment,
n(t) = Noise Source at Input,
n'(t) = Output due to Noise at Input,
m(t) = Noise Source at Output.

Fig. 2-19-Illustration of idealized and actual linear systems (Nazarian, 1984).

CHAPTER 3

THE SPECTRAL ANALYSIS OF SURFACE WAVES METHOD

3.1 Introduction

The spectral analysis of surface waves (SASW) method is a seismic method for measuring in situ elastic moduli of layered systems, like soils and pavements. The method is a modification of the steady state Rayleigh wave method which is discussed in the following paragraph.

Steady-state surface wave method is one of the nondestructive seismic surface methods. This method is used to determine the thicknesses and corresponding shear wave velocities of the layers of a soil or pavement system by determining the in-situ Rayleigh wave dispersion curve. In the original steady-state Rayleigh wave method, a steady-state vibrator acting vertically on the surface of the soil or pavement generated vibrations of a known frequency that propagated along the surface (Jones, 1962 and Ballard, 1964).

The generated vibrations are detected by a receiver (accelerometer or geophone) with vertical motion sensitivity located at the surface of the half-space. The receiver is moved progressively away from the vibrator and successive positions are found at which the vertical surface motions are in phase with the vibrator (Richart et al. 1970). The distance between any two in-phase points is equivalent to one wavelength (λ) of the Rayleigh wave (Fig. 3.1). Since the frequency (f) of vibration is known, the velocity of the wave propagating at that frequency is calculated using:

$$V_{ph} = \lambda f \qquad [3.1]$$

A plot of surface wave phase velocity versus frequency or wavelength is obtained by repeating this process for different excitation frequencies. This plot is called "dispersion curve". The effective depth of a sampling is assumed to be 1/2 to 1/3 of the wavelength, and shear wave velocity is assumed in the range of 1.0 to 1.10 times the phase velocity. These assumptions are empirical and have no rigorous theoretical background. Therefore, the analysis based on the above assumption cannot provide reliable shear wave profile in all cases.

The major advantage of the steady-state technique is its analytical simplicity because the shear wave velocity profile is obtained directly from the field dispersion curve. It also has low initial cost and requires neither time measurement nor signal analysis. It is, however, time consuming and impractical for investigating relatively deep-seated deposits with monochromatic signals since receiver spacing becomes inconveniently large. The weakness of the method also lies in its neglect of the dispersive characteristic of surface waves in the inversion process. With the development of digital electronic equipment in the 1970s, this shortcoming has been overcome.

The advances and modification of the steady-state surface wave method resulted in a new nondestructive technique known as spectral analysis of surface waves (SASW) (Hesiey et al. 1982; Stokoe and Nazarian 1983). Rather than using a harmonic source, the SASW method employs an impact source and results are obtained using FFT analyses.

The complete testing procedure for investigating a site with the SASW method can be divided into three parts:

1-collection of data in the field,

2-determination of dispersion curve (a plot of phase velocity versus wavelength or frequency) and,

3-inversion of dispersion curve to obtain the shear wave velocity profile.

Details of these three parts are discussed in this chapter.

3.2 Field Equipment and Procedure

A schematic of the testing setup of SASW method is presented in Fig. 3.2. Surface waves are generated by an impact source at distance S from the near receiver, and are then detected by a pair of receivers, and recorded on an appropriate recording device. In the following sections source type, receiver and recording device, and effect of configuration setup such as source-to-near-receiver spacing, receiver-to-receiver spacing, and source-receiver geometry are discussed.

3.2.1 Source Type

The ideal impact source for SASW testing should be able to generate dominantly Rayleigh waves over a wide range of frequencies with adequate amplitude so that they can be detected by the receivers. The choice of source depends on the frequency range of interest which varies with material properties and receiver spacing. The frequencies of interest for testing typical soil deposits are 2 to 80 Hz, and for a flexible pavement up to 6 kHz. For a rigid pavement, the upper boundary is about 10 to 20 kHz (Nazarian 1984).

Small, lightweight sources produce high frequencies necessary for sampling shallow depths, and therefore are used with short receiver spacing. While larger, heavier sources produce low frequencies for sampling greater depths and hence are used with large receiver spacing. To generate waves at low frequencies (in the order of 2 to 5 Hz) a source which can generate an impulse with long duration is required. Based on his experiments, Nazarian (1984) estimated that a period of 100 msec or more is required. In order to increase the duration of the impact, it can be applied on a soft surface, such as a rubber pad.

The weight of the source has a dramatic influence on the dispersion curves obtained. Hiltunen and Woods (1990) reported that both the upper and lower cutoff frequencies decreased as the weight of the source increased.

Depending on the receiver spacings, several types of sources are used in SASW (Stokoe et al. 1988). At close receiver spacing, small, hand-held hammers are used. At 2.5 to 5 m spacing, sledge hammers or large drop weights, weighing from 220 to 440 N, are employed. For receiver spacing greater than 5 m, a variety of sources have been used including drop weights ranging from 670 to 8900 N, bulldozers, and a very large weight used for dynamic compaction (290 kN).

For generating low frequencies, the large dynamic compaction weight is used permitting wavelengths as long as 150 m to be measured at soil sites. Bulldozers have proven to be a valuable source of surface wave for those situations in which impact sources such as drop weights were not able to generate sufficient energy over wide range of frequencies or where these sources were not available.

Hiltuunen and Woods (1990) reported that single source types failed to consistently duplicate the optimum results at all frequencies.

3.2.2 Receivers

In the SASW method, the generated surface waves are detected by vertically oriented receivers. Acceleration transducers (accelerometers) and velocity transducers (geophones) are two convenient types of receivers which are used. The useful frequency range, sensitivity, and coupling between the receivers and the surface are the most important parameters which influence the selection and performance of receivers.

A schematic sketch of an accelerometer construction is shown in Fig. 3.3a. The piezoelectricity phenomenon is used in design of accelerometers. A piezoelectric material

is one that generates an electric output when subjected to mechanical shock or vibration, i.e. deformation.

The ratio of the accelerometer›s electrical output to the mechanical input is defined as the sensitivity of the accelerometer. Accelerometers are used over a wide range of frequencies (up to 20 kHz). They have high natural frequencies and perform well in this range. Also they are much smaller than geophones making them more appropriate for measurements at close spacings. Nazarian (1984), based on his experiments, suggested that accelerometers were more suitable to reduce the effect of environmental noise.

Velocity transducers or geophones are instruments which generate an electrical output proportional to the magnitude of motion of the surface onto which they are mounted and are electromagnetic in nature. The electromagnetic geophone operates on the principal of voltage generation due to relative motion between the coil and magnet. Fig. 3.3b shows a schematic sketch of a geophone. The ratio of the electrical output of geophone to the mechanical input is defined as transductivity which depends on the strength of the magnetic field, the number of turns in the coil and the relative velocity of the coil with respect to the magnet. The motion of the coil is attenuated with time due to damping of the system.

The useful frequency range of velocity transducers is between 1 to 1000 Hz. Since the output of an accelerometer is generally lower than the output of a geophone at low frequencies, velocity transducers are used in testing of soils. For testing pavements either geophones or combination of accelerometers and geophones are employed.

3.2.3 Receiver Coupling

Good coupling between the receivers and test surface is necessary to ensure that their movement is identical. They should be capable of faithfully transmitting to the transducer the actual motion of the ground over the frequency range of interest. Improper coupling

often causes errors resulting in the measurement of distorted signal amplitudes. In the case of soil testing, velocity transducers are generally coupled by using spikes (in firm soil) or by partially burying (in loose soil). In testing of pavements, both velocity transducers and accelerometers can be successfully attached by using epoxy and cyanoacrelate cements.

3.2.4 Recording Devices

The signals detected by the receivers are transmitted by cables to a recording device and are stored for future analysis. The spectral analyzer is a common recording device for performing SASW test. It is a digital oscilloscope that, by means of a microprocessor, is able to perform signal analysis directly in either time or frequency domain. It also yields various functions of the signals such as linear spectra, transfer function, cross power spectra and coherence function. For the calculation of the dispersion curve, the phase spectrum of the transfer function or the cross power spectrum is required. The coherence function is also required for judging the quality of the signal, which may be enhanced by frequency domain averaging of several repetitions of the same test.

Nazarian and Stokoe, (1985) estimated that an averaging of five signals is considered to be adequate. Data in frequency domain is then transferred to a microcomputer for calculating the dispersion curve.

3.2.5 Source-Receiver Configuration

Two possible arrangements of source and receiver are used in SASW tests. These are the common receiver mid point (CRMP), and common source configuration (CS). In the CRMP set-up (Fig. 3.4a), two receivers are placed equidistant on both sides of an imaginary centerline. The source is placed in line with the receivers and the distance to the near receiver S, is equal to the receiver spacing. In the CS set-up (Fig. 3.4b), the

location of the source and one receiver remains unchanged during the test, while the second receiver is moved further away from the other receiver for a new test. The CS configuration takes less work in field, since only one receiver has to be coupled for additional spacing.

Nazarian and Stokoe (1983) performed a series of tests using two source and receiver configurations. The dispersion curves obtained from two configurations are shown in Figs.3.5 and 3.6. It is observed that the scattering in curve obtained using the CRMP set-up is much less than that obtained from the CS set-up. This is attributed to the fact that lateral inhomogenity of testing material is influenced more by the CS than CRMP set-up. Since the materials in pavements are usually placed under more controlled conditions than natural soil, and the lateral extent of the test array is short, it might be reasonable to expect that the effect of source and receiver configuration is less for pavements than for soil.

In CRMP set-up, by fixing the receiver locations and by averaging the records from forward and reversed tests, the effect of any internal phase shift between the two geophones can be eliminated. In addition, it helps to detect dipping or inhomogenity in the layer.

The CRMP and CS configurations are normally performed using a dual channel analyzer. This means that data collection might be time-consuming, since several receiver spacings are usually required to fully investigate a site. By using multiple-channel spectrum analyzers all the data for a given site can be obtained with least number of sources. Hiltunen and Woods (1990) report that the CS configuration is the preferred configuration for multiple-receiver array testing since it has the practical advantage of a fixed source location.

Ideally, it should be possible to use a single receiver spacing to perform an entire test. However, factors such as the attenuation of particle motion with horizontal propagation

distance dictate that the test is performed for several different receiver spacings. Then the data is combined.

3.2.6 Reversing of the Source

Reversing of the source is a process that a test is performed from two opposites of receiver array as shown in Fig. 3.7. In this process first the SASW test is performed from one side that is called forward. Then without changing receivers from their original position, the source is moved to opposite side of the array. The test performed with new configuration is called reverse. In the reverse process test, the near receiver is the far receiver of the forward test and vise versa. Reversing of the source has an advantage that any dipping in a layer can be detected by comparing the relative phase angle spectra from forward and reverse.

Generally the SASW test is performed for both configurations and then the results are averaged. By this process the effects of any internal phase shifts associated with receivers or recording device are minimized or eliminated.

3.2.7 Source-to-near-Receiver Spacing

The distance between the source and near receiver S should be far enough to ensure that Rayleigh waves are fully established and the amplitudes of body waves are sufficiently attenuated before arriving at the first receiver. However, if the source is too far away from the receivers, the Rayleigh wave energy associated with the frequencies of interest may not be sufficient for detection by the receivers, and background noise may dominate the record.

Based on theoretical studies, Lysmer (1968) indicated that, at a distance of two and a half wavelength from the source, surface wave forms are virtually fully established.

Heisey et al. (1982) have recommended that the receiver spacing (D) should be equal to the source-to-near-receiver spacing (S). They also recommended that wavelengths smaller the 0.5 D or larger the 3 D be eliminated from the data. Nazarian (1984) has pointed out that since velocities of layers are initially unknown, the above criterion cannot be applied before testing.

However, theoretical studies performed by Sanchez-Salinero et al. (1987) have indicated criteria that are different from those suggested by Heisey (1982). They report for a typical SASW setup in which D = S, waves with wavelength larger than one-half the distance between receivers (D) carry a substantial amount of body wave energy. Therefore it is recommended that field data be filtered so that the value of D/λ_{ph} is kept greater than 2. This was also supported by experimental studies on pavements by Sheu et al. (1988).

3.2.8 Receiver-to-Receiver Spacing

On the basis of experimental studies, Heisey (1982), concluded that factors which affect appropriate receiver spacing are the velocity of the material, sampling depth, frequency range, the attenuation properties of the medium and sensitivity of instrumentation. Heisey et al. (1982) suggested that the distance between receiver (D) should be less than two times the desired wavelengths and greater than one-third of the desired wavelength. This relation can be summarized as

$$\frac{\lambda_{ph}}{3} < D < 2\lambda_{ph} \qquad [3.2a]$$

or

$$0.5D < \lambda_{ph} < 3D \qquad [3.2b]$$

In order to cover the wavelength range required to sample the various layers of a site, SASW tests need to be performed with several receiver spacings (D). Distances between receivers of 7.5 cm to 200 cm are typically employed for near-surface profiling of pavement sites.

The maximum receiver spacing can be determined by estimating the longest wavelength that is required to evaluate the shear wave velocity profile. For instance, if a profile to a depth of 10 m is desired, a maximum wavelength from 2 to 3 times of this depth should be measured.

Since high frequencies attenuate with distance faster than low frequencies, and therefore, might be dominated by background noise, applying the above criterion ensures that short wavelengths (λ_{ph}<0.5D) picked up by the receivers are eliminated. Also the above criterion with the condition S≈D seem to ensure that long Rayleigh wavelengths (λ_{ph}>3D) are eliminated.

Since surface waves might not be fully developed when they arrive at the near receiver and also are contaminated by body waves, Sanchez-Slinro et al. (1987), based on theoretical studies, suggest that only wavelengths less than 0.5 D should be included in the analyses to ensure the condition that body waves are insignificant and Rayleigh waves are developed.

Hiltunen and Woods (1990), based on their experimental studies, concluded that the S/D ratio should be ≤ 2 and recommended that CS configuration with S/D=1 be used for a multiple-transducer array. They also found that the measured phase velocities are practically independent of S/D for wavelengths larger than 1.5 m (5 ft) and for all values of D/λ_{ph}. Secondly, the measured phase velocities are significantly dependent on S/D for small values of D/λ_{ph} for wavelengths less than 1.5 m (5 ft). Thirdly, the measured phase velocities are practically independent of S/D for values of D/λ_{ph} of 0.5 or greater, for all wavelengths.

Roesset et al. (1990) report that the best result should be expected if S/D ratio is of the order of 1 to 2. Also values of S/λ_{ph} between 0.5 and 2 generally produce results that are very close to those of the plane Rayleigh waves.

Gucunski and Woods (1992) examined several filtering criteria and suggested a new criteria:

$$\lambda_{ph} < D < 4\lambda_{ph} \qquad [3.3]$$

They have shown that applying the filtering criteria given by Eq. 3.3 significantly reduces the errors in the field dispersion curve for irregular soil systems. Implementation of the above filtering would lead to a profile which is approximately three times shallower than the profile that would be obtained by Heisey's criterion. Therefore this increases the need for a powerful impact source even more whenever deep soil measurements are to be performed.

3.2.9 Signal Quality

As signals propagate from the source to the receivers, they decay and are mixed by signals from other sources in the vicinity of the test location. These undesirable signals are called noise.

Fig. 3.8 shows typical time histories, denoted $y_1(t)$ and $y_2(t)$ for receivers 1 and 2, respectively. Acceptable signals usually are very similar to those in Fig. 3.8. These signals are characterized by an initial quiet period followed by the arrival of the impulse after which the ground surface return to its at rest position. The operator after viewing them on the display of a dynamic signal analyzer may choose or reject these time signals. Possible reasons for rejecting signals include the presence of extraneous noise, a double hit, etc.

Noises may be categorized into two groups: coherent noise and incoherent noise. Coherent noise is characterized by a fairly narrow bandwidth. Incoherent noise is

composed of unpredictable signals of random amplitude and onset. The incoherent noise is believed to be due to winds, sea waves and unintentional man-made disturbances.

Incoherent noise is generally minimized by adequate signal averaging. In the SASW test, to enhance signal quality, i.e., increased signal to noise ratio, the results from five signals are averaged (Nazarian and Stokoe 1983). One way of indirectly determining the quality of signal at a particular frequency is to determine the coherence function between the source and measured signals at that frequency (see Section 2.3.9). If coherence is low, more averages improves the situation.

The effect of coherent noise can only be minimized or eliminated by ignoring the frequencies common to the signal and the noise.

3.3 Construction of the Field Rayleigh Wave Dispersion Curve

In a perfectly elastic, homogeneous, isotropic, half-space, surface wave velocity is independent of the frequency. However, these assumptions are not valid for soil profiles, which typically exhibit variations with depth. Therefore, surface wave velocity vary with the wave frequency. This variation of wave velocity with frequency (or wavelength) is known as dispersion, and a plot of velocity versus wavelength is called a dispersion curve.

The dispersion curve is developed from phase information of the cross power spectrum. This information is used to obtain the relative phase shift between two signals at each frequency. The phase shift results from the waves sensed at the near receiver having to travel an additional distance D to be sensed at the far receiver. This phase shift can be translated into travel time as explained in the following section .

For a travel time equal to the period of the wave (T), the phase difference is 360 degrees.

Therefore for each frequency the travel time between receivers can be expressed by

$$t = \frac{\phi(f)T}{360} = \frac{\phi(f)}{360f} \qquad [3.4]$$

where

f = frequency,

t = travel time of the wave at the given frequency, and

ϕ(f) = phase shift in degrees for the frequency.

Because the travel distance is represented by the receiver spacing D, the Rayleigh wave velocity V_{ph} is simply calculated by

$$V_{ph}(f) = \frac{D}{t(f)} \qquad [3.5]$$

and the corresponding wavelength can be determined by

$$\lambda_{ph} = \frac{V_{ph}}{f} = \frac{360D}{\phi} \qquad [3.6]$$

By repeating the above procedure for every frequency, the Rayleigh wave velocity corresponding to each wave length is evaluated and the dispersion curve is determined.

The dispersion curve generated according to equations [3.5] and [3.6] are filtered by applying the suggested criterion discussed in this chapter. The filtered dispersion curves for all receiver spacings and both, the forward and reverse, directions are finally statistically combined to obtain an average dispersion curve.

Generally, a spectral analyzer displays the phase of the cross spectrum in the range of ± 180 (wrapped or folded) and needs to be transformed to a continuous format. This process is known as unfolding or unwrapping and is performed by adding the correct number of 360° cycles as shown in Fig. 3.9b. For example, consider the point marked as A in Fig. 3.9a in the raw phase spectrum, the phase is read as 100° whereas the actual unwrapped phase is 980°.

The coherence function provides a guide for choosing which points of the phase of spectrum should be used in determining surface wave phase velocities. In an ideal system the coherence function will be equal to unity but for the reasons described in Chapter 2 (section 2.3.9), this value is normally less than unity. The low coherence ranges that are discarded from the construction of dispersion curve are marked as shaded region in Fig. 3.9c. Nazarian and Stokoe (1986) have recommended that only frequency ranges for which coherence is greater than 0.90 should be accepted in construction of field dispersion curves while, Sayyedsadr and Drnevich (1989) used a default value of 0.98 as the minimum acceptable data. Nazarian and Stokoe (1986) and Sheu et al. (1987) recommended that the data points having a phase of less than 120° be eliminated from calculation (Heisey's criterion).

On the basis of experimental studies Al-Hunaidi (1992) found that using the usual manner for unwrapping phase angles (Nazarian and Stokoe 1986) can sometimes lead to unrepresentative dispersion curves of the tested site. He reports that under some conditions spurious cycles may exist in the relative phase spectrum which can be mistakenly counted as true ones, and proposed a correction procedure.

The criteria for source to near receiver distance and wavelength are applied to ensure that only one surface mode is predominant. Therefore if more than one surface mode or other wave types are propagated, phase angles will then represent some average corresponding to all participating surface modes (Douglas et al. 1989). Therefore, such phase angle will not be suitable as angles for use in the SASW.

The construction of dispersion curve is time-consuming and sometimes requires personal judgment. Nazarian and Desai (1993) developed an automated method for construction of field dispersion curve. At each receiver spacing, knowing the phase angle, phase velocity and wavelength associated with a particular frequency are calculated. By using the least absolute value best-fit criterion, these raw data are combined to construct the dispersion curve.

Generally, unrepresentative experimental dispersion curves due to erroneous phase unwrapping and incorrect assumption of single surface mode lead to erroneous back calculation (inversion).

In summary, the process of the construction of field dispersion curve can be summarized in the following steps:

1-Find the unwrapped phase angle by adding the correct number of 360° cycles to the phase angles of cross power function.

2-Discard the phase data which fall within a low coherence range.

3-At each frequency that is not eliminated, calculate phase velocities and wavelengths using Eq. 3.4 through 3.6.

4-Combine dispersion curves constructed from different spacings to generate the final dispersion curve.

The shape of dispersion curve depends on the variation of soil properties with depth. The particle motion at a given frequency and wavelength is restricted to a soil depth of the same order of the wavelength. Also the velocity of propagation of the surface waves depend almost exclusively on the soil properties over that depth.

3.4 Inversion of the Rayleigh Wave Dispersion Curve

Inversion of the Rayleigh wave dispersion curve is a process of obtaining the actual propagation velocities at different depths from the dispersion curve. In other words, inversion is the process of determining the depth of each layer and shear wave velocity for each layer from the apparent Rayleigh wave velocity versus wavelength.

The inversion process in the steady-state surface wave method as described by Richart et al. (1970), is based on two approximate relationships. The first is based on the

theoretical observation that, within normal range of Poisson's ratio ($0 \leq \nu \leq 0.5$), the shear wave velocity is approximately 110 percent of the phase velocity, i.e.,

$$V_s = 1.10 V_{ph} \qquad [3.7]$$

The second relationship is based on the theoretical attenuation of both components of the Rayleigh wave as shown in Fig. 2.3. It is reasonable to assume that the bulk of the Rayleigh wave travels through a zone of the half-space about one-wave-length deep. It could further be postulated that the average properties are those at depth of one-half to one third wavelength. Using an equivalent depth equal to one-third of Rayleigh wavelength was found to give a reasonable estimate of the actual profile of a pavement site (Szendrei and Freeme 1970).

In the preliminary inversion of the SASW method, Heisey et al. (1982) considered that the effective depth of sampling is equal to one-third of a wavelength. They also assumed that the apparent and actual Rayleigh wave velocities for each wavelength were equal. Nazarian and Stokoe (1983), based on experimental studies, found that the above assumption is applicable to soil sites with relatively uniform, thick layers. In other cases when the contrast in shear wave velocities is larger this method can often lead to doubtful results. A new inversion process was developed by Nazarian (1984).

The refinement process is an iterative procedure based on forward modeling. In this process a theoretical dispersion curve is matched to the experimental curve obtained in the field. In calculation of the theoretical dispersion curve, the actual site is modeled as a layered half-space with uniform, elastic layers of infinite horizontal extent. The shear wave velocities, thickness, Poisson's ratio, and mass density of the layers in the profile are assigned initial values. For this assumed layering, a theoretical dispersion curve is determined using a modified version of the Haskell-Thomson matrix solution (Thrower 1965). The theoretical dispersion curve is then compared to the experimental dispersion curve obtained in the field. The assumed shear wave velocities and thickness of the layers

in the model are adjusted until satisfactory agreement between theoretical and experimental dispersion curves is obtained. At that point the shear wave profile is accepted as a solution.

Parametric study of dispersive characteristic of Rayleigh wave by Ewing et al. (1957) shows that the variation in values of Poisson's ratio and mass density have less than 10 percent effect on the final shear wave velocities for reasonable choices and, therefore, are generally not varied after the initial choice is made.

Hossian and Drnevich (1989), Addo and Robertson (1992), also developed inversion procedures. These methods are different from the one developed by Nazarian (1984) in two ways: (i) they use a modified version of the Thomson-Haskell method developed by Knopoff (1964) and (ii) they automate the dispersion curves matching using optimization techniques with least squares criterion. Hossian and Drnevich (1989) used Powell's conjugate directions method while Addo and Robertson used Nelder and Meads (1965) Simplex method for minimizing least squares errors. Hossian and Drnevich also used the discrete layer stiffness matrix method originally developed by Lysmer and Waas (1972) to calculate theoretical dispersion curves.

This method, unlike the Knopoff or Haskell-Thomson methods lead to a nontranscendental quadratic eigenvalue problem which does not require root search techniques to solve. Later Nazarian automated his inversion procedure using least squares fitting with linear approximation (Yuan and Nazarian, 1993). Lately, Meier and Rix (1993) and Williams and Gucunski (1995), introduced automated inversion procedure using Nueral Networks which are trained using a large data base of theoretical dispersion curves.

An artificial neural network is used to invert surface wave dispersion. In order to generate the data base, synthetic dispersion curves are calculated for representative shear wave velocity profiles. Then an artificial neural network is taught to map these dispersion

curves back into their respective shear wave velocity profiles. Artificial neural networks are much less sensitive to incomplete and noisy data than optimization techniques. However, because neural networks approximate the mapping of dispersion curves into velocity profiles, their results may not be as accurate as those obtained using optimization techniques. Therefore, in situations where time is not as critical as accuracy, an artificial neural network can provide a good initial profile for optimization method.

In all existing SASW inversion methods, plane Rayleigh waves are used for calculation of theoretical dispersion curves. It is also assumed that the first mode of surface waves is the predominant propagation mode. Roesset et al. (1991), show that the use of the plane Rayleigh wave solution with the dispersion curve corresponding to the first mode of propagation is reasonable for soil deposits with gradual variation of properties but cannot reflect sudden jumps and discontinuities in the slope of the curve caused by wave reflection or refraction. They recommend to use the more accurate three dimensional solution for more complicated soil profiles and most pavement systems. Theoretical studies conducted by Sanchez-Salinero et al. (1987), and Gucunski and Woods (1991) show that higher Rayleigh modes provide a significant, and in many cases, a dominant influence on the overall wave propagation along the surface of a system. Therefore the inversion of the dispersion curve should not be guided solely by the theoretical first Rayleigh mode.

Gucunski and Woods (1992) have suggested the use of a simulated dispersion curve to overcome difficulties associated with multi-modes. In this method, the inversion procedure is performed by comparing the dispersion curve obtained from SASW field tests in the usual manner with the dispersion curve obtained from analytical or numerical simulation of the actual SASW tests used in the field. Tokimatsu et al. (1991) suggested that use of particle orbits together with dispersion data to overcome difficulties associated with multi-modes propagation.

The inversion procedures based on simulated dispersion curves may be computationally complicated and expensive. An alternative way is to separate the experimental dispersion curves into participating modes and to compare those to the theoretical dispersion curves. Al-Hunaidi (1994) has applied the multiple filter/crosscorrelation method for resolving the actual dispersion curves belonging to the various modes contributions to SASW signals. He found that this method is effective for phase velocity calculation if the modes comprising the signals are well separated. But in situations where the propagation velocities of the modes are similar or vibrations belonging to different modes interfere with each other, the modes yield poor results. However, in the case where SASW signals are dominated by one surface mode only, the multiple filter/crosscorrelation method yields representative results even when mode jumping occurs in comparison with the usual phase unwrapping procedure.

3.5 Conclusion and Research Needs

The Spectral-Analysis-of-Surface-Waves (SASW) method, is an improvement of the steady-state Rayleigh-wave method of in situ seismic testing. The SASW is a nondestructive testing procedure for determining in situ elastic moduli and thickness of layered system, like soils and pavement. The test is performed from the ground surface and thus requires no boreholes. The method has been under development since 1980.

Unfortunately, there are still no standard procedures for performing the SASW method. The main disadvantages at present are that field testing and data analysis are not performed rapidly. An important step toward reducing testing time in the field is the development of a multiple transducer testing procedure in which all the data for a given site can be obtained with the least number of source excitation on the test surface.

Also, there is uncertainty regarding source-to-near-receiver spacing and wavelength selection criteria to ensure that one surface wave mode is predominant. Since at certain

frequencies, the wave field may be compromised of more than one surface wave mode and (or) types, the phase angle obtained represents some average of all participating surface wave modes. Therefore, these phase angles will not be suitable as an analysis parameter in the SASW method. Currently there are no methods of detecting these invalid phase angles that are causing inconsistency in the dispersion curves. The filtering criteria suggested by Sanchez-Salinero et al. (1987), is contrary to the suggestion of Heisey et al. (1982). This conflict may be due to performing the tests at sites with different properties. Obviously, further investigation of these conflicting criteria is needed.

The inversion process is normally based on two dimensional solution in which only plane Rayleigh waves are considered. The experimental dispersion curve which is a result of three-dimensional wave propagation, and includes both body and Rayleigh waves is compared with theoretical dispersion curves for the plane Rayleigh wave. Therefore, it seems there is discrepancy between analysis and measurement in the site. This discrepancy is more pronounced when there are sharp changes in the properties of the layers. Therefore, development of a three dimensional procedure for inversion is needed.

In case of irregular stratification i.e., when the shear wave velocity does not increase with depth, the higher Rayleigh modes provide a significant, and in many cases, a dominant influence on the overall wave propagation along the surface of a system. The inversion of the dispersion curve for such sites should not be guided solely by the theoretical first Rayleigh mode. Therefore, improvement of the SASW method requires the development of an inversion program that can handle multi-modes in the inversion procedure. Also, it is necessary to explore the impact devices for measurements in deep deposits.

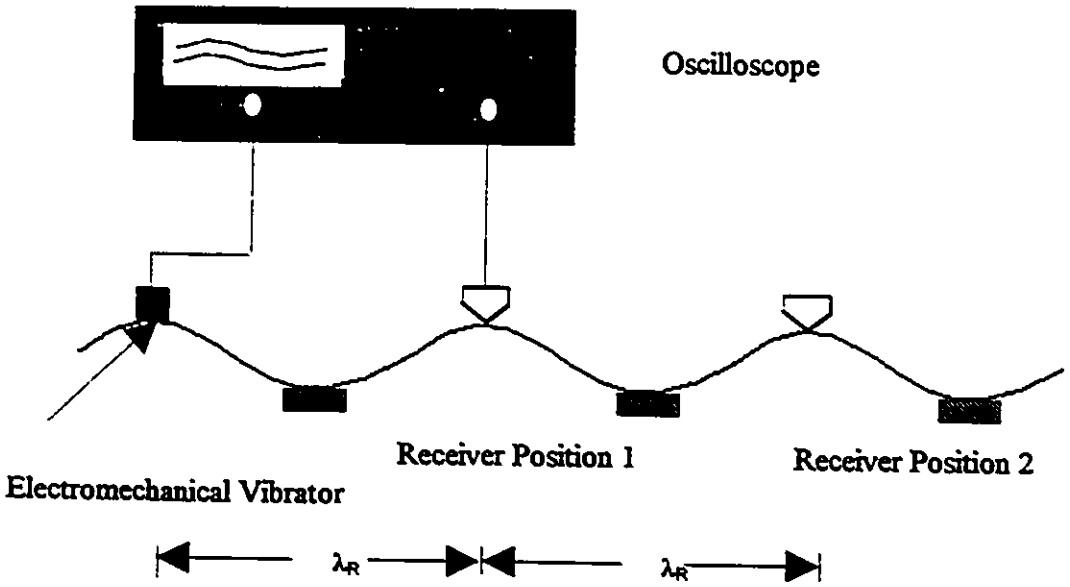

Fig. 3.1-Layout of the testing setup of the Steady-State Rayleigh wave method.

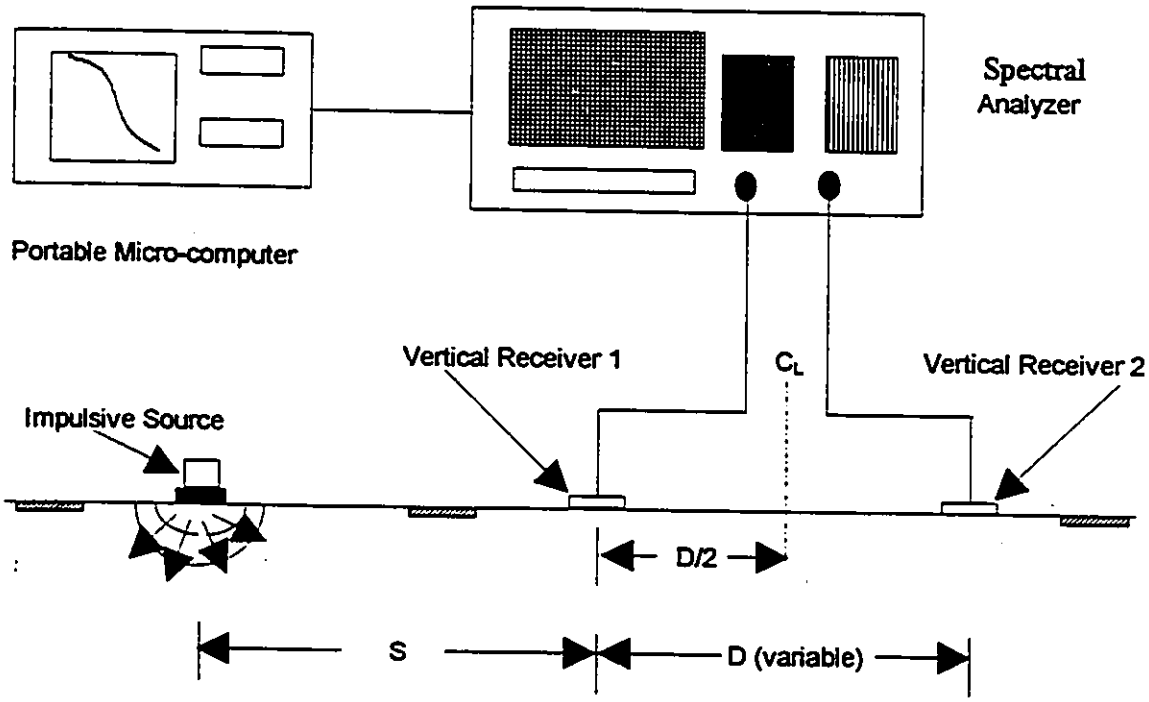

Fig. 3.2-Layout of the testing setup of the SASW method (after Roesset et al. 1990).

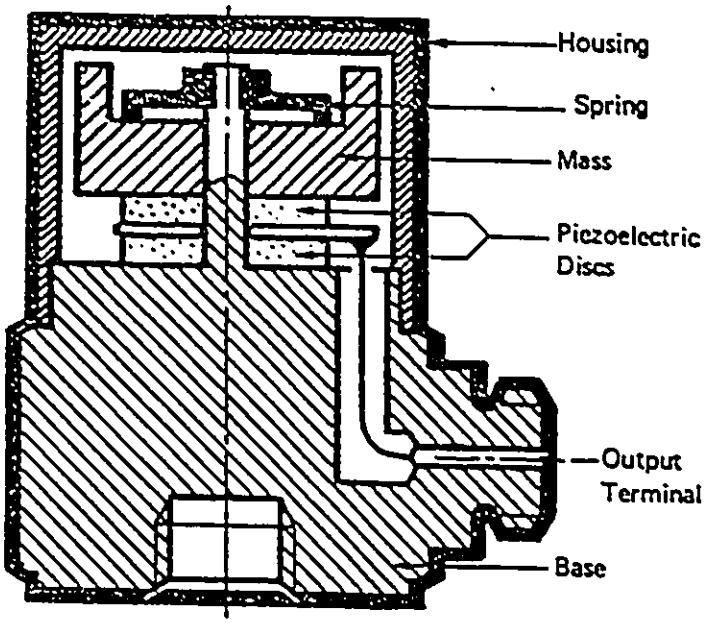

(a).The Piezoelectric Accelerometer (After Bruel and Kjar, 1978).

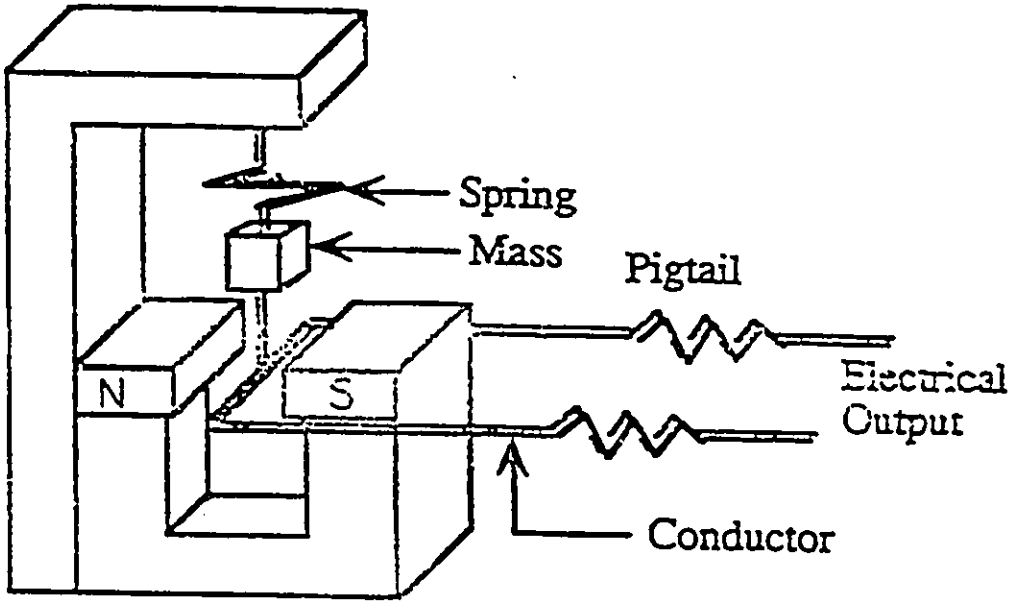

(b).Basic Geophone Construction

Fig. 3.3-Schematic diagram of Signal Receivers

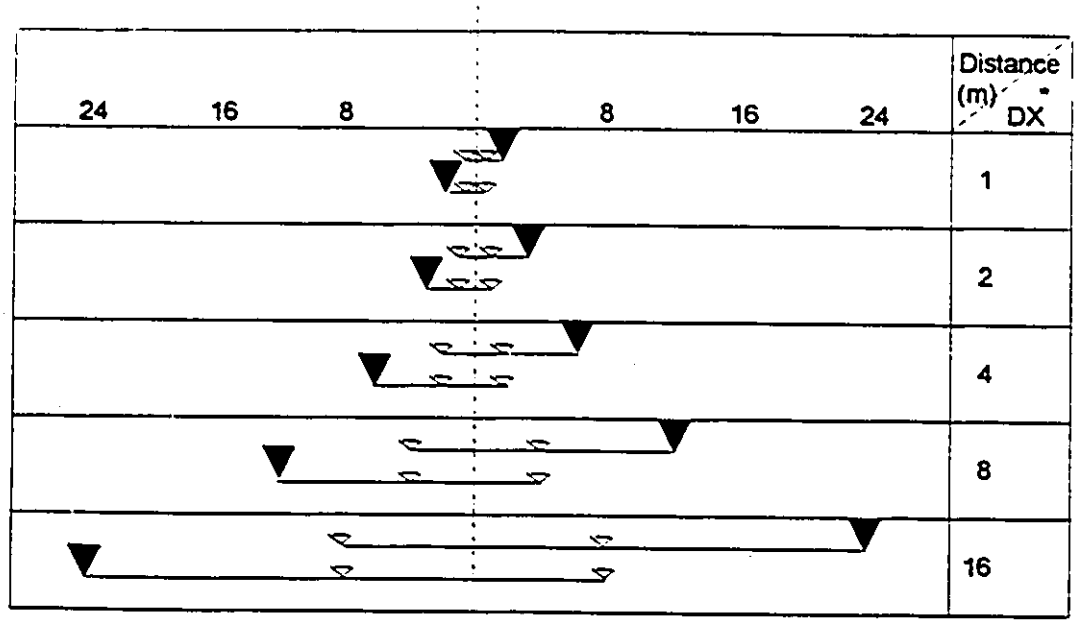

* DX: Receiver Spacings
▼:Source
▽:Receiver

(a)

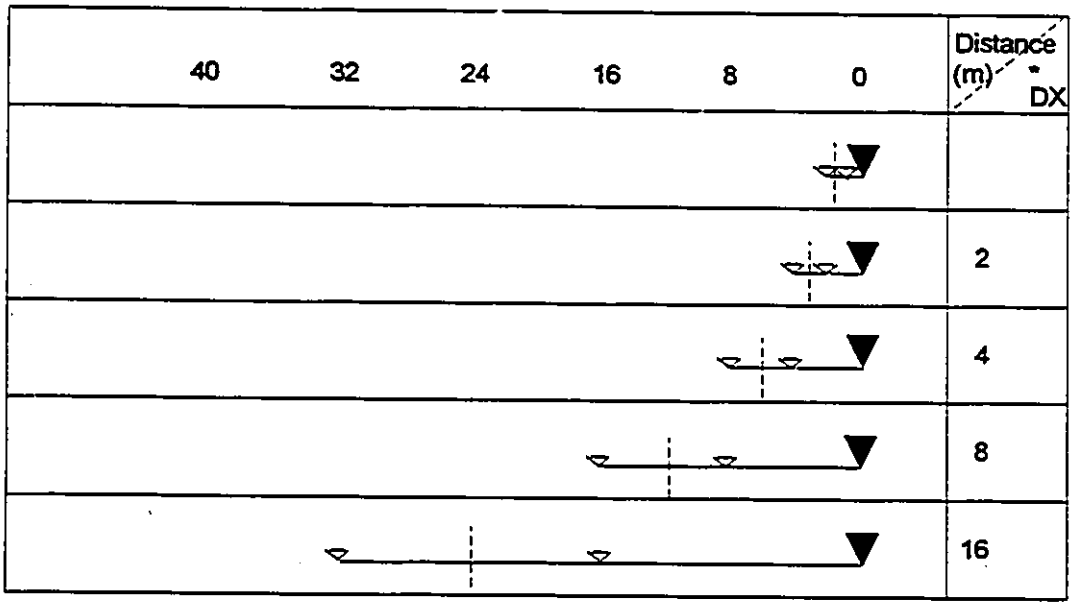

* DX: Receiver Spacings
▼:Source
▽:Receiver

(b)

Fig. 3.4-Source-receiver geometry: (a) common receivers midpoint geometry, (b) common source geometry (After Nazarian & Stokoe, 1985).

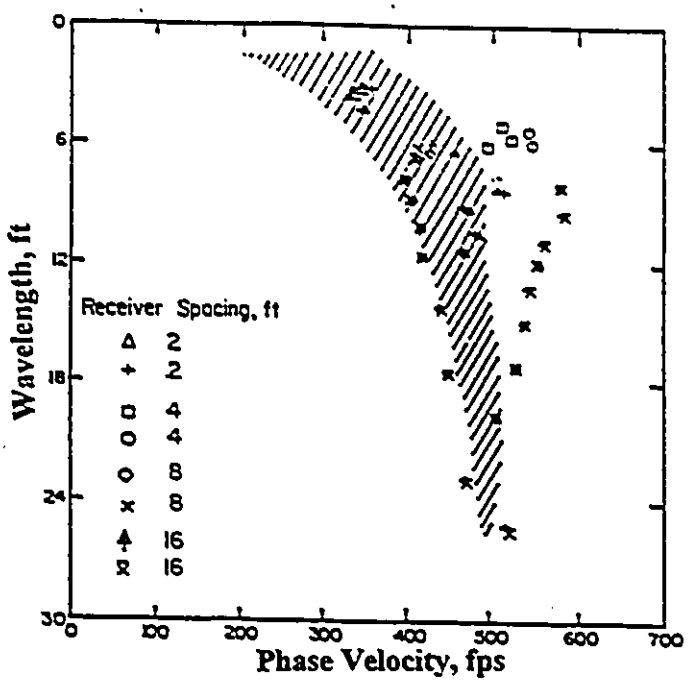

Fig. 3.5-Dispersion curve from SASW tests performed using common source geometry (from Nazarian and Stokoe, 1983).

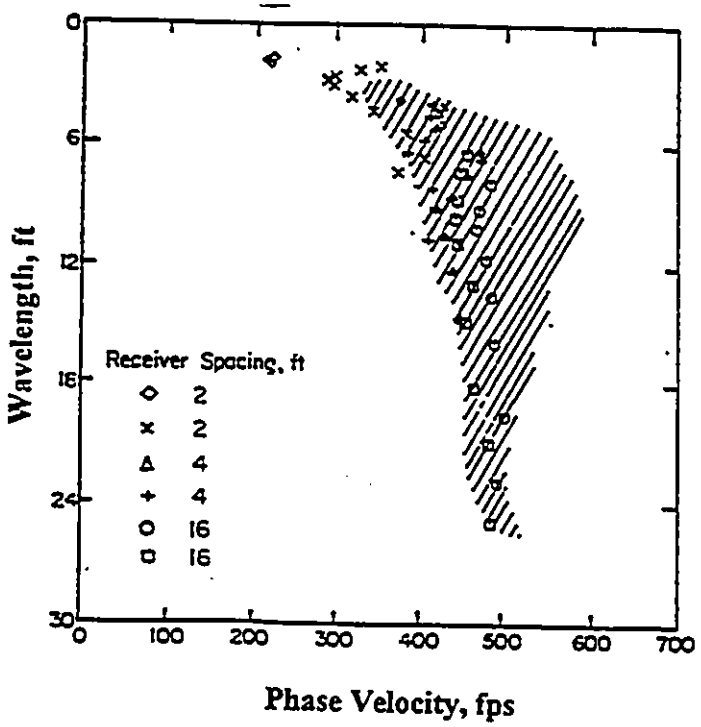

Fig. 3.6-Dispersion curve from SASW tests performed using common receivers midpoint geometry (from Nazarian and Stoke, 1983).

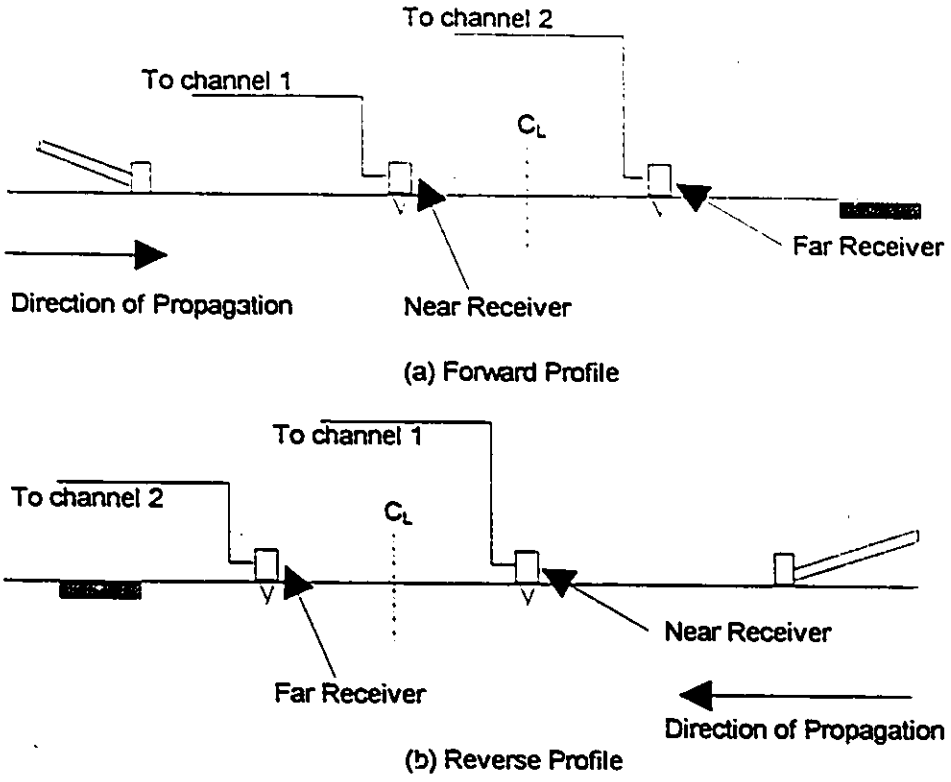

Fig. 3.7-Schematic illustration of Forward and Reverse profile tests.

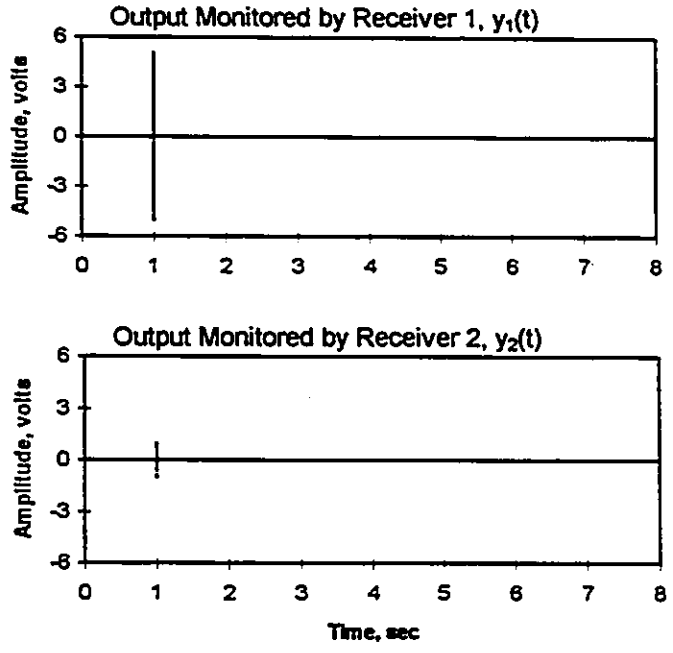

Fig. 3.8-Typical time histories resulting from an impact source.

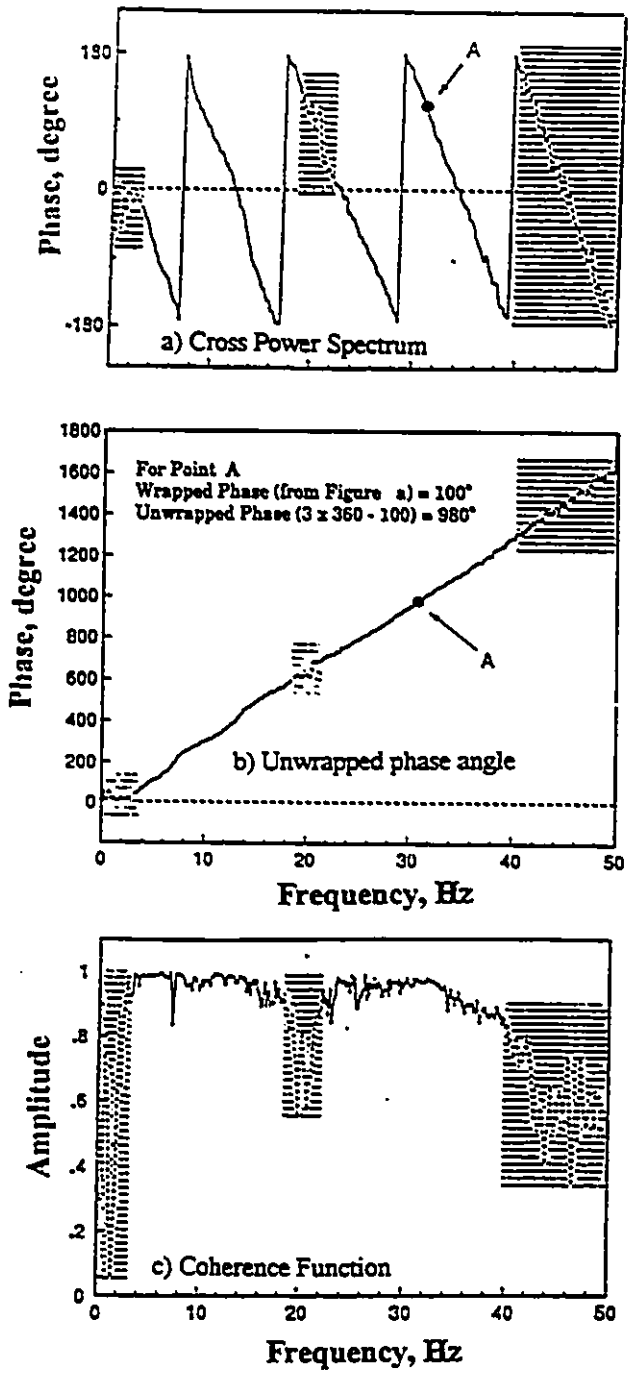

Fig. 3.9-Typical spectral functions:

(a)Wrapped phase information of cross power spectrum;

(b) Unwrapped phase information of cross power spectrum;

(c) Coherence function (Nazarian and Desai, 1993).

CHAPTER 4

CALCULATION OF THE DISPERSION CURVE

4.1 Introduction

In a homogeneous, isotropic, elastic half-space, Rayleigh wave velocity does not vary with frequency. However, Rayleigh wave velocity varies with frequency in a layered soil system because of variation of stiffness with depth. This frequency dependency of surface wave velocity in a layered system is termed dispersion and a plot of velocity versus frequency or wavelength is called dispersion curve. Procedures for calculation of thecretical dispersion curves are discussed in this chapter.

4.2 Dispersion of Plane Rayleigh Waves

The plane Rayleigh wave dispersion curve can be calculated using the theory of propagation of elastic surface waves in a layered half-space. The mathematical model consists of a horizontally layered half-space with properties varying from one layer to

another but constant within each layer as shown in Fig. 4.1. The dispersion equation can be derived either by the transfer or the stiffness matrix approach.

4.2.1 The Transfer Matrix Approach

The transfer matrix of a layered soil system was first derived by Thomson (1950) and later was corrected by Haskell (1953).

In this section, the transfer matrix approach is presented briefly. More detailed discussion on the subject can be found in the above references and in Nazarian (1984), Nazarian and Stokoe (1986) and Sanchez-Salinero et al. (1987).

The transform matrix [T] or propagator matrix gives displacements and stresses at the bottom of the layer in terms of displacements and stress at the top of the layer as follows:

$$\begin{bmatrix} U_h \\ S_h \end{bmatrix}_j = [T]_j \begin{bmatrix} U_o \\ S_o \end{bmatrix}_j \qquad [4.1]$$

where

$$= \begin{bmatrix} u \\ w \end{bmatrix}$$

$$S = \begin{bmatrix} \tau_{xz} \\ \sigma_z \end{bmatrix}$$

u is the displacement in the x-direction, w is the displacement in the z-direction, the subscripts h and o indicate bottom and top of layer respectively, τ_{xz} and σ_z are the stresses on a horizontal plane.

The compatibility of displacements and stresses at the interface of any two adjacent layers can be written as

$$\begin{bmatrix} U_h \\ S_h \end{bmatrix}_j = \begin{bmatrix} U_o \\ S_o \end{bmatrix}_{j+1} \qquad [4.2]$$

Substituting Equation 4.2 in Equation 4.1 results in

$$\begin{bmatrix} U_o \\ S_o \end{bmatrix}_{j+1} = [T]_j \begin{bmatrix} U_o \\ S_o \end{bmatrix}_j \qquad [4.3]$$

By repeating the above procedure for all of the layers, a relationship can be obtained between the displacements and stresses at the surface of the layered system and those at any depth:

$$\begin{bmatrix} U_o \\ S_o \end{bmatrix}_{n+1} = [T]_n [T]_{n-1} \cdots [T]_1 \begin{bmatrix} U_o \\ S_o \end{bmatrix}_1 \qquad [4.4]$$

Considering the half-space layer number n+1, one can write an equation that relates displacements and stresses at the top of the half-space with the amplitudes of the upward and downward propagating waves in the half-space as

$$\begin{bmatrix} U_o \\ S_o \end{bmatrix}_{n+1} = [H]_{n+1} \begin{bmatrix} A \\ B \\ C \\ D \end{bmatrix}_{n+1} \qquad [4.5]$$

Where A, B, C and D are proportional to the amplitudes of the waves propagating in the downward (A,B) and upward directions (C,D), in the half-space, respectively.

Substituting Equation 4.5 into Equation 4.4 results in

$$\begin{bmatrix} A \\ B \\ C \\ D \end{bmatrix}_{n+1} = \begin{bmatrix} L_{11} & \vdots & L_{12} \\ \cdots\cdots & \vdots & \cdots\cdots \\ L_{21} & \vdots & L_{22} \end{bmatrix} \begin{bmatrix} U_o \\ S_o \end{bmatrix}_1 \qquad [4.6]$$

where matrix [L] which relates the amplitudes of the outgoing and ingoing waves in the half-space and the displacements at the surface is a 4×4 matrix

$$[L] = [H]_{n+1}^{-1} [T]_n [T]_{n-1} \cdots [T]_1 \qquad [4.7]$$

Rayleigh wave modes represent natural modes of wave propagation. That means no forces are applied at the top of the layered system (i.e., $S_{o1} = 0$) and no waves are assumed to travel upward in the half-space (i.e, $C_{n+1} = D_{n+1} = 0$). Therefore, equation 4.6 becomes

$$\begin{bmatrix} A \\ B \\ 0 \\ 0 \end{bmatrix}_{n+1} = \begin{bmatrix} L_{11} & \vdots & L_{12} \\ \cdots\cdots & \vdots & \cdots\cdots \\ L_{21} & \vdots & L_{22} \end{bmatrix} \begin{bmatrix} U_o \\ 0 \end{bmatrix}_1 \qquad [4.8]$$

In order to find a nontrivial solution, the determinant of the submatrix L_{21} must be zero, i.e:

$$|L_{21}| = 0 \qquad [4.9]$$

This equation is called the characteristic equation which relates frequency (ω) with phase velocity (V_{ph}). At any frequency, there may be several values of velocity that satisfy this equation. Each value of velocity corresponds to a different mode of propagation and defines a different dispersion curve.

The transfer matrix approach caused difficulties during numerical implementations in the high frequency range. That is, some components of the matrix become large, causing a loss of significant figures which makes it impossible to obtain accurate value of the roots. This problem was later solved by Knopoff (1964), Dunkin (1965), Thrower (1965), and Watson (1970) by techniques that use second and third order subdeterminants of a layer. The problematic terms are eliminated by these techniques before computing products of matrices. However, they require more computer memory and time compared to the original Thomson-Haskell solution as programmed by Press et al. (1961).

4.2.2 The Stiffness Matrix Approach

An alternative method for computing the modes of propagation and their dispersion curves is the stiffness matrix approach. The stiffness matrix of a layer, as described in section 2.2.4 relates forces and displacements at top and bottom of the layer in the frequency-wave number domain.

If the soil system consists of several layers, the global stiffness matrix is constructed by overlapping the contribution of the layer matrix at each node (interface) of the system. In

this case the global load vector corresponds to the prescribed external forces at the interfaces between layers. Therefore, the assembly and solution of the equation is formally analogous to the solution of structural dynamics problems in the frequency domain.

The assembly process is shown in Fig. 4.2. It leads to the system of equations defined by

$$[K]\{U\} = \{P\} \qquad [4.10]$$

where [K] represents the system stiffness matrix, {U} the vector of interface displacements, and {P} the vector of external interface loadings. Since Rayleigh wave modes represent natural modes of wave propagation, the latter are obtained from the eigenvalue problem that follows from setting the load vector equal to zero.

$$[K]\{U\} = 0 \qquad [4.11]$$

where for a fixed angular frequency ω, the eigenvalues represent phase velocities of the Rayleigh wave while U represents its shape as a function of depth. For a nontrivial solution the determinant of matrix [K] must be zero

$$|K| = 0 \qquad [4.12]$$

4.3 Root Searching

Because the stiffness matrices include transcendental functions, theoretically an infinite number of modes is possible. To solve Equation 4.12, either the value of frequency or phase velocity should be assumed. The resulting equation is then solved using numerical search techniques as an explicit solution is not available, except for simple one or two layered media.

Schwab and Knopoff (1970) have shown that a dispersion curve can be obtained with a single computer run by a procedure that specifies a set of frequencies and iterates over velocity at each frequency. At very high and very low frequencies, phase velocities do not vary by much, and they are approximately equal to the Rayleigh wave velocities of

the top and bottom layers, respectively. As the number of increments increase, reasonable results can be obtained. However, as the number of increment increase, the computation time is increased.

At each frequency, a number of velocities (roots) that satisfy Equation 4.12 exist. These different roots correspond to various modes of propagation. The root with minimum magnitude is called the fundamental mode. The first higher root than the fundamental is called first mode and so on.

In this study, for solving Equation 4.12, a computer program was developed in which the frequency is assumed as the independent variable. In the first version of this program damping of soil layers was not considered, therefore the determinant and the phase velocity are real and the phase velocity is equal to the apparent velocity. At each selected frequency, the program computes the determinant for each increment of velocity in the range of velocities selected. A root of the dispersion equation for a selected frequency is first located between two phase velocities whose determinants have opposite signs. Then, the root is pinpointed using one of several methods as discussed next.

4.3.1 Bisection Method

The bisection method was first used to locate the roots. This method is simple. Over some interval the function is known to pass through zero because it changes sign. It is assumed that for a continuous function f, defined on the interval [a,b], with f(a) and f(b) of opposite sign there exists p, $a<p<b$, for which $f(p)=0$. Next, the function at the midpoint of the interval is evaluated and its sign is examined. The midpoint is used to replace whichever limit has the same sign. After each iteration the bounds containing the root decrease by a factor of two.

To illustrate how the Bisection method works (Fig. 4.3a), set $a = a_1$ and $b = b_1$, and let p_1 be the midpoint of [a, b], i.e. $p_1 = 1/2(a_1 + b_1)$. If $f(p_1) = 0$, then $p = p_1$; if not, then $f(p_1)$ has the same sign as either $f(a_1)$ or $f(b_1)$. If $f(p_1)$ and $f(a_1)$ have the same sign, then $p \in (p_1, b_1)$, and we set $a_2 = p_1$ and $b_2 = b_1$. If $f(p_1)$ and $f(a_1)$ have opposite signs, then $p \in (a_1, p_1)$, and we set $a_2 = a_1$ and $b_2 = p_1$. We then reapply the process to the interval $[a_2, b_2]$.

The Bisection method, though conceptually clear, has significant drawbacks. If the interval happens to contain two or more roots, the bisection method will only find one of them. If the interval contains no roots and merely straddles a singularity, it will converge on the singularity. Due to the above difficulties and those shown in Fig. 4.3b to 4.3d in finding the roots of the determinant, this method was abandoned. In the second version of the program, the Newton-Raphson method was applied.

4.3.2 Newton-Raphson Method

The Newton-Raphson method requires the evaluation of both the function f(x), and the derivative f'(x), at arbitrary point x. The Newton-Raphson formula consists geometrically of extending the tangent line at a current point x_i until it crosses zero, then setting the next guess x_{i+1} to the abscissa of that zero-crossing (see Fig. 4.4). Applying this method for finding the roots of Eq. 4.12, gives satisfactory results as discussed later.

4.3.3 Steepest-descent Method

In the second version of the inversion program, damping of the layered soil system is considered. For nonzero damping, the determinant and hence the phase velocity are complex. Under this condition Eq. 4.12 was solved based on a steepest-descent

procedure as recommend by Wolf (1985). This method replaces the root-finding problem by an equivalent problem of minimization. For example, solving

$$f(x,y)=0 \qquad g(x,y)=0 \qquad [4.13]$$

is clearly equivalent to minimizing

$$S(x,y)=[f(x,y)]^2+[g(x,y)]^2 \qquad [4.14]$$

Beginning at an initial approximation (x_0,y_0), we select the next approximation in the form

$$x_1=x_0-tS_{x0} \qquad y_1=y_0-tS_{y0} \qquad [4.15]$$

Where S_{x0} and S_{y0} are the components of the gradient vector at (x_0,y_0). Thus progress is in the direction of steepest descent. The number t may be chosen to minimize S in this direction. Similar steps follow.

In this version of program the real and imaginary parts of phase velocity are iterated for the specified frequency until the real and imaginary parts of the determinant vanish. However, computational difficulty (overflow) at high frequencies was encountered when using this method, and consequently Muller's method described next was investigated.

4.3.4 Muller's Method

This method is a generalization of the Secant method. The Secant method begins with two initial approximations x_0 and x_1 and determines the next approximation x_2 as the intersection of the x-axis with the line through $(x_0, f(x_0))$ and $(x_1, f(x_1))$ (see Fig. 4.5a).

Muller's method uses three initial approximations x_0, x_1, and x_2 and determines the next approximation x_3 by considering the intersection of the x-axis with the parabola through $(x_0, f(x_0))$, $(x_1, f(x_1))$, and $(x_3, f(x_3))$ (see Fig. 4.5b). No numerical difficulties were encountered with this method.

Detailed description of the Muller, Bisection and Newton-Rophson methods can be found in most numerical text books (e.g. Burden and Faires, 1988). To reduce computational time in the case of non-zero damping, the program first finds the range of the imaginary part of phase velocity. This is done by interpreting the ratio of imaginary to real parts as the effective damping ratio.

4.3.5 Verification of Computer Code

The computer program developed here was tested by finding the dispersion curves for several different soil stratifications. Fig. 4.6 shows the results obtained with the program developed in this study for a homogeneous layer resting on the half-space with and without damping and the dispersion curve reported by Wolf and Obernhuber (1982). Fig. 4.6 shows that first Rayleigh mode begins at Rayleigh wave velocity of half-space for frequency f=0 and converges to the top layer's Rayleigh wave velocity for frequency $f \rightarrow \infty$.

The results obtained (see Fig. 4.6) indicate that material damping does not affect Rayleigh wave dispersion curve. The damping only causes attenuation of waves, while the apparent velocity remains almost equivalent to the phase velocity of undamped system.

Further verification of the program was done by considering three more cases of stratified soil sites as shown in Fig. 4.7. Case one represents a soil profile of regular soil stratification, i.e., when the shear wave velocity increases with depth, while case two represent irregular soil stratification, with a soft layer trapped between harder surface layer and a half space. Case three is an example of a system with a hard layer trapped between softer layers. The obtained dispersion curves are shown in Figs.4.8a, 4.9a, and 4.10a.

Gucunski (1991), Gucunski and Woods (1992) calculated dispersion curves for the same cases as shown in Figs. 4.8b, 4.9b, 4.10b. By comparing these figures to Figs. 4.8a, 4.89a, 4.10a, it is verified that the program performs well for soil stratification problems.

4.4 Difficulty in Construction of Field Dispersion Curve

As discussed earlier, presently there is no standard procedure available for performing the SASW method in the field. More development is needed for field testing and data analysis. The main goal in performing the SASW test in the field is to obtain the experimental dispersion curve. To develop the field dispersion curve, it is first necessary to obtain the relative phase shift, ϕ, between two signals as a function of frequency from phase information of cross power spectrum or transfer function. Then the relative phase shift is used to calculate the time (Eq. 3.4) for each frequency component of the signal to travel between the two receivers. Knowing the distance D between the two receivers, the phase velocity and corresponding wavelength can be obtained from Eqs 3.5 and 3.6. By repeating the above procedure for each frequency and for all spacings, the Rayleigh wave velocity corresponding to each wave length can be evaluated and by combining these data, the dispersion curve is determined.

Generally, the signal analyzer displays the phase of the cross power between -180° and 180° (wrapped) and needs to be transformed to a continuous format (unwrapped). This is performed by adding the correct number of 360° cycles. The coherence function should be used as a tool for assessing the quality of the observed signals. The low coherence parts of the signal must be discarded from construction of dispersion curve.

As reported by Al-Hunaidi (1993), under some conditions, spurious cycles may exist in relative phase angle spectra that may be mistakenly counted as true ones and thus leading to an error in unwrapping of phase angles. This situation exists for sites where, dominant surface wave propagation from one mode shifts to another mode. The phenomenon is

called mode jumping. Therefore, the usual procedure for unwrapping is unreliable for sites where mode jumping occurs.

Also, in the usual phase unwrapping procedure, the distance between receivers is taken equal to the spacing between the source and the near receiver. Currently used wavelength filtering criteria, e.g. Heisey et al. (1982) and Sanchez-Salinero et al. (1987) may not be enough to ensure that only one surface wave mode is dominant at a particular frequency.

4.5 Case Study

To demonstrate the above mentioned difficulties, a SASW test was performed on a flexible pavement section of a service road at the National Research Council, Ottawa campus.

4.5.1 Field Testing Setup and Data acquisition

The CS array geometry was used, and the spacings between receivers were 0.125, 0.25, 0.5, 1.0, 4.0, 8.0, and 16 meters. Four types of accelerometer transducers were used to pick up the seismic signal, depending on the frequency range of interest. For spacing 0.125 m, to profile shallow layers using short wave lengths, accelerometers which are sensitive in the high frequency range were used (PCB model 309 A). PCB model 308b10 and PCB model 306C accelerometers were used for (0.25, 0.50 m) and (1.0, 2.0, 4.0 m) spacings, respectively. To pick up low frequency signals to profile deeper layers B&K 8306 accelerometer was employed for the 8.0 m spacing. The transducers were attached to small aluminum plates using steel studs or double sided tape. The plates were glued to the pavement surface using 5-minute epoxy glue to ensure good coupling. A portable dual channel FFT analyzer (HP 35670 A) was utilized for recording and analyzing the data.

As mentioned in Chapter 3, Section 3.2.1, the dynamic signal is generated in the pavement using a variety of sources depending on the frequency range of interest or the desired depth of sampling. For 0.125 m spacings a small steel ball was used, and a light ball peen hammer (0.3 kg) was used for 0.25, 0.5, 1.0 m spacings to produce high frequency vibration which is necessary to sample shallow layers. A heavy sledge hammer (8 kg) and drop weight (approximately 100 kg and height varied between 1 to 2 m) were employed for large spacings to induce a signal with low frequency. To enhance signal quality, i.e., increases signal to noise ratio, the results from five signals were averaged. In order to produce a signal with high coherence in the frequency range of interest, the test was repeated using different sources or impact surfaces, e.g., by employing rubber pads. To detect dipping or inhomogenity in the layer the test was perform for both forward and reverse configuration.

4.5.2 Construction of the Field Dispersion Curve

The relative phase angle spectra and corresponding coherence function for 0.125, 0.25, 0.5, 1.0, 2.0, 4.0 and 8.m receiver spacings are shown in Fig. 4.11, respectively. The usual procedure for unwrapping was used and the phase velocity and the wavelength was evaluated (using equations 3.4 through 3.6). These calculations were performed in a commercial spread-sheet program (Excel). Data points with low coherence (e.g., less than 0.90) were eliminated. Since forward and reverse tests of the relative phase angle spectra for 16.0 m spacings (Fig. 4.11) are different from each other this implies that the layers are not horizontal and hence this spectrum was not included in the analysis.

In filtering the wavelength the following three criteria were applied :

i) Points for which the wavelength does not satisfy Heisey criterion $0.5\ D < \lambda < 3D$ are discarded (where λ is wavelength and D is receiver-to-receiver spacing). The corresponding dispersion curve is shown in Fig. 4.12 a.

ii) Applying the Sanchez-Salinero et al. criterion, $\lambda < 0.5\ D$

iii) Applying Gucunski and Woods criterion $0.25\ D < \lambda < D$.

The dispersion curves obtained with criteria (ii) and (iii) are shown in Figs 4.12b, 4.12c.

From Figs. 4.12a, 4.12b, 4.12c it can be seen that different dispersion curves are obtained for this site depending on the filtering criterion used. This may be due to the participation of more than one surface wave mode or other type of motions that can not be distinguished by available criteria. However, it seems that Sanchez-Salinero filter criterion works better than other criteria but the implementation of this criteria increases the need for powerful impact sources as the depth of sampling increases. Therefore, it is necessary to find a method that enables the separation of modes from each other. Such a procedure will significantly assist the interpretation of SASW results.

In order to find a reliable dispersion curve the following criterion is introduced. Since the SASW test is usually performed for several receiver spacings, therefore the dispersion data from different spacing are overlapped over wide frequency ranges and for each frequency several dispersion data may be available. These dispersion data must be combined to generate the average dispersion. In the new filtering criterion, the data points at same frequency but obtained from two different receiver spacings are rejected if they are not in close agreement. The dispersion curve obtained in this way is shown in Fig. 4.13.

4.5.3 Inversion of the Field Dispersion Curve

Inversion is the process of determining the thickness and shear wave velocity of each layer from the field dispersion curve. The inverse problem is difficult to solve, because interpretation from a dispersion curve to a structural model is nonlinear and nonunique (Knopoff 1961; Thrower 1965; Mora 1988). Generally, the adopted procedure for handling this nonlinear problem is to employ a technique that only requires solution to forward problem to find the inverse mapping. This technique was first adopted by

Dorman and Ewing (1962). They computed the theoretical dispersion curve for an assumed initial structure and then iterated until a theoretical dispersion curve matched the experimental curve obtained in the field.

In calculating the theoretical dispersion curve, the actual site is modeled as a layered half-space with uniform elastic layers of infinite horizontal extent. The shear wave velocities, thickness, Poisson's ratio and mass density of the layers in the profile are assigned initial values. Nazarian (1984) has numerically shown that the effects of Poisson's ratio (ν) and mass density (ρ) in most practical cases are less than 5%.

In this study the forward modeling is adopted. For assumed layering, a theoretical dispersion curve is determined using the stiffness matrix approach suggested by Kausel and Roesset (1981). The theoretical dispersion curve is then compared to the experimental dispersion curve obtained in the field. The assumed shear wave velocities and thickness of the layers in the model are adjusted until satisfactory agreement between theoretical and experimental dispersion curves is obtained. At that point the shear wave profile is accepted as a solution.

To invert the field dispersion curve of the case study, the dispersion curve was divided into two sections as shown in Fig. 4.14. From wavelength of about 2.0 m the propagation velocity is constant and it does not vary with the wavelength. This means that the layered soil system is located over half-space, since in the case of a uniform half-space the zero determinant matrices [Eq. 4.12] lead to a frequency (or wavelength) independent solution for the characteristic equation. Thus the dispersion curve becomes a horizontal line. The initial profile is selected using the simplified inversion method as used in the steady-state surface wave method discussed in Chapter Three, Section 3.4. The shear wave velocities and thickness of each layer are estimated assuming that shear wave velocity is approximately 110 percent of the phase velocity, and using equivalent depth equal to one-half of Rayleigh wavelength.

An alternative way for the first estimation of the shear wave velocities and the thickness of layers is to use the relative phase angle of cross spectra as a guide. The sharp change in gradient of phase angle is a sign that waves have started to propagate in another layer. For example at relative phase angle of cross spectrum of the 0.125 m spacing (Fig. 4.11), at the frequency equal to 4864 Hz, significant change occurs in the gradient of the relative phase spectrum. This sharp change is taken as a sign that layer stiffness has changed. The wrapped phase angle in this frequency equals to 139° and the corresponding unwrapped phase angle and wavelength are equal to 221° and 0.20 m, respectively. Therefore, the first guesses of thickness of layer and shear wave velocity are equal to 0.20 m and 1100 m/s, respectively.

The properties of layered soil for the first iteration are shown in Table 4.1. The corresponding theoretical dispersion curve was produced by running the program developed during this study (see Fig. 4.15). Then soil properties were changed until the computed and the experimental dispersion curves match as in Fig. 4.16. Soil properties in last stage are shown in Table 4.2. From Fig. 4.16 it is obvious that none of the theoretical dispersion curves match with the field dispersion curve at short wavelengths (1-2 m). This is due to transition of dominant influence from the first towards higher modes as frequency increases (See Fig. 4.17 which is produced from same data as Fig. 4.16 but instead of wavelength, the frequency versus phase velocity is used). The important fact is that at high frequency the theoretical dispersion curves approach the shear wave velocity of the second layer. This is in contrast to the expectation that phase velocity of the modes at high frequencies should approach the Rayleigh wave velocity of the surface layer.

4.6 Conclusion

Currently there are no standard methods available for filtering the wavelength. Filtering criterion suggested by Sanchez-Salinero et al. (1987), is contrary to the suggestion of

Heisey et al. (1982). The construction of field dispersion curve and the inversion process by iteration is tedious and time-consuming, and therefore, it needs to be automated. Also to overcome difficulties associated with multi-mode SASW signals, an attempt should be made to simulate dispersion curves as suggested by Gucunski and Woods, (1991) and Tokimatsu et al. (1992). In this method, the field dispersion curve is compared to simulated dispersion curves.

Table 4.1-Soil properties for first iteration.

	Shear Wave Velocity (m/s)	Thickness (m)	Damping ratio	Poisson's ratio	Unit Weight (kN/m^3)
Layer 1	1600	0.12	0.0	0.35	22
Layer 2	900	0.13	0.0	0.35	18
Layer 3	600	0.10	0.0	0.35	17
Layer 4	460	0.15	0.0	0.35	17
Layer 5	390	0.30	0.0	0.35	17
Layer 6	250	0.20	0.0	0.35	17
Half-space	200	------	0.0	0.35	17

Table 4.2-Soil properties for final iteration.

	Shear Wave Velocity (m/s)	Thickness (m)	Damping ratio	Poisson's ratio	Unit Weight (kN/m^3)
Layer 1	1400	0.20	0.0	0.35	22
Layer 2	500	0.25	0.0	0.35	18
Layer 3	400	0.25	0.0	0.35	17
Layer 4	310	0.30	0.0	0.35	17
Half-space	160	------	0.0	0.35	17

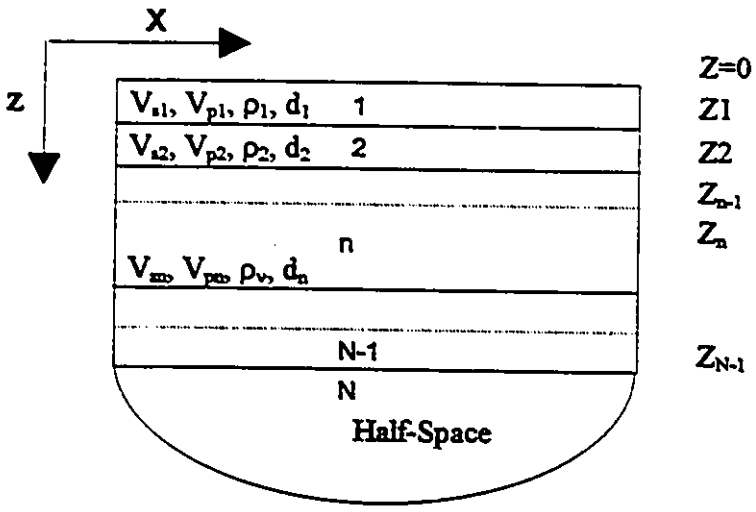

Fig. 4.1-Idealized layered Half-space.

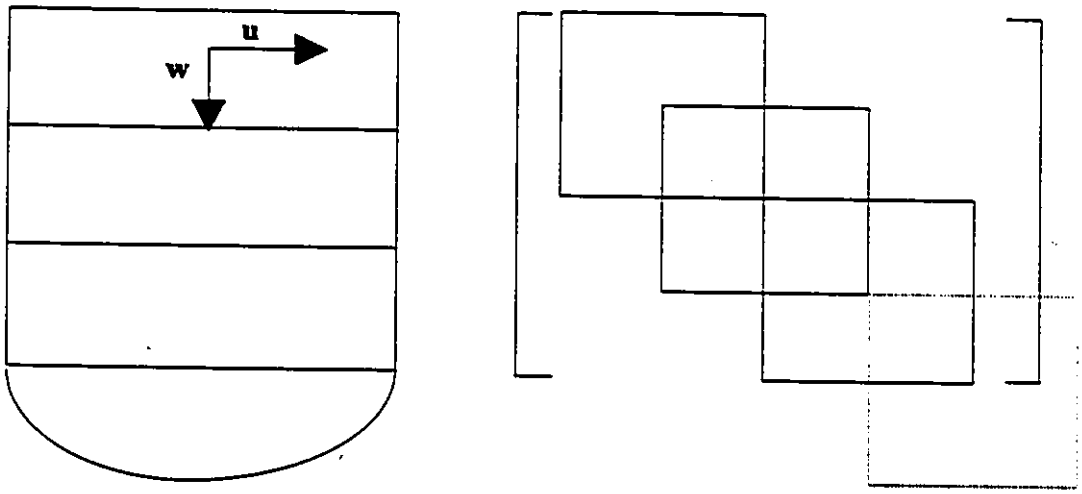

Fig. 4.2-Assembly process of the global stiffness matrix.

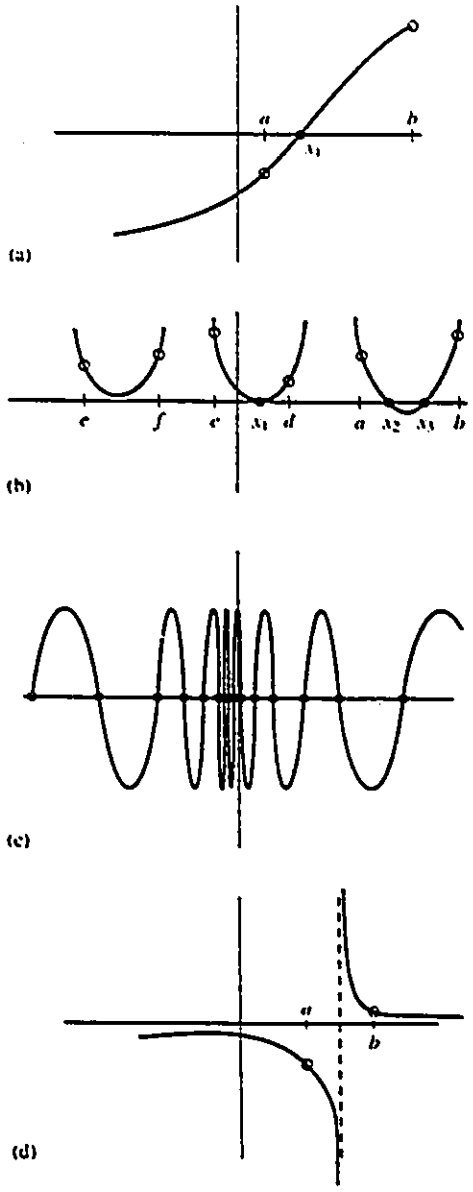

Fig. 4.3-Illustration of the Bisection method procedure and some situations encountered while root finding: (a) shows an isolated root p bracket by two points a and b at which the function has opposite signs; (b) illustrates that there is not necessarily a sign change in the function near a double root (in fact, there is not necessarily a root!); (c) is a pathological function with many roots; and (d) the function has opposite signs at points a and b, but the points bracket a singularity, not a root (Press et al. 1992).

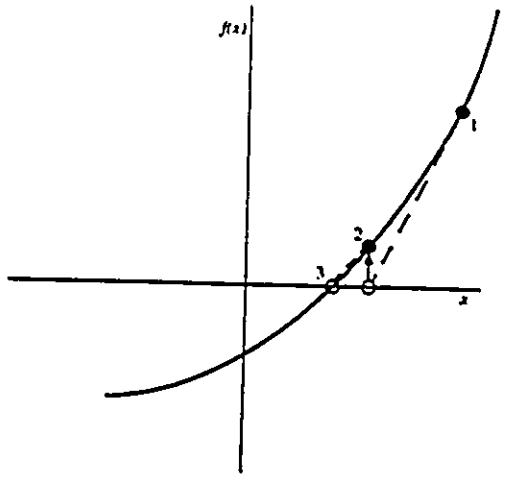

Fig. 4.4-Illustration of Newton's method in which the local derivative is extrapolates to find the next estimate of the root (Press et al. 1992).

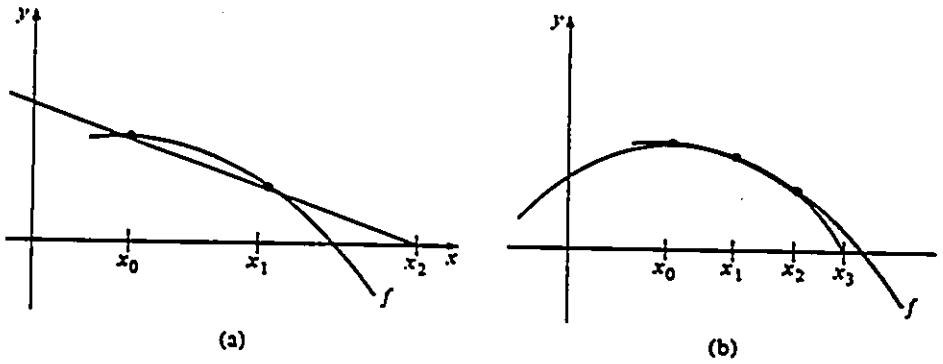

Fig. 4.5-Illustration of Muller's method (Burden and Faires 1985).

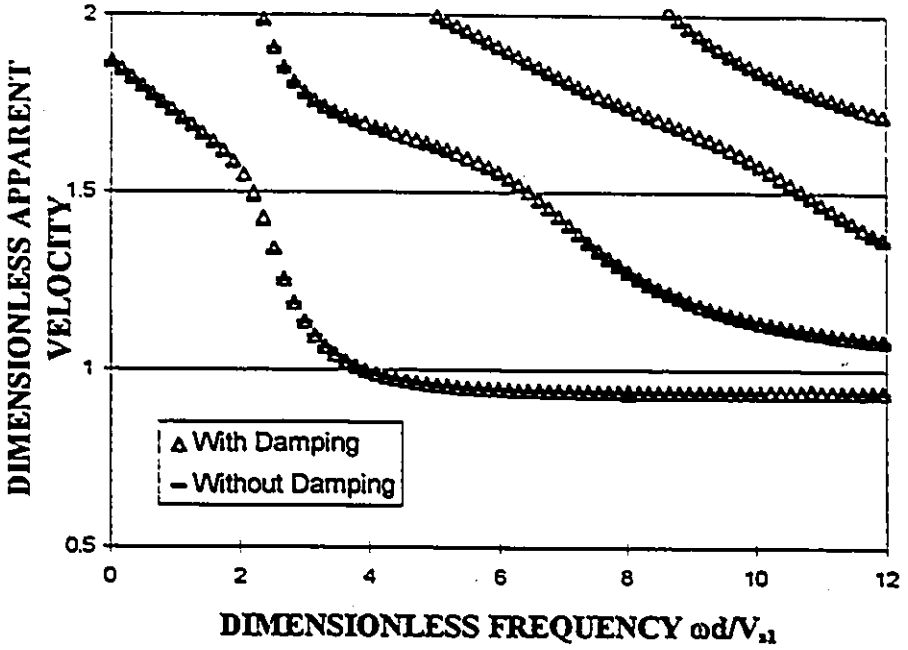

(a)

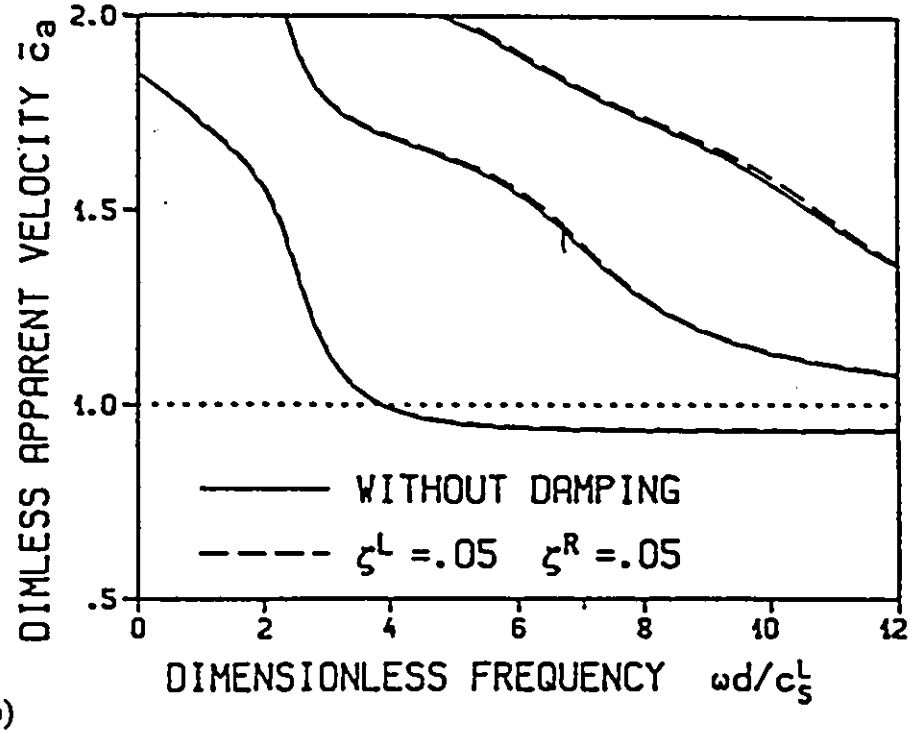

(b)

Fig. 4.6-DISPERSION CURVE-homogeneous layer, Vs_1=600 m/s, Vs_2=1200 m/s, d_1 1=1.50 m, ν_1=.33, ν_2=.33, ρ_1/ρ_2=1
(a) from developed program, (b) from Wolf and Obernhuber (1982).

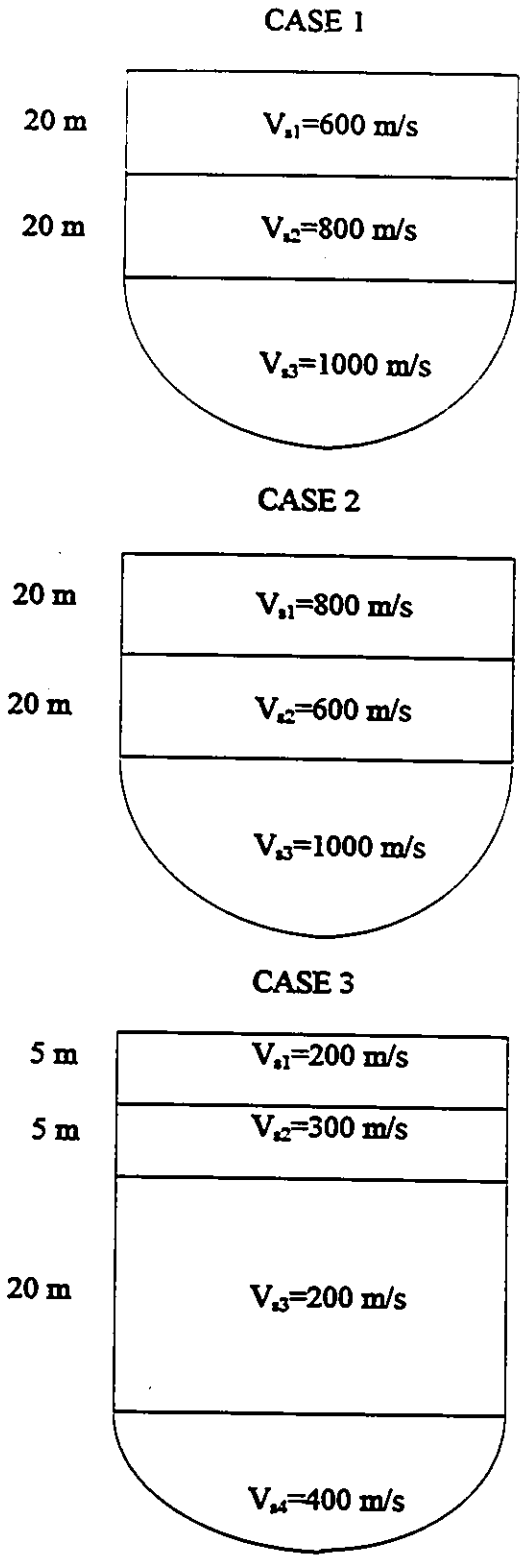

Fig. 4.7-Analyzed soil profiles.

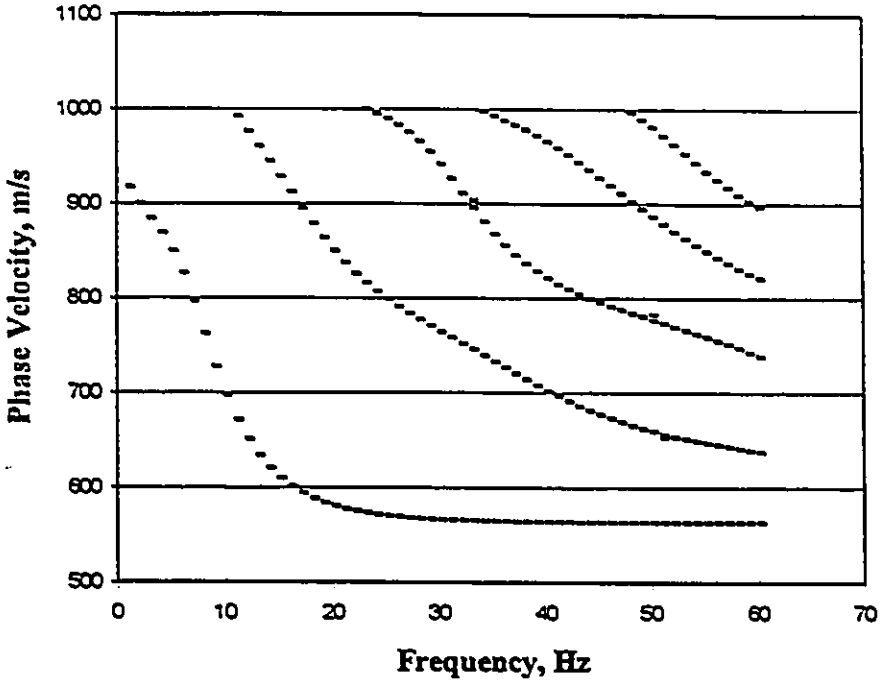

(a)

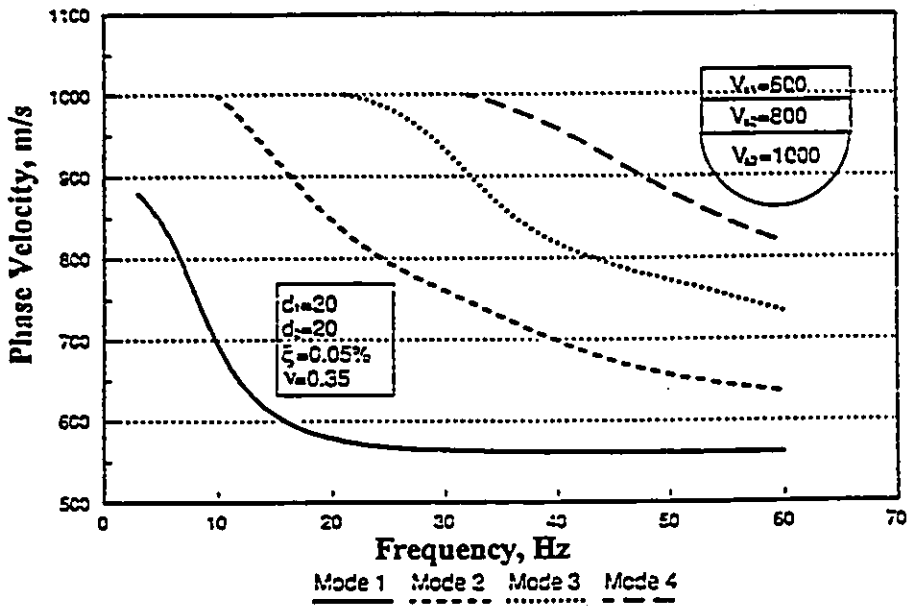

(b)

Fig. 4.8-DISPERSION CURVE FOR CASE 1 (a) from developed program, (b) from Gucunski (1991).

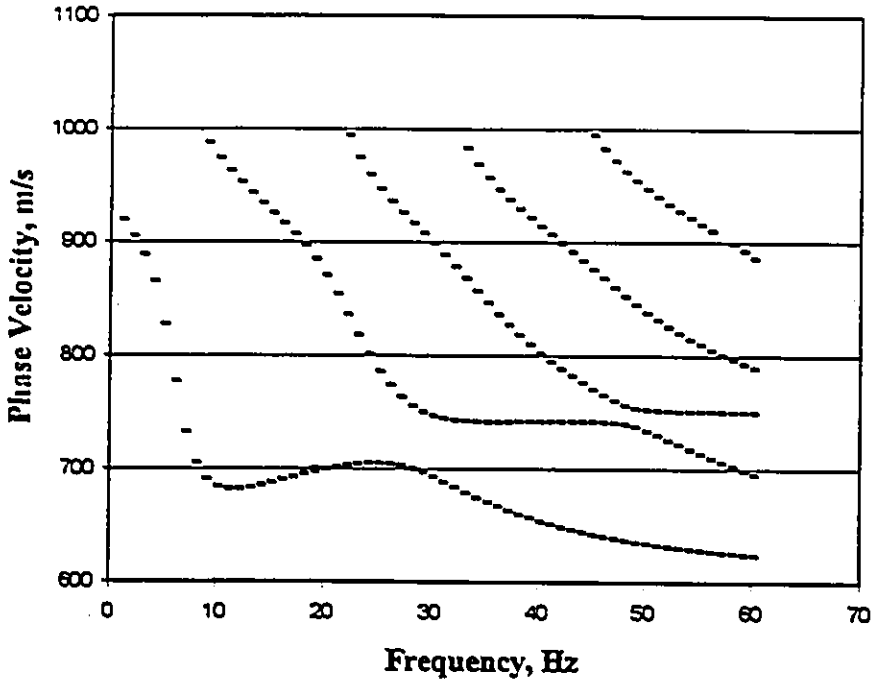

(a)

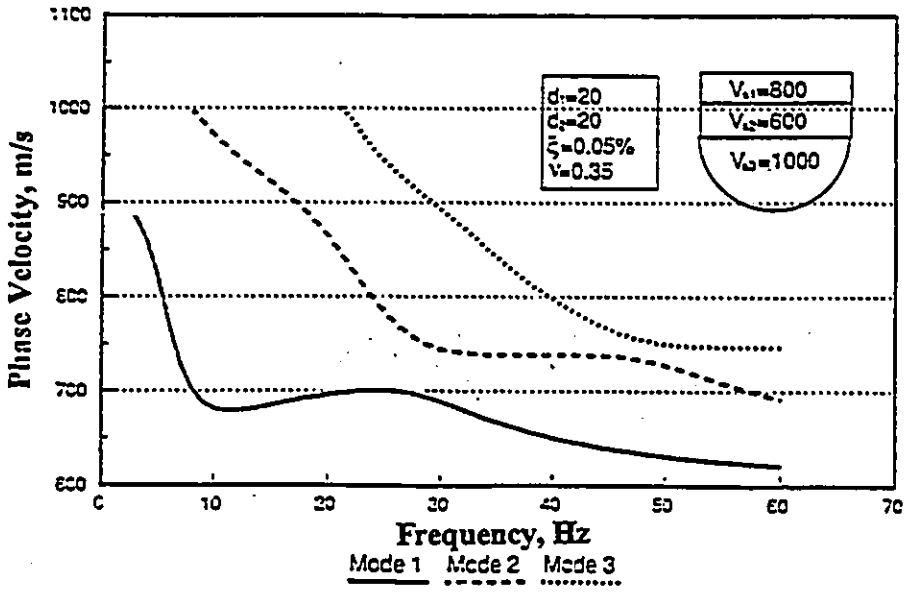

(b)

Fig. 4.9-DISPERSION CURVE FOR CASE 2 (a) from developed program, (b) from Gucunski (1991).

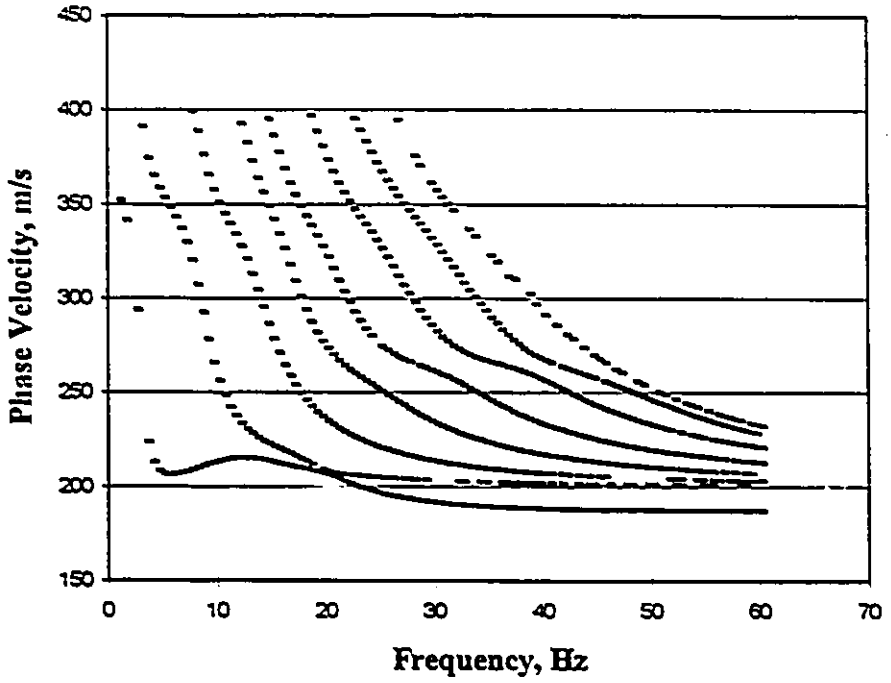

(a)

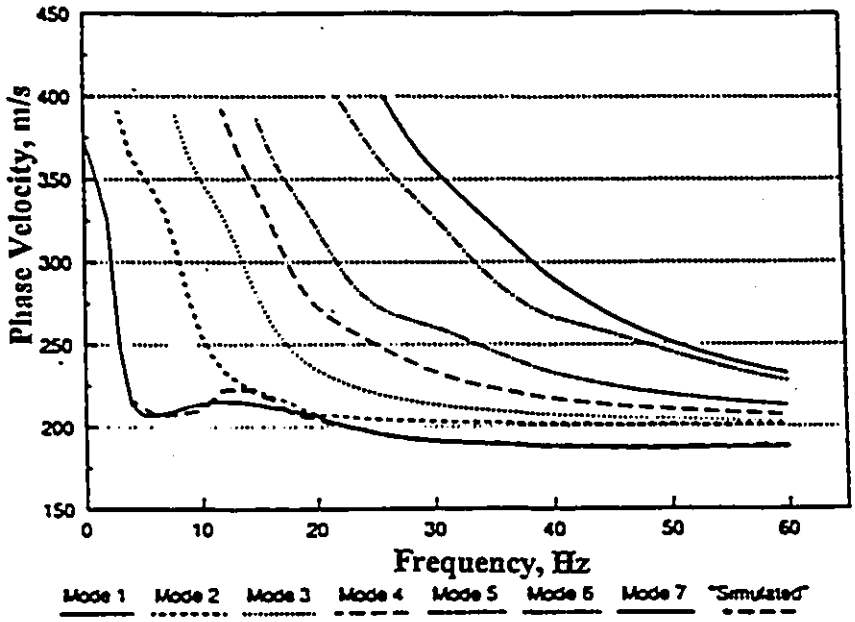

(b)

Fig. 4.10-DISPERSION CURVE FOR CASE 3 (a) from developed program, (b) from Gucunski (1991).

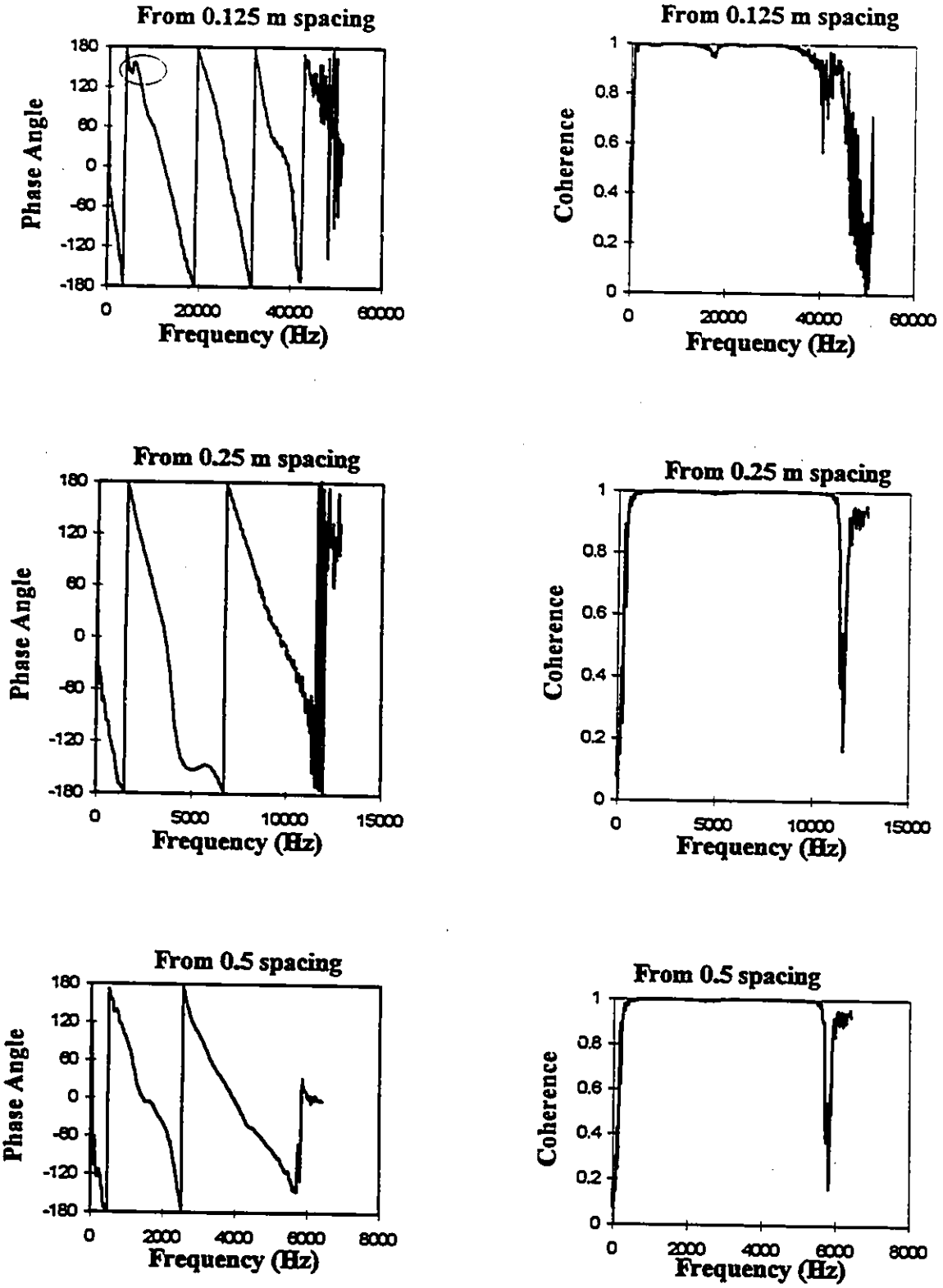

Fig. 4.11-Relative Phase angle spectra and Coherence function for different spacings.

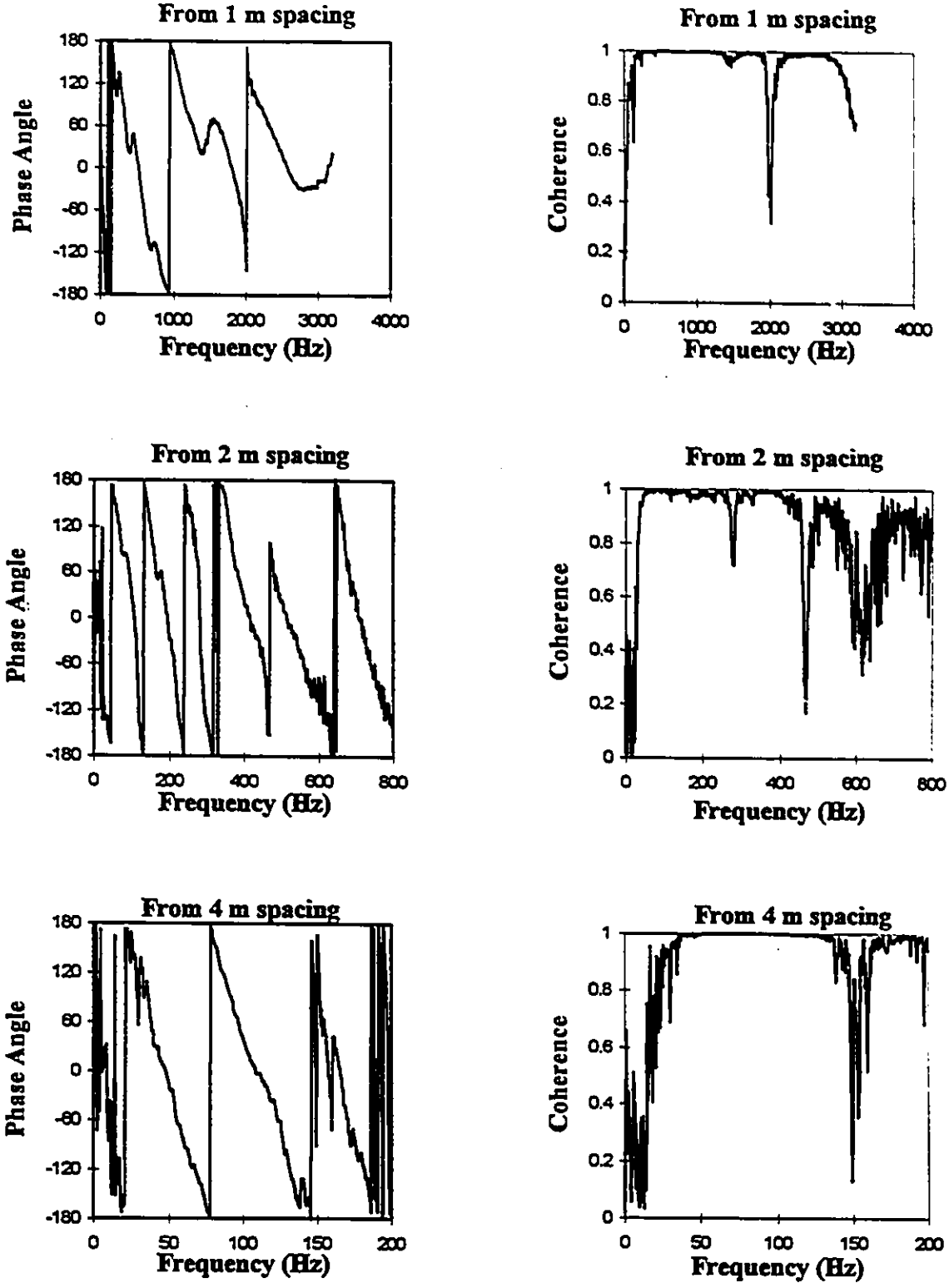

Fig. 4.11-Relative Phase angle spectra and Coherence function for different spacings (continued).

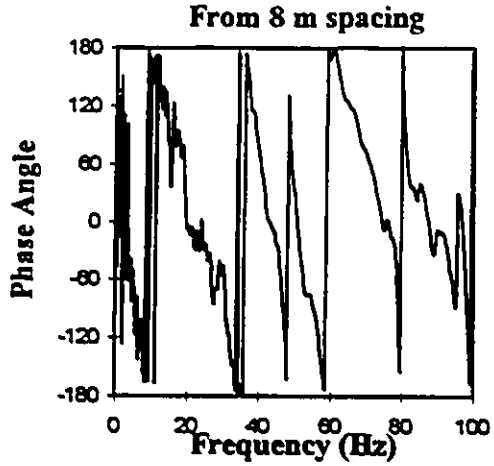

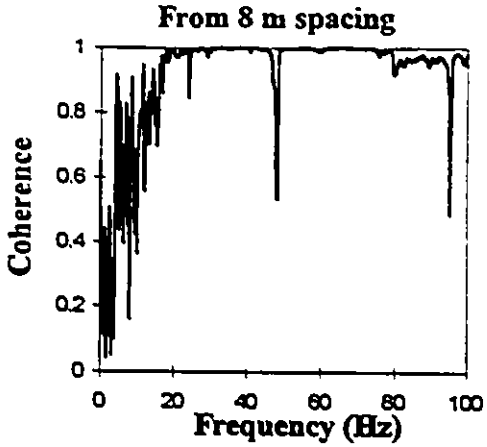

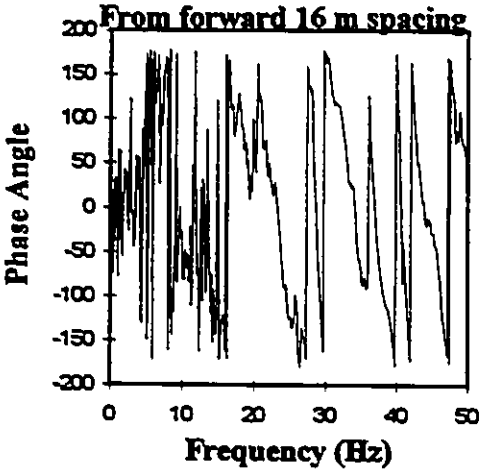

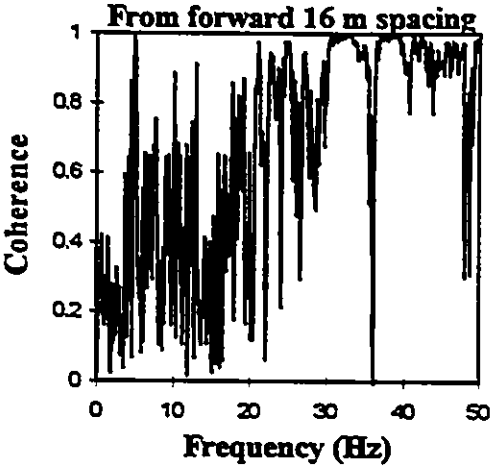

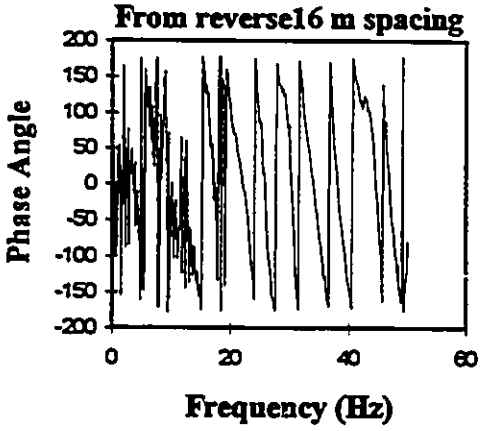

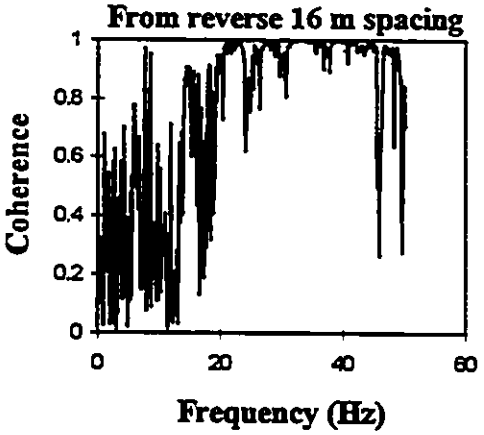

Fig. 4.11-Relative Phase angle spectra and Coherence function for different spacings (continued).

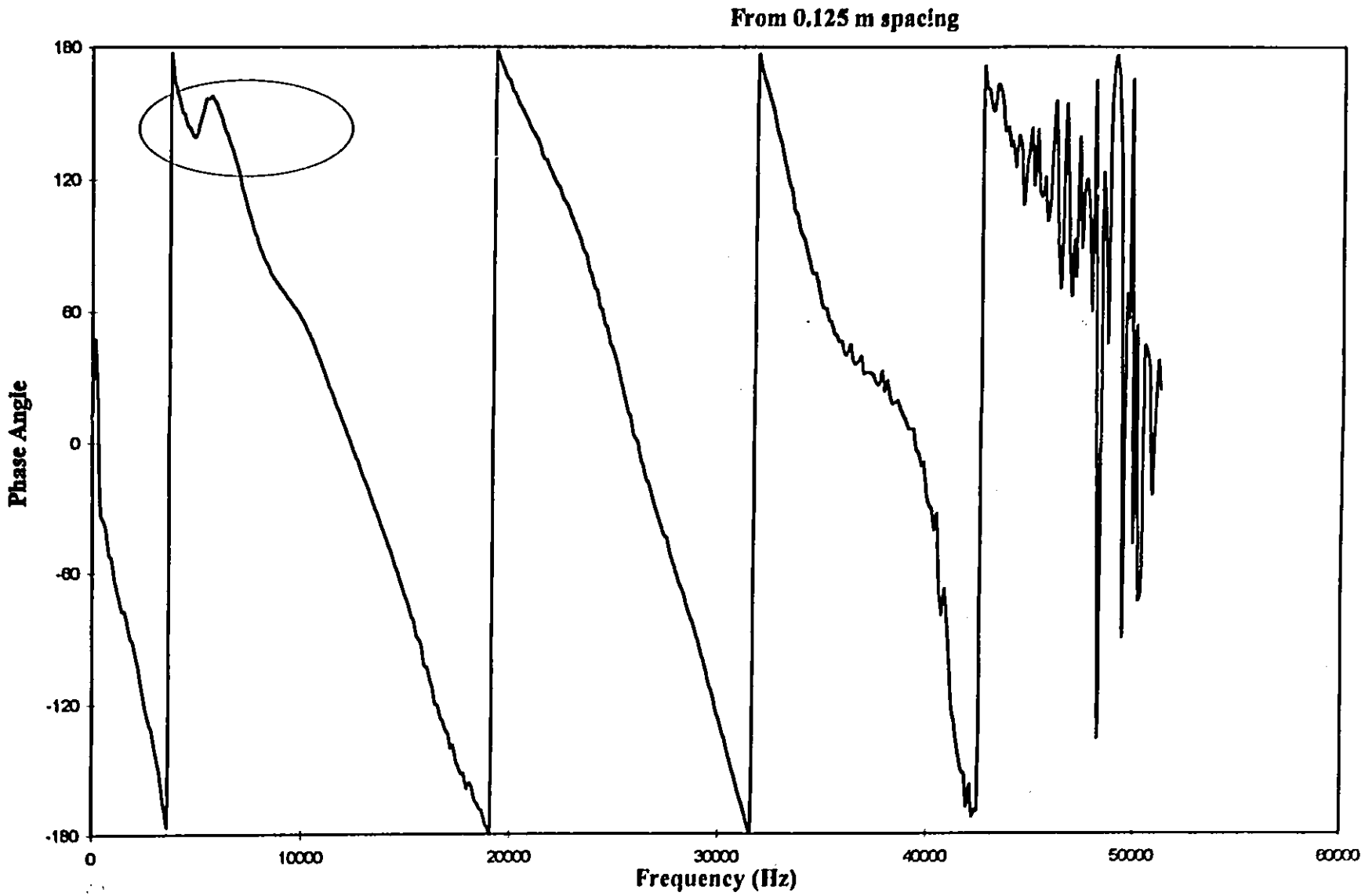

Fig.4.11-Relative Phase angle spectra and Coherence function for different spacings (continued).

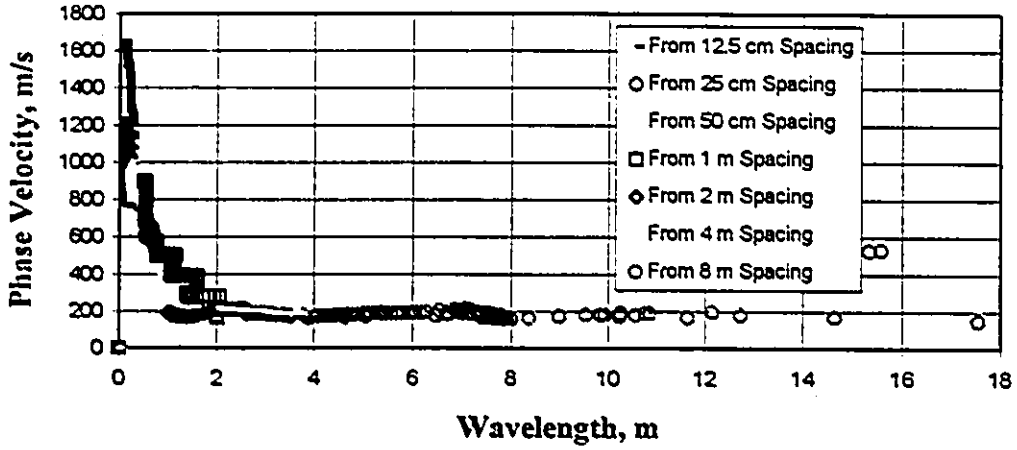

Fig. 4.12a-Dispersion Curve based on Heisey et al. Criterion.

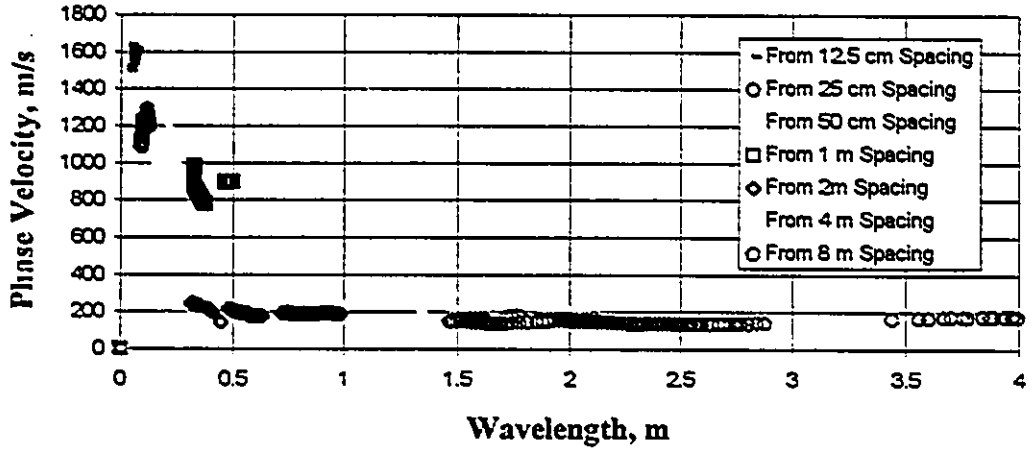

Fig. 4.12b-Dispersion Curve based on Sanchez-Salinero et al. Criterion.

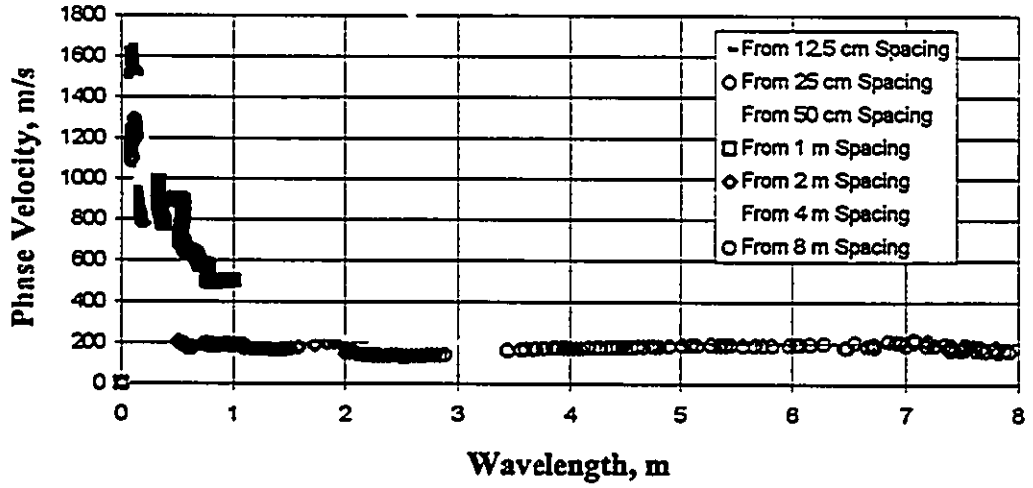

Fig. 4.12c-Dispersion Curve based on Gucunski & Woods Criterion.

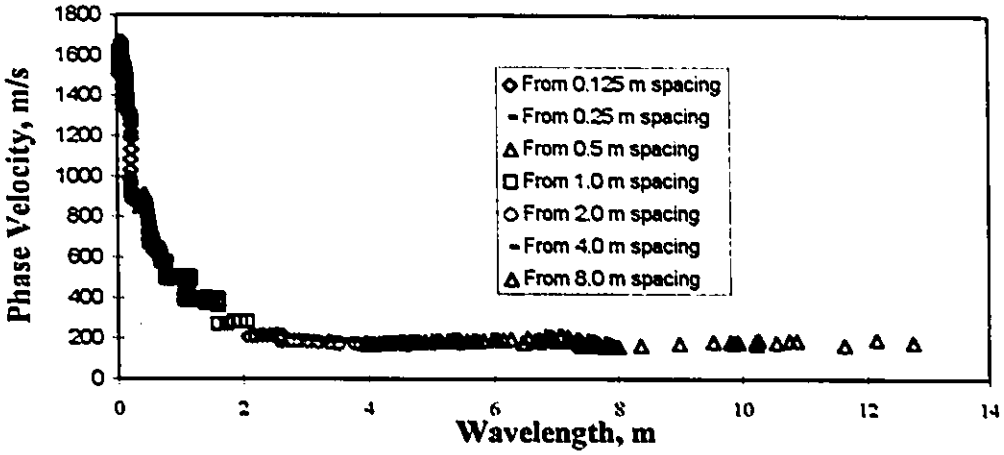

Fig. 4.13-Field Dispersion Curve.

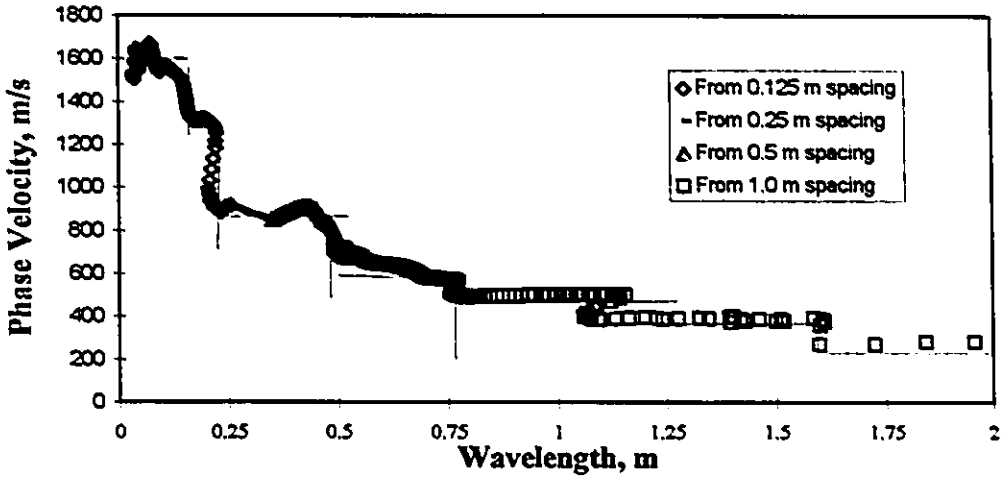

Fig. 4.14a-Field Dispersion Curve divided into layers (0-2 m).

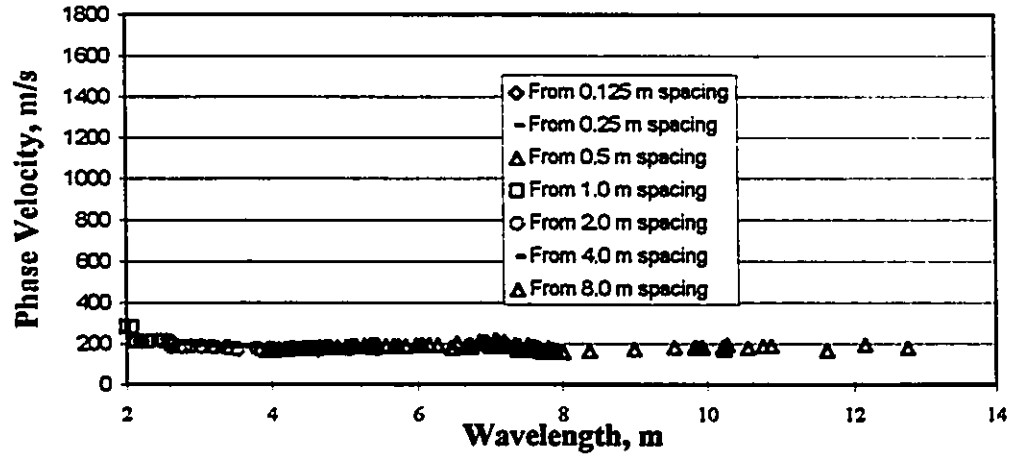

Fig. 4.14b-Field Dispersion Curve divided into layers (2-14 m).

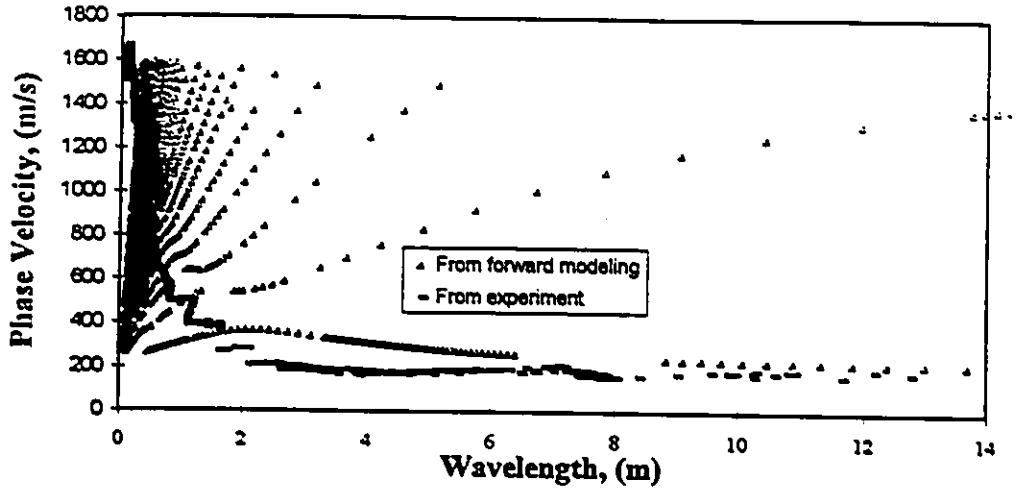

Fig. 4.15-Inversion process (first modeling).

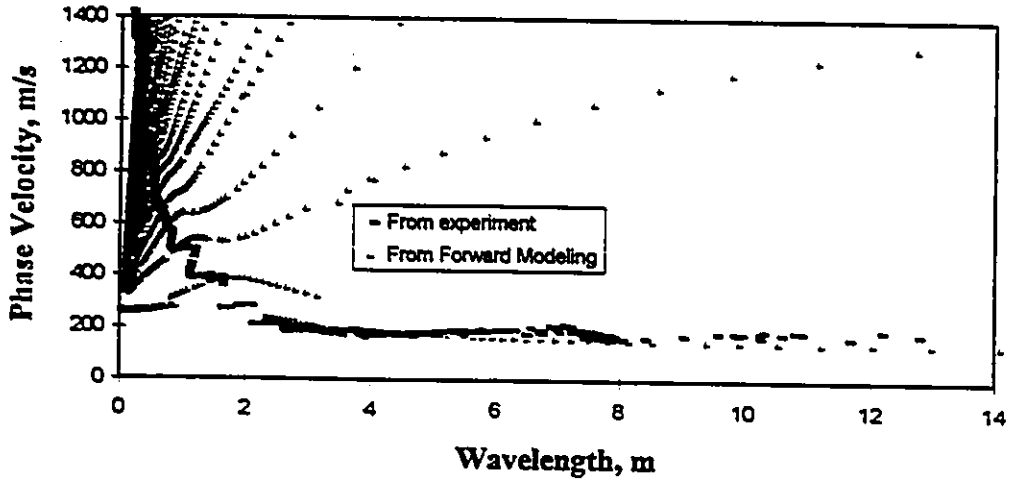

Fig. 4.16-Inversion process (final modeling).

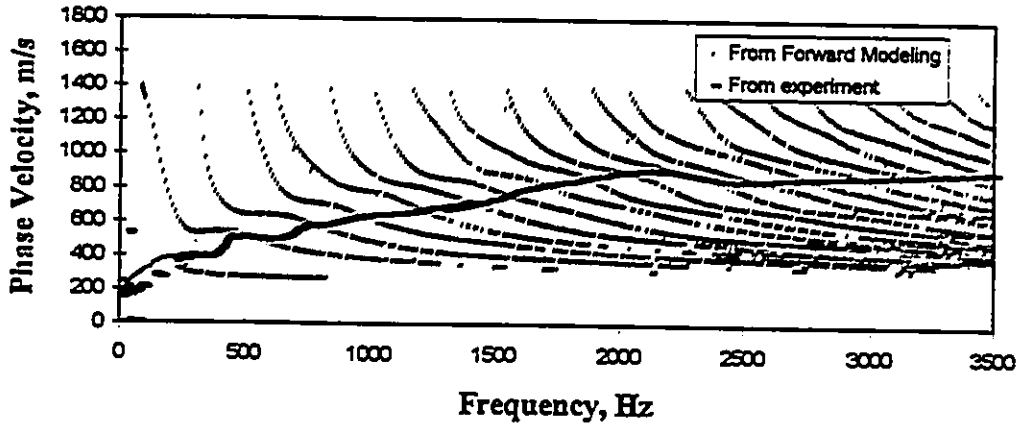

Fig. 4.17-Dispersion Curve.

CHAPTER 5

NUMERICAL SIMULATION OF THE SASW TEST

5.1 Introduction

Surface wave tests are simulated by applying a harmonic load on the surface of the soil layer or pavement. Simulation of SASW tests involves the solution of an axisymmetric wave propagation problem in which the source is represented by a disk load on the surface of a layered soil system (Fig. 5.1).

As stated in Chapter 4, Section 4.2.2, the mathematical formulation of wave propagation in a layered system as used in this study is based on the stiffness matrix approach. In this approach, the external forces that are applied at the layer boundaries are related to the their displacement through a stiffness matrix. The stiffness matrix is function of both frequency and wave number. For a soil system consisting of several layers, the stiffness matrices of individual layers are assembled, in a fashion similar to that in structural analysis, to form the global stiffness matrix [K]. The global stiffness matrix relates

displacements {u} to external forces {P} in the frequency-wave number domain as follows:

$$[K]\{u\} = \{P\} \qquad [5.1]$$

5.2 Transformation of Loading into Frequency-Wave number Domain

To find the solution for arbitrary loads using Eq. 5.1, the loads need to be transformed from the spatial coordinate domain to the frequency-wave number domain. In axisymmetric loading, a common procedure is to expand the loading function in terms of Fourier series in the circumferential direction θ (n=0, 1, ...) and in terms of Bessel functions in the radial direction r. This transformation can be written as:

$$q(k,n) = a_n \int_{r=0}^{\infty} r\, C_n(kr) \int_{\theta=0}^{2\pi} D(n\theta) P(r,\theta) d\theta dr \qquad [5.2]$$

Where

$$a_n = \begin{Bmatrix} \frac{1}{2\pi} & \text{for } n=0 \\ \frac{1}{\pi} & \text{for } n \neq 0 \end{Bmatrix} \qquad [5.3]$$

P(r,θ) equals loading vector in the spatial domain with components in the radial, tangential and vertical direction, and q(k,n) equals loading vector in the frequency-wave number domain. In the symmetric case:

$$D(n\theta) = \begin{vmatrix} |\cos(n\theta)| & & \\ & |-\sin(n\theta)| & \\ & & |\cos(n\theta)| \end{vmatrix} \qquad [5.4]$$

And for an antisymmetric case

$$D(n\theta) = \begin{vmatrix} |\sin(n\theta)| & & \\ & |\cos(n\theta)| & \\ & & |\sin(n\theta)| \end{vmatrix} \qquad [5.5]$$

and

$$C_n(kr)=\begin{vmatrix} \frac{1}{k}\frac{\partial J_n(kr)}{\partial r} & \frac{n}{kr}J_n(kr) & 0 \\ \frac{n}{kr}J_n(kr) & \frac{1}{k}\frac{\partial J_n(kr)}{\partial r} & 0 \\ 0 & 0 & -J_n(kr) \end{vmatrix} \qquad [5.6]$$

Where $J_n(kr)$ is the Bessel function of the first kind of order n. In the axisymmetric case, coordinate θ and the corresponding displacement v can be eliminated. Considering a uniform vertical circular loading with intensity of p_o and radius R_o, the corresponding loading in wave number domain for which only the zeroth symmetric Fourier term (n=0) need to be considered, can be written as

$$q_o(k)=-\frac{1}{2\pi}\int_{r=0}^{R} rJ_o(kr)\int_{\theta=0}^{2\pi} P_o\,d\theta\,dr \qquad [5.7]$$

$$=-P_o\int_{r=0}^{R} rJ_o(kr)\,dr \qquad [5.8]$$

The following two identities of the Bessel functions are used:

$$\left[x^n J_n(x)\right]_x = x^n J_{n-1}(x) \qquad [5.9]$$

which in integral form is equal to

$$\int x^n J_{n-1}(x)\,dx = x^n J_n(x)+\text{constant} \qquad [5.10]$$

and

$$\left[x^{-n} J_n(x)\right]_x = -x^{-n} J_{n+1}(x) \qquad [5.11]$$

Using Eq. 5.11, Eq. 5.8 is formulated as

$$q_o(k)=-\frac{P_o R_o}{k}J_1(kR_o) \qquad [5.12]$$

5.3 Determination of Vertical Flexibility Coefficient

For the axisymmetric case, only u and w displacement components exist. The displacements u(k) and w(k) in the frequency-wave number domain can be obtained by solving Eq. 5.1 for the loading vector q(k). The loading vector q has only one nonzero component, the vertical component at the surface q_o, given by Eq. 5.12.

The displacement amplitudes at the surface can be expressed in terms of flexibility coefficients as

$$\begin{Bmatrix} u(k) \\ w(k) \end{Bmatrix} = \begin{Bmatrix} F_{uw} \\ F_{ww} \end{Bmatrix} q_o(k) \qquad [5.13]$$

Where F_{uw} and F_{ww} are elements of $[k]^{-1}$ that are condensed at the surface.

5.4 Computer Program for Vertical Flexibility Coefficient

A program was developed for finding vertical flexibility coefficients F_{ww}. This program was written in Fortran language. First the stiffness matrix of the each layer is constructed (see section 4.2.2). Then for a soil system consisting of several layers, the global stiffness matrix is constructed by overlapping the contribution of the layer matrices at each node (interface) of the system. The program calculates the flexibility coefficient in the wave-number domain by inverting the stiffness matrix.

The program was verified for several cases. The first verification of the program was done by finding the vertical-flexibility coefficient for a layer of thickness d over half-space (see Fig. 5.2). The shear wave velocity of the half space is twice that of the layer. Poisson's ratio equals 0.33 for both layer and half-space. The dimensionless frequency ($\omega d/Vs$, Vs: shear wave velocity of a layer, and ω: circular frequency) of 7 and damping ratio of ξ=0.001 are selected. The vertical flexibility coefficient in the k-domain is plotted as a function of the dimensionless wave number kd in Fig. 5.3. The real and

imaginary parts at four distinct numbers, exhibit sharp peaks, where the real part changes sign. The same site was reported by Wolf and Darbre, 1983 (see Fig. 5.4).

The second case is two layers over half-space as shown in Fig. 5.5. The shear-wave velocity of the first layer is 800 m/s, the second layer 600 m/s, and the shear wave velocity of the half space is 1000 m/s. Poisson's ratio equals 0.35. Frequency of 40 Hz and damping ratio of ξ=0.0005 were selected. The vertical-flexibility coefficient in the k-domain is plotted as a function of the wave number k (see Fig. 5.6). Again, the real and imaginary parts at several distinct numbers, exhibit sharp peaks, whereby the real part changes sign. The vertical flexibility for the same site that was reported by Gucunski and Woods, 1992 is shown in Fig. 5.7.

The peaks of vertical flexibility coefficient correspond to different modes of surface wave propagation. The peak with the largest amplitude corresponds to the predominant mode of propagation. The importance of these coefficients in the SASW analysis will be explained in Chapter 6.

5.5 Determination of Displacements In Spatial Domain

To obtain the displacements in the spatial domain, inverse Hankel transform is applied to displacements in the wave number domain. The relation for this operation is

$$U_s(r,\theta) = \sum_{n=0}^{\infty} D(n\theta) \int_{k=0}^{\infty} kC_n(kr)U_w(k,n)dk \qquad [5.14]$$

Where U_s is the displacement vector in the spatial domain and U_w the displacement vector in the wave number domain. In axisymmetric, case only u and w displacements exist and therefore, the second row and column of matrices D and C_n can be eliminated. Surface displacements in spatial domain (u_s, w_s) can be found in term of displacements in the wave number domain by the following relation:

$$\begin{Bmatrix} u_{\infty}(r) \\ w_{\infty}(r) \end{Bmatrix} = \int_{k=0}^{\infty} \begin{bmatrix} \frac{\partial J_0(kr)}{\partial r} & 0 \\ 0 & -kJ_{0(kr)} \end{bmatrix} \begin{Bmatrix} u_o(k) \\ w_0(k) \end{Bmatrix} dk \qquad [5.15]$$

Only the vertical surface displacement is of interest in SASW tests. It can be obtained by making use of the identity of Eq. 5.9 and substituting Eq. 5.12 leading to

$$w_{\infty}(r) = -\int_{k=0}^{\infty} kJ_0(kr)w_o(k)dk \qquad [5.16]$$

Combining Eq. 5.12 and 5.17

$$w_{\infty}(r) = -p_o R \int_{k=0}^{\infty} J_1(kR_o)J_o(kr)w_o(k)dk \qquad [5.17]$$

Knowing the surface vertical displacement, the wave length of the simulated dispersion curve can be evaluated by two ways. The first method evaluates an average wavelength from the displacement curve at each particular frequency (see Fig. 5.8). This procedure should be repeated for a set of frequencies. The second method evaluates the transfer function H(f) between two prescribed points representing receiver locations at each frequency. The transfer function as described in Section 2.9.8, is the ratio of the spectrum of the far receiver to the spectrum of the near receiver. Then the phase difference between these two prescribed points is easily evaluated. Knowing the phase difference, the phase velocity, and the wavelength can be calculated using Equation 3.4 through 3.6.

5.5.1 Computer Simulation of the SASW Test

To perform the simulation of SASW test, a computer program was developed. The program calculates the exact flexibility coefficient in the wave number domain by inverting the stiffness matrix. Then using numerical integration, Equation [5.17] is evaluated. The only approximation introduced in this procedure is the use of the

trapezoidal integration method. Errors due to this approximation are minimized by reducing the interval of integration. The program has the capability of considering layered system in three different ways:

1-layered system over half-space;

2-layered system over fixed base;

3-layered system over free base;

5.5.2 Verification of the Simulation Program

The program was tested using several cases. The first verification of the program was done by finding the vertical flexibility-influence function w(s) for the two sites for which the vertical-flexibility coefficient was calculated in the previous section. The vertical-flexibility-influence function w(s) for one layer over half-space system having a disk load with radius $R_o = 0.0705*d$ was calculated. Fig. 5.9 shows w(r) as a function of r/d. The vertical-flexibility influence function for the same site reported by Wolf and Darbre (1983) is shown in Fig. 5.10.

Fig. 5.11 shows the vertical flexibility-influence function w(s) for a disk load with radius $R_o = 1$ m, w(r) for site 2 as a function of r. The same site was reported by Gucunski and Woods (1992) for which the vertical-flexibility coefficient and vertical flexibility-influence function are shown in Fig. 5.12.

The second case is the numerical simulation of a pavement site for which experimental results were reported by Jones (1962). The site consists of an asphalt layer, nominally 10 cm thick, overlying a sand sub-base, nominally 40 cm thick. The subgrade is a 7.50 m thick clay. Other material properties used in the computer simulation are given in Table 5.1. The analysis is performed for frequencies in the range from 2 to 500 Hz. The excitation frequencies are increased by increments of 2 Hz. Phase angle spectra are generated for several receivers spacings usually used in SASW tests. Simulated relative phase angle spectra for 0.5, 1.0, and 2.0 m receiver spacings are shown in Fig. 5.13. The

simulation of same site using the discrete layer stiffness matrix method was reported by Al-Hunaidi (1993). In this approach the pavement, sublayer, and the supporting soil are considered to be horizontally unbounded in all direction. The layered pavement system under the action of a harmonic surface load is discretized as shown in Fig. 5.14. Then this system is modeled by frequency-dependent dynamic stiffness matrix of nodal points in Fig. 5.14. The matrix is obtained by means of the discrete layer stiffness matrix approach developed for site resting on a rigid base by Waas (1972) and Lysmer and Waas (1972) and Lysmer and Drake (1972) and Watkins et al. (1974). The layered system is discretized into thin layers having small thickness in comparison to the wave lengths of interest. By using standard finite element procedures, the stiffness and mass matrices for each layer are then derived and assembled to form global matrices of the complete layered system. The transcendental coefficients of layer stiffness matrices are expanded using Taylor's series in terms of the wave number k keeping only terms up to second degree which is an acceptable estimation when ktd is small.

$$\sin ktd = ktd - \frac{k^3 t^3 d^3}{6} \qquad [5.18]$$

$$\cos ktd = 1 - \frac{k^2 t^2 d^2}{2} \qquad [5.19]$$

Therefore, this substitution leads to non-transcendental quadratic eigenvalue problem. The wave numbers and mode shapes of all waves that can propagate in the layered medium for a particular frequency are determined by solving an algebraic eigenvalue problem resulting from imposing the condition of no external forces in the discretized equations of motion and assuming a rigid base. The wave number corresponding to the waves that propagate in the desired direction are then selected. By expanding displacements in the layered system using the modal shapes corresponding to the selected wave numbers, the dynamic stiffness matrix relating nodal forces and displacement in Fig. 5.14 can then be derived by satisfying the equilibrium conditions. The motion at any point in the layered medium is then easily calculated using modal shapes and participation factors. A complete description of the discrete layer stiffness

matrix approach and its numerical implementation details can be found in the original work by Waas (1972).

The simulated relative phase angle spectra for same spacings from this approach are shown in Fig. 5.13.

The third verification of the program was done by finding simulated dispersion curve for the actual layered soil system reported by Nazarian and Desai (1993). The material properties used in the computer simulation are given in Table 5.2 and Fig. 5.15. The frequency range used in the analysis was from 0.1 to 520 Hz. The excitation frequencies from 0.1 to 50 Hz and from 51 to 520 were increased by increments of 0.1 and 1 Hz, respectively. Phase angle spectra are generated for 1, 2, 4, 8, 16, 32, 64 m receivers spacings. Simulated relative phase angle spectra for these receiver spacings are given in Fig. 5.16. The simulated dispersion curves for the site obtained with applying the different filtering criteria described in Section 3.3 are shown in Fig. 5.17. As explained in section 4.4.1.2, the available filtering criteria produce different dispersion curves. The dispersion curve for the site obtained with the filtering method proposed in this study is shown in Fig. 5.18. Fig. 5.19 shows the experimental dispersion curve reported by Nazarian and Desai (1993). This dispersion curve is obtained by the following procedures:

1) using a weighted least-squares best fit solution, estimate the phase at each frequency with a weighted function chosen based on coherence;
2) by knowing the phase at each frequency and distance between receivers, the corresponding phase velocity and wavelength are calculated;
3) the least-absolute value best-fit criterion is used to combine these raw data and construct the dispersion curve.

By comparing Fig. 5.18 and Fig. 5.19 one can conclude that the simple proposed filtering criteria yields a dispersion curve similar to the one obtained by Nazarian and Desai (1993) using cumbersome analysis procedures.

5.6 Summary and Conclusion

To evaluate the test and data analysis procedures of the SASW method, a computer program for simulation of actual tests was presented. The developed computer program for simulation is tested using several cases. Inversion procedure based on simulated dispersion curve involves substantial computation time. As the number of layers and frequency increases, computer storage and run-time requirement increase significantly. In addition it is demonstrated that usual source-to-receiver distance taken to be equal to the spacing between receivers and application of existing filtering criteria are insufficient to ensure the condition that the measured wave field is due to one predominant mode only for the considered site. The proposed filtering criteria overcomes this difficulty.

Table 5.1-Material properties of simulated pavement site.

Layer	Thickness (m)	Shear wave velocity (m/s)	Unit Weight (kN/m^3)	Poisson's ratio	Damping ratio
Asphalt	0.1	1570	22	0.333	0.02
Subbase	0.4	127	18.3	0.314	0.04
Subgrade	7.5	122	20	0.474	0.08

Table 5.2-Material properties of simulated layered soil site.

Layer	Thickness (m)	Shear wave velocity (m/s)	Unit Weight (kN/m^3)	Poisson's ratio	Damping ratio
Sandy Silt	3	110	20	0.45	0.05
Silty Clay	5	135	20	0.45	0.05
Sandy Silt	11	175	20	0.45	0.05
Sand	Inf	320	20	0.45	0.05

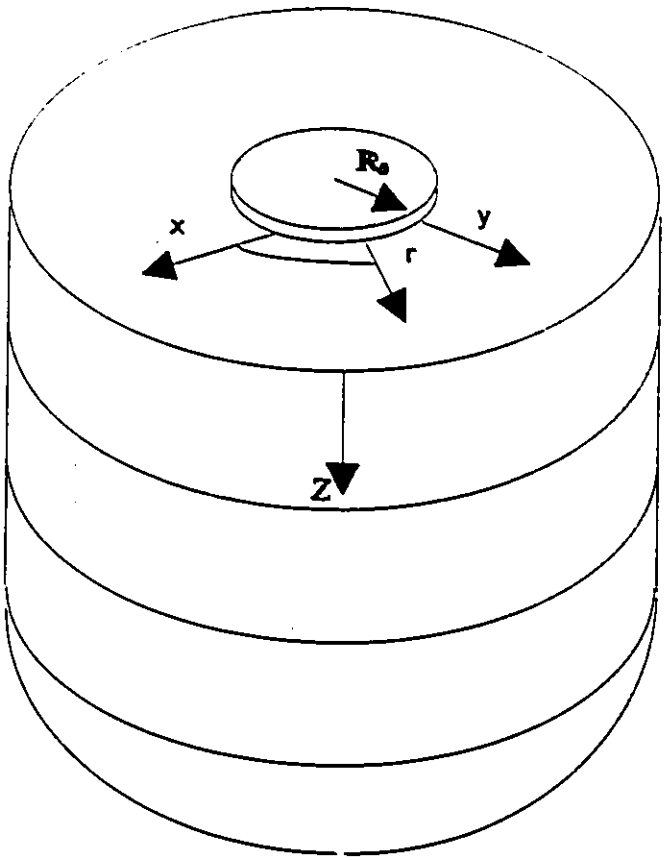

Fig. 5.1-An axisymmetric model of a soil system with circular loading.

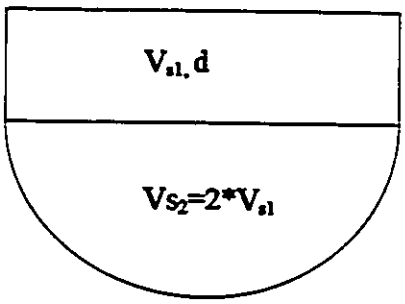

Fig. 5.2-Soil system.

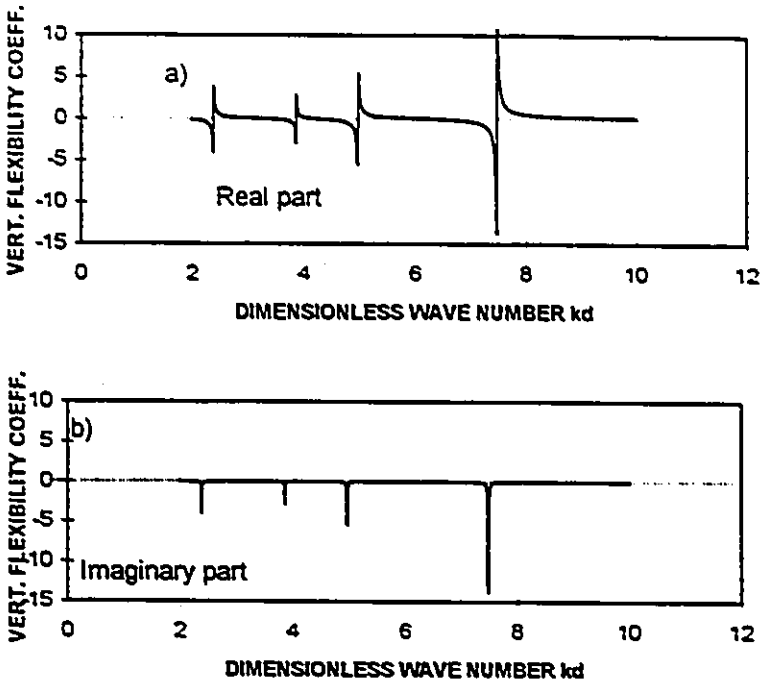

Fig. 5.3-Vertical flexibility coefficient in the wave-number domain (a) Real part; (b) imaginary part.

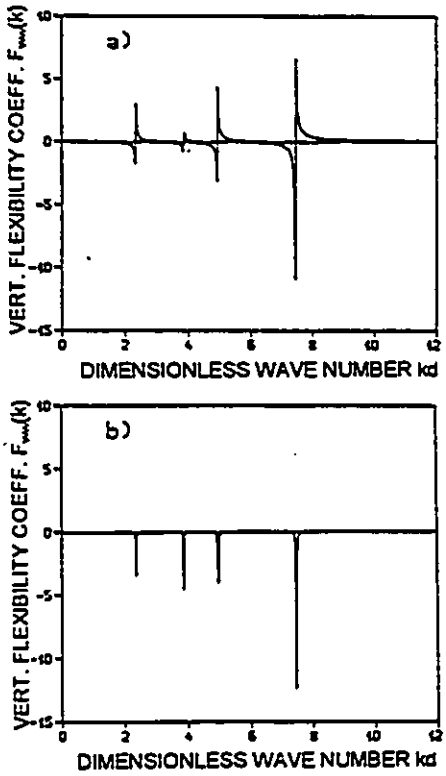

Fig. 5.4-Vertical flexibility coefficient in the wave-number domain (a) Real part; (b) imaginary part from Wolf et al. 1983.

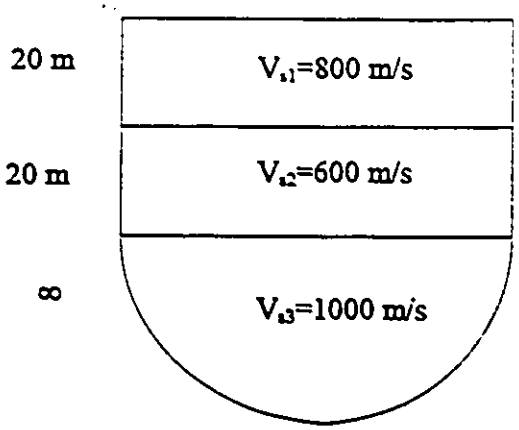

Fig.5.5-Soil profile

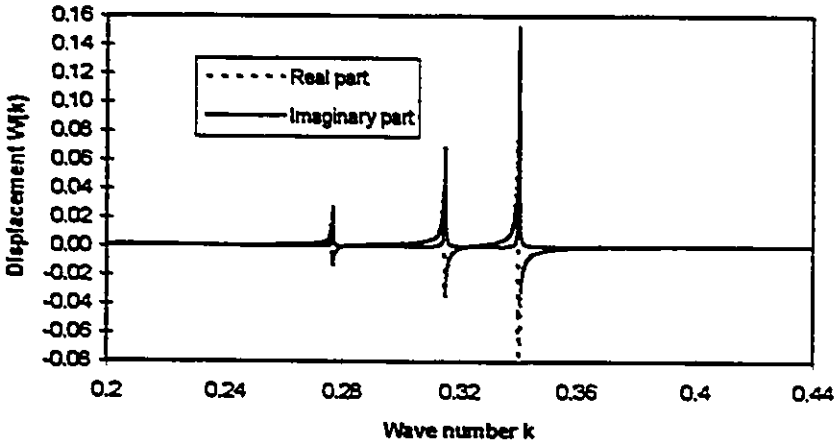

Fig. 5.6-Vertical flexibility coefficient in the wave-number domain at 40 Hz.

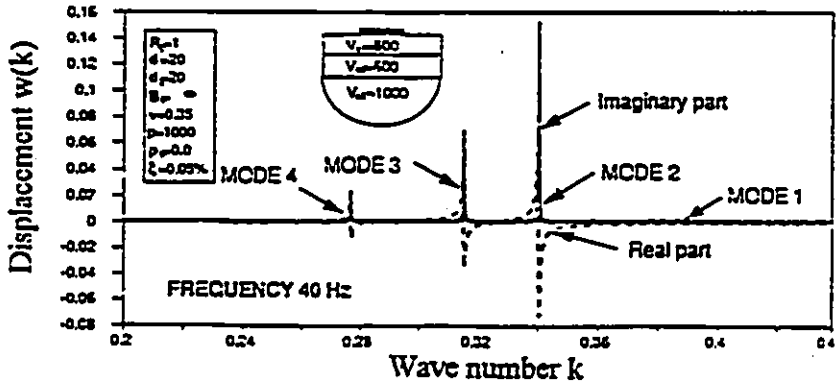

Fig. 5.7-Vertical flexibility coefficient in the wave-number domain at 40 Hz from Gucunski and Woods, 1992.

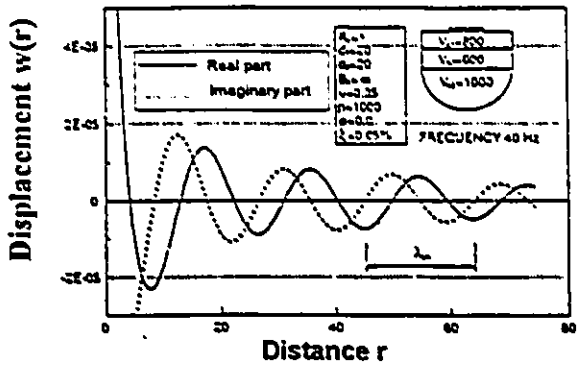

Fig. 5.8-Surface vertical displacements in the spatial domain and evaluation of the wavelength of the simulated dispersion curve (Gucunski and Woods, 1992).

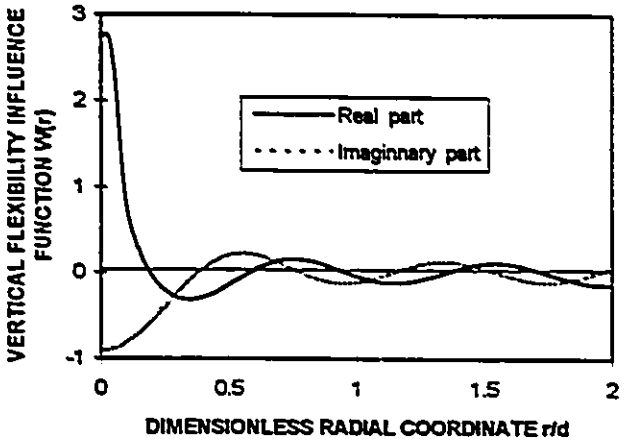

Fig. 5.9-Vertical flexibility-influence function.

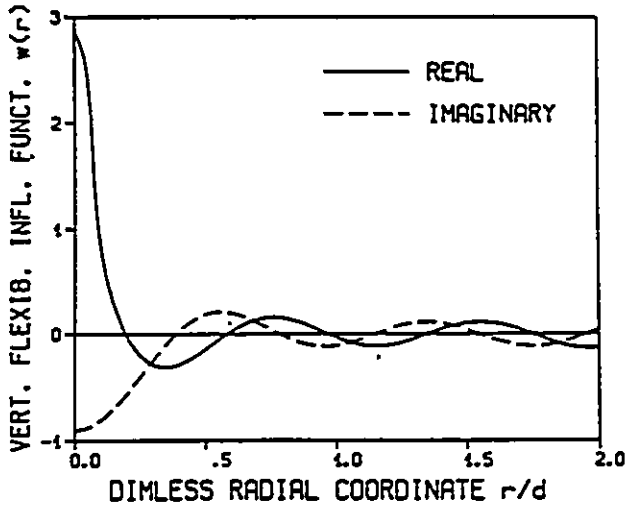

Fig. 5.10-Vertical flexibility-influence function from Wolf et al. 1983.

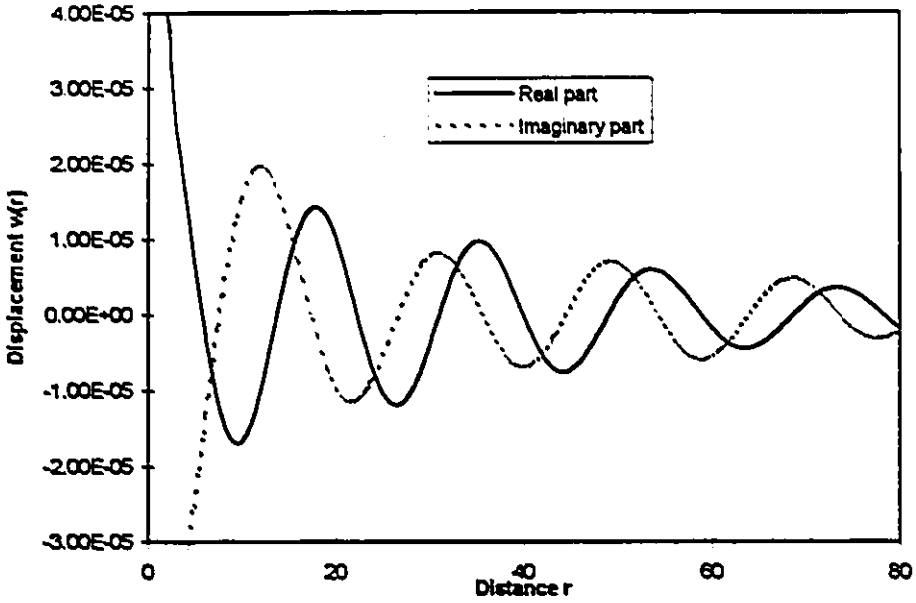

Fig. 5.11-Surface vertical displacement at 40 Hz.

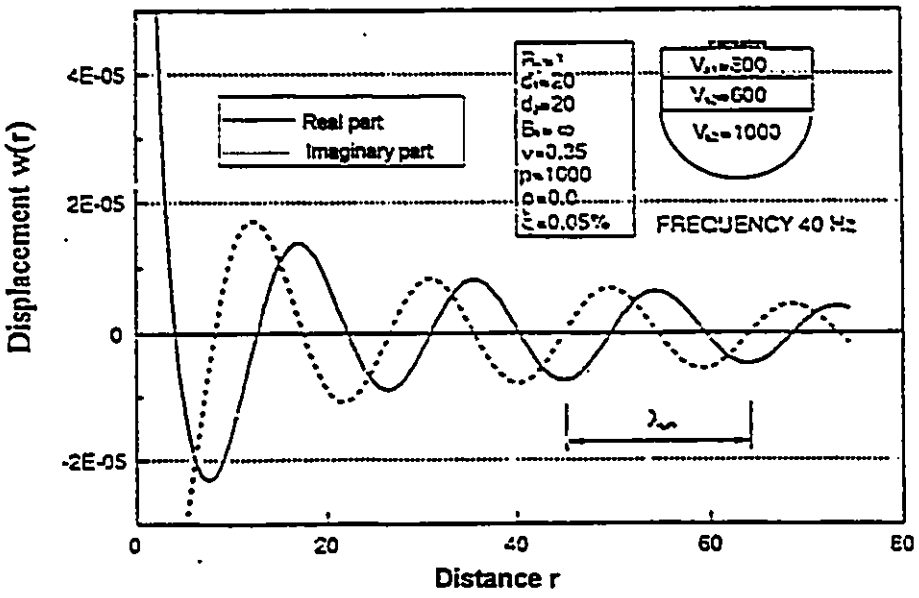

Fig. 5.12-Surface vertical displacement at 40 Hz from Gucunski and Woods, 1992.

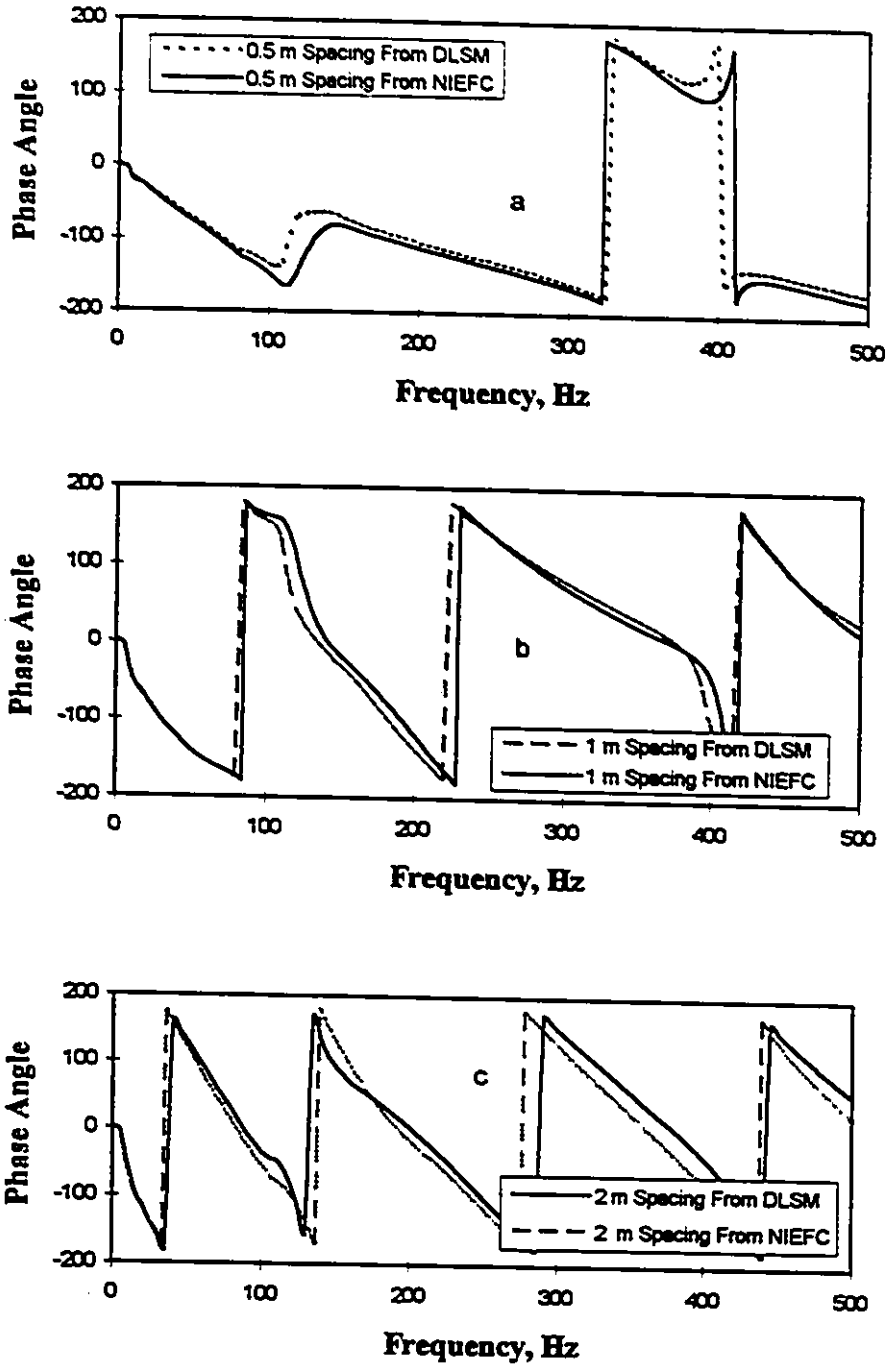

Fig. 5.13-Simulated relative phase angle spectra (in degrees) for various spacings:
(a) 0.5 m spacing, (b) 1 m spacing, and (c) 2 m spacing.
Source-to-near-receiver distance equals receiver spacing.
(DLSM: Discrete layer stiffness matrix approach,
NIEFC: Numerical integration exact flexibility coefficient approach)

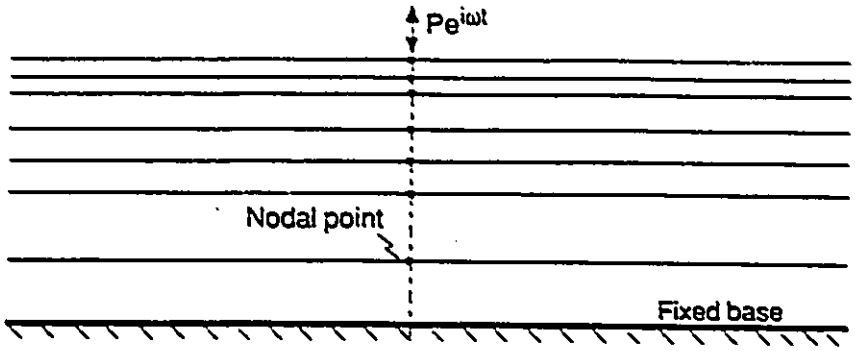

Fig. 5.14-Discretized model of pavement site.

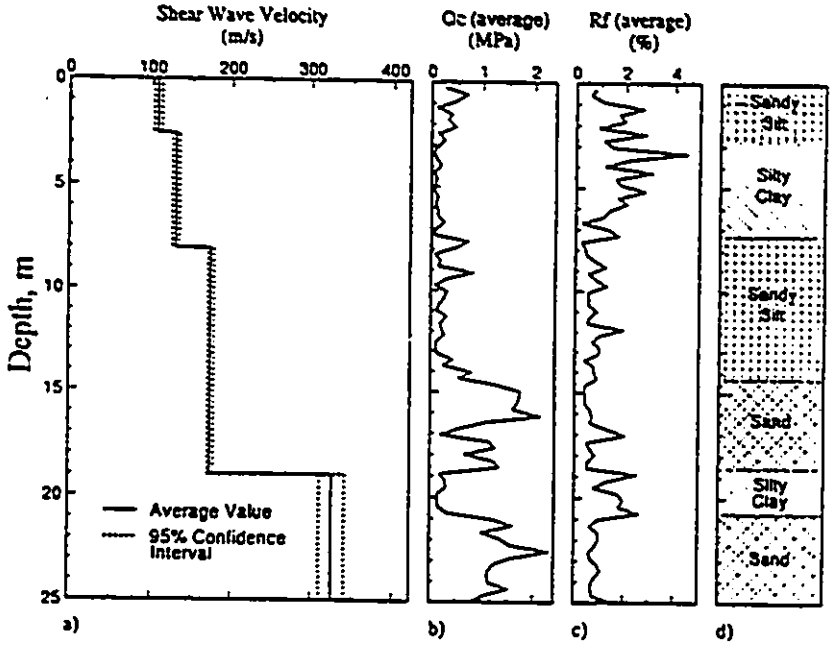

Fig. 5.15-Composite profile (from Yuan and Nazarian): (a) Stiffness profile; (b) Tip resistance; (c) Friction ratio; (d) Material profile.

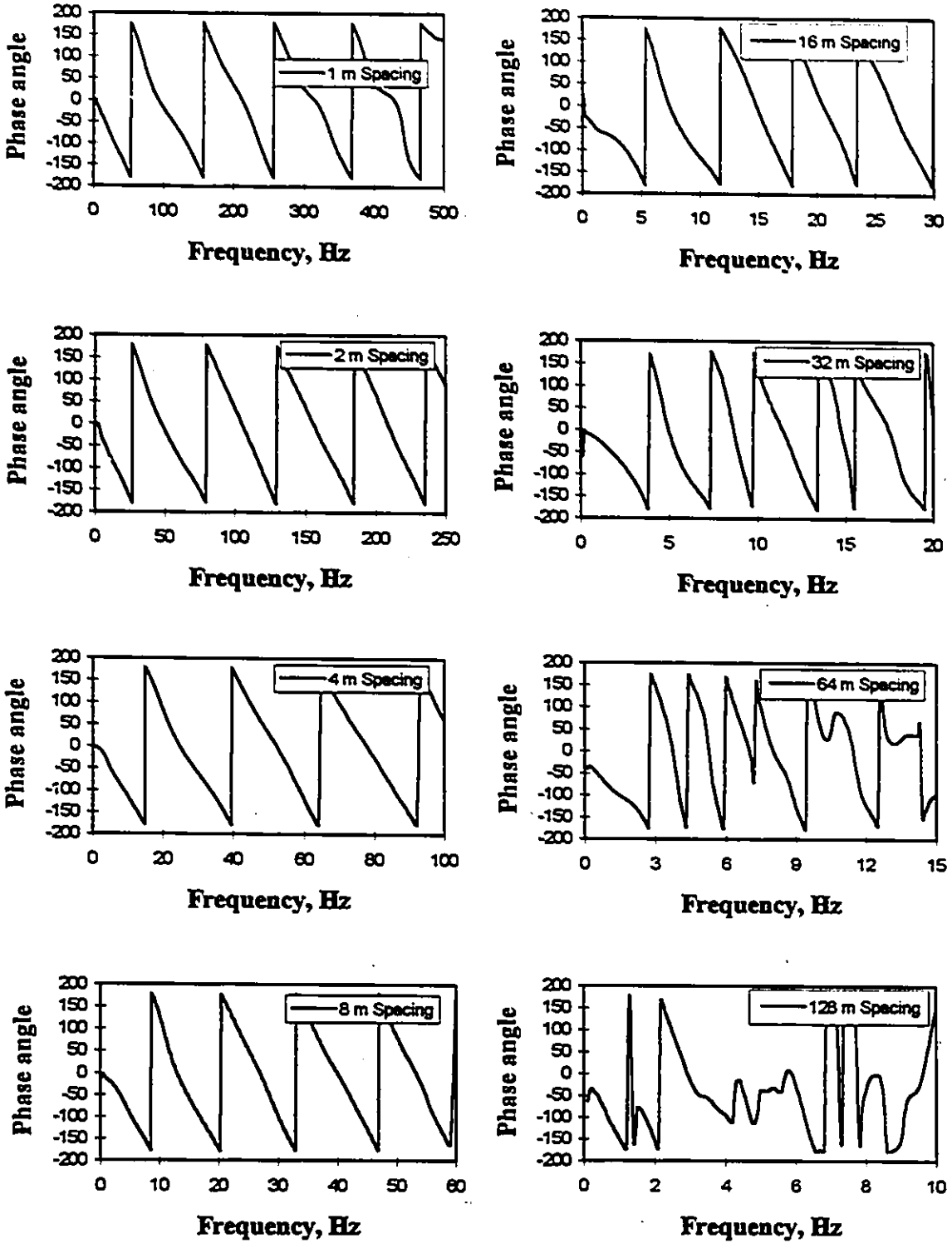

Fig. 5.16-Simulated relative phase angle spectra (in degrees) for various spacings. Source-to-near-receiver distance equals receiver spacing

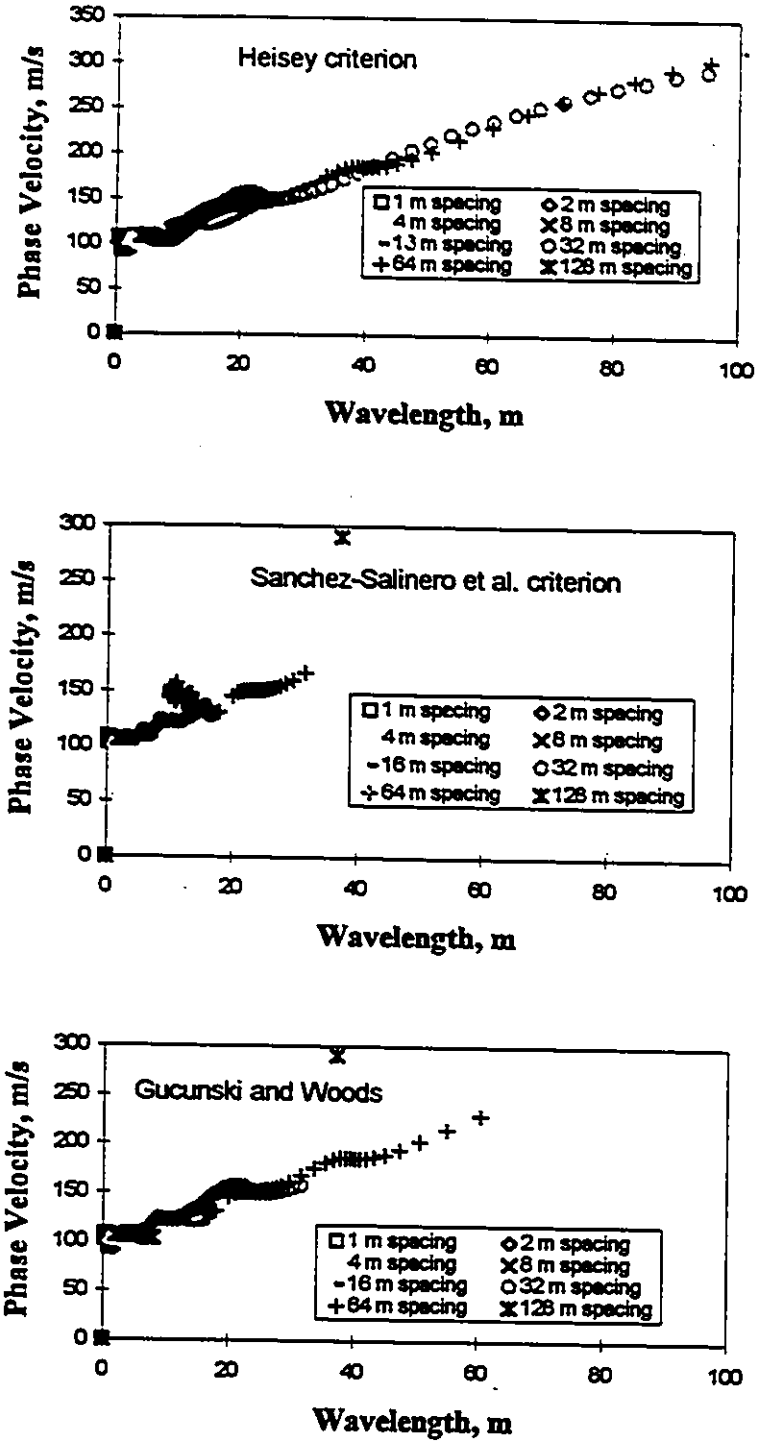

Fig. 5.17-Dispersion curves from available filtering criteria.

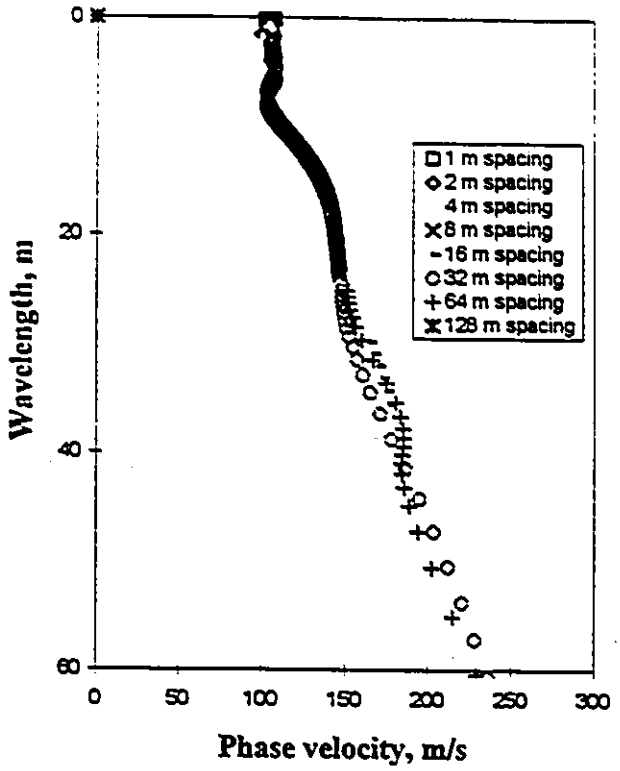

Fig. 5.18-Dispersion curve from proposed filtering criterion.

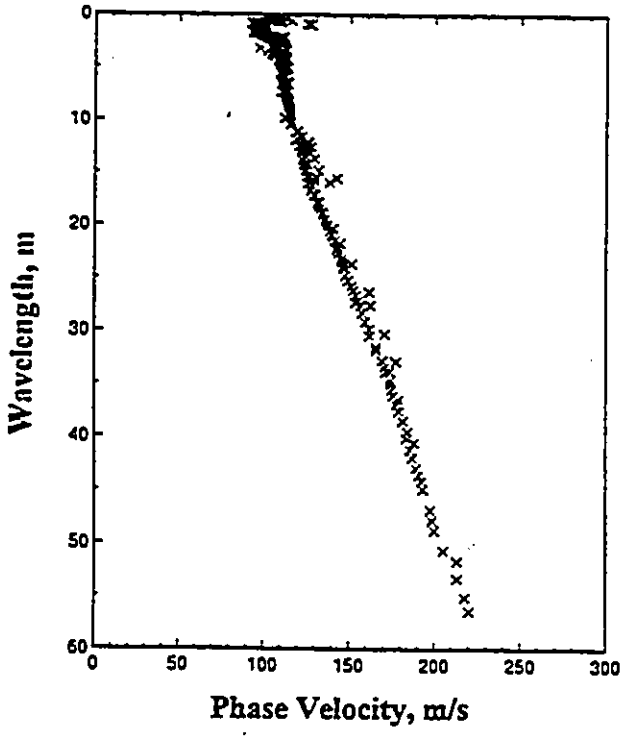

Fig. 5.19-Dispersion curve by Nazarian and Desai (1993).

CHAPTER 6

A NEW METHOD FOR CALCULATING THEORETICAL DISPERSION CURVES

6.1 Introduction

As explained in Section 3.4, the inversion procedures currently used for the SASW tests is based on forward modeling of the soil site. In these procedures, the field dispersion curve is compared with the theoretical dispersion curve obtained for the first mode of surface wave propagation. However, Rayleigh waves have different modes of propagation, thus different velocities at any frequency. The participation of each mode varies depending on soil stratification as well as frequency. Difficulties associated with these procedures were reported by Roesset et al. (1991), Sanchez-Salinero et al. (1987), and Gucunski and Woods (1991). They have shown that the use of the plane Rayleigh wave solution with the dispersion curve corresponding to the first mode of propagation is only suitable for soil deposits with gradual variation of properties. However, these procedures cannot reflect sudden jumps and discontinuities in the slope of the curve caused by wave reflection or refraction. Simulation of SASW tests is one remedy for this problem (Gucunski and Woods 1992; Roesset et al. 1991; and Tokimatsu et al. 1992). Using the multiple filter/crosscorrelation method is an alternative way (Al-Humaidi, 1994). Difficulties associated with applying both of these solution methods have been previously discussed.

In the absence of a reliable and simple method to separate the dispersion curves of the various modes in SASW signals, the following inversion method is introduced. This method has an advantage over existing methods in back calculating the correct profile of a site in comparison to the usual methods, since it has the ability to calculate the predominant mode at each frequency. The existing methods perform inversion by matching experimental dispersion points to theoretical dispersion points of the fundamental propagation mode. The proposed method, however, matches the experimental points to theoretical dispersion points corresponding to the predominant mode for the frequency being considered.

If the first mode happens to be the predominant mode at the site, the proposed method as well as existing methods will backcalculate the true profile. Otherwise, only the proposed method will be able to provide the true profile. The proposed method is presented next.

The determination of the vertical flexibility coefficients was described in Section 5.3. In order to show their use in the proposed inversion method, vertical flexibility coefficients are calculated here for two soil systems. The first soil system represents a regular soil profile where the shear wave velocity increases with depth (Fig. 6.1). The second soil system represents an irregular soil profile in which a soft layer is trapped between a harder layer and harder half-space (Fig. 6.2). The soil properties for both soil systems are presented in Table 1 and 2, respectively. The vertical flexibility coefficients calculated for soil system 1 in the frequency range of 10 to 60 Hz in increments of 10 Hz are shown in Fig. 6.3. The figures indicate that at distinct wave numbers, the real and imaginary parts of the vertical flexibility coefficients exhibit sharp peak, whereby the real part changes sign. Wave numbers where these peaks occur correspond to modes of surface waves in the layered system. Using the vertical flexibility coefficient, one can then calculate the theoretical dispersion curve as explained in next section.

6.2 Calculation of Phase Velocity

The wave number is defined by the following relation:

$$k = \frac{\omega}{C} \qquad [6.1]$$

where

k = wave number;

ω = circular frequency, and

C = phase velocity

Generally, the wave number and phase velocity are complex numbers. For surface wave modes, the real part of the wave number is large compared to the imaginary part (Lysmer and Drake, 1972). By ignoring the imaginary part of the wave number no major error occurs in calculation of phase data. Therefore, from now on only real part of wave number is considered in computation.

To find the wave numbers of propagation modes at a given frequency, the vertical flexibility coefficient is calculated for a wide range of the wave number. Wave numbers corresponding to the maxima of the flexibility coefficient are then identified. By substituting these wave numbers in Eq. 6.1, phase velocity of each propagation mode is calculated. For example at frequency of 10 Hz, the maximum flexibility coefficient occurred at wave number equal to 0.215. Therefore, the calculated phase velocity is equal to 292.24 m/s. This procedure is repeated for all frequencies of interest and the dispersion curve calculated by this procedure is presented in Fig. 6.4.

It is known that the Rayleigh wave modes represent natural modes of wave propagation. The latter are obtained from the eigenvalue problem that follows from setting the load vector in Eq. 5.1 equal to zero, i.e.

$$[K]\{U\} = 0 \qquad [6.2]$$

where for a fixed angular frequency ω, the eigenvalues represent velocities of the Rayleigh wave while U represents its shape as a function of depth. For a nontrivial solution the determinant of matrix [K] must be zero

$$|K| = 0 \qquad [6.3]$$

The solution of Eq. 6.3 was discussed in Section 4.3.

In this study, for solving Eq. 6.3 a computer program was developed in which the frequency is assumed as the independent variable. The above equation was solved for system 1 at a frequency of 10 Hz, which results in phase velocity equals to 292.95 m/s. Equation 6.3 was solved for other frequencies and the calculated dispersion curve is shown in Fig. 6.4. By comparing the dispersion curves it can be observed the dispersion curve obtained with the maximum flexibility coefficient method follows very well the dispersion curve of the first Rayleigh mode. The first mode remains the dominant mode of propagation through the entire frequency range. Fig. 6.5 shows the vertical maximum flexibility coefficients for system 2 at different frequencies. The dispersion curves for system 2 derived by both flexibility coefficient and root-searching methods are shown in Fig. 6.6. These curves show that the dominant mode shifts to higher modes as the frequency increases.

6.3 Comparison of Dispersion Curves from Different Procedures

The SASW test is simulated for the two soil systems as described in Section 5.5. Frequencies used for the analysis are in the range of 0.1 to 700 Hz. The increments of excitation frequencies from 0.1 to 30 Hz and from 31 to 700 Hz were 0.1 and 1 Hz, receptively. The relative phase angle spectra are generated for receiver spacing of 1, 2, 4, 8, 16, 32, 64, 128 m that are shown in Fig. 6.7 and Fig. 6.8. To process the SASW phase data, the unwrapped phase angles are calculated for each spacing. Then phase velocity and the wavelength are calculated using Eq. 3.2 through 3.6. The simulated dispersion curves after applying different filtering criteria are shown in Fig. 6.9 and 6.10. Fig. 6.11 and 6.12 show the dispersion curves from simulated SASW test with the proposed

filtering criteria and dispersion curves obtained by using maximum vertical flexibility coefficient approach. These figures indicate that the simulated dispersion curves for both systems agree with the those obtained from maximum vertical flexibility coefficients. Therefore, instead of using SASW simulation, which involves substantial computation time, the maximum vertical flexibility coefficient approach can be used to obtain the theoretical dispersion curves.

6.4 Comparison of Results from the New Method with the Results of Tokimatsu et al. (1992)

To demonstrate the effectiveness of the proposed method for calculating the theoretical dispersion curve, those for 3 four-layer models listed in Table 6.3 are computed and compared with the results obtained for the sites by Tokimatsu et al., 1993. In Case 1, the stiffness of soil layers increases with depth. While in Case 2 and 3, the stiffness varies irregularly with depth. Fig. 6.13 shows the dispersion curves for case 1, where the fundamental mode is consistently the dominant mode except at the frequency of 5 Hz. In contrast, for Case 2 (Fig. 6.15), higher modes play a significant role in some range of frequency in addition to the fundamental mode. It can be seen from Fig. 6.15 that modes of higher order become the dominant modes. Fig. 6.17 shows the dispersion curves for Case 3. In this case again, the fundamental mode is the dominant mode through out the whole frequency range except at frequency range of 10-13 Hz.

The dispersion curves for the above sites as reported by Tokimatsu et al. (1992) were derived by simulation of the SASW test. The theoretical formulae used in the simulation process were based on the transfer matrix method proposed by Thomson (1950). In this method phase lag of vertical and horizontal particle motions between the sensors at each frequency are calculated. Then the apparent phase velocity for vertical and horizontal motion are determined though Equation 3.2 to 3.6.

The reported dispersion curves for the three four-layer systems are show in Figs. 6.14, 6.16, 6.18. By comparing the results, there is good agreement between the two methods in the three cases.

To check that the new method produces the correct dispersion curve, the simulation of the SASW test was carried out for case 3. The phase angle data for the site at different spacing are shown in Fig. 6.19. After processing the phase data, the simulated dispersion curve was obtained for different filtering criteria (see Fig. 6.20). The comparison of dispersion curves, obtained from the simulation of SASW test, and the dispersion curve derived from root-searching are presented in Fig. 6.20d. Fig. 6.20d shows that the simulated dispersion curve follows the dispersion curve obtained for first mode through the entire frequency range except at frequency range between 10 to 13 Hz. In these frequencies the Rayleigh wave shifts to higher mode. This further confirms that only the dispersion curve derived by the proposed filtering criteria can produce an acceptable dispersion curve, since it lies close to the results from the steady state test.

6.5 Simulation of the Steady-State Rayleigh Wave Test

An alternative way to check the results of the new method is to compare the results with simulation of a Steady-State Rayleigh wave test. The numerical simulation of the Steady-State Rayleigh wave test can be performed by calculating of the vertical displacement as a function of distance for each frequency. In-phase positions of surface motion are then found by the same procedure as in the case of original Steady-State Rayleigh wave test. The wavelength and phase velocity are calculated based on the average of two to three cycles of surface wave motion.

The surface motions for sites two and three are calculated by the developed simulation program. Figs. 6.21, 6.22 show the surface motion. These curves indicate that there are significant variations of the amplitude of motion with distance from source. In the frequency range below cut-off frequencies of higher Rayleigh modes, the variation

results from a contamination of Rayleigh waves with direct and reflected body waves. The in-phase positions of surface motion for the two soil systems are calculated at each frequency and are shown in Figs. 6.23, 24. The dispersion curves derived by simulation of the Steady-State Rayleigh wave test and new method for both sites are given in Figs. 6.25, 26. By comparing the results it is found that there is good agreement between the simulated dispersion curves from the Steady-State and the new method.

6.5 Parametric Study

6.6.1 Effect of Poisson's Ratio on Dispersion Curves

For most soils, Poisson's ratio is always positive but less than 0.5. To investigate the effect of Poisson's ratio on the predominant mode of dispersion curve, a parametric study was conducted using two soil systems with different value of Poisson's ratio. These systems are analyzed and the dispersion curves were derived based on the new method. Figs. 6.27, 6.28 show dispersion curves of the dominant mode of propagation. It appears from Fig. 6.27 that the variation of Poisson's ratio as reported by Ewing et al. (1957) doesn't change the phase velocity value by more than ten percent. However, the variation of Poisson's ratio changes the phase velocity by a little more than ten percent especially when transition of mode occurred (see Fig. 6.28).

6.6.2 Effect of Damping on Dispersion Curves

As discussed in Chapter 4, material damping does not affect Rayleigh wave dispersion curve obtained by root searching technique. The damping only causes attenuation of waves, while apparent velocity is almost equivalent to the phase velocity of undamped system.

In practice, the damping ratio at the low-strain level may be chosen in the range of 1% to 5% based on the soil classification and viscosity level (Richart and Woods, 1970). To

investigate effect of damping ratio on the dispersion curves calculated by the new method, the developed program was run for two soil systems. Fig. 6.29 shows the dispersion curves for different damping ratios. For zero damping ratio the peaks in the vertical flexibility coefficient that correspond to different mode of propagation become infinite. For the selected small value of damping ratio, these peaks remain finite. These dispersion curves indicate different damping ratios do not change dispersion curves significantly.

6.7 Summary and Conclusions

The Rayleigh wave has different modes of propagation, and thus may have different velocities at any frequency. The participation of each mode varies depending on the soil's stratification as well as the frequency. Generally, inversion procedures require the calculation of the theoretical dispersion curve. Available procedures assume that the first mode of the Rayleigh wave is the predominant one and the dispersion curve of the first mode is then compared with the field dispersion curve. For irregular stratification, i.e., when the shear wave velocity does not increase with depth, higher Rayleigh modes provide a significant, and in many cases, a dominant influence on the overall wave propagation along the surface of a system. The inversion of the dispersion curve for such sites should not be guided solely by the theoretical first Rayleigh mode. A new method for calculating theoretical dispersion curves was introduced. At each frequency the method makes use of the vertical flexibility coefficients and finds the maximum one. Then using definition of the wave number, the corresponding phase velocity is calculated.

However, the new method for calculating of dispersion curves yields the same results as simulated SASW test, or simulated Steady-State Rayleigh wave test. It should be noted that although the proposed maximum flexibility coefficient for calculating of dispersion curves is superior to root-searching method, it suffers from two limitations. First, it fails

to find the predominant mode in a situation where several modes have the same amplitude. In such a case, the new method can only find one of them. Second, when the increment used for the wave number is too coarse, the proposed method can miss some modes of propagation. This difficulty, however, can be overcome by using a small wave number increment (having of course to bear the additional expense of increased computational time).

Table 6.1 Soil properties for system one.

	Shear Wave Velocity (m/s)	Thickness (m)	Damping ratio	Poisson's ratio	Unit Weight (kN/m^3)
Layer 1	300	20	0.005	0.35	20
Layer 2	500	20	0.005	0.35	20
Layer 3	700	----	0.005	0.35	20

Table 6.2 Soil properties for system two.

	Shear Wave Velocity (m/s)	Thickness (m)	Damping ratio	Poisson's ratio	Unit Weight (kN/m^3)
Layer 1	500	20	0.005	0.35	20
Layer 2	300	20	0.005	0.35	20
Layer 3	700	----------	0.005	0.35	20

Table 6.3 Soil properties for Four-layer system.

Layer number	Shear Wave Velocity (m/s) Case (1)	(2)	(3)	Thickness (m)	Damping ratio	Poisson's ratio	Unit Weight (kN/m^3)
1	80	180	80	2	0.005	0.35	18
2	120	120	180	4	0.005	0.35	18
3	180	180	120	8	0.005	0.35	18
3	360	360	360	----------	0.005	0.35	18

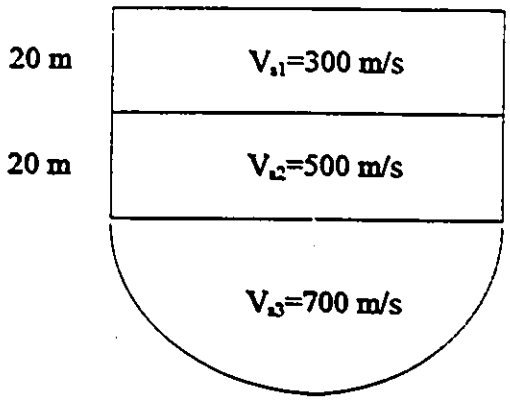

Fig. 6.1-Soil system one.

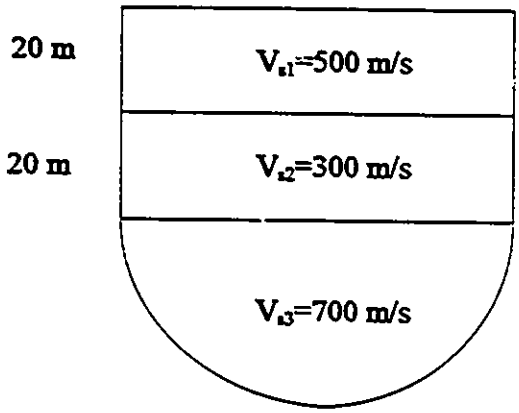

Fig. 6.2-Soil system two.

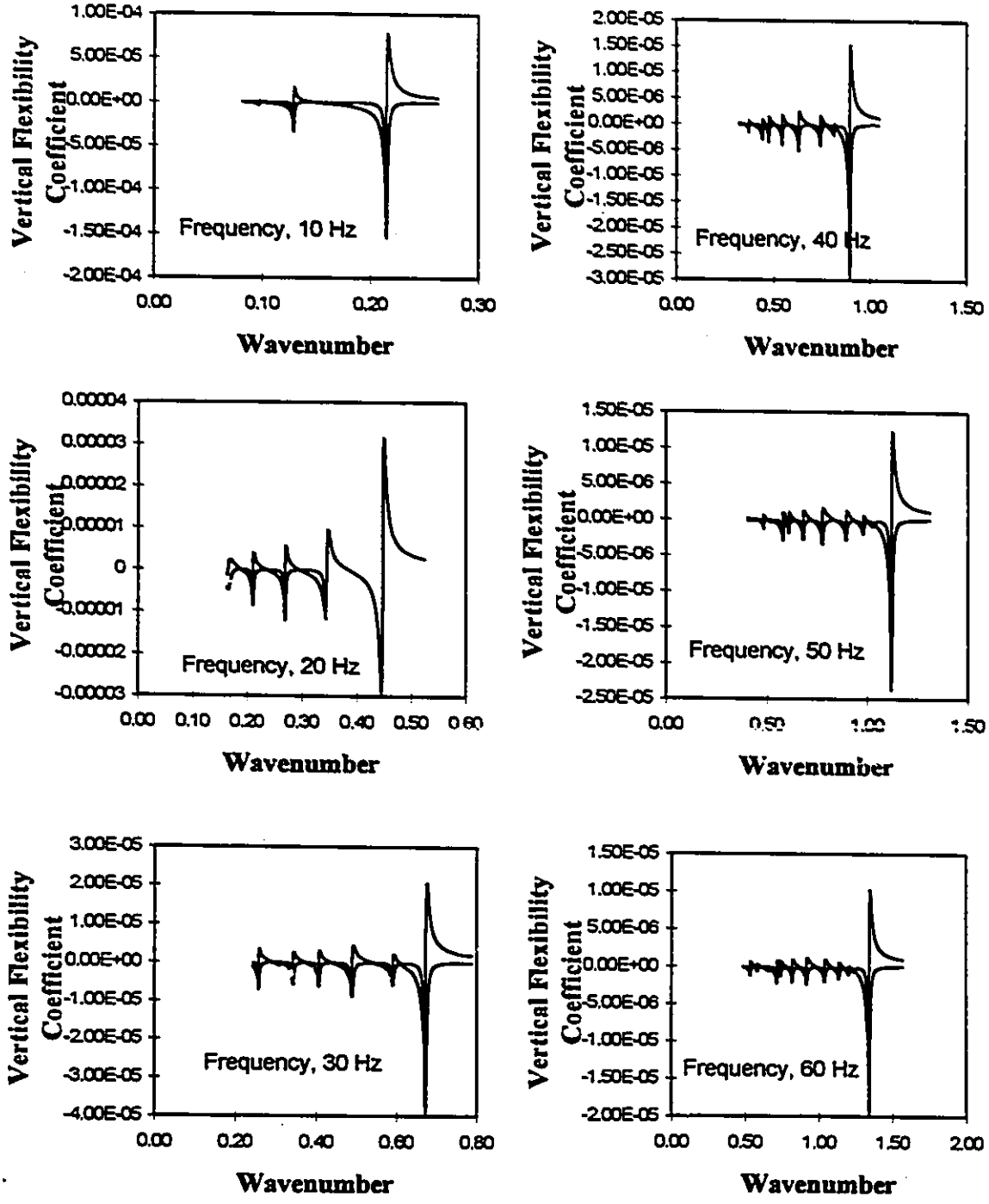

Fig. 6.3-Vertical flexibility coefficient for system one in the wavenumber domain at different frequencies.

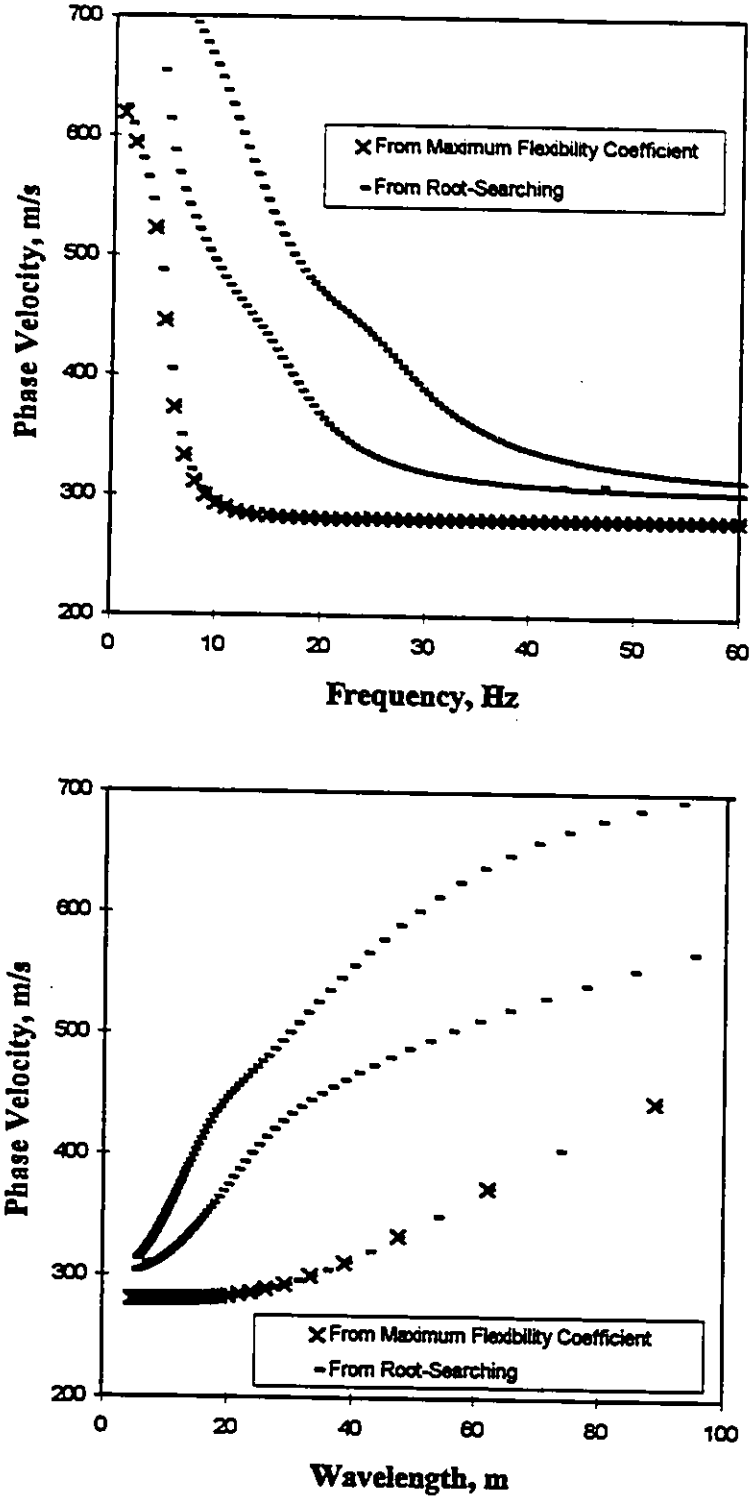

Fig. 6.4-Dispersion curve for system one.

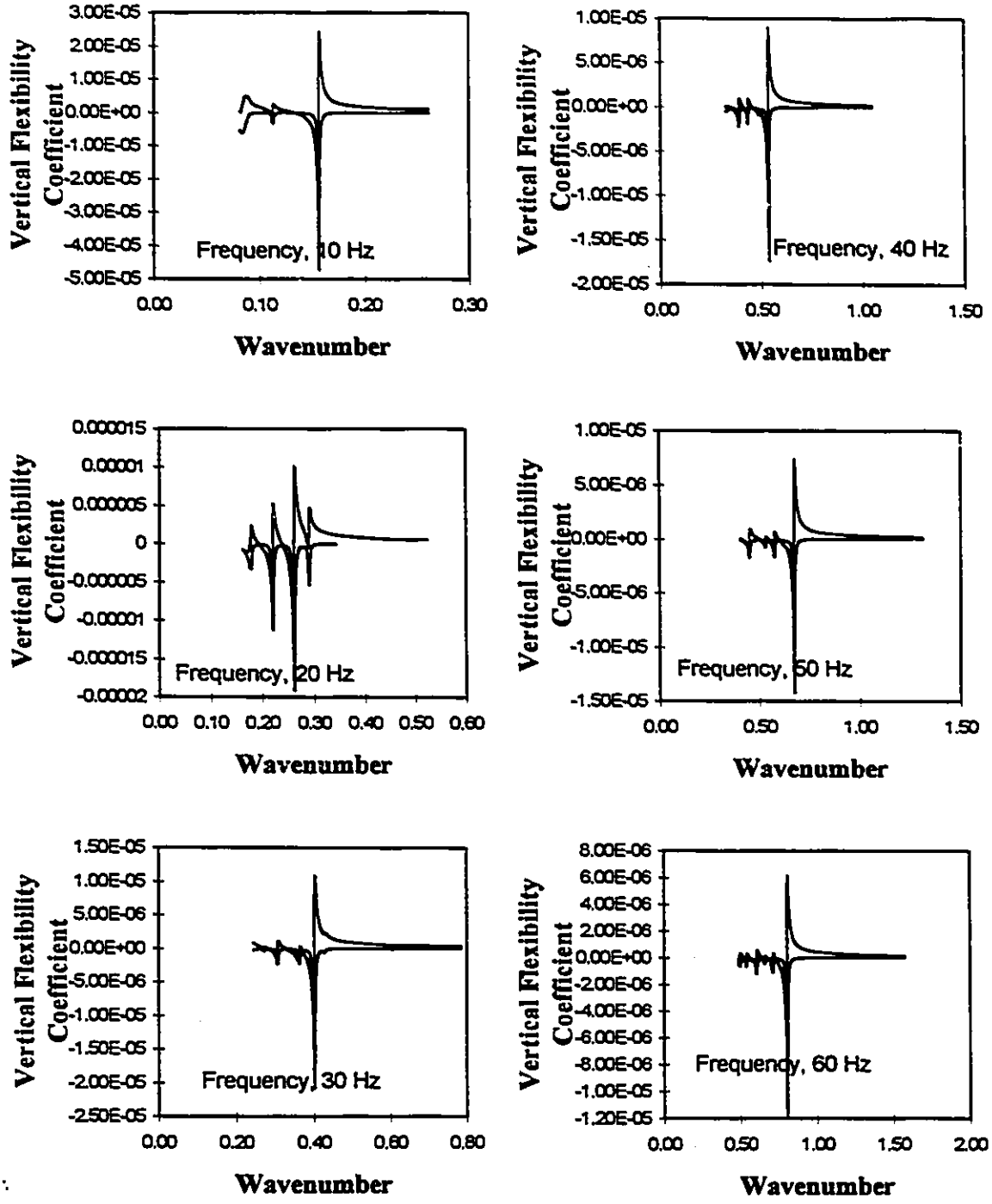

Fig. 6.5-Vertical flexibility coefficient for system two in the wavenumber domain at different frequencies.

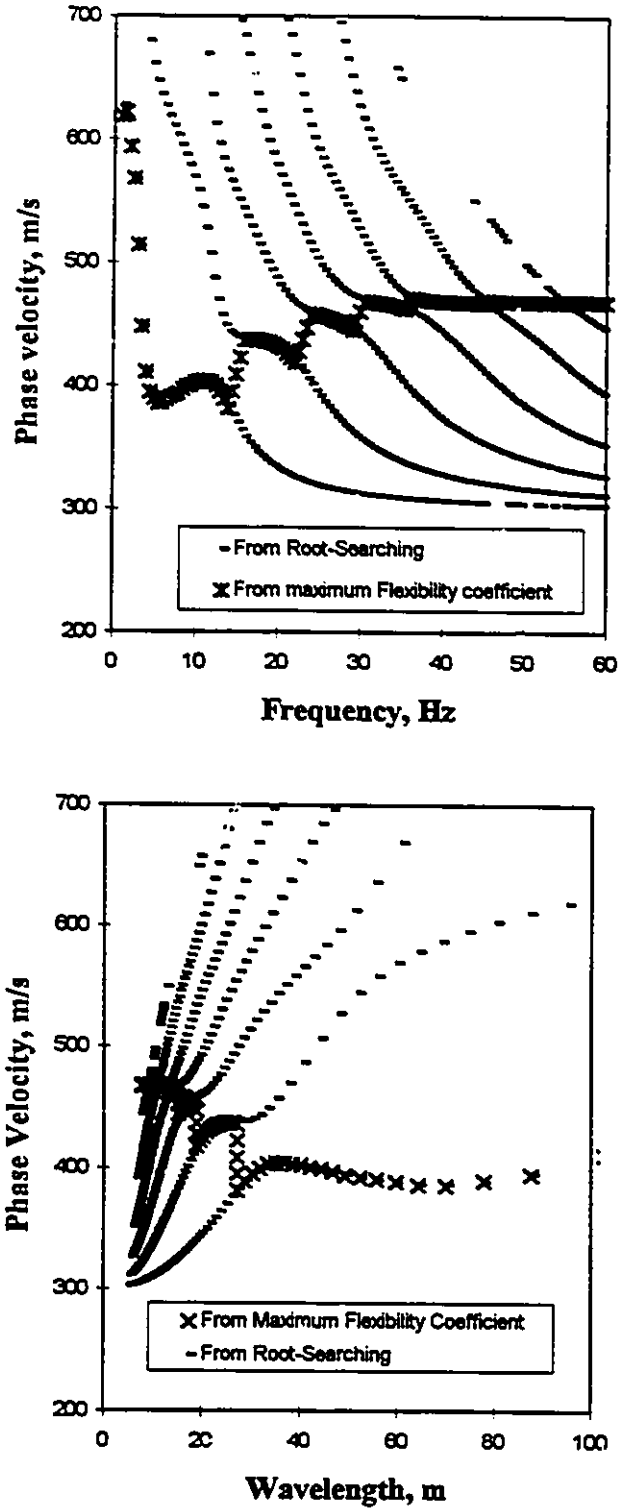

Fig. 6.6-Dispersion curve for system two.

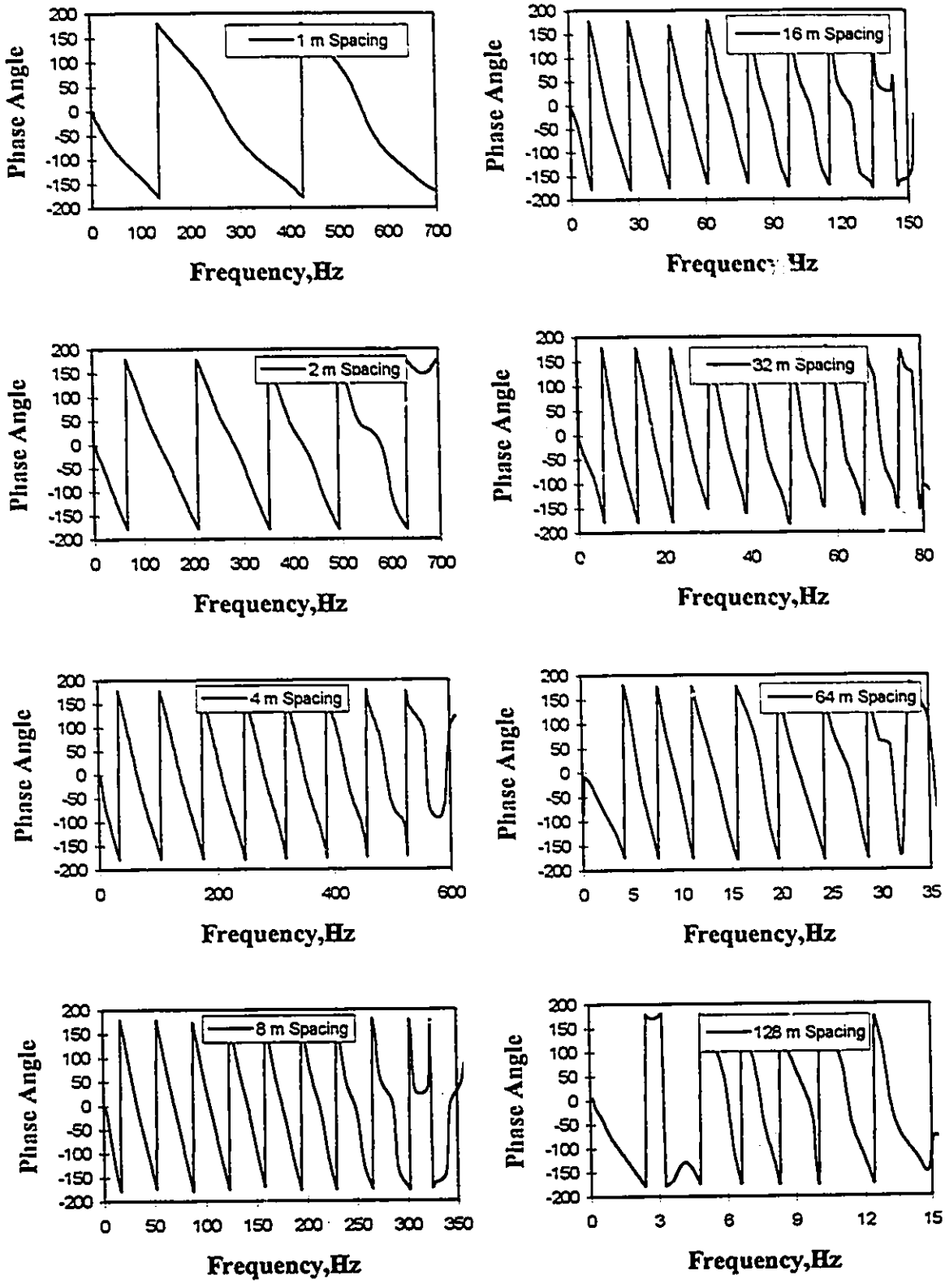

Fig. 6.7-Simulated relative phase angle spectra (in degrees) for various spacings for system one.

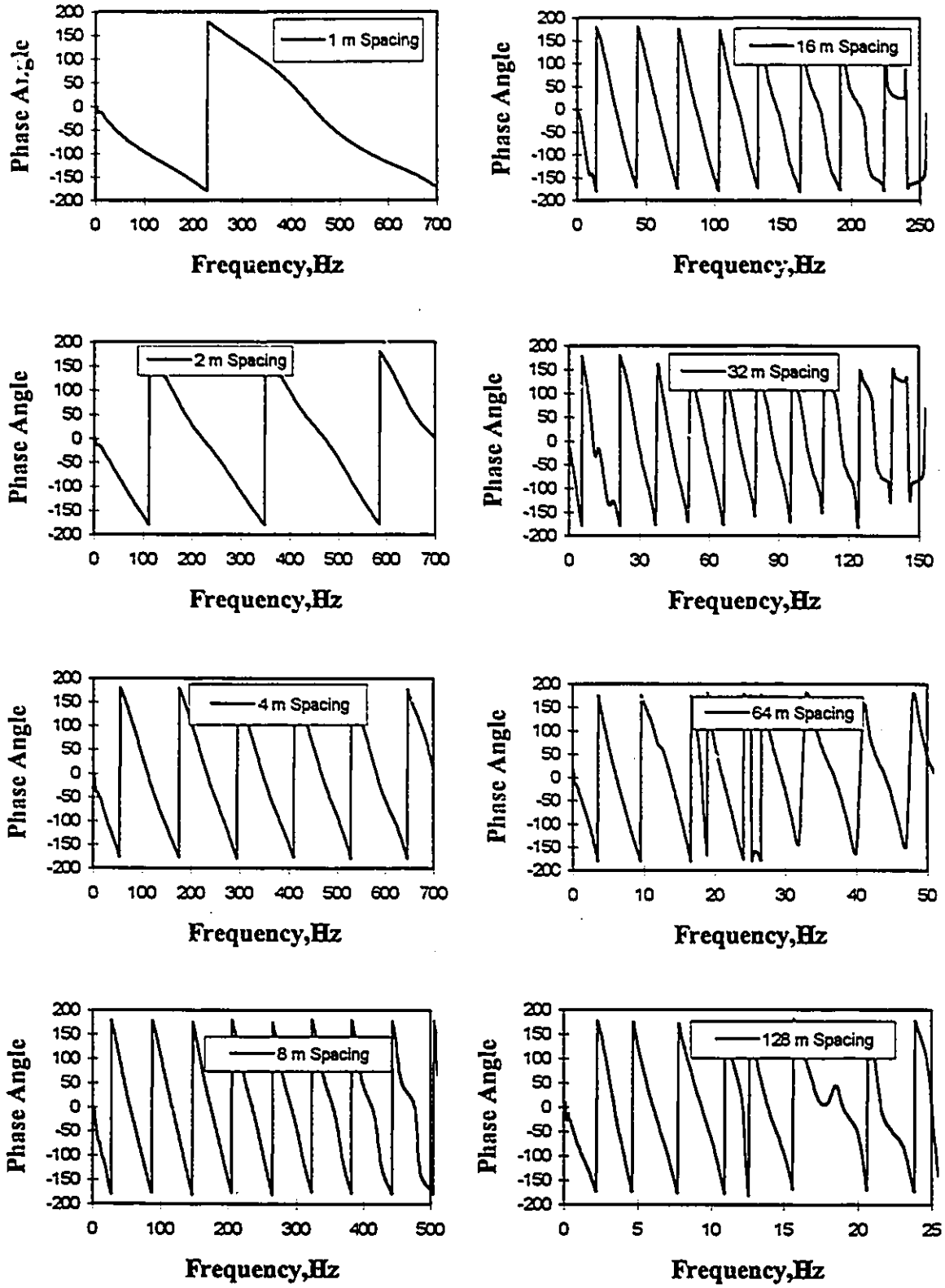

Fig. 6.8-Simulated relative phase angle spectra (in degrees) for various spacings for system two.

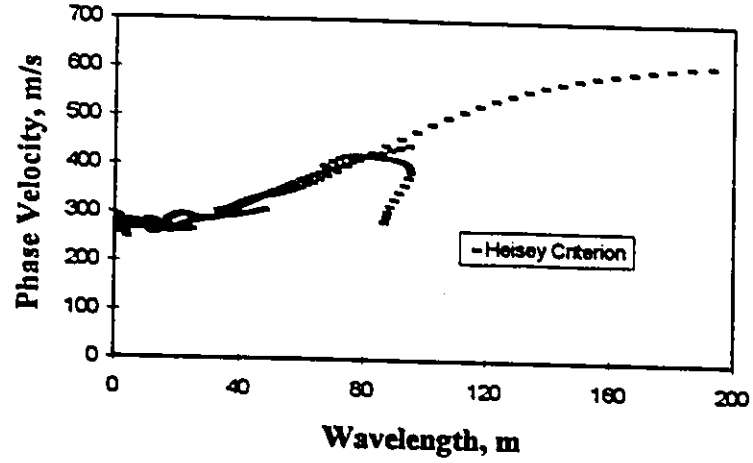

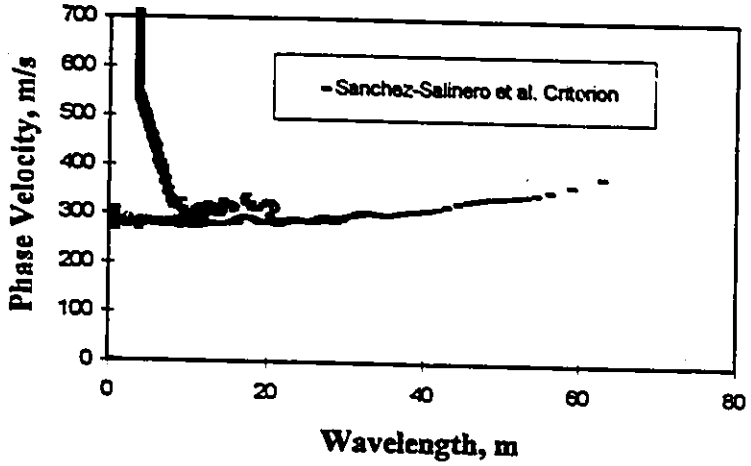

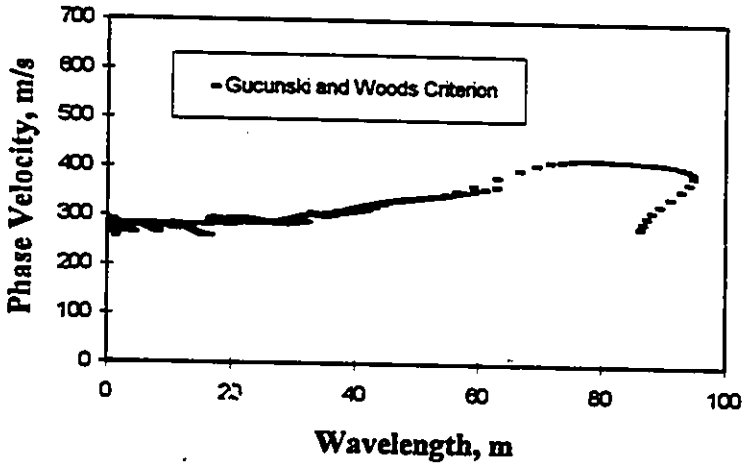

Fig. 6.9-Dispersion curves for system one from different filtering criteria.

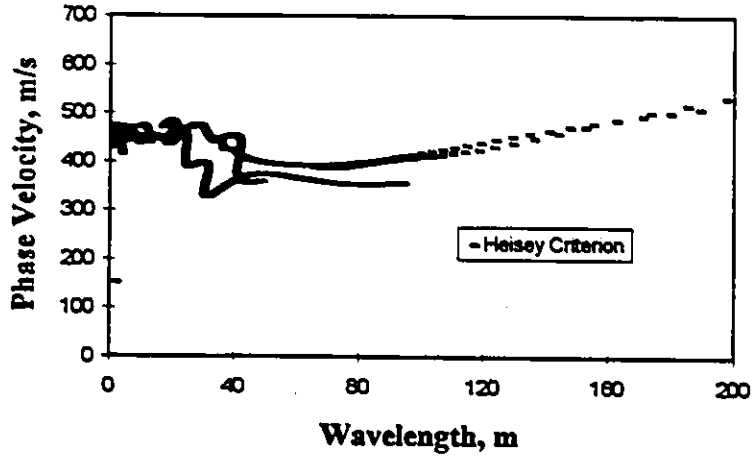

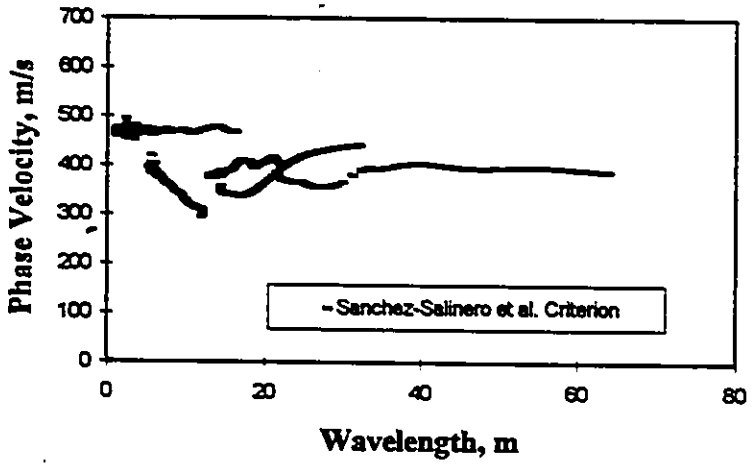

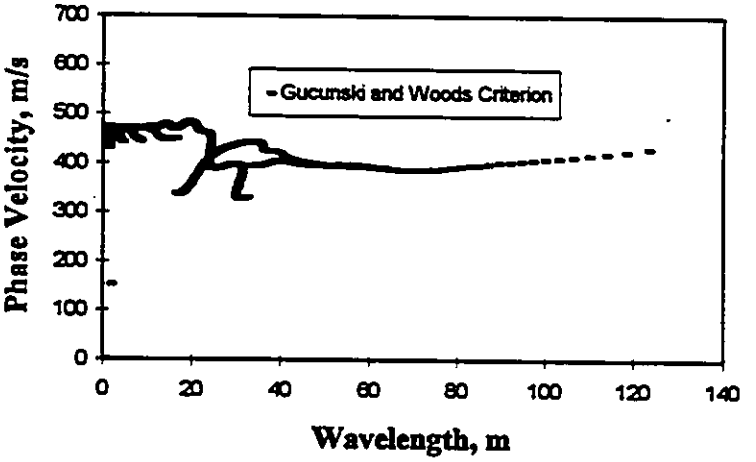

Fig. 6.10-Dispersion curves for system two from different filtering criteria.

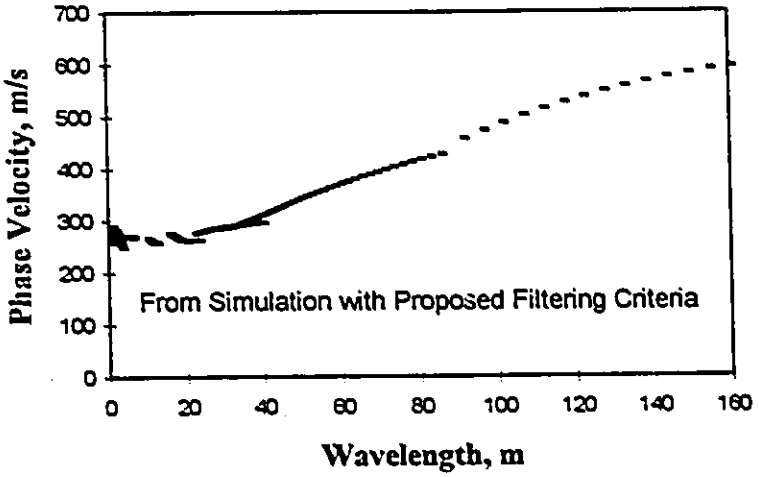

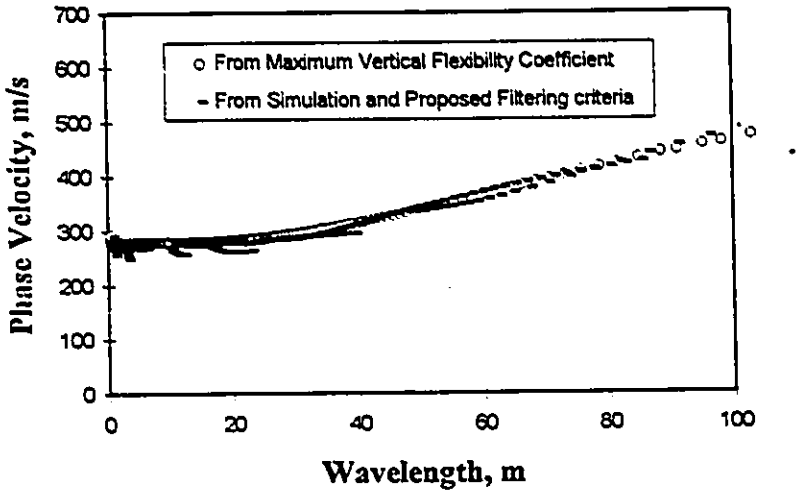

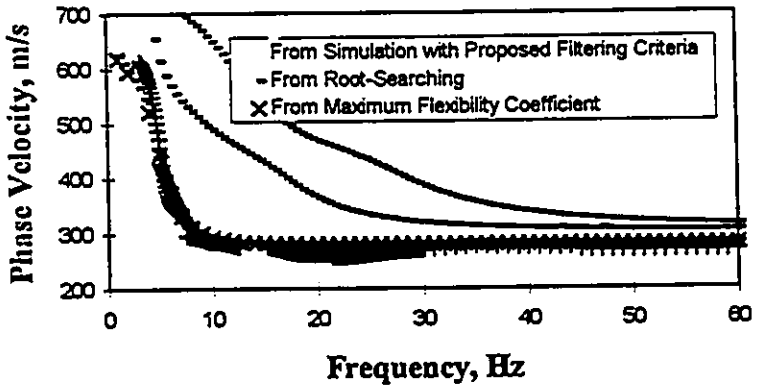

Fig. 6.11-Dispersion curves for system one from simulation, maximum flexibility coefficient methods, and the root searching method.

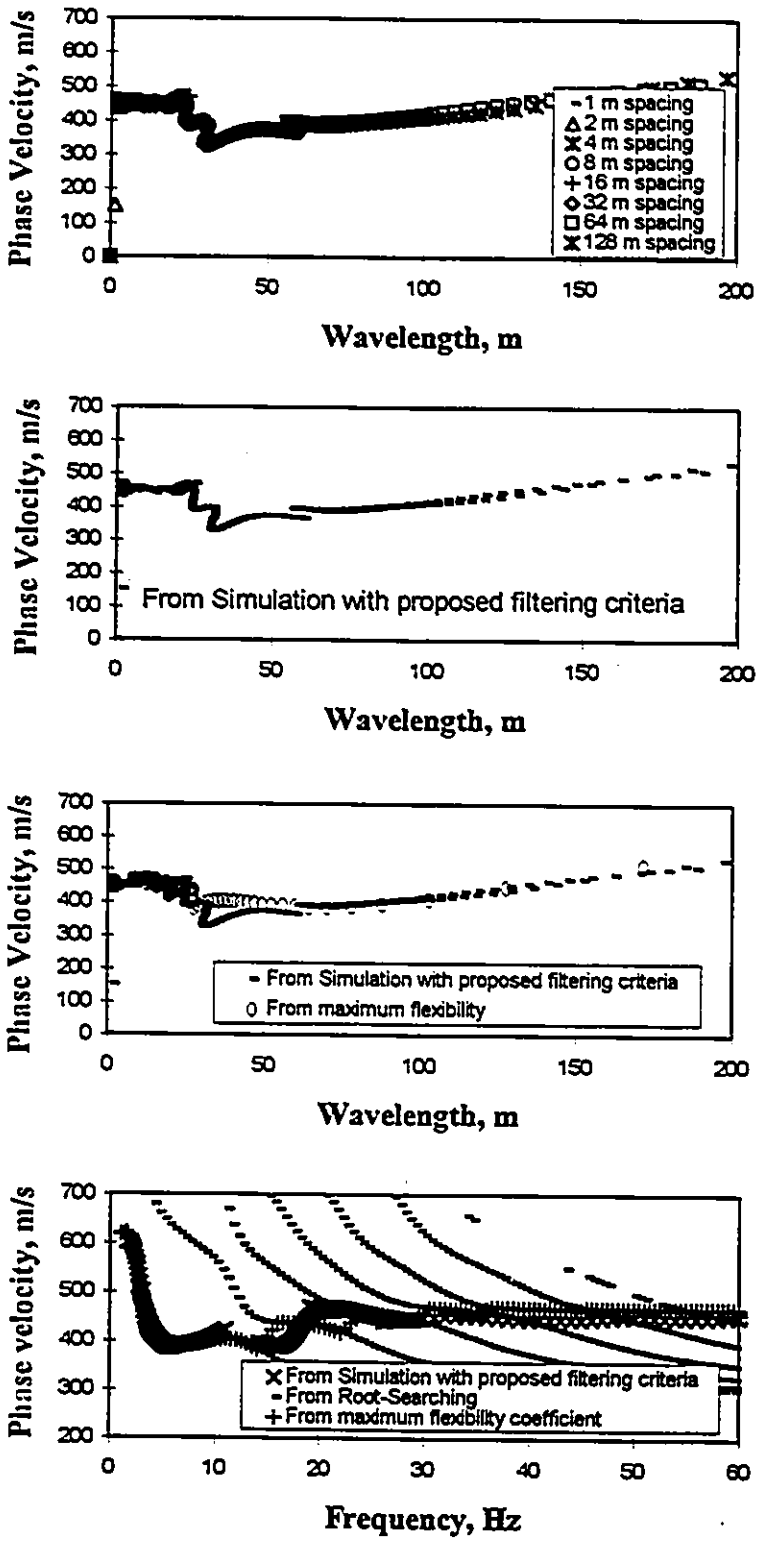

Fig. 6.12-Dispersion curves for system two from simulation, maximum flexibility coefficient methods, and the root searching method.

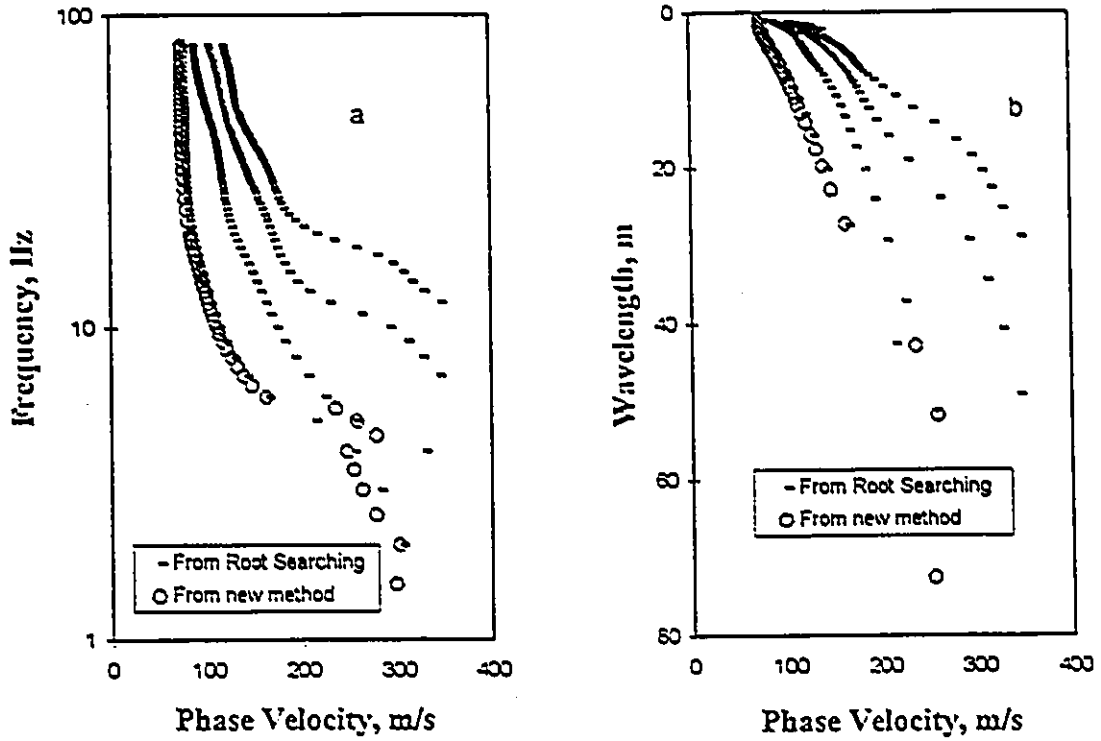

Fig. 6.13.a)-Variation of Phase Velocity with Frequency for Case 1
b)-Variation of Phase Velocity with Wavelength for Case 1

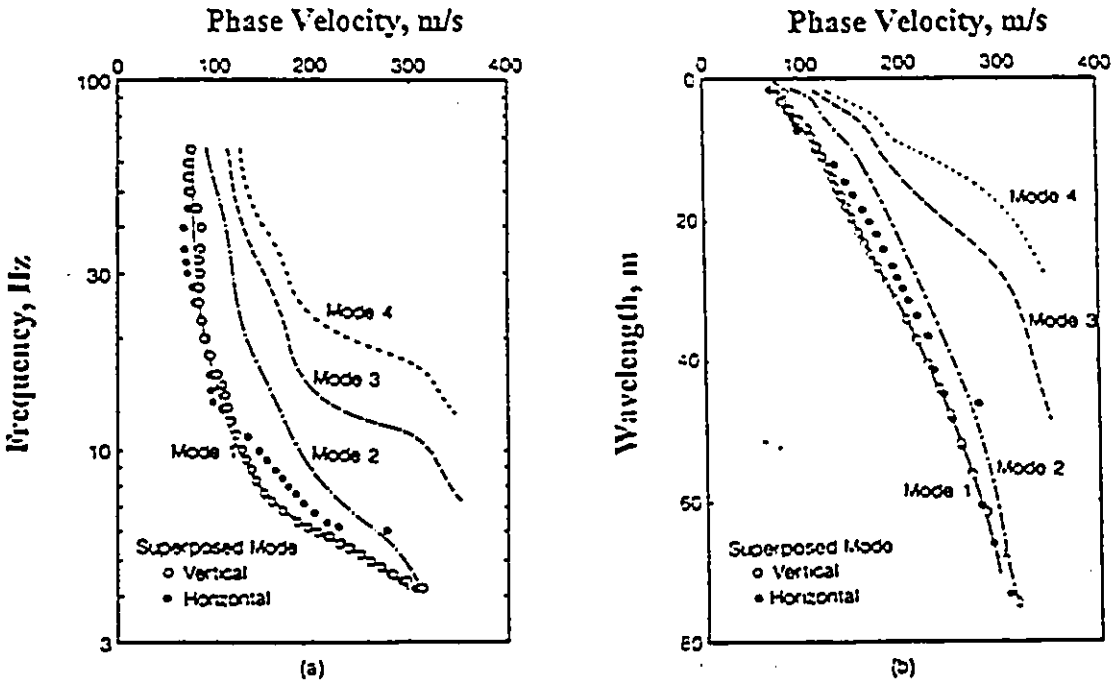

Fig. 6.14.a)-Variation of Phase Velocity with Frequency for Case 1
b)-Variation of Phase Velocity with Wavelength for Case 1 from Tokimatsu et al. 1992.

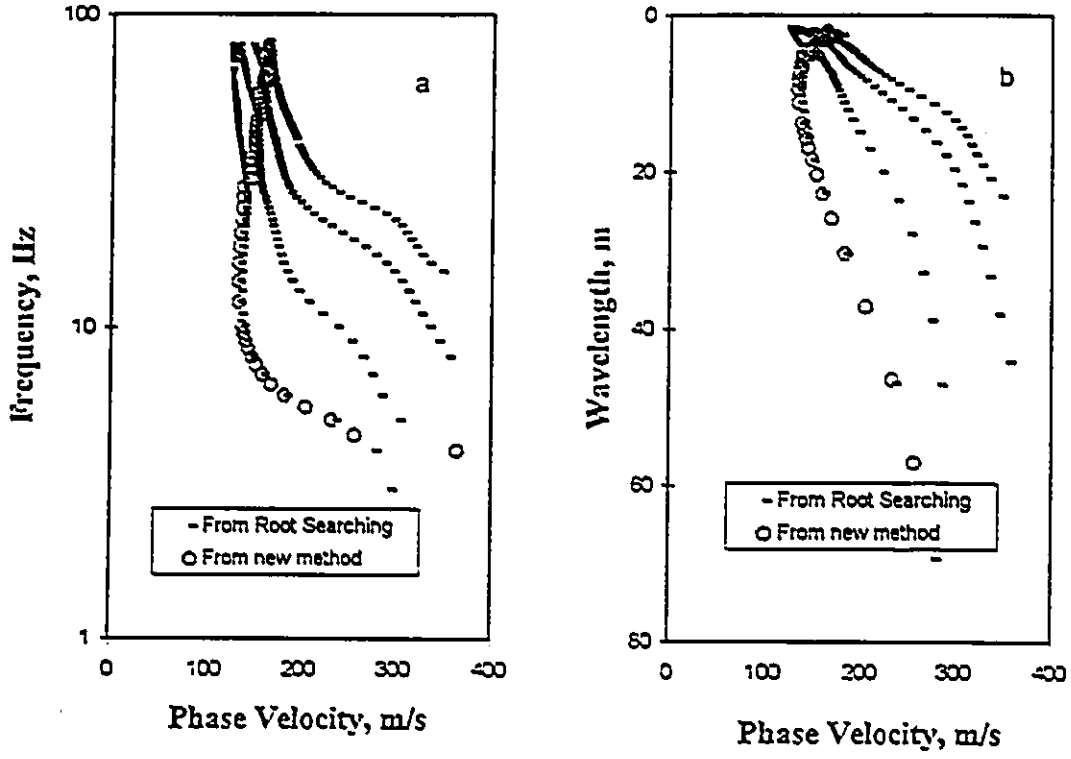

Fig. 6.15.a)-Variation of Phase Velocity with Frequency for Case 2
b)-Variation of Phase Velocity with Wavelength for Case 2.

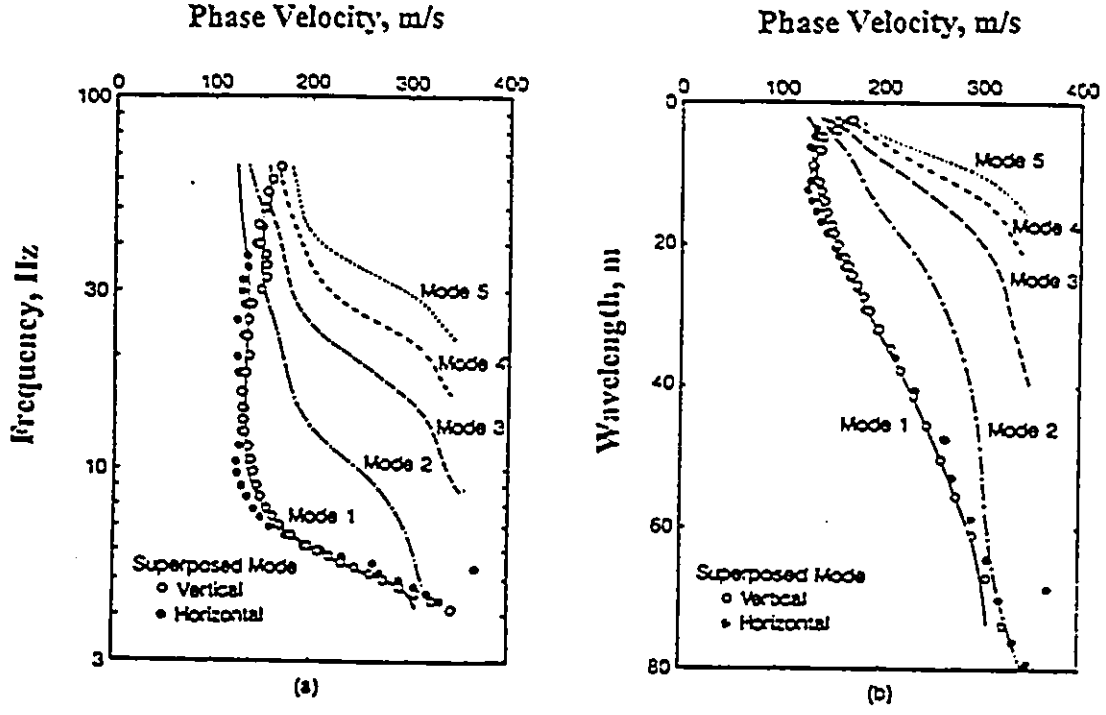

Fig. 6.16.a)-Variation of Phase Velocity with Frequency for Case 2
b)-Variation of Phase Velocity with Wavelength for Case 2 from Tokimatsu et al. 1992.

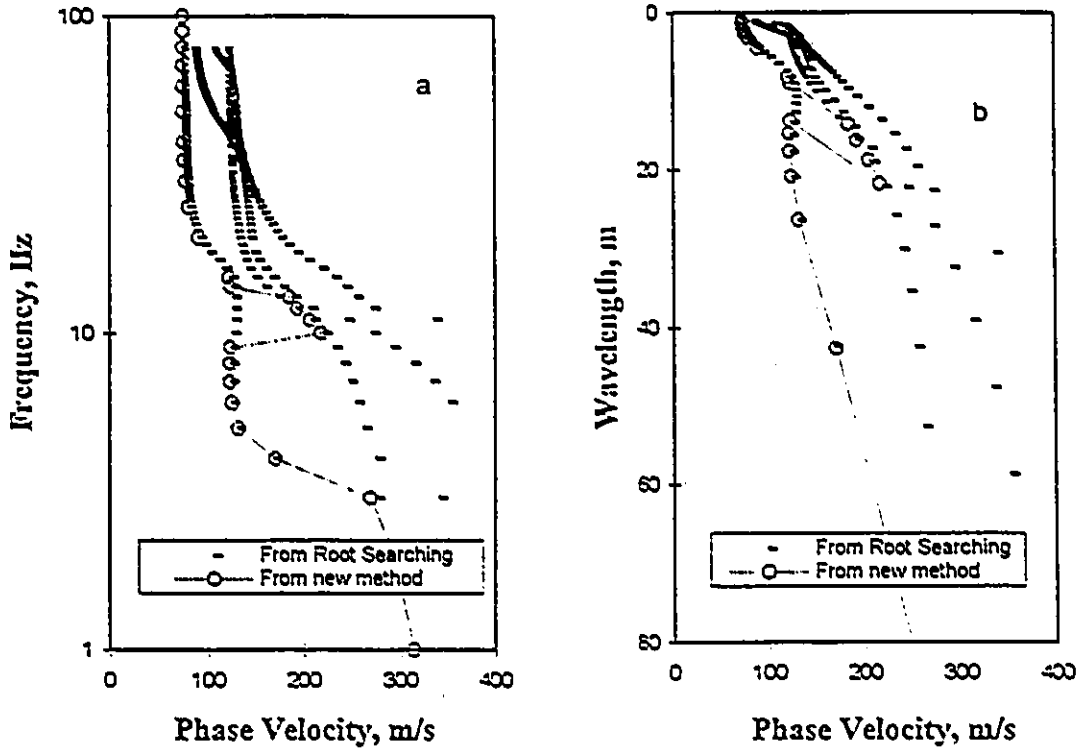

Fig. 6.17.a)-Variation of Phase Velocity with Frequency for Case 3
b)-Variation of Phase Velocity with Wavelength for Case 3.

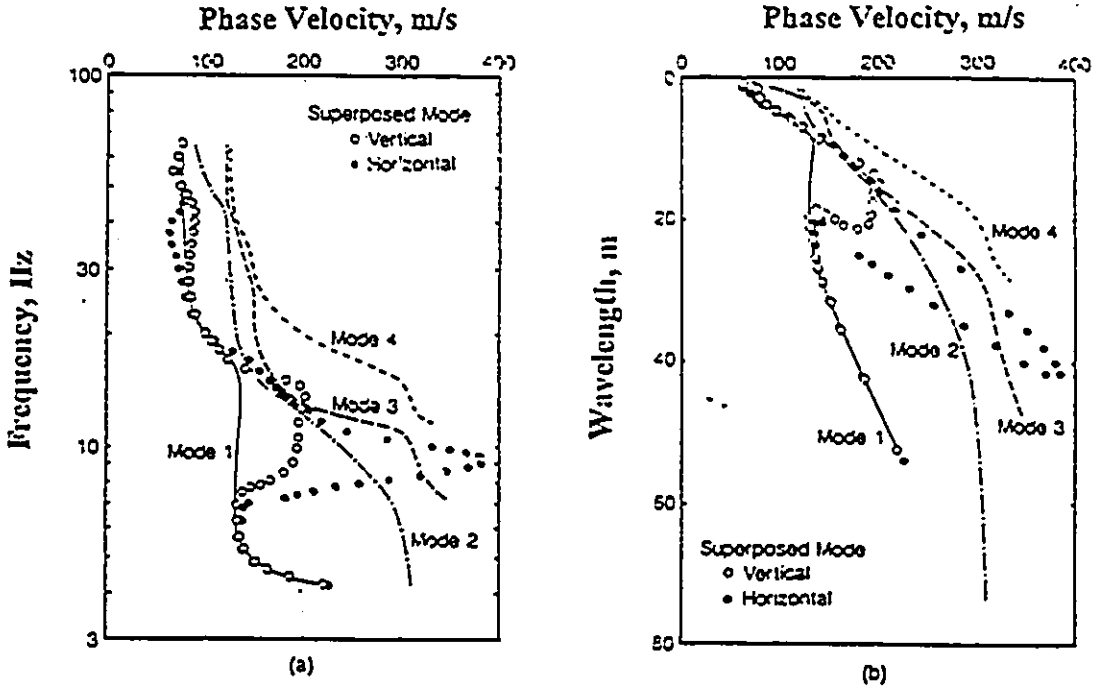

Fig. 6.18.a)-Variation of Phase Velocity with Frequency for Case 3
b)-Variation of Phase Velocity with Wavelength for Case 3 from Tokimatsu et al. 1992.

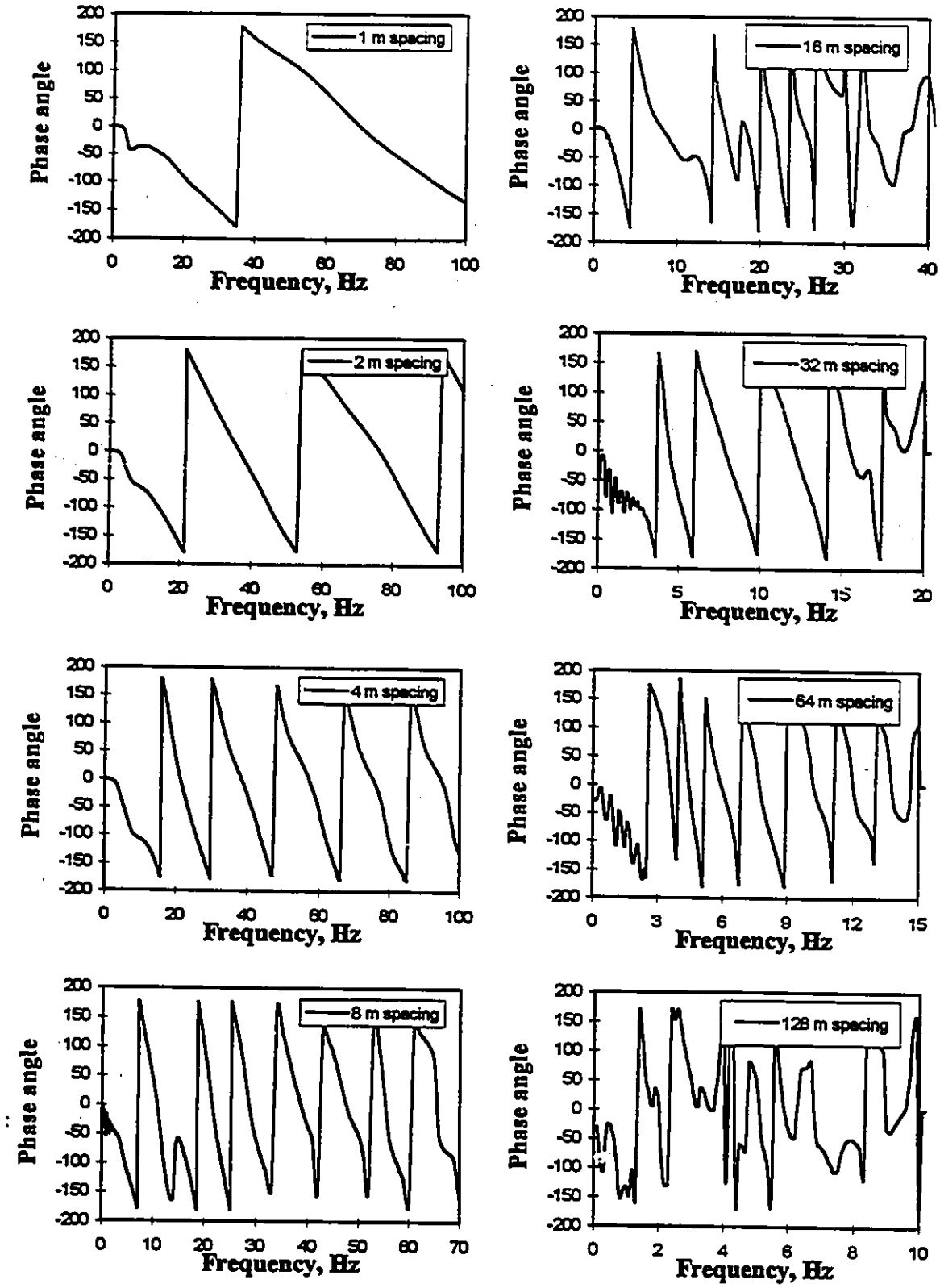

Fig. 6.19-Simulated relative phase angle spectra (in degrees) for various spacings for case 3.

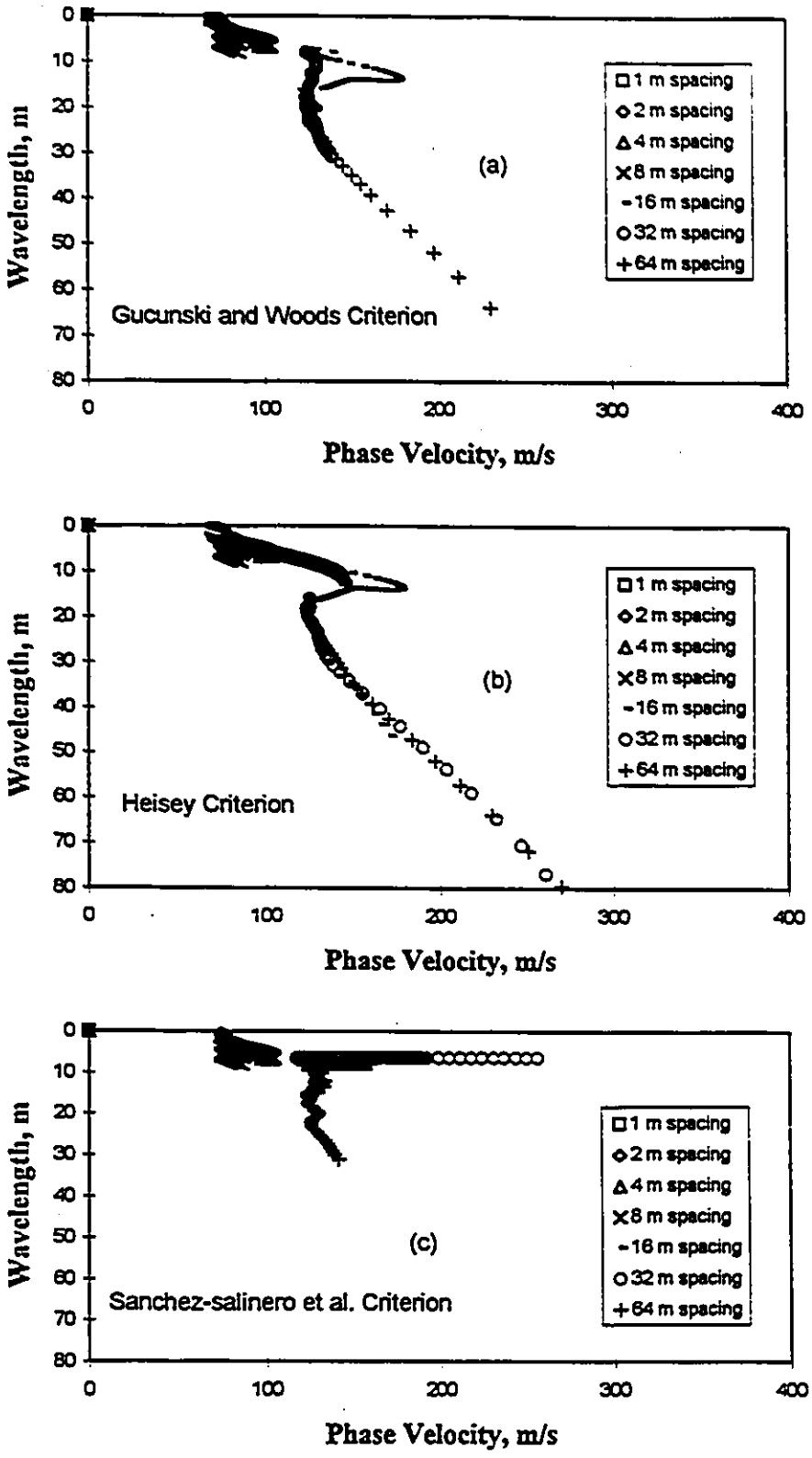

Fig. 6.20-Dispersion curve for case 3 from different filtering criteria.

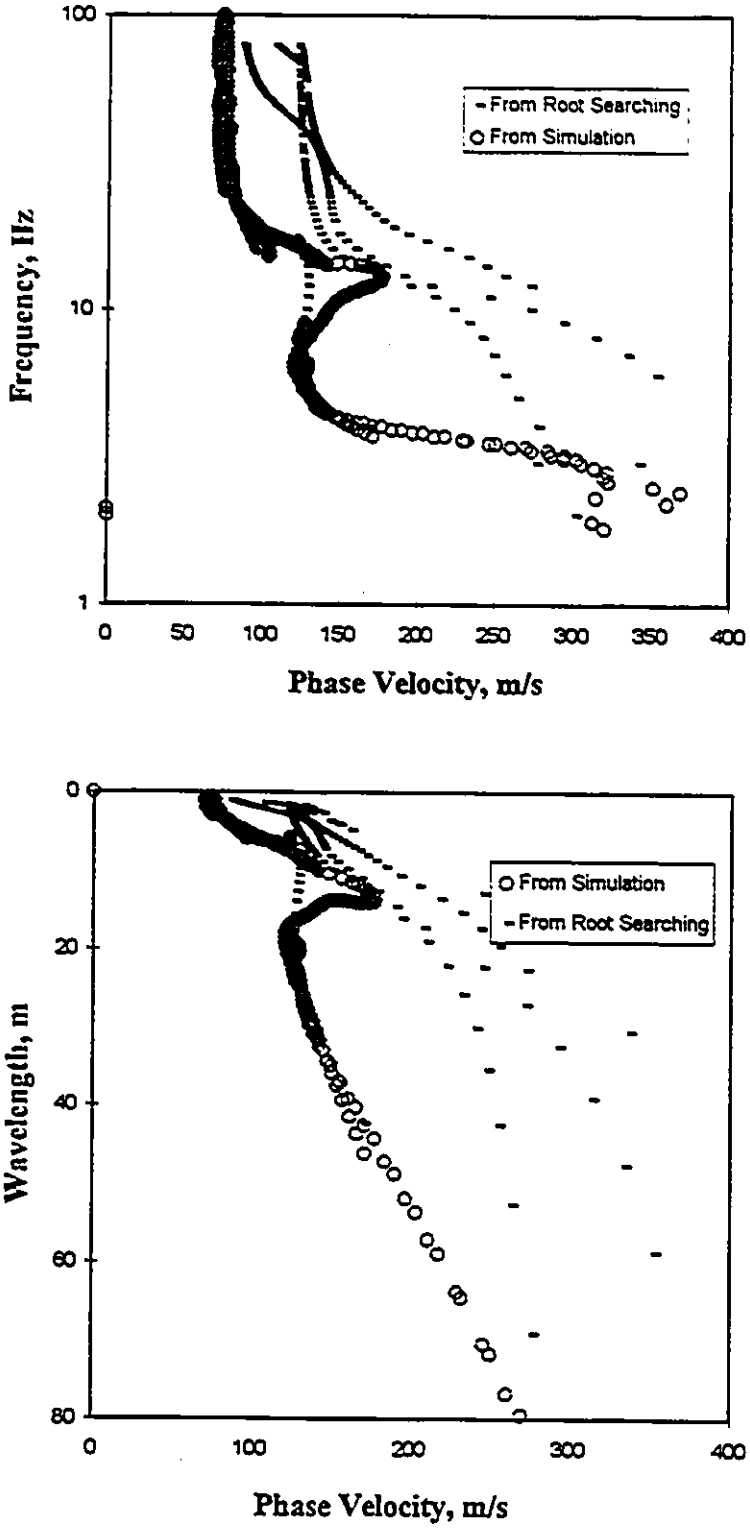

Fig. 6.20d-Dispersion curves for case 3 from root searching and simulation.

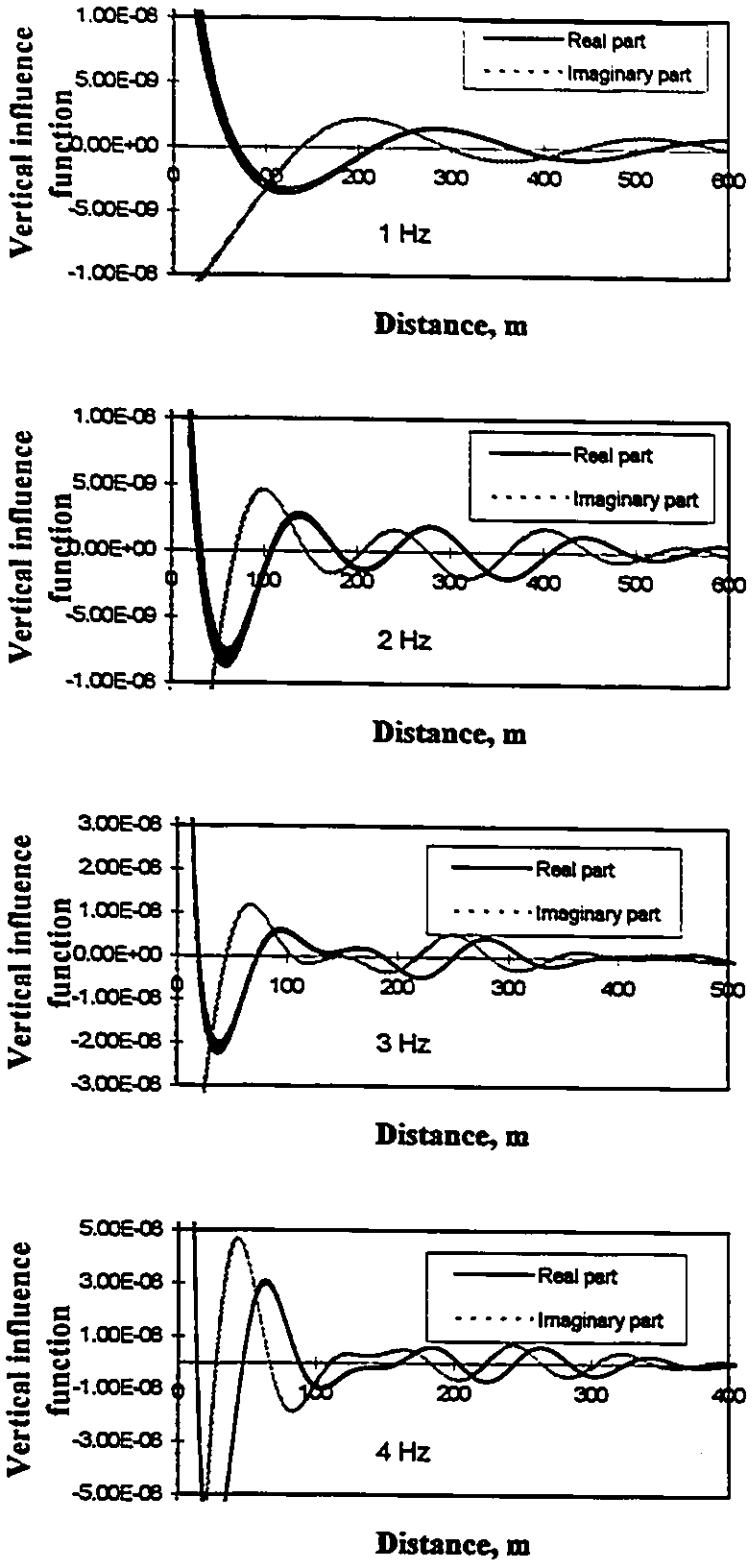

Fig. 6.21-Simulated vertical motion at surface for case 2 at different frequencies.

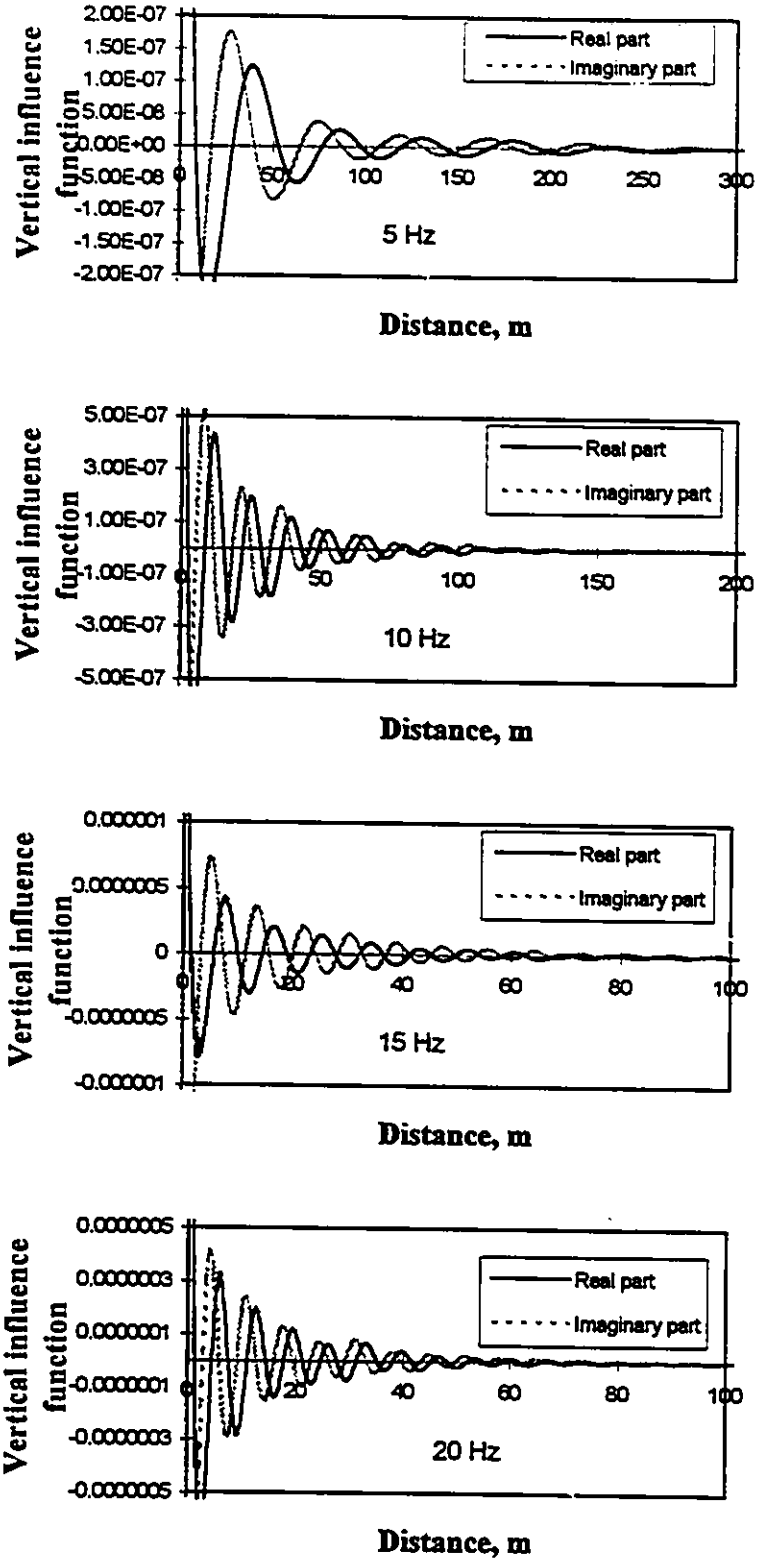

Fig. 6.21-Simulated vertical motion at surface for case 2 at different frequencies (continued).

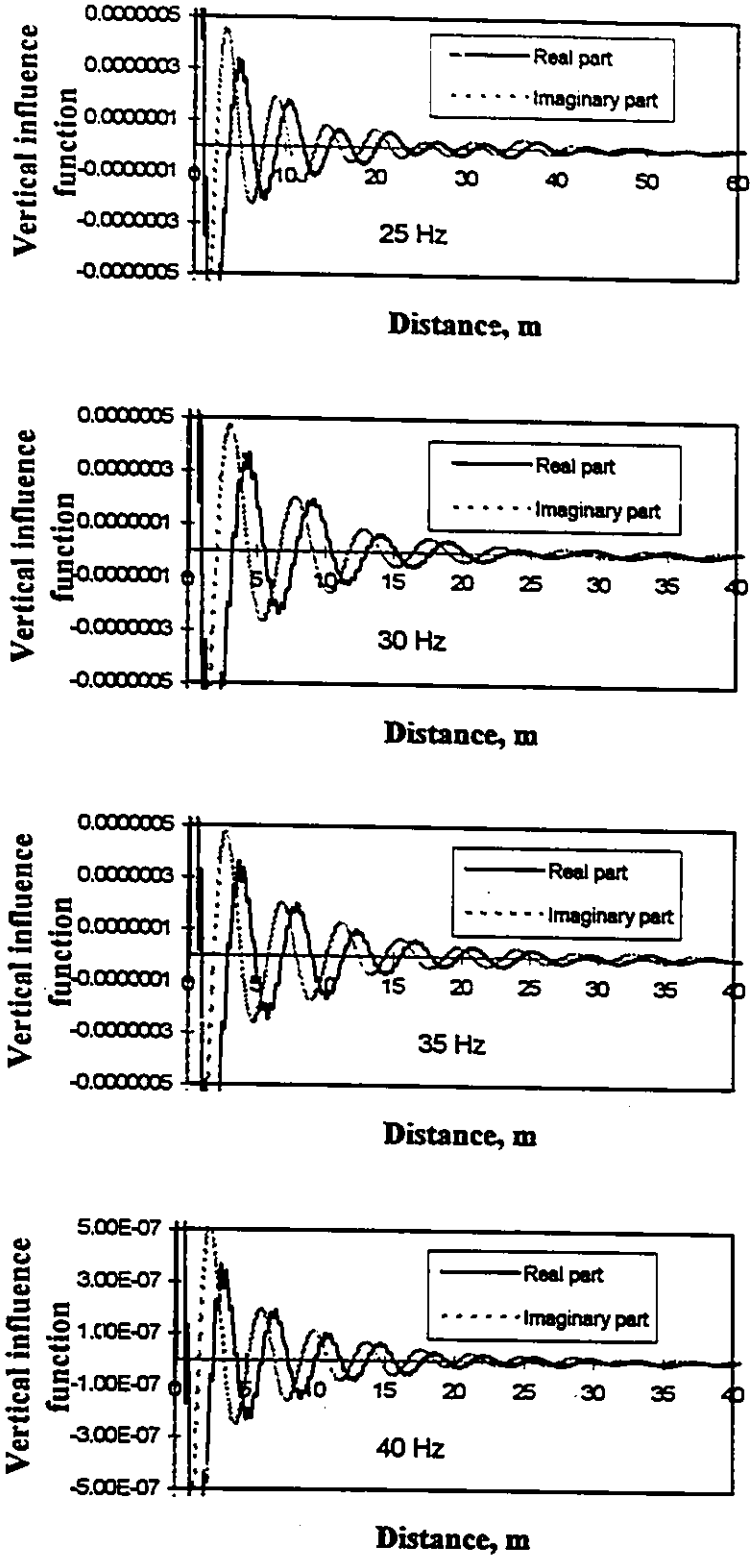

Fig. 6.21-Simulated vertical motion at surface for case 2 at different frequencies (continued).

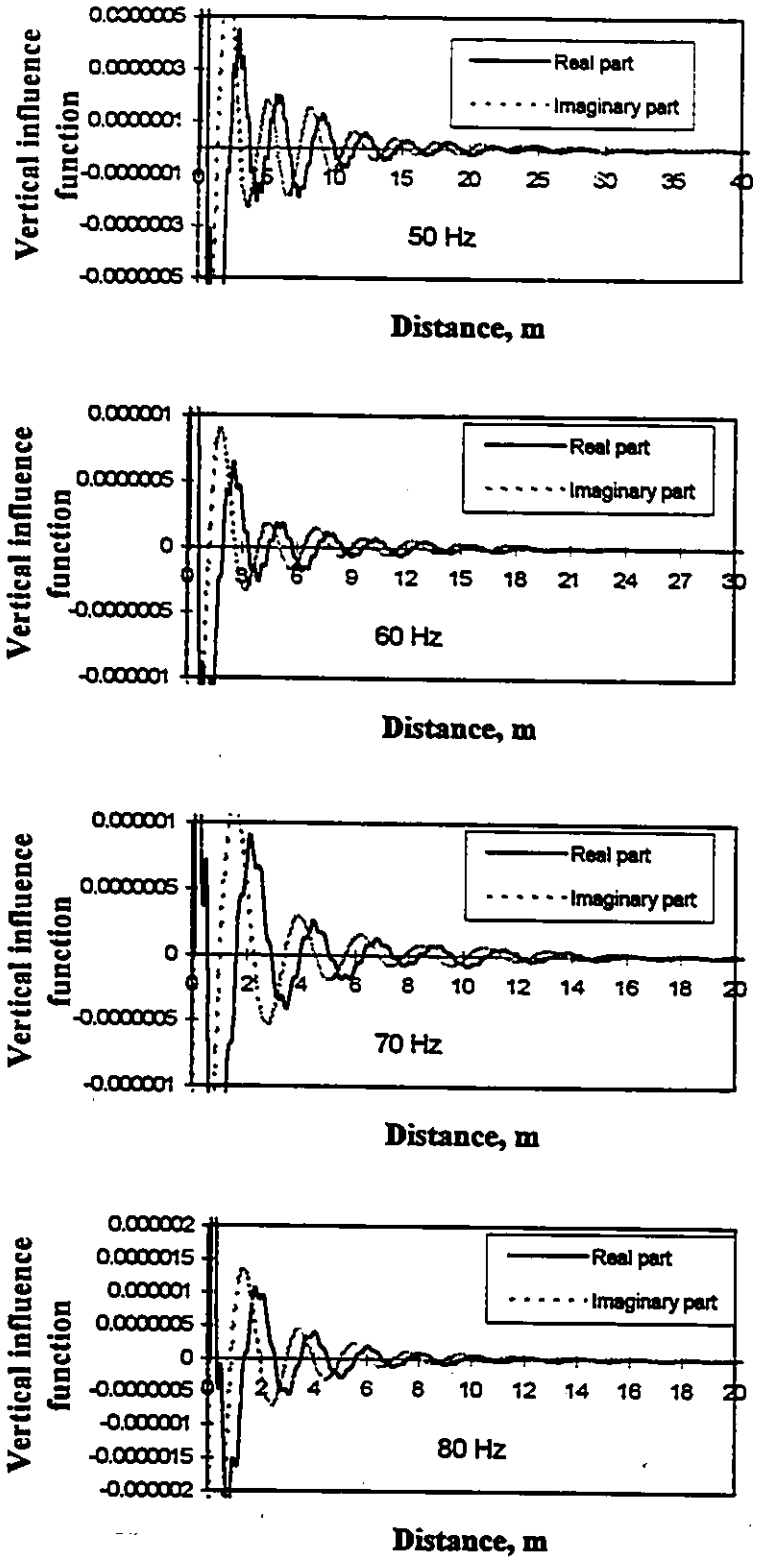

Fig. 6.21-Simulated vertical motion at surface for case 2 at different frequencies (continued).

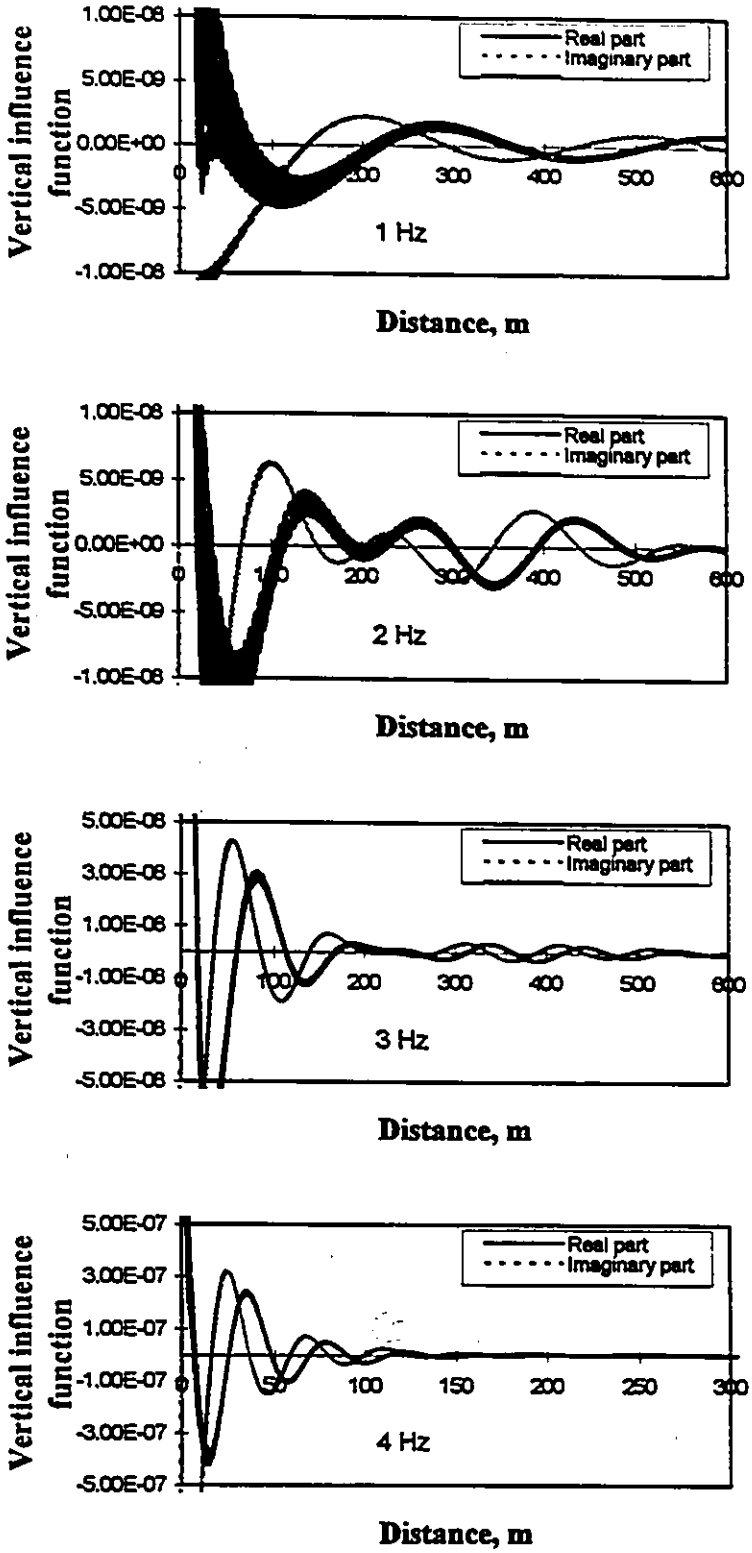

Fig. 6.22-Simulated vertical motion at surface for case 3 at different frequencies.

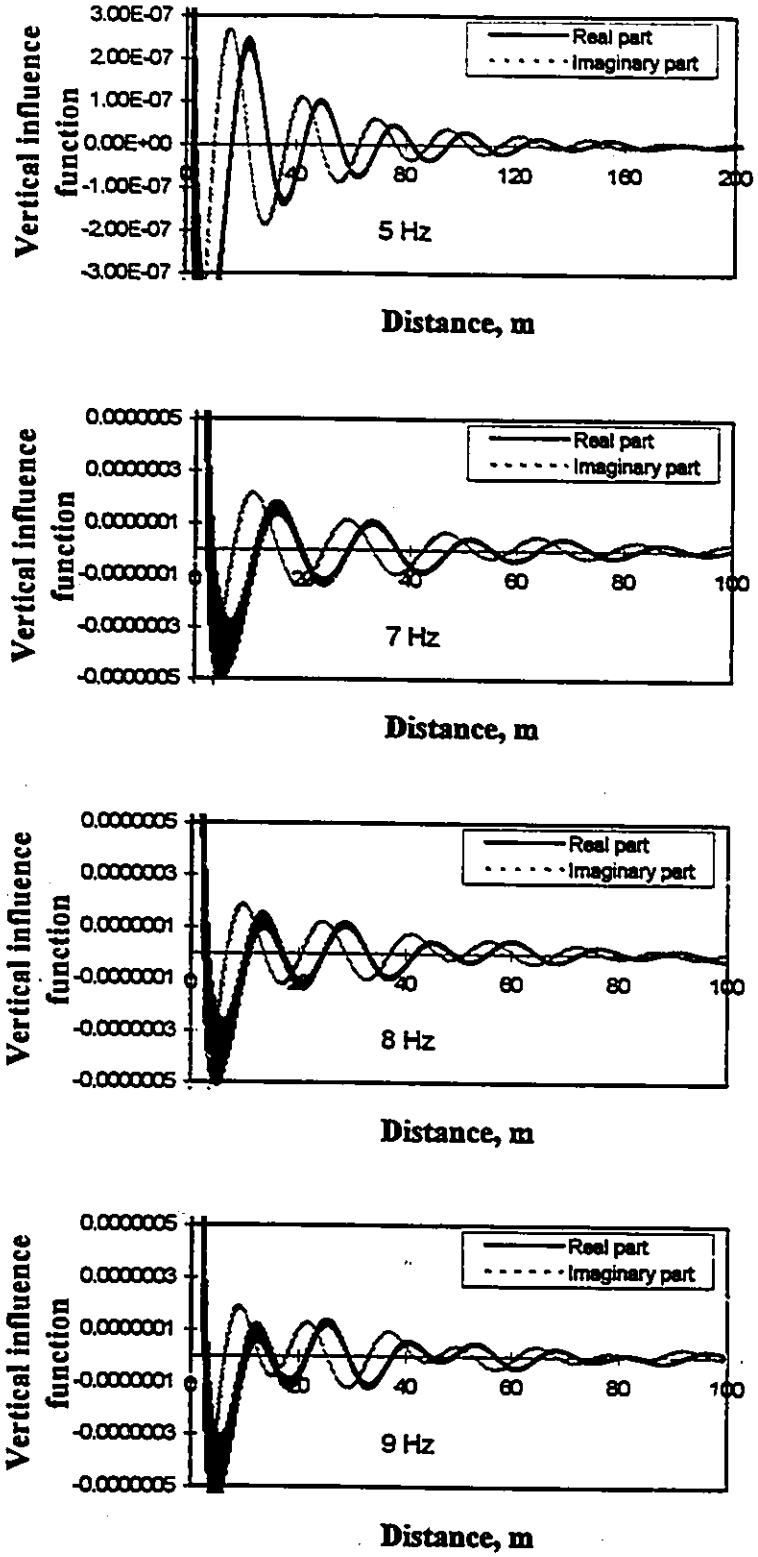

Fig. 6.22-Simulated vertical motion at surface for case 3 at different frequencies (continued).

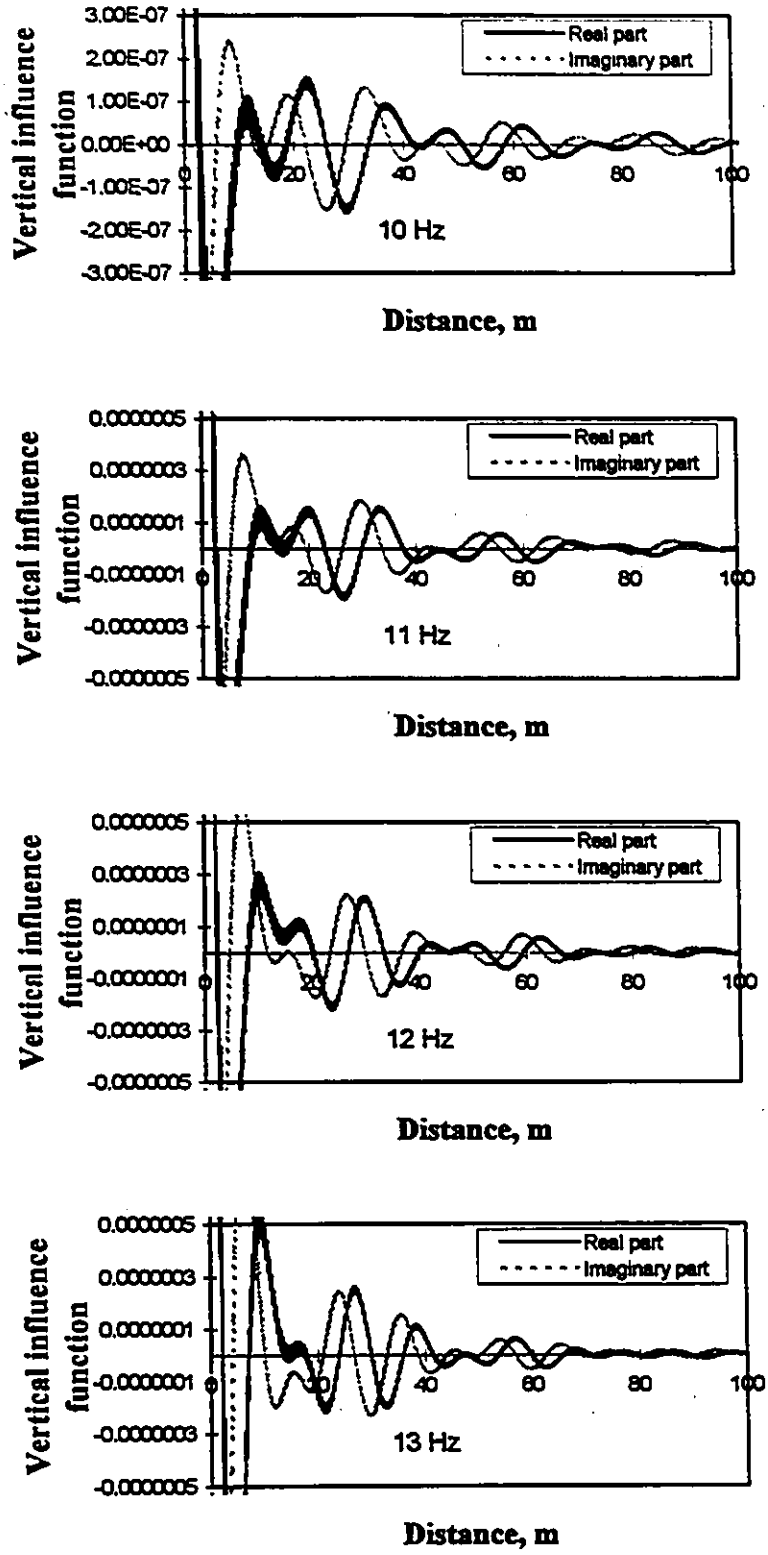

Fig. 6.22-Simulated vertical motion at surface for case 3 at different frequencies (continued).

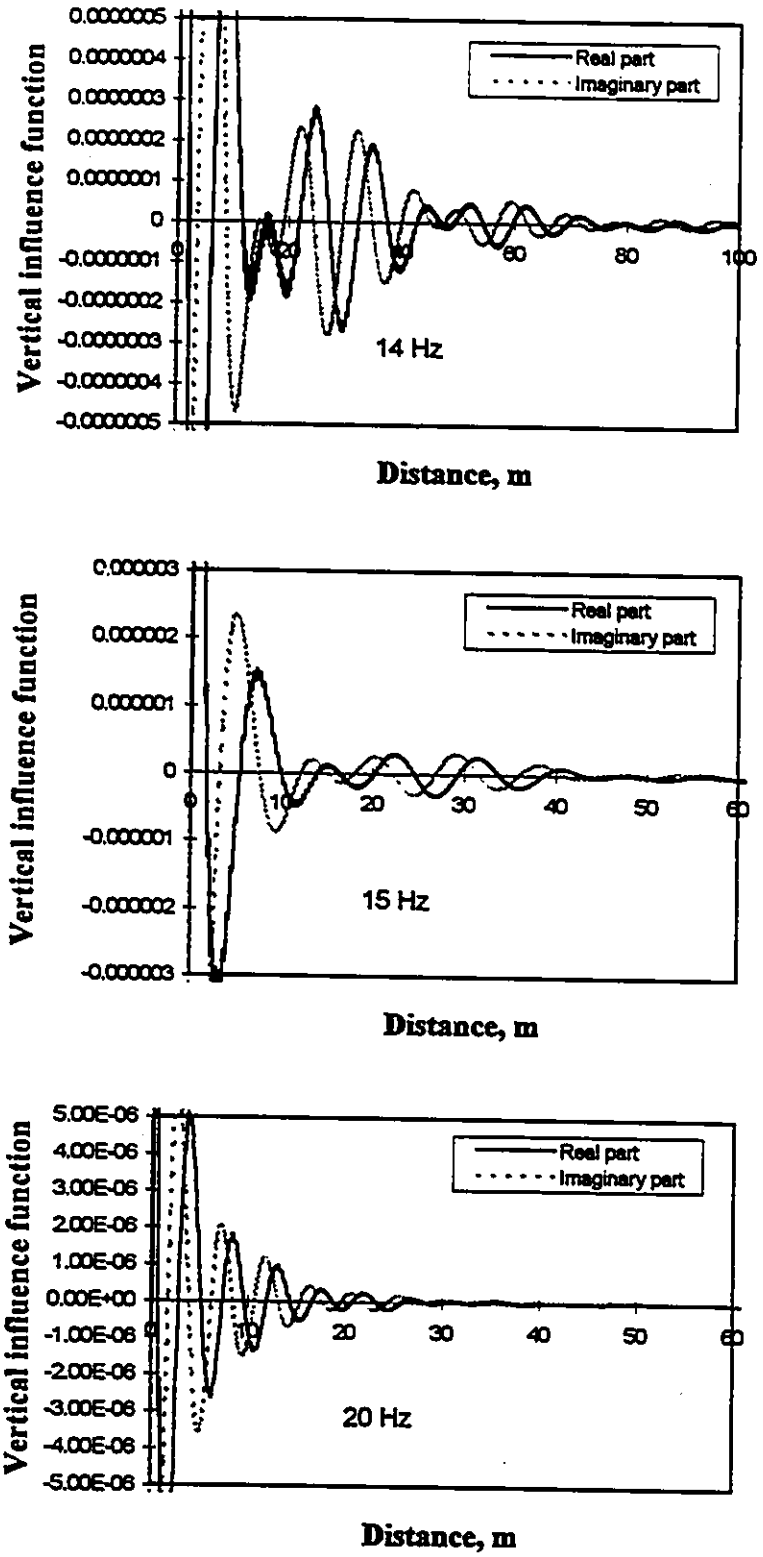

Fig. 6.22-Simulated vertical motion at surface for case 3 at different frequencies (continued).

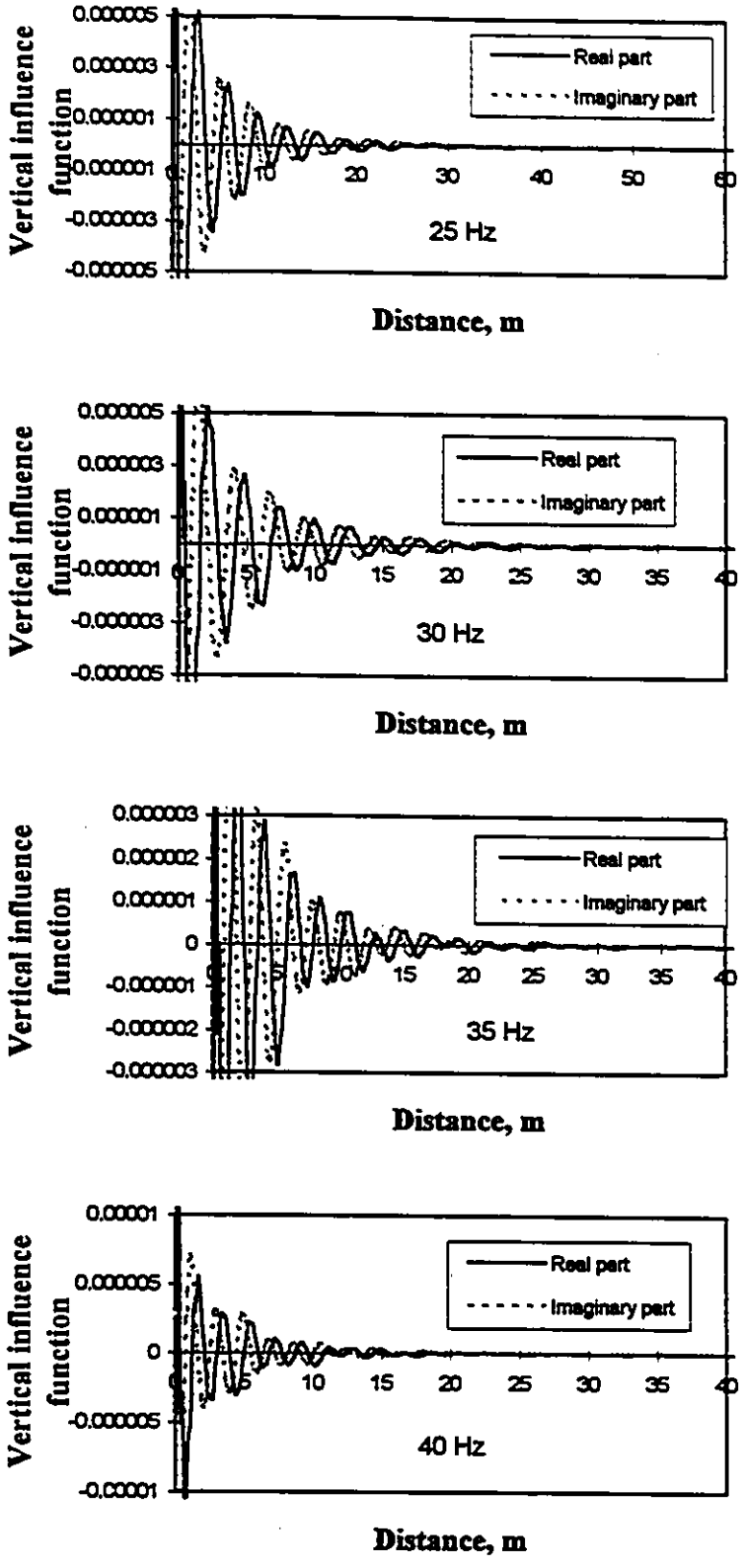

Fig. 6.22-Simulated vertical motion at surface for case 3 at different frequencies (continued).

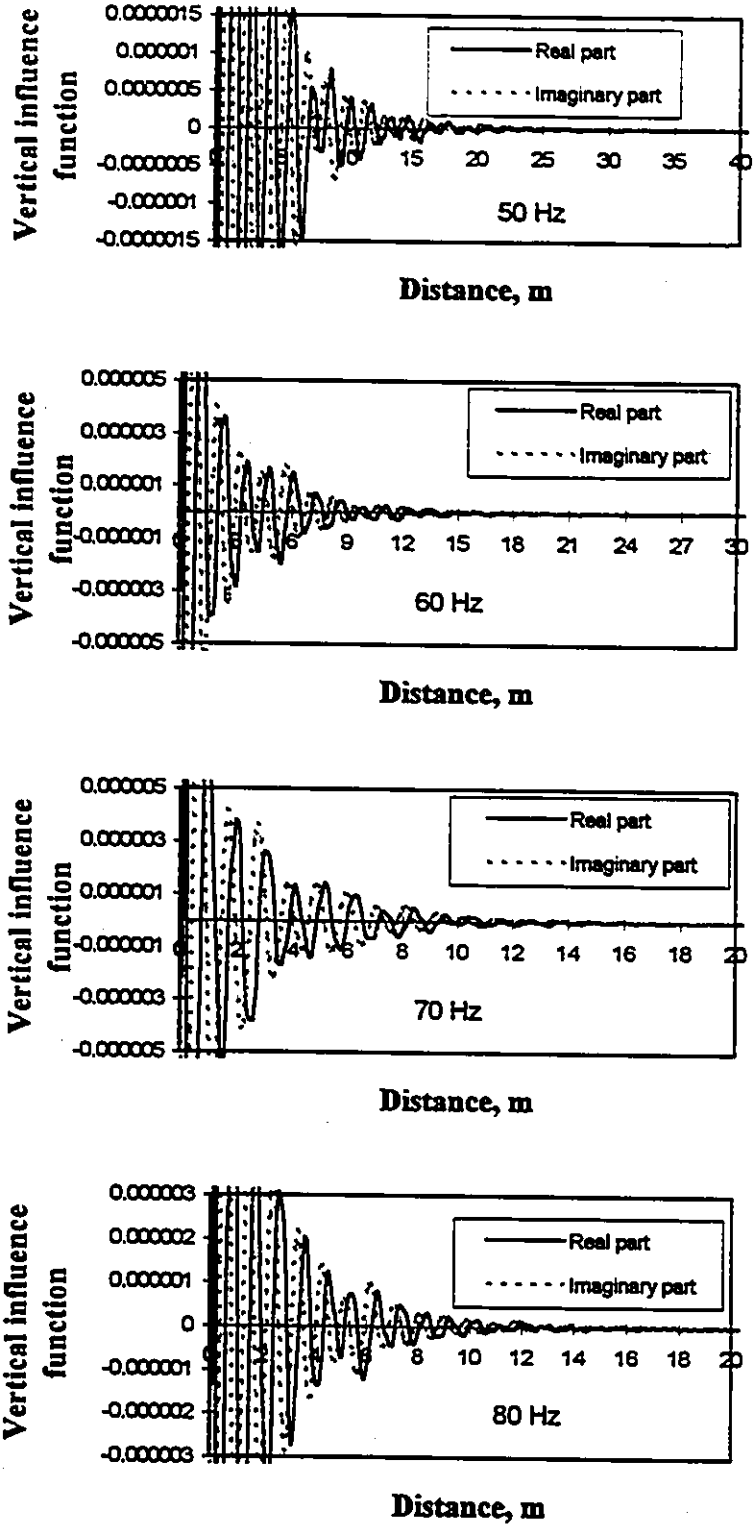

Fig. 6.22-Simulated vertical motion at surface for case 3 at different frequencies (continued).

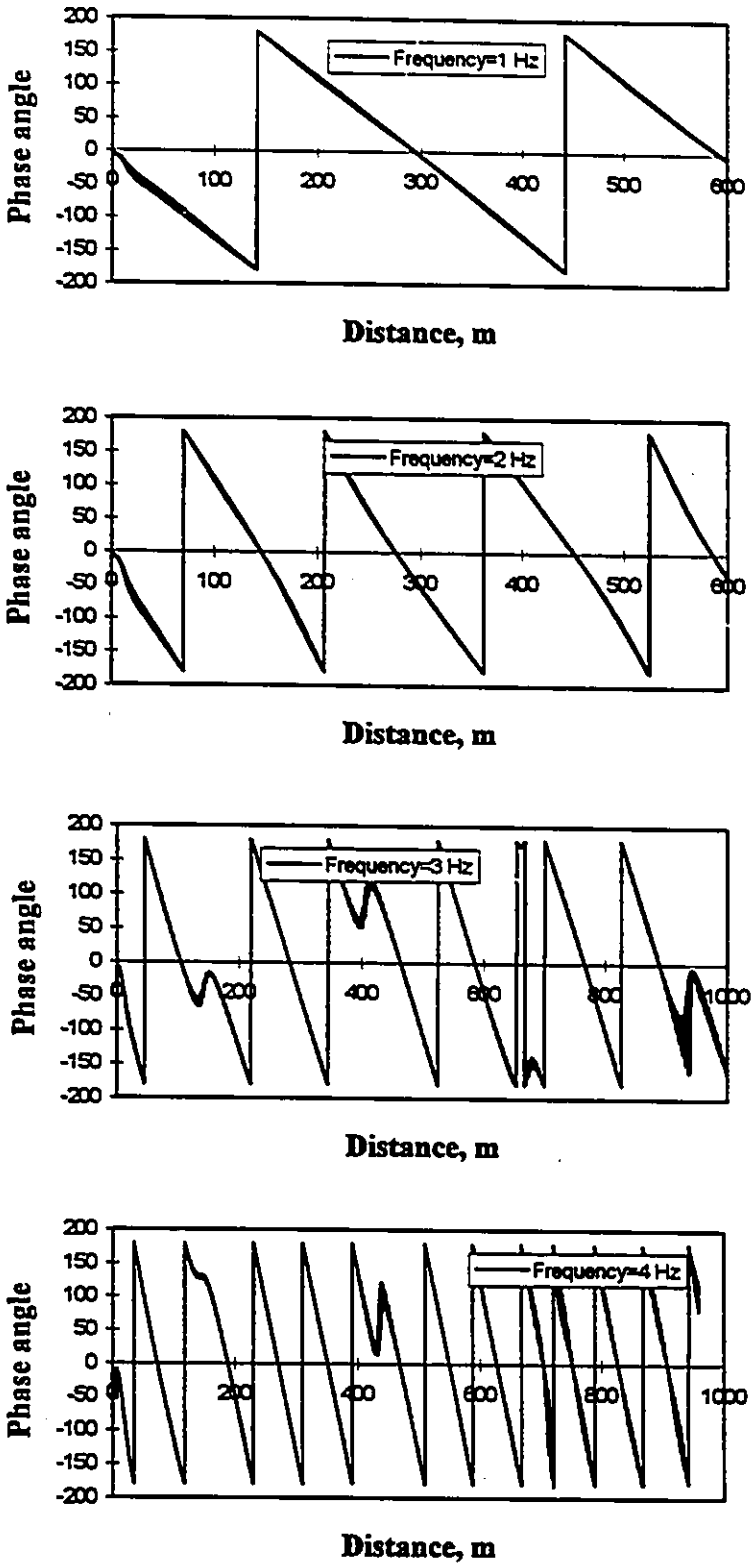

Fig. 6.23-In-phase positions of surface motion for case 2 at different frequencies.

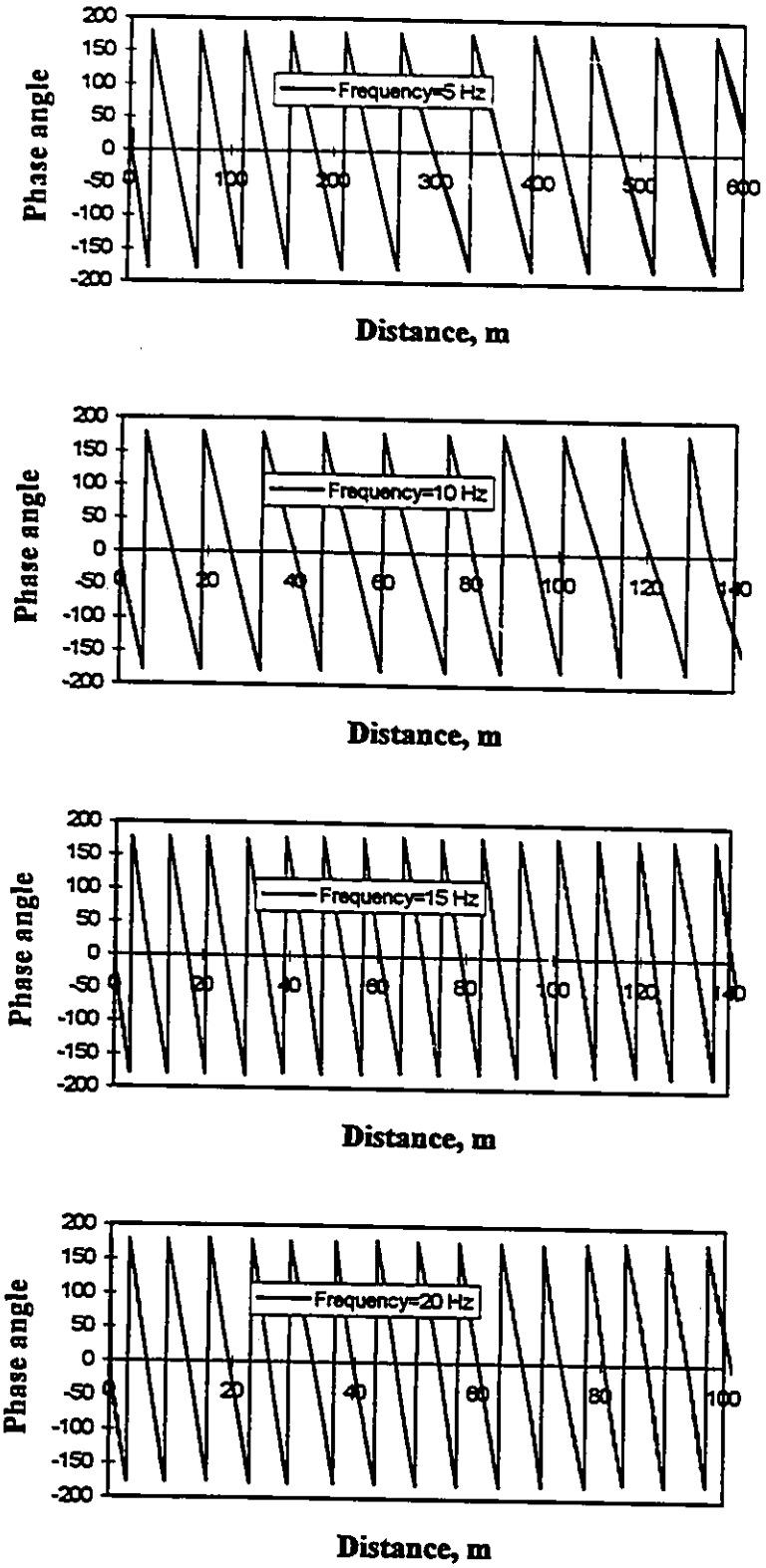

Fig. 6.23-In-phase positions of surface motion for case 2 at different frequencies (continued).

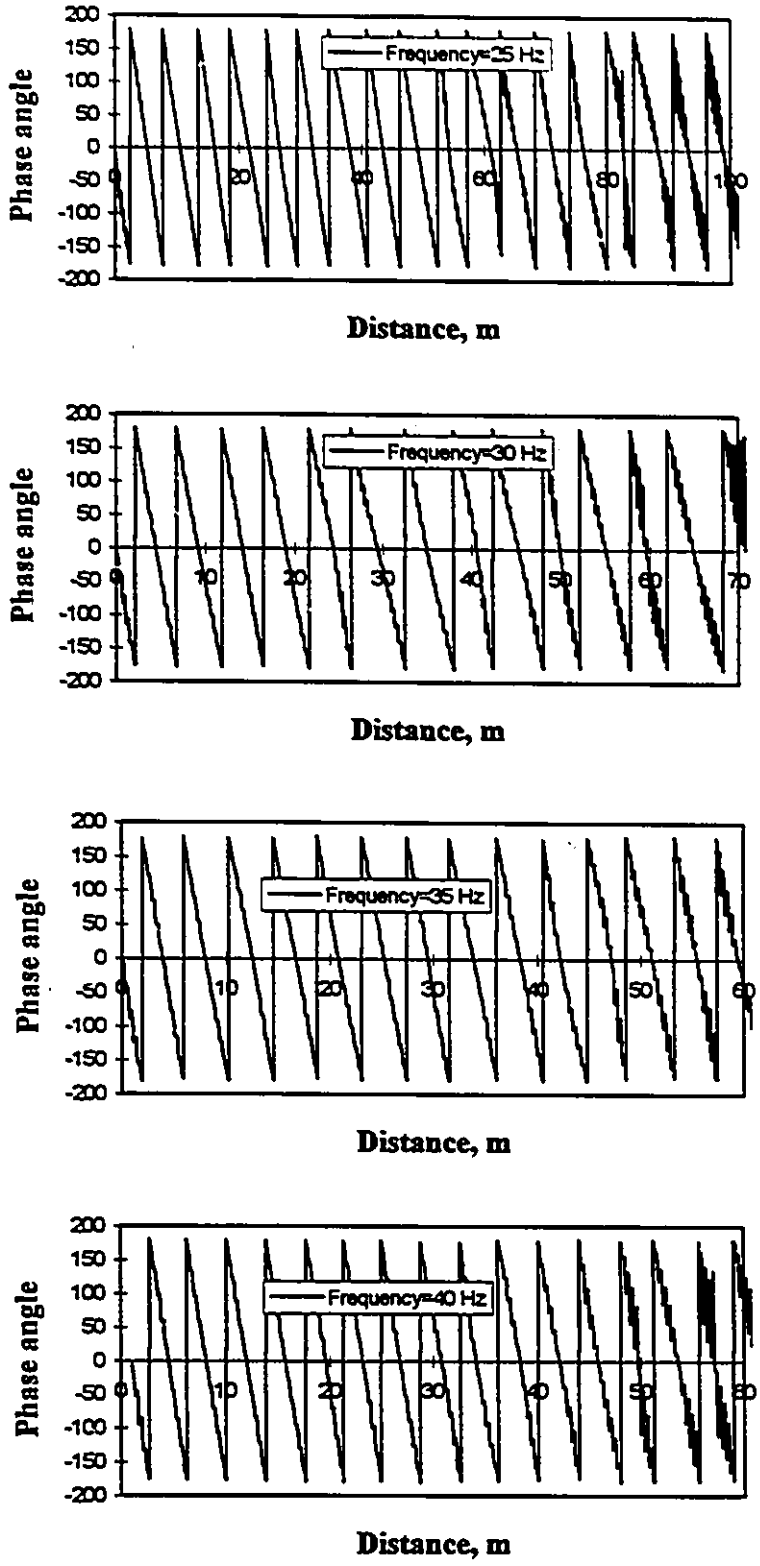

Fig. 6.23-In-phase positions of surface motion for case 2 at different frequencies (continued).

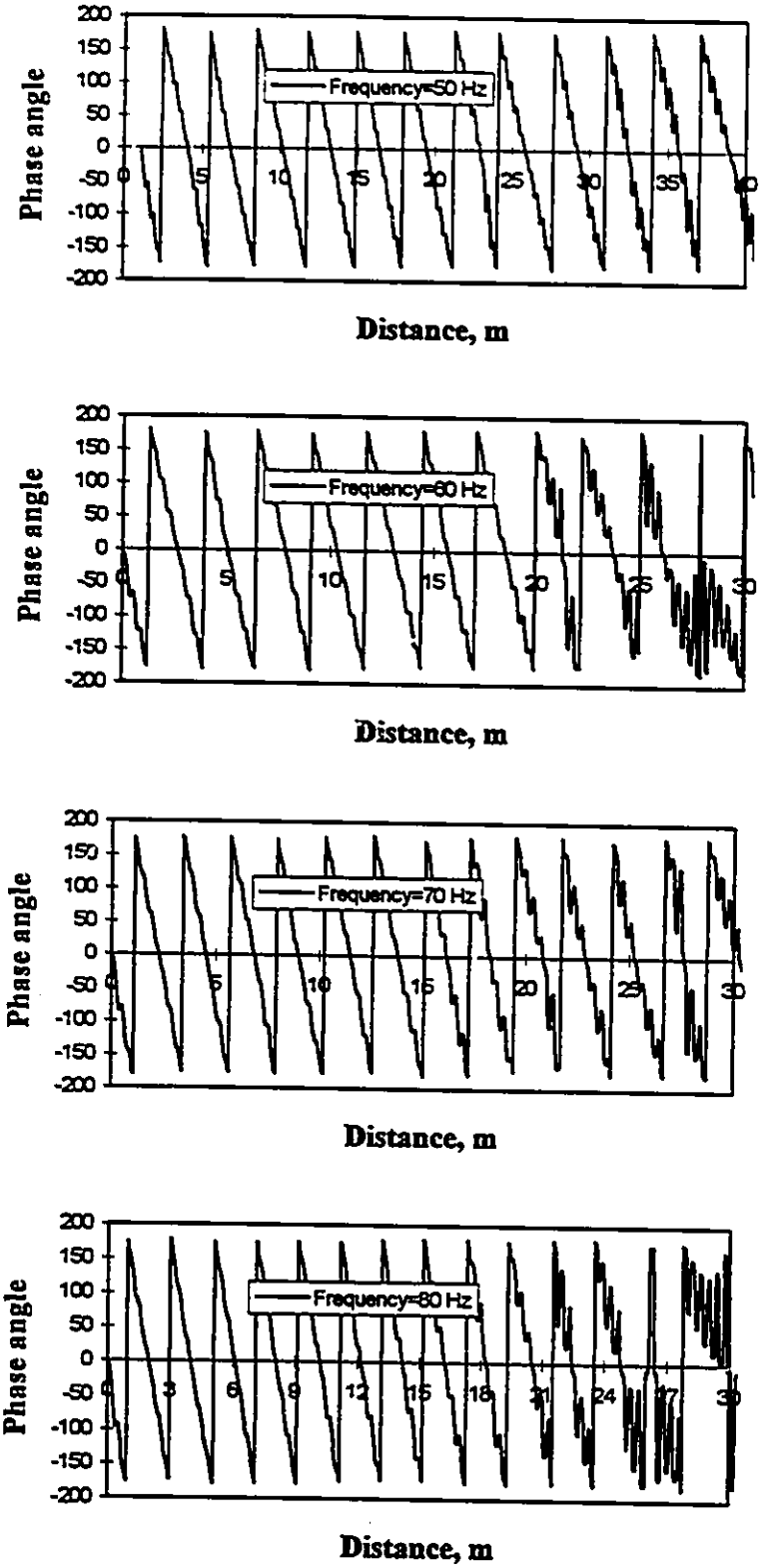

Fig. 6.23-In-phase positions of surface motion for case 2 at different frequencies (continued).

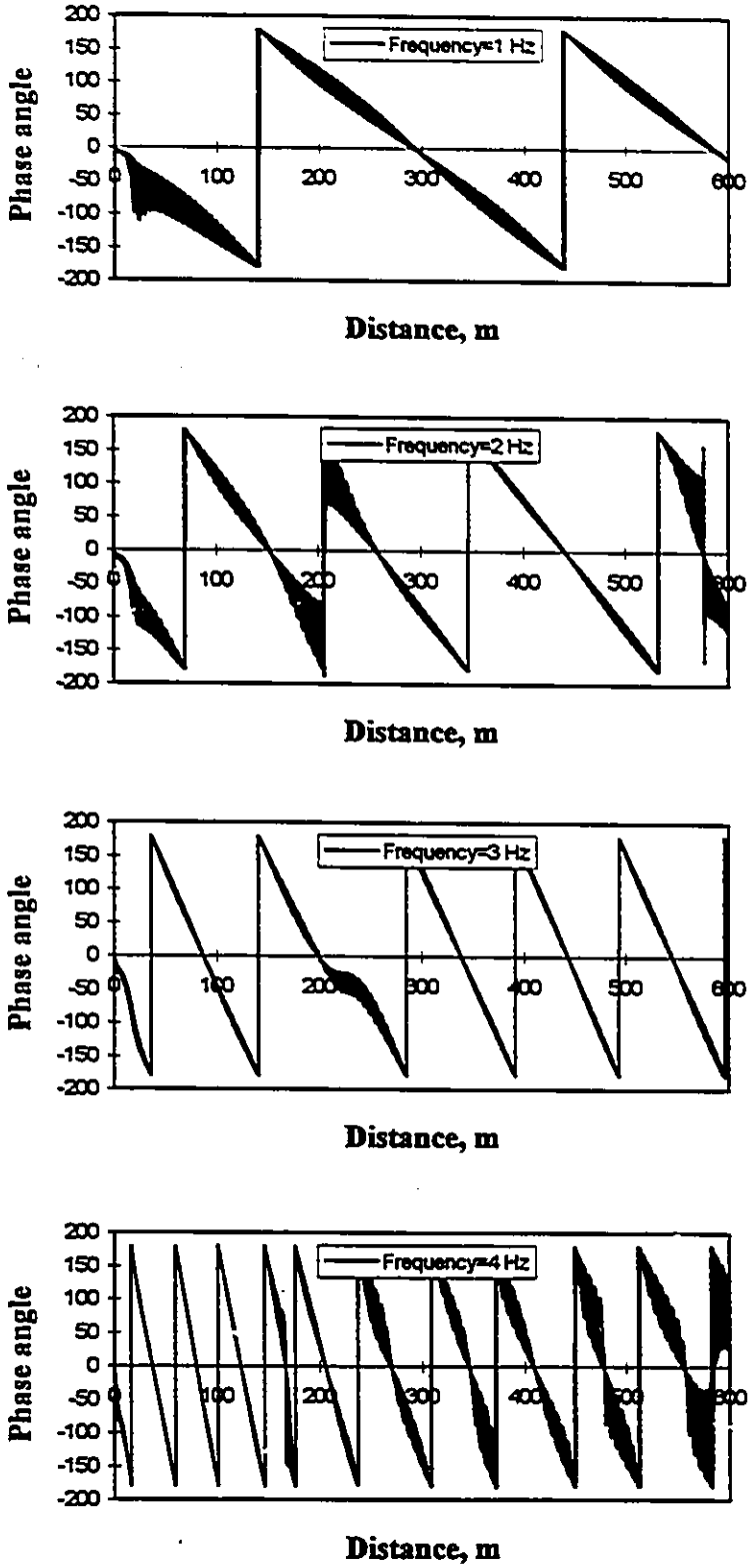

Fig. 6.24-In-phase positions of surface motion for case 3 at different frequencies.

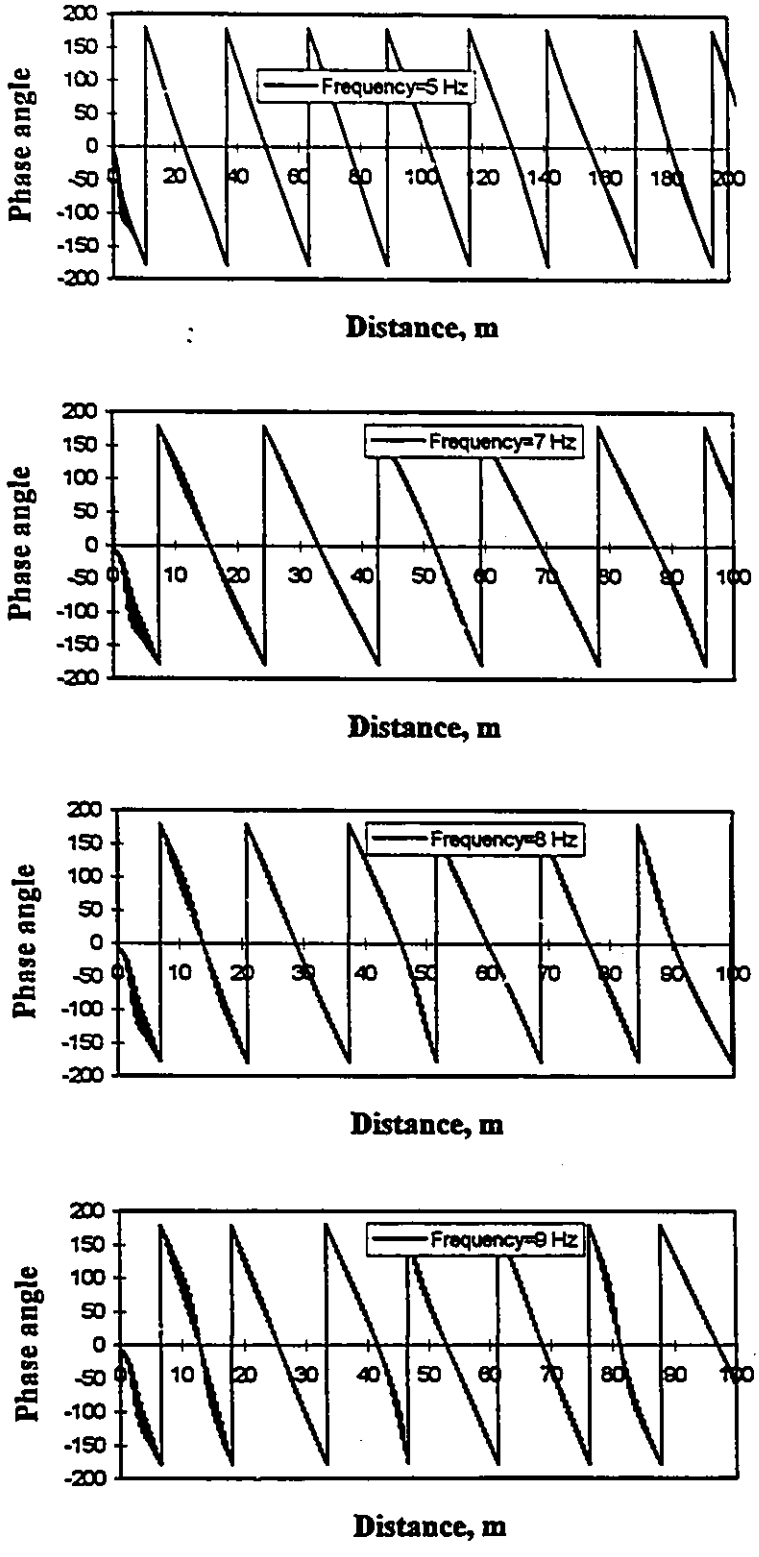

Fig. 6.24-In-phase positions of surface motion for case 3 at different frequencies (continued).

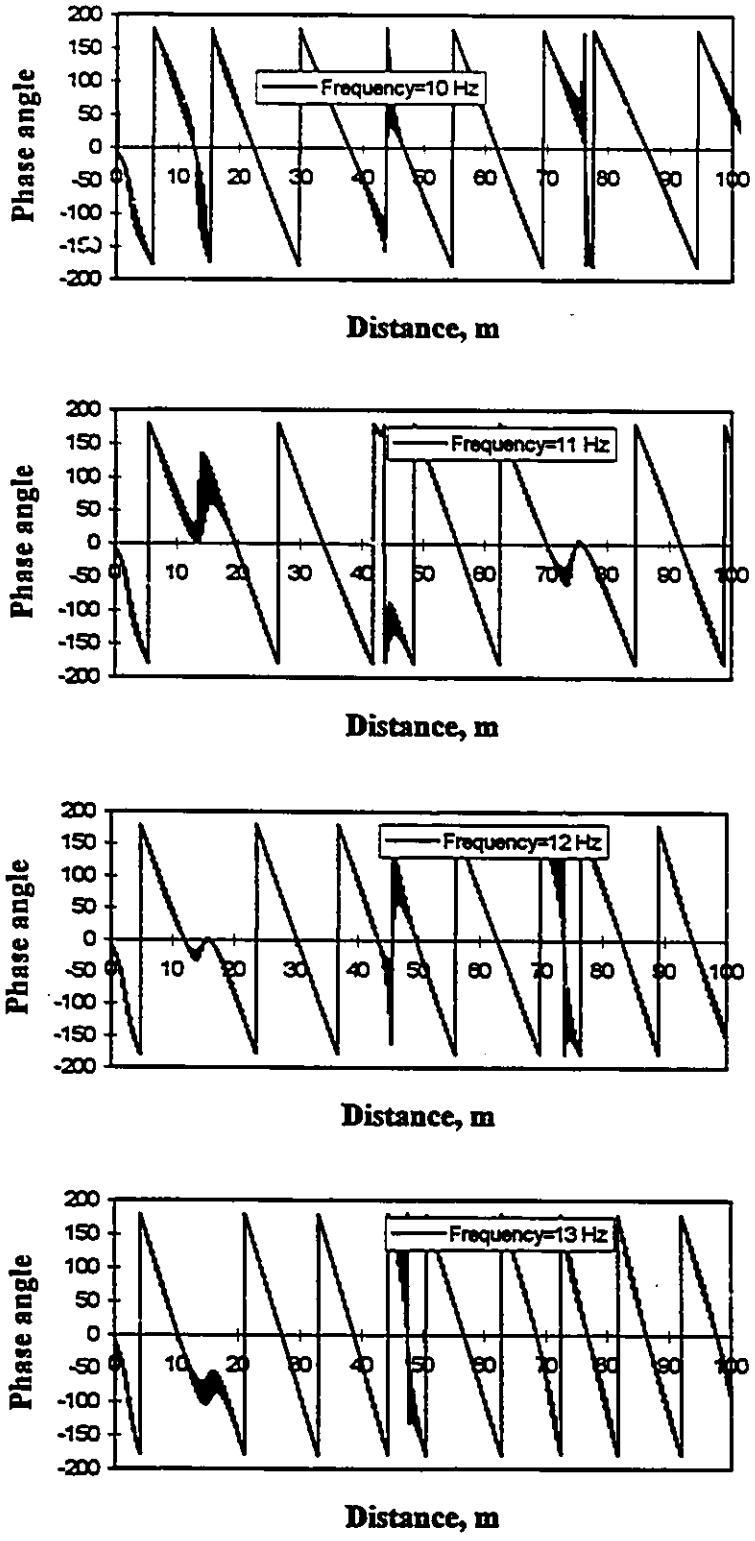

Fig. 6.24-In-phase positions of surface motion for case 3 at different frequencies (continued).

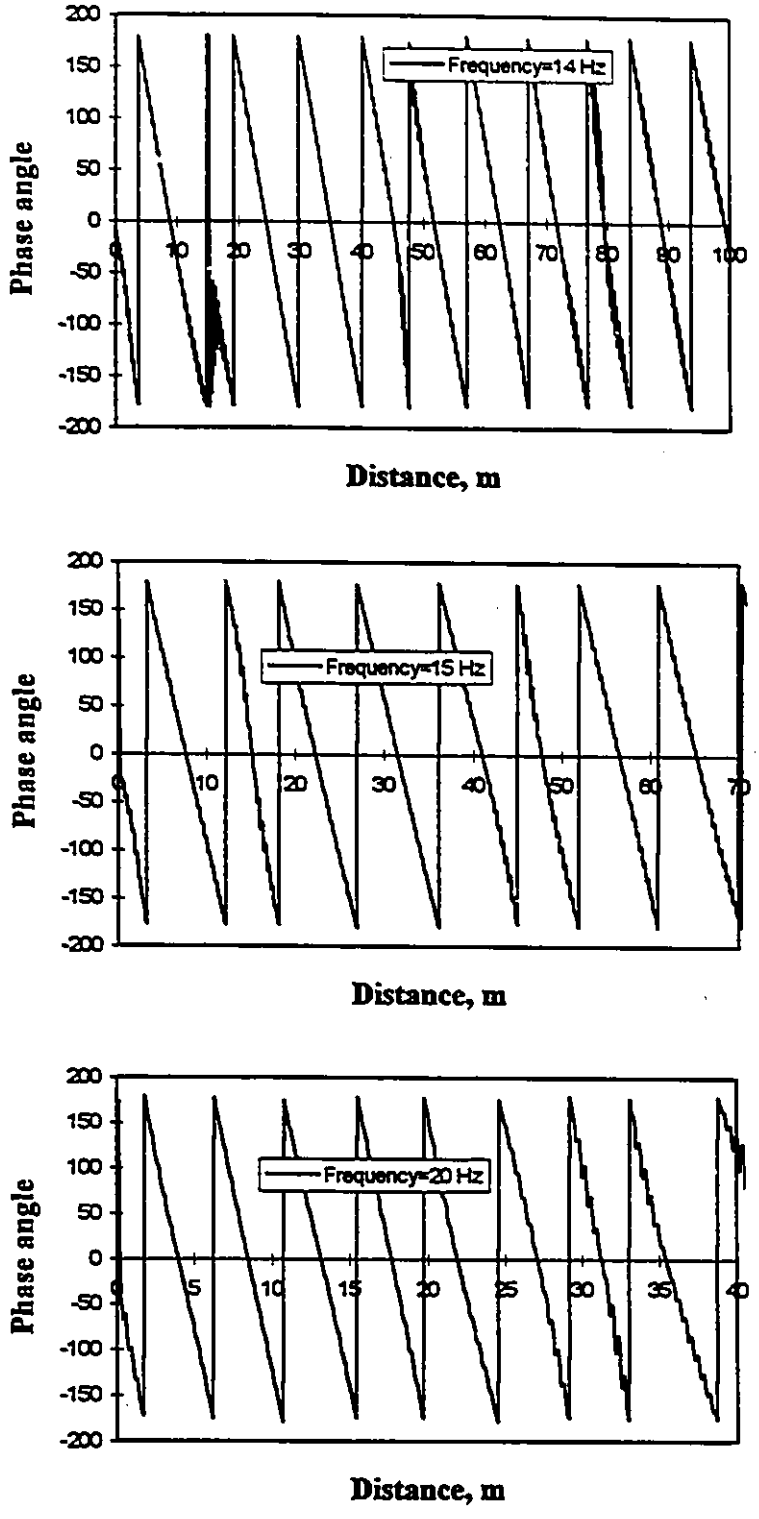

Fig. 6.24-In-phase positions of surface motion for case 3 at different frequencies (continued).

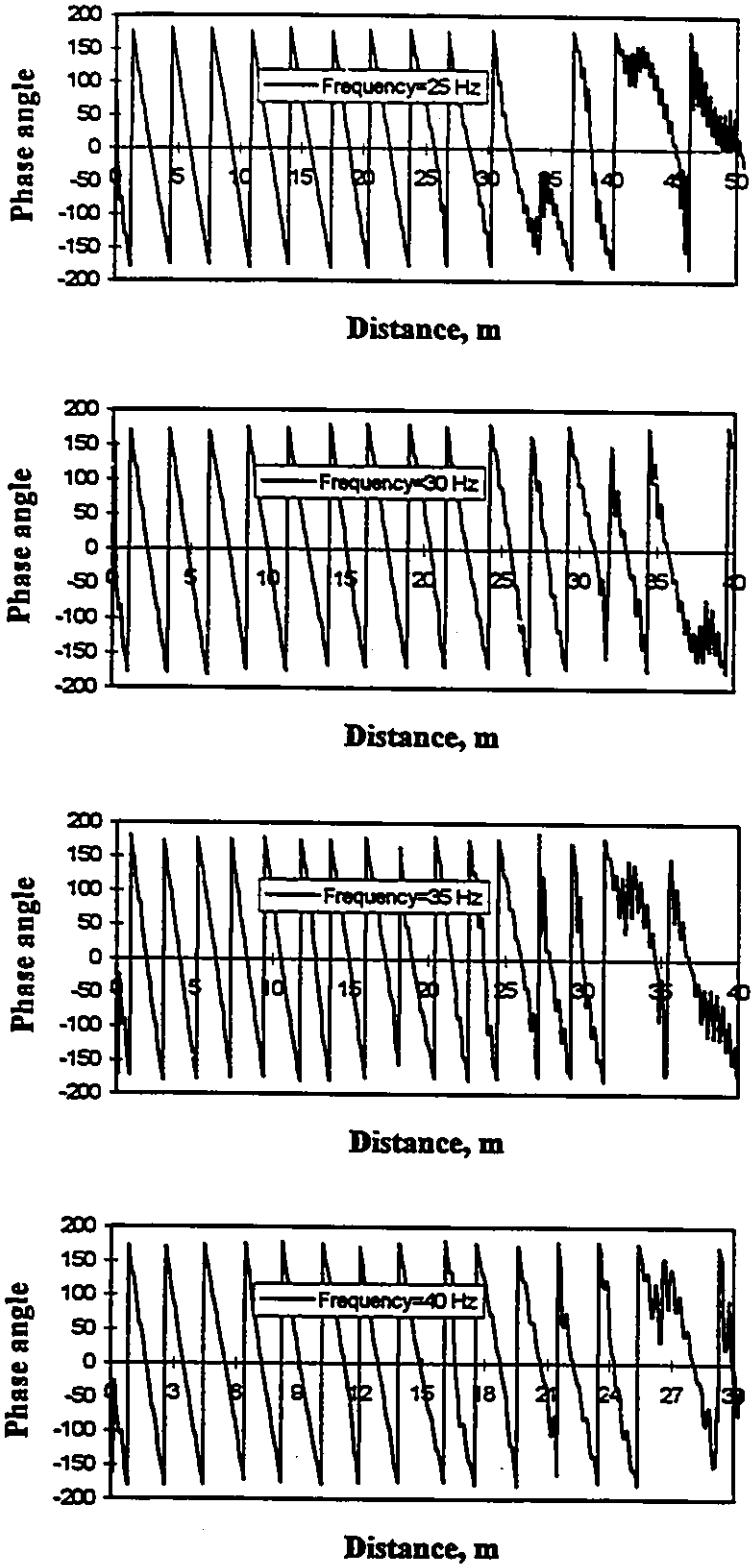

Fig. 6.24-In-phase positions of surface motion for case 3 at different frequencies (continued).

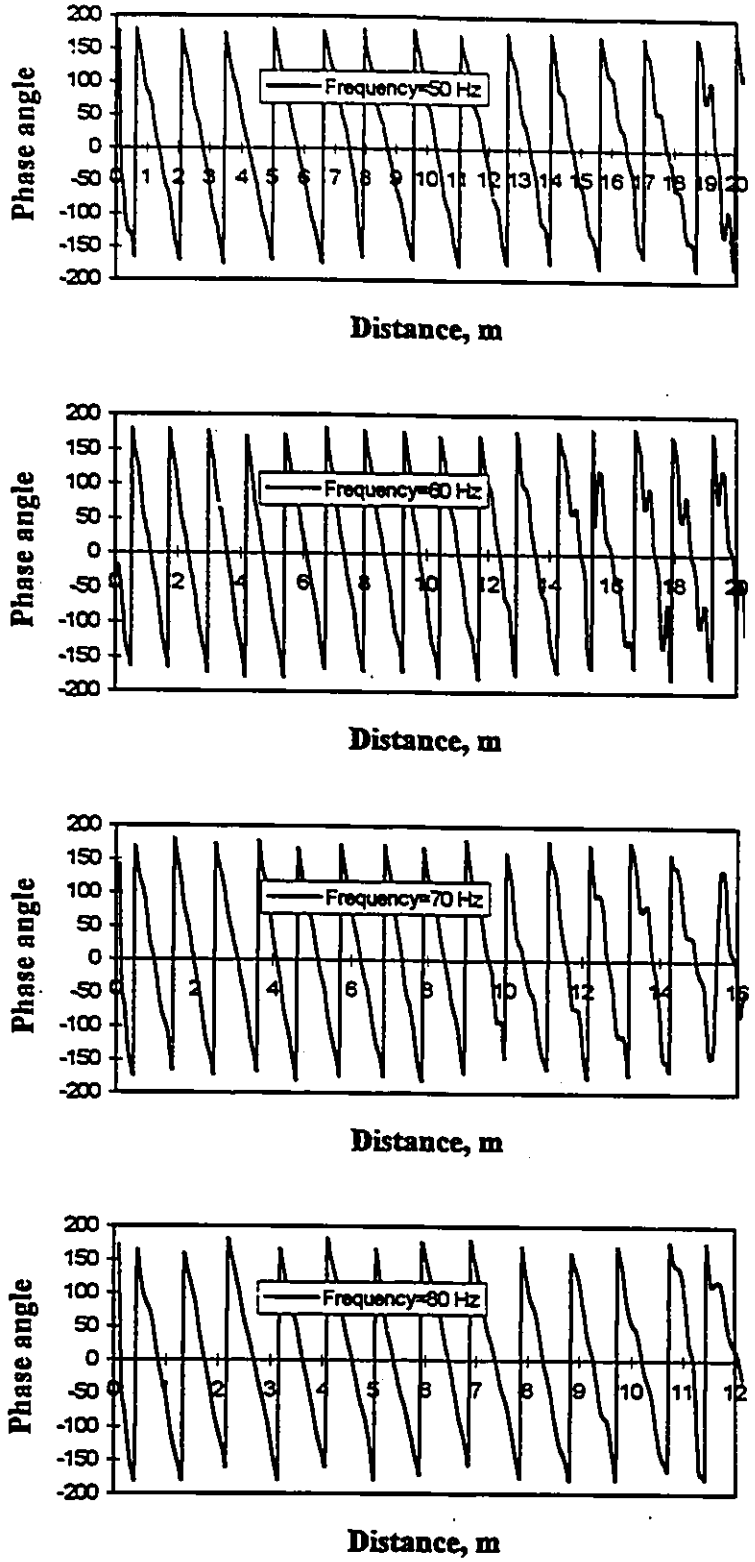

Fig. 6.24-In-phase positions of surface motion for case 3 at different frequencies (continued).

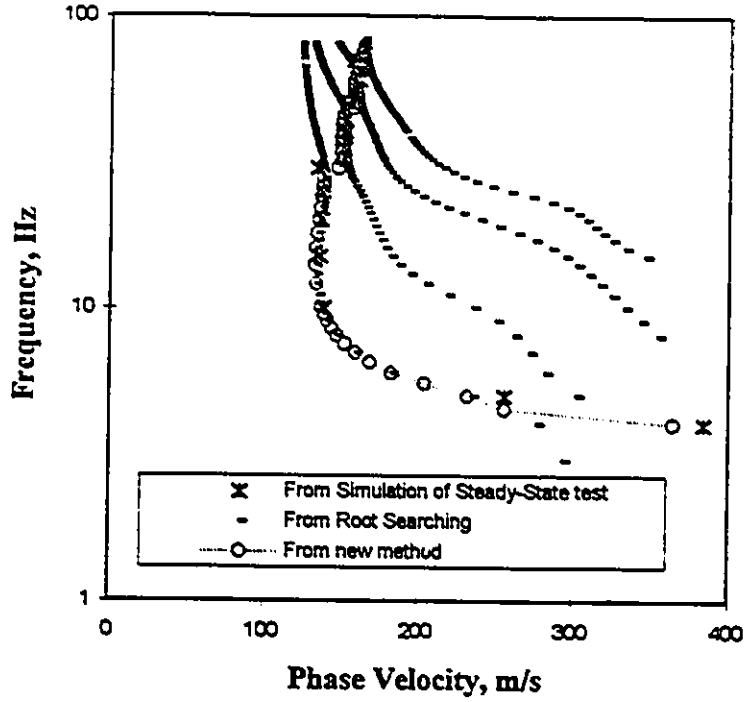

Fig. 6.25-Dispersion curve for case 2 from different procedures.

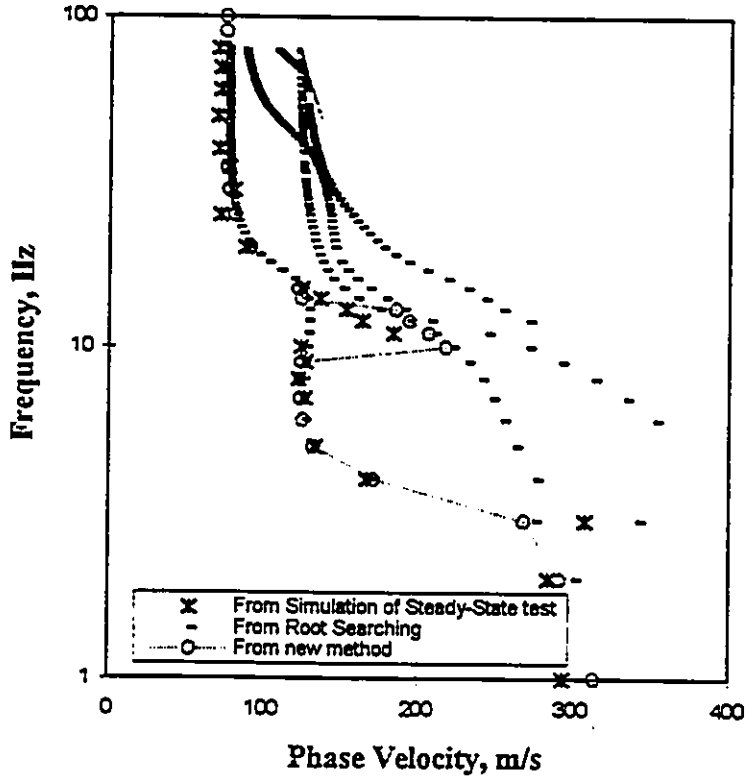

Fig. 6.26-Dispersion curve for case 3 from different procedures.

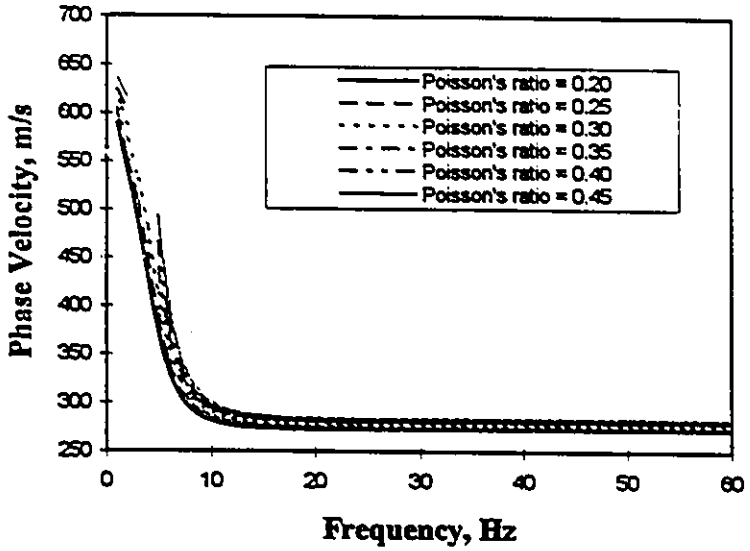

Fig. 6.27-Dispersion curve for layered soil system one with different Poisson's ratios.

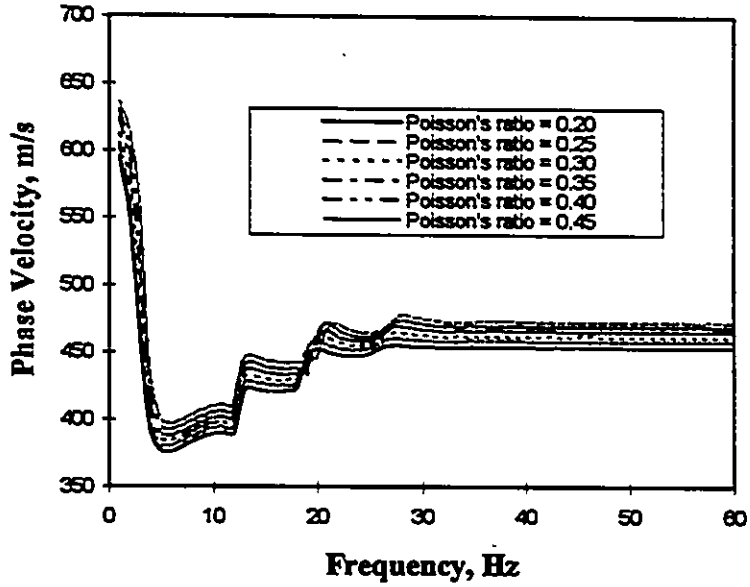

Fig. 6.28-Dispersion curve for layered soil system two with different Poisson's ratios.

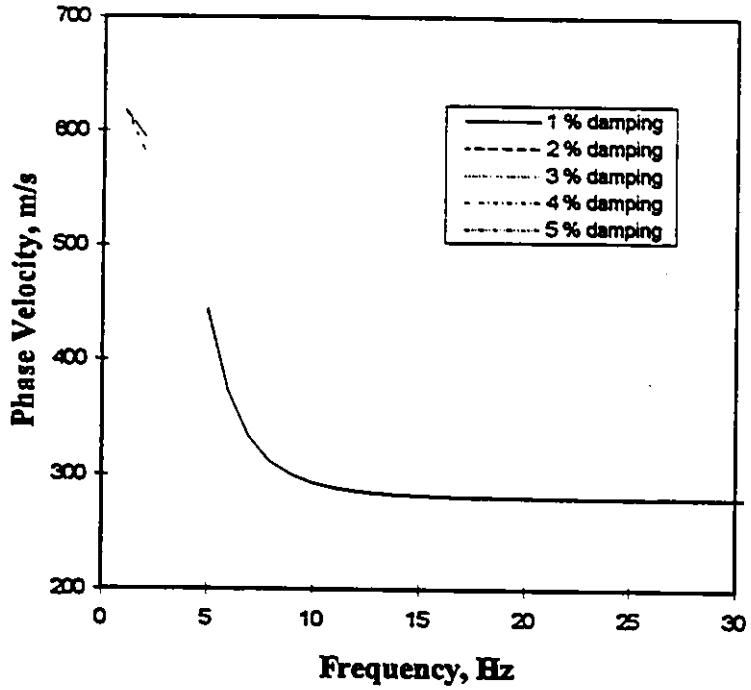

Fig. 6.29-Dispersion curve for layered soil system one with different damping ratios.

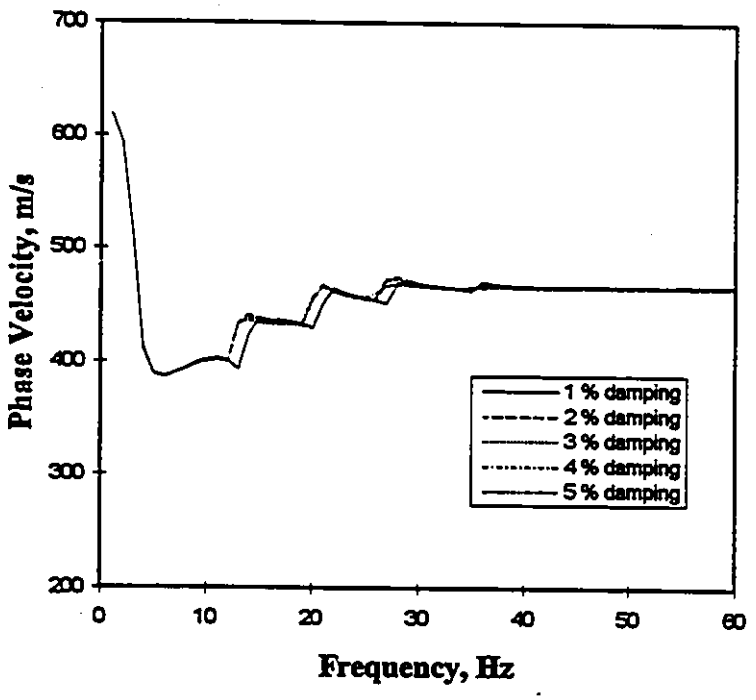

Fig. 6.30-Dispersion curve for layered soil system two with different damping ratios.

CHAPTER 7

AUTOMATION OF INVERSION PROCEDURE

7.1 Matching of Dispersion Curves

The process of matching theoretical and field dispersion curves by iteration is time consuming. To overcome this difficulty, the inversion process is based on matching techniques employing optimization theory. For an initial layered soil system (model), parameters such as thickness (h), shear wave velocity (V_s), mass density (ρ), Poisson's ratio (ν), etc. are assumed. Then a set of theoretical dispersion points is calculated for assumed profile. The soil parameters are changed until the theoretical points match with experimental points. Given n phase velocity (v^{obs}) versus frequency experimental dispersion points, a corresponding number of theoretical phase velocity (v^{the}) versus frequency dispersion points are calculated. The optimization process minimizes the differences between experimental and theoretical dispersion points. Usually the sum of $(v_1^{obs} - v_1^{the})^2 + (v_2^{obs} - v_2^{the})^2 + \cdots\cdots + (v_n^{obs} - v_n^{the})^2$, which is called the sum of the squared residuals, is chosen as the function to be minimized, i.e. merit function.

The matching process therefore involves finding:

$$\sum_{i=1}^{n}(v_i^{obs} - v_i^{the})^2 = \text{minimum} \qquad [7.1]$$

For an N layered soil system, the number of unknown parameters is equal to 4N-1. Since the effects of changing the mass density and Poisson's ratio are negligibly small, the total number of layer properties to be determined in the inversion analysis can be reduced to 2N-1. For a soil deposit in which thickness of each layer is known in advance, the total number of properties may be further reduced to N.

Various optimization methods that can be used to solve Equation [7.1] are presented in this chapter.

7.2 Down-Hill Simplex Method

The simplex method was first proposed by Nelder and Mead, in 1965. The method requires only function evaluations, not derivatives. A simplex is a geometric figure that has one vertex more than the dimension of space in which it is defined. A triangule and a tetrahedron are examples of a simplex in a two and three-dimensional space, respectively.

To minimize a function of n variables, a set of initial values P_0, P_1, P_2,..P_n are assumed to be the n+1 points in n-dimensional space defining the current "simplex". The function value at P_i is represented by y_i. Also, P_h and P_l are defined as points with the highest and lowest function values, respectively. Also, $\bar{P}$ is defined as the centroid of all points except P_h, and $[P_i\ P_j]$ is defined as the distance from P_i to P_j. At each stage of the minimization process, the objective is to find the point with the highest function value and to replace it with a new point which has a smaller function value. To achieve this goal, three main operations called reflection, contraction, and expansion are applied (see Fig. 7.1).

The reflection of P_h is denoted by P^*, whose coordinates are obtained from the coordinates of P_h by the following relation:

$$P^* = (1+\alpha)\bar{P} - \alpha P_h \qquad [7.2]$$

where α is a positive constant called the reflection coefficient and typically assumed to be 1. Thus P^* is located on the line joining P_h and $\bar{P}$, on the far side of $\bar{P}$ from P_h with $[P^* \bar{P}] = \alpha[P_h \bar{P}]$. For α assumed equal to 1, then

$$[P^* \bar{P}] = \alpha[P_h \bar{P}] = [P_h \bar{P}] \qquad [7.3]$$

If y^* lies between y_h and y_l, then the reflection operation produces a new minimum (i.e. a better point). In this case, P_h is replaced by P^*, and the whole process is re-started with the new simplex.

If $y^* < y_l$, i.e. reflection produces a new minimum, then a new point P^{**} is calculated by an expansion operation defined by the relation:

$$P^{**} = \gamma P^* + (1-\gamma)\bar{P} \qquad [7.4]$$

where γ is the expansion coefficient, that is greater than unity, and is defined by the

$$\gamma = \frac{[P^{**} \bar{P}]}{[P^* \bar{P}]} \qquad [7.5]$$

If $y^{**} < y_l$, P_h is replaced by P^{**} and the process is restarted. However, if $y^{**} > y_l$, P_h is replaced by P^* before re-starting. In the case where $y^* > y_i$ for all values of y_i, where $i \neq h$, replacing P by P^* leaves y^* as the maximum. Then, a new P_h is defined as either the old P_h or P^*, whichever has the lower y value. Therefore, in this case, the next step is to contract the new P_h by the following relation:

$$P^{**} = \beta P_h + (1-\beta)\bar{P} \qquad [7.6]$$

where β is a contraction coefficient that lies between 0 and 1 and is defined by

$$\beta = \frac{[P^{**}\,\bar{P}]}{[P\,\bar{P}]} \qquad [7.7]$$

P_h is then replaced by P^{**} and the process is re-started, unless $y^{**} > \min(y_h, y^*)$ (i.e. the contracted point is worse than the better of P_h and P^*). If $y^{**} > \min(y_h, y^*)$, all the P_i's are replaced by the following points.

$$P_i = \frac{(P_i + P_l)}{2} \qquad [7.8]$$

and then the process is re-started.

A flow chart of the down-hill simplex method as described above is shown in Fig. 7.2. Further details are given by Nelder and Mead (1965).

7.2.1 Program SASW-INVERT

SASW-INVERT is a program developed during this study for calculating a theoretical dispersion curve that matches a given in-situ curve. The program is written in Fortran language.

The following input is required by the program SASW-INVERT:

1. Initial soil profile including shear wave velocity, thickness, Poisson's ratio, mass density, and damping ratio of each layer,
2. The number of measured dispersion points.
3. The maximum number of iterations, and
4. The range of wave numbers.

The initial guess of shear wave velocity and thickness may be made by using the simple empirical inversion procedure (Richart et al. 1970):

$$V_s = 1.10 V_{ph} \qquad [7.9]$$

$$H = 0.5\lambda_{ph} \qquad [7.10]$$

where V_s is shear wave velocity, V_{ph} is phase velocity, H is thickness (equivalent sampling depth), and λ_{ph} is wavelength.

For each frequency, SASW-INVERT calculates the vertical flexibility coefficients for the specified range of the wave number. Then, it finds the wave number corresponding to the maximum vertical flexibility coefficient. Knowing the wave number, phase velocity is calculated by

$$V_{ph} = \frac{\omega}{k} \qquad [7.11]$$

where ω is the circular frequency, and k is the wave number.

This procedure is repeated for all frequencies. The sum of squares of the difference between experimental and theoretical points is then calculated.

Using the down-hill simplex algorithm, the parameters of the model are adjusted until a set of best-fit parameters are found for which theoretical wavelengths and phase velocities match the experimental ones.

As stated in Section 3.4, for most soil sites, the variation in values of Poisson's ratio and mass density has no significant effect on the dispersion curve. Therefore, they are generally not changed after the initial choice is made.

The convergence of successive iterations is monitored by the following root-mean-square error criterion:

$$\varepsilon = \sqrt{\frac{1}{N}\sum_{i=1}^{N}\Delta V_i^2} \qquad [7.12]$$

where N is number of dispersion data points, and $\Delta V_i = V_i^{obs} - V_i^{the}$.

The iteration procedure is terminated when ε reaches an acceptable small value or when all elements of vector ΔV are within the other pre-specified limits.

7.2.2 Verification Of SASW-INVERT

To ensure that program SASW-INVERT was producing correct results, the following test was carried out.

First, SASW tests were simulated for the site is shown in Fig. 7.3. The dispersion curve for this site, after reducing the number of points, is shown in Fig. 7.4. To determine the shear wave velocity profile, two different inversion procedures were implemented. In the first one, the thickness of each layer was assumed as known, and only the shear wave velocity of each layer was determined. This procedure is called shear wave velocity inversion. In the second procedure, both the thickness and the shear wave velocity of layers were assumed as unknown. This inversion procedure is called shear wave velocity and thickness inversion. During the inversion process, a Poisson's ratio of 0.45 and mass density of 2000 Kg/m^3 were assumed for all layers.

Using the simple empirical inversion procedure, given by Eq. 7.9 and 7.10, initial values of shear wave velocity and layer thickness were assumed. The initial guesses for the above two procedures are shown in Tables 7.1, 7.2. The final shear wave velocity profiles and theoretical dispersion curves obtained with SASW-INVERT are shown in Tables 7.3 and 7.4 and Figs. 7.5 and 7.6 respectively. The inversion for same site as reported by Yuan and Nazarian (1993) is shown in Fig. 7.7. By comparing the results in Figs. 7.6 and 7.7 and the shear wave velocity profiles in Tables 7.3 and 7.4 with exact profile it is verified that program SASW-INVERT works well.

7.2.3 Difficulties with Down-Hill Simplex Method

The simplex method is simple and requires only function evaluations, not derivatives, which makes suitable for optimization of discontinuous functions. However, it is not very efficient in terms of the number of function evaluations required.

Another drawback of this method is false convergence. This problem, however, is found in almost all minimization routines. To avoid this problem in the case of the Simplex Down-Hill method, Press et al. (1992) suggest to re-start the minimization process at a point where the method claims to have found a minimum.

To investigate the effect of selection of initial profile to reach a good match, the SASW-INVERT was re-run for the initial profiles as given in Table 7.5. Fig. 7.8 shows the theoretical and field dispersion points for this case. The final profile is shown in Fig. 7.9. In this case the program converges to the local minimum and by comparing the result, it was found that the initial estimated values have significant role in the inversion algorithm.

To overcome the above shortcomings simulated annealing was implemented in conjunction with the simplex method.

7.3 Simulated Annealing

Simulated annealing is an attractive technique for optimization of large scale problems, especially ones where a desired global extremum is hidden among many, poorer, local extrema.

The simulated annealing can be described with a thermodynamics analogy, namely with the way that liquids freeze and crystallize, or metals cool and anneal. The molecules of a

liquid can move freely with respect to one another at high temperature. If the liquid is cooled slowly, thermal mobility is lost and system reaches a minimum energy state.
To minimize function f(x), where x is an N-dimensional vector, four elements are required as follows: The value of the objective function f, the temperature, with an annealing schedule by which it is gradually reduced, and a generator of random changes in the configuration, and a procedure for taking a random step from x to $x+\Delta x$. The last element, choosing Δx is the most problematical.

Simulated annealing was applied to minimize the difference between theoretical and experimental phase data by using a modified version of the down-hill simplex method. In this procedure, the single point x was replaced as a description of the system state, by a simplex of N+1 points. The next step is applied using the same operations as described in Section 7.2 (i.e. reflections, expansions, and contraction). In addition, a positive logarithmically distributed of random variable, proportional to the temperature T, was added to the stored function values. These values are associated with every vertex of the simplex and a similar variable is subtracted from the function value of every new point which is tried as a replacement point. In the limit $T\rightarrow 0$, this algorithm reduces exactly to the downhill simplex method and converges to a local minimum.

At a final value of T, the simplex expands to a scale that approximates the size of the region that can be reached at this temperature, and then executes a stochastic, tumbling Brownian motion within the region, sampling new, approximately random, point as it does so. If the temperature is reduced sufficiently slowly, it becomes highly likely that the simplex will shrink into that containing the lowest relative minimum encountered. The success or failure of simulated annealing is quite often determined by the choice of annealing schedule. Details of this method were described by Kirkpatrick, (1984).

By implementing simulated annealing inversion procedure and running several cases, it was found again that the initial estimation has significant influence on the final result.

7.4 Linearized Least-Squares Method

In another step, to find a more efficient procedure for matching theoretical dispersion curves and experimental data, a modified version of the nonlinear optimizing method was used. This approximate procedure was originally proposed by Dorman and Ewing, (1962).

Assume that on a soil profile with M layers, a series of SASW tests has been carried out. Then an experimental dispersion curve containing N data point has been constructed. The number of N data depends on the quality of field data. The dispersion curve shows the corresponding experimental phase velocity v_i^{obs} at each frequency f_i. To invert the dispersion curve an initial profile P is first assumed. Mathematically, P is a vector with elements containing shear wave velocity and thickness of each layer. Theoretical phase velocity v_i^{thr} at each frequency is calculated based upon the assumed profile. The goal is to find the P profile for which the difference between the observed and theoretical data points is minimum, i.e.

$$LS = \sum_{i=1}^{N} (v_i^{obs} - v_i^{thr})^2 = \text{minimum} \quad [7.13]$$

In this inversion process, Poisson's ratio, mass density, and damping ratio are fixed. Therefore, the theoretical phase velocity is only a function of the thickness of the layer and shear wave velocity:

$$v = f(p_1, p_2, p_3, \ldots\ldots p_k) \qquad [7.14]$$

If V is defined as a column vector that has N elements, $v_i^{obs} - v_i^{thc}$, then in matrix notation Eq. 7.13 can be written as:

$$V^T V = \text{minimum} \qquad [7.15]$$

In order to satisfy Equation [7.15] a set of corrections, Δp_i, denoted by the column vector, D, are sought.

The change in p_j due to the increment Δp_j will also correspond to a small incremental change in v_{ij} at frequency f_i. This small incremental change, Δv_{ij} is evaluated numerically by the modeling Equation [7.14]:

$$\Delta v_{ij} = f(p_1, p_2, \ldots\ldots, p_j + \Delta p_j, \ldots p_k) - v_i \qquad [7.16]$$

The partial derivative of v at frequency f_i with respect to p_j can be expressed as:

$$\frac{\partial v_i}{\partial p_j} = \frac{\Delta v_{ij}}{\Delta p_j} \qquad [7.17]$$

Using the partial derivatives evaluated at a given frequency, Equation [7.17] can be written in the form of the following linear expression which relates the required corrections dp_j, to the observed residual $v_i^{obs} - v_i^{thc}$

$$\frac{\partial v_i}{\partial p_1} dp_1 + \frac{\partial v_i}{\partial p_2} dp_2 + \ldots \frac{\partial v_i}{\partial p_k} dp_k = v_i^{obs} - v_i^{thc} \qquad [7.18]$$

A similar equation can be written for each observed frequency. The above equation can be written in matrix notation:

$$[A]\{\Delta p\} = \{V^{obs} - V^{thc}\} \qquad [7.19]$$

or

$$AD = V \qquad [7.20]$$

Where A is the matrix of partial derivatives with N rows and K columns whose elements are $A_{ij} = \frac{\partial v_i^{thc}}{\partial p_j}$ for the assumed profile. D represents a column vector of K elements which are the Δp_j's.

Solving Equation [7.20], the vector D is found where $D = (\Delta p_1, \Delta p_2, \ldots\ldots \Delta p_k)^T$, and then used to modify the vector for next iteration. The modified value of the profile for the next iteration is:

$$P = P + \Delta p \qquad [7.21]$$

The above computation is repeated until the least squares, LS (Equation [7.13]), become practically zero, i.e., the computed dispersion curve matches with the observed one. Generally, matrix A is not square and may be singular or close to singular. Therefore, Eq. 7.20 can not be solved by inversion of the matrix A. Singular value decomposition or SVD will resolve this difficulty.

SVD methods are based on the following theorem of linear algebra that any N×K matrix [A] whose number of rows N is greater than or equal to its number of columns K, can be written as the product of an N×K column-orthogonal ($UU^T=I$) matrix U, an K×K diagonal matrix W with positive or zero elements, and the transpose of an K×K orthogonal matrix S, i.e.

$$A = UWS^T \qquad [7.22]$$

Substituting Eq. 7.17 in Eq. 7.15 results in

$$D = SW^{-1}U^TV \qquad [7.23]$$

Usually w_i (an element of W) is nonzero but for some elements the value is very small. This can result in very large numbers that can cause instability in the solution. To remedy this instability w_i's with very small values are set to zero.

Iteration is stopped when V reaches a small value. To monitor V, the following error criterion is applied:

$$\varepsilon = \sqrt{\frac{1}{N}\sum_{i}^{N}(v_i)^2} \qquad [7.24]$$

The iteration procedure is stopped when the ε reaches an acceptable pre-set value.

A computer program SVD-INVERT was written to implement the above inversion procedure. Derivatives were calculated numerically using central difference. SVD-INVERT was able to solve cases with 2 to 3 layers successfully but as number of layers increased, it did not converge. A possible explanation is due to difficulty in calculating the derivatives numerically.

SVD-INVERT program was verified using the following case. First the dispersion curve for the site shown in Fig. 7.10 was obtained using the new method as described in Section 6.2. Table 7.6 shows the soil properties and Fig. 7.11 shows dispersion curve for the site after reducing number of points. Then, the SVD-INVERT program was run for two different initial shear wave velocity profiles as shown in Table 7.7. The initial and final shear wave velocity profiles are presented in Fig. 7.12.

7.5 Summary and Conclusions

A brief overview of three optimization techniques that are implemented for inversion of dispersion curve is presented. These techniques worked better than trial-and-error inversion, but they still have several disadvantages:

1 They are sensitive to errant input data and incomplete data.

2 If the initial estimate of the shear wave velocity profile is far from the actual (but unknown) solution, the inversion algorithm may never converge to solution.

3 As the number of layers and the number of field dispersion point increase, computer storage and run-time requirement are increased significantly.

Table 7.1-Initial guess of soil properties for shear wave velocity inversion.

	Shear Wave Velocity (m/s)	Thickness (m)	Damping ratio	Poisson's ratio	Unit Weight (kN/m^3)
Layer 1	100	3.0	0.05	0.45	20
Layer 2	115	3.0	0.05	0.45	20
Layer 3	130	3.0	0.05	0.45	20
Layer 4	150	3.0	0.05	0.45	20
Layer 5	165	3.0	0.05	0.45	20
Layer 6	180	3.0	0.05	0.45	20
Layer 7	200	3.0	0.05	0.45	20
Layer 8	215	3.0	0.05	0.45	20
Layer 9	230	3.0	0.05	0.45	20
Layer 10	245	3.0	0.05	0.45	20
Half-space	310	∞	0.05	0.45	20

Table 7.2-Initial guess of soil properties for shear wave velocity and thickness inversion.

	Shear Wave Velocity (m/s)	Thickness (m)	Damping ratio	Poisson's ratio	Unit Weight (kN/m^3)
Layer 1	110	4.3	0.05	0.45	20
Layer 2	155	8.0	0.05	0.45	20
Layer 3	200	13.4	0.05	0.45	20
Layer 4	400	∞	0.05	0.45	20

Table 7.3-Final soil properties for shear wave velocity inversion.

	Shear Wave Velocity (m/s)	Thickness (m)	Damping ratio	Poisson's ratio	Unit Weight (kN/m^3)
Layer 1	115	3.0	0.05	0.45	20
Layer 2	131	3.0	0.05	0.45	20
Layer 3	148	3.0	0.05	0.45	20
Layer 4	171	3.0	0.05	0.45	20
Layer 5	188	3.0	0.05	0.45	20
Layer 6	205	3.0	0.05	0.45	20
Layer 7	228	3.0	0.05	0.45	20
Layer 8	245	3.0	0.05	0.45	20
Layer 9	262	3.0	0.05	0.45	20
Layer 10	279	3.0	0.05	0.45	20
Half-space	353	∞	0.05	0.45	20

Table 7.4-Final soil properties for shear wave velocity and thickness inversion.

	Shear Wave Velocity (m/s)	Thickness (m)	Damping ratio	Poisson's ratio	Unit Weight (kN/m^3)
Layer 1	115	4.46	0.05	0.45	20
Layer 2	160	8.36	0.05	0.45	20
Layer 3	209	13.9	0.05	0.45	20
Layer 4	418	∞	0.05	0.45	20

Table 7.5-Initial guess of soil properties for shear wave velocity inversion.

	Shear Wave Velocity (m/s)	Thickness (m)	Damping ratio	Poisson's ratio	Unit Weight (kN/m^3)
Layer 1	150	3.0	0.05	0.45	20
Layer 2	150	3.0	0.05	0.45	20
Layer 3	150	3.0	0.05	0.45	20
Layer 4	150	3.0	0.05	0.45	20
Layer 5	150	3.0	0.05	0.45	20
Layer 6	150	3.0	0.05	0.45	20
Layer 7	150	3.0	0.05	0.45	20
Layer 8	150	3.0	0.05	0.45	20
Layer 9	150	3.0	0.05	0.45	20
Layer 10	150	3.0	0.05	0.45	20
Half-space	500	∞	0.05	0.45	20

Table 7.6-Soil properties for analyzed profile.

	Shear Wave Velocity (m/s)	Thickness (m)	Damping ratio	Poisson's ratio	Unit Weight (kN/m^3)
Layer 1	220	2	0.05	0.35	18
Layer 2	350	5	0.05	0.35	18
Half-space	800	∞	0.05	0.35	21

Table 7.7-Initial guess of soil properties for two different inversion.

	Shear wave velocity m/s (1)	Shear wave velocity m/s (2)
Layer 1	180	180
Layer 2	180	270
Half-space	180	500

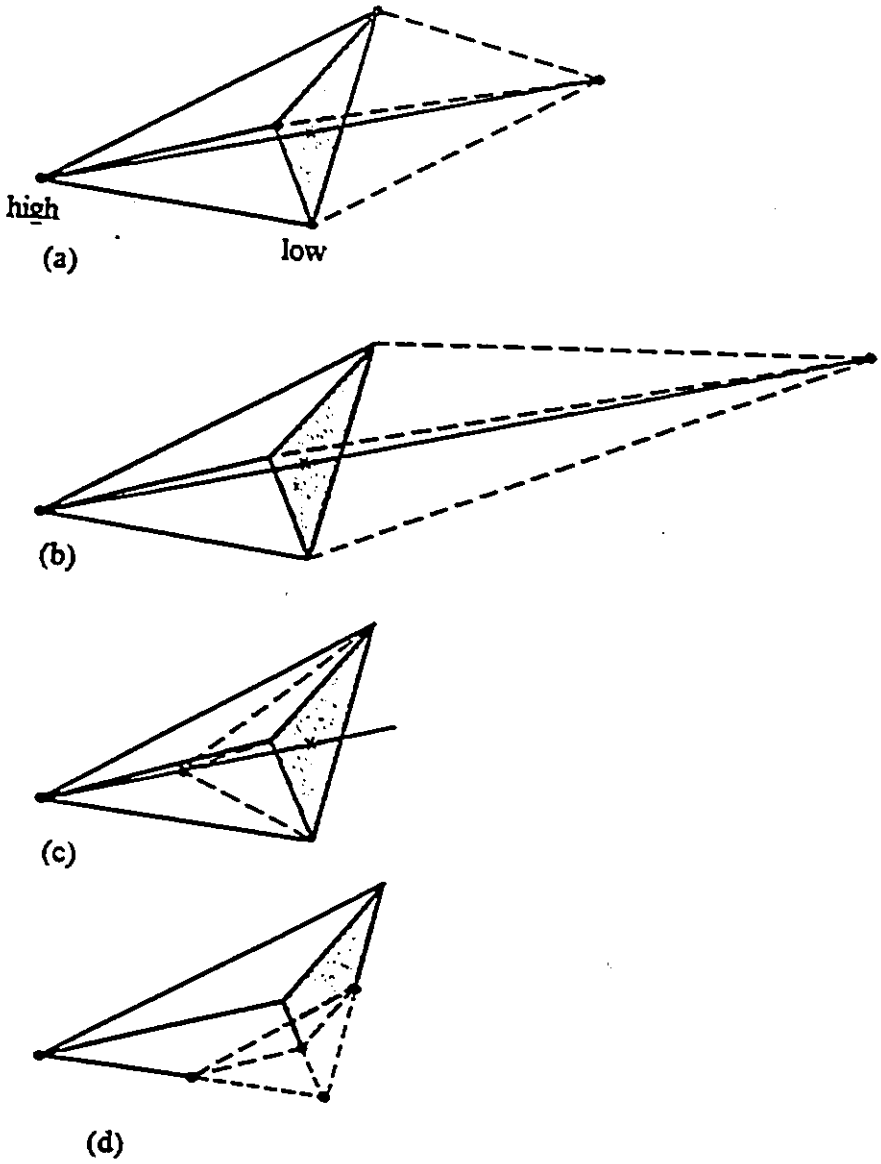

Fig. 7.1-Possible outcomes for a step in the downhill simplex method. The simplex at the beginning of the step, a tetrahedron, is drawn with solid lines. The simplex at the end of the step (drawn dashed) can be either (a) a reflection away from high point, (b) a reflection and expansion away from the high point, (c) a contraction along one dimension from the high point, or (d) a contraction along all dimensions toward the low point (Press et al. 1992).

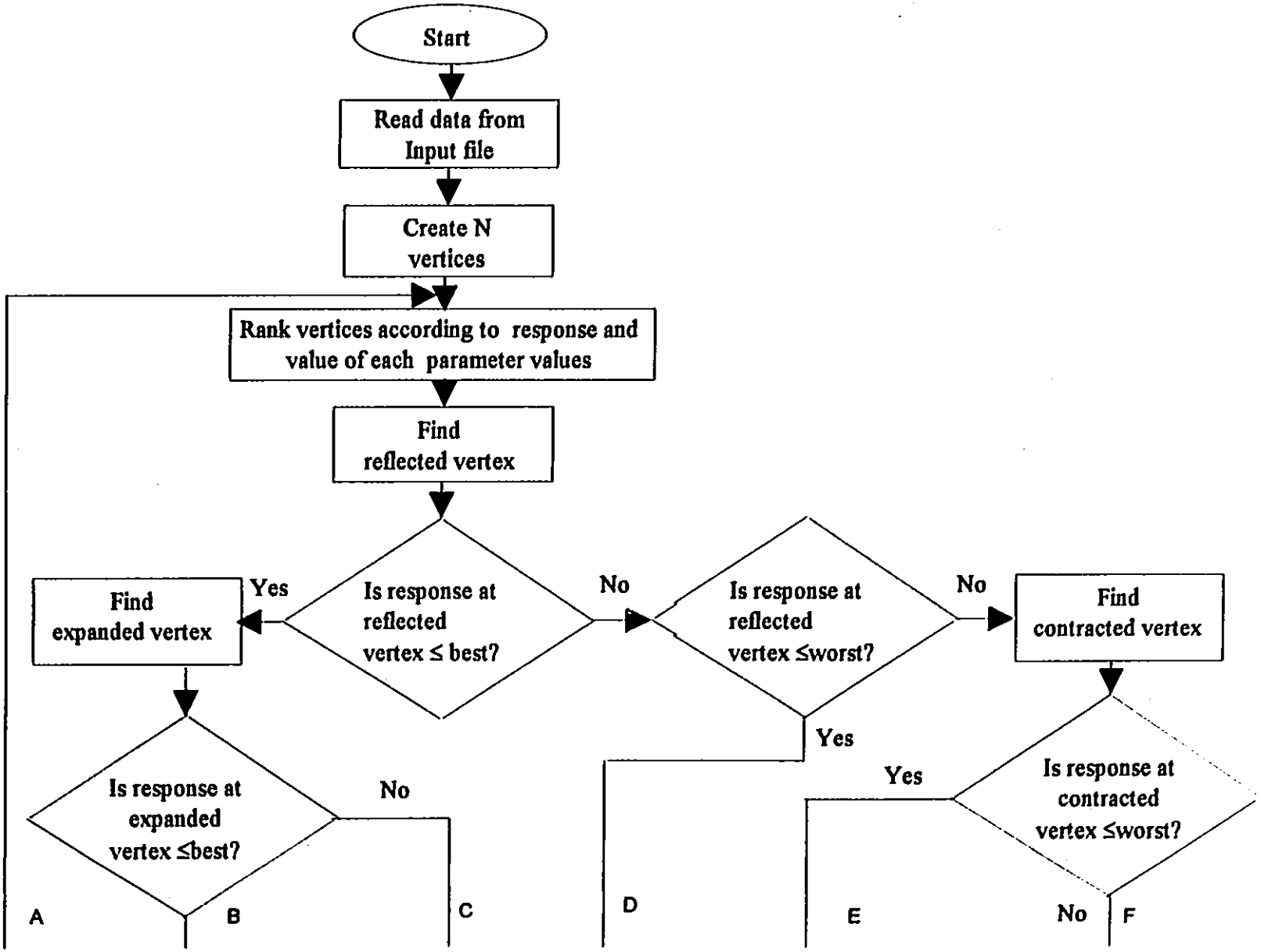
Start
Read data from Input file
Create N vertices
Rank vertices according to response and value of each parameter values
Find reflected vertex
Is response at reflected vertex ≤ best?
Yes
Find expanded vertex
Is response at expanded vertex ≤best?
No
A
B
C
No
Is response at reflected vertex ≤worst?
No
Find contracted vertex
Yes
D
Yes
Is response at contracted vertex ≤worst?
Yes
E
No
F

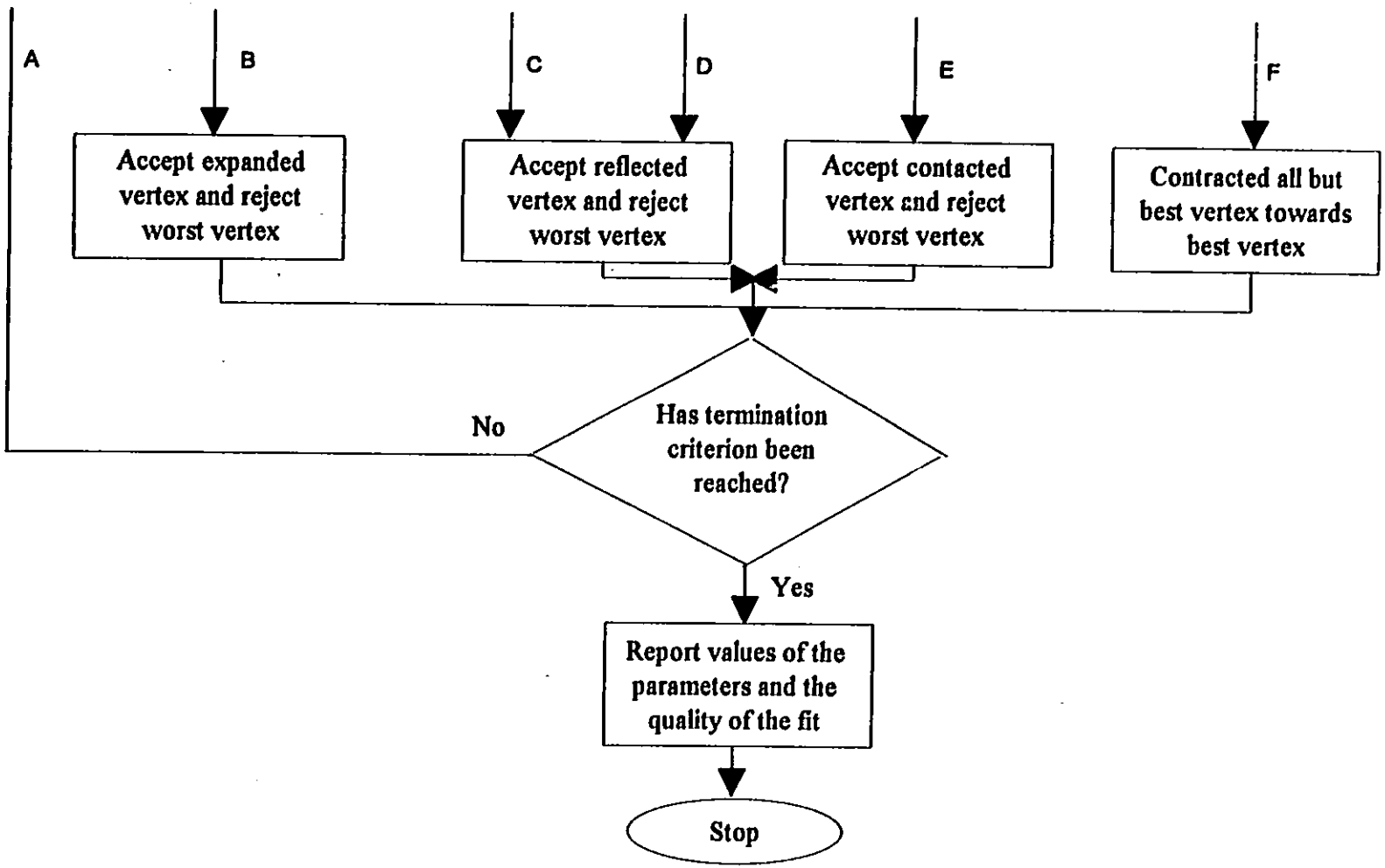

Fig. 7.2-Flow chart of the Simplex algorithm (After Caceci and Cacheris, 1984).

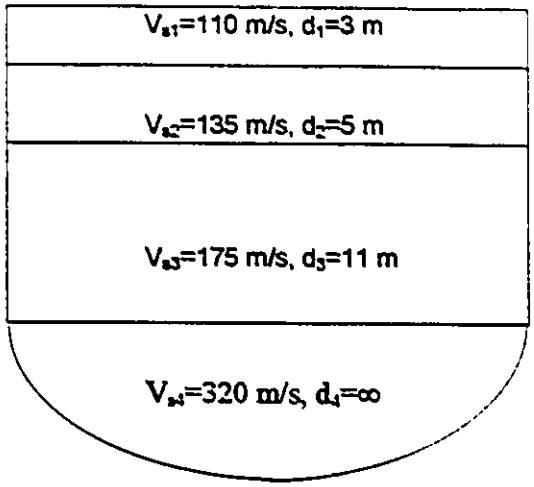

Fig. 7.3-Shear wave velocity profile.

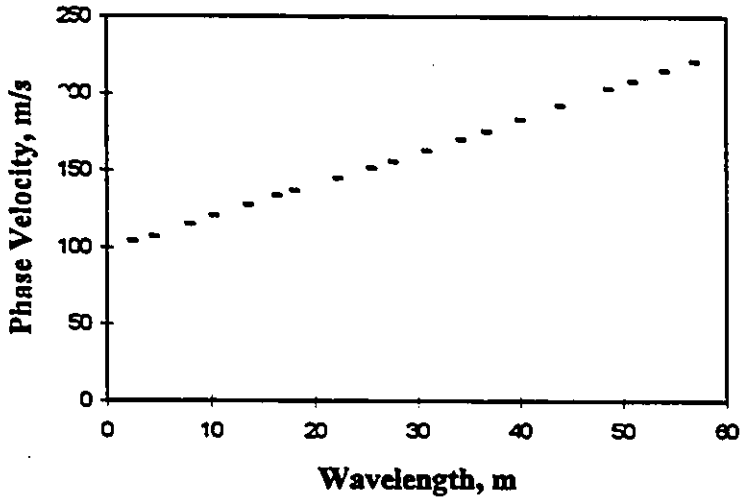

Fig. 7.4-Dispersion curve from simulation of SASW test.

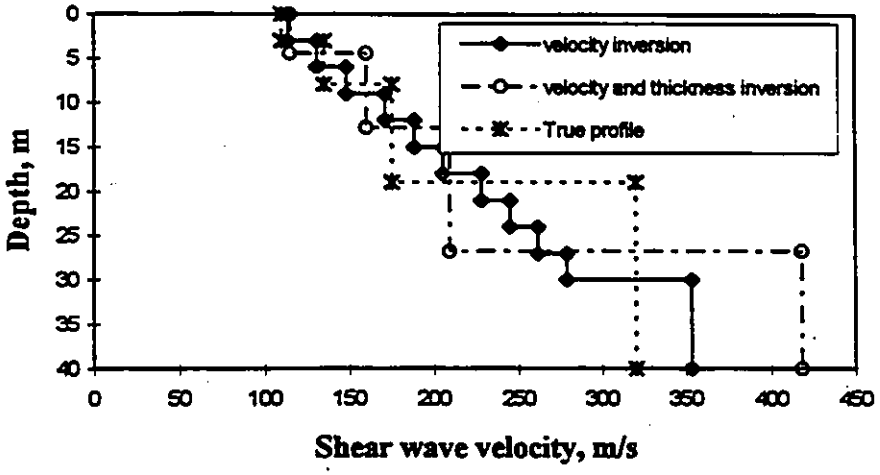

Fig. 7.5-Shear wave velocity profile.

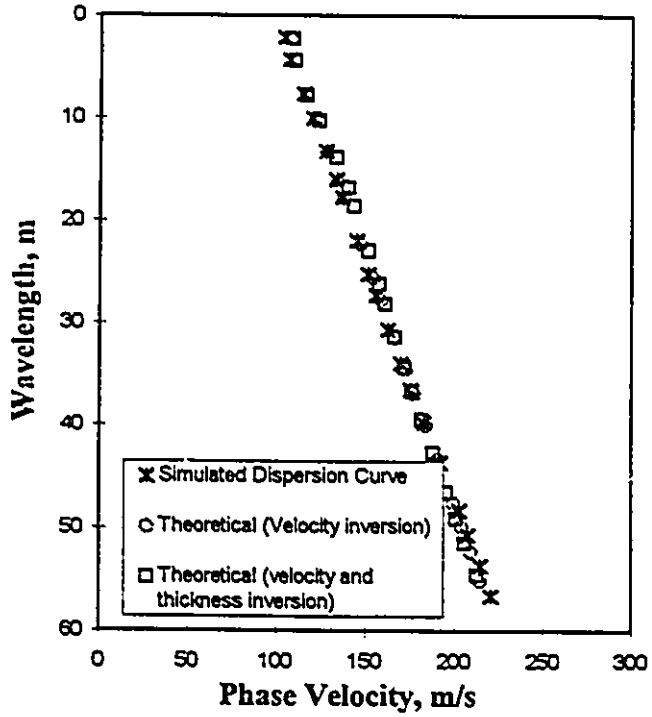

Fig. 7.6-Comparison of experimental and theoretical dispersion curve after completion of inversion.

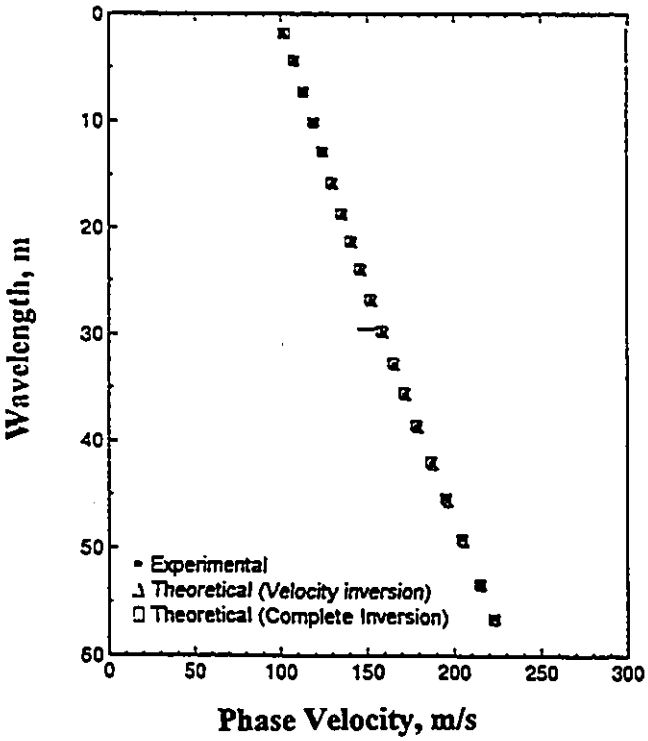

Fig. 7.7-Comparison of experimental and theoretical dispersion curve after completion of inversion (Yuan and Nazarian, 1993).

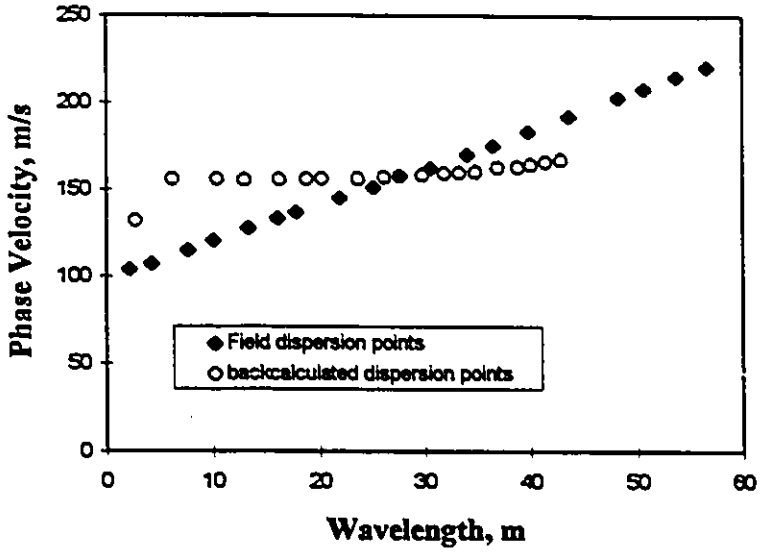

Fig. 7.8-Dispersion curves.

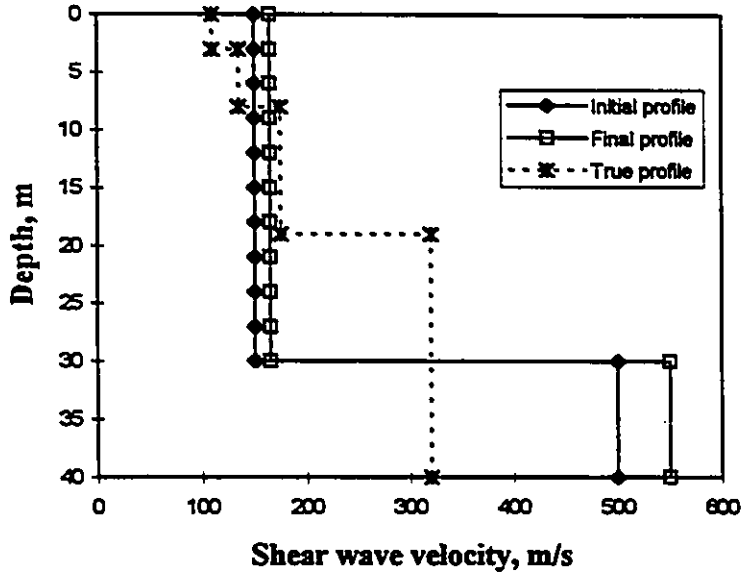

Fig. 7.9-Shear wave velocity profile.

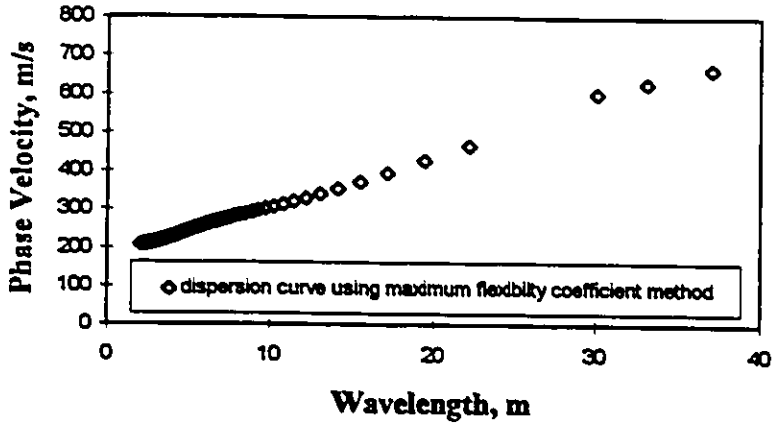

Fig. 7.10-Simulated dispersion curve.

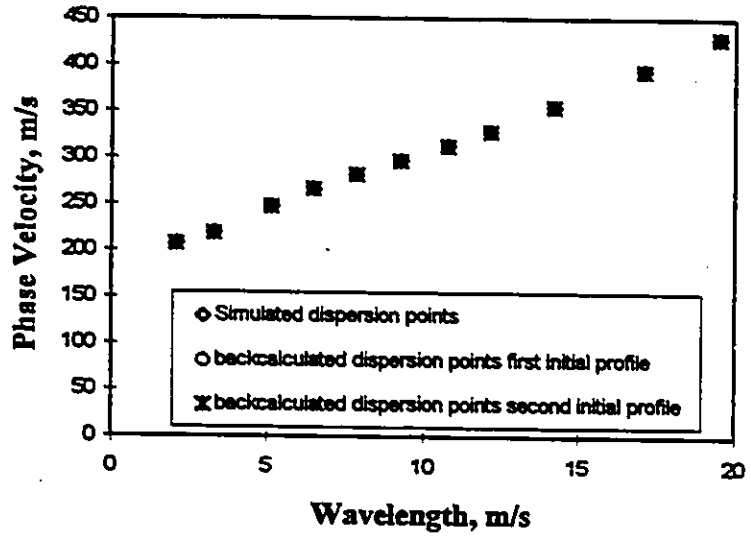

Fig. 7.11-Dispersion curve.

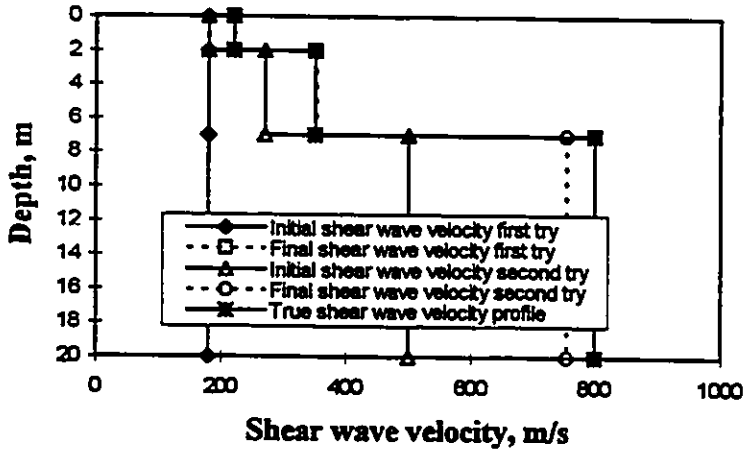

Fig. 7.12- Shear wave velocity profile.

CHAPTER 8

RESULTS OF FIELD TESTS USING THE SASW METHOD

This chapter presents the results of several SASW tests. However, to provide a preliminary information regarding soil sites used in this study a brief description of sites, field equipment, data collection, and construction of field dispersion curves are given at the beginning of each test. The inversion results are subsequently presented and discussed.

8.1 Service Road at the National Research Council, Ottawa Campus

The SASW test was performed on a flexible pavement section of a service road at the National Research Council, Ottawa Campus in September 1994.

8.1.1 Field Testing Setup and Data Acquisition

The CS array geometry was used, and the spacings between receivers were 0.125, 0.25, 0.5, 1, 2, 4, 8, and 16 meters. Four types of accelerometer transducers were used to pick up the seismic signal, depending on the frequency range of interest. For spacing 0.125 m, to profile shallow layers using short wave lengths, accelerometers which are sensitive in the high frequency range were used (PCB model 309 A). PCB model 308b10 and PCB model 306C accelerometers were used for (0.25, 0.50 m) and (1, 2, 4 m) spacings, respectively. To pick up low frequency signals to profile deeper layers B&K 8306

accelerometer was employed for the 8 m spacing. The transducers were attached to small aluminum plates using steel studs or double sided tape. The plates were glued to the pavement surface using 5-minute epoxy glue to ensure good coupling. A portable dual channel FFT analyzer (HP 35670 A) was utilized for recording and analyzing the data.

The dynamic signal is generated in the pavement using a variety of sources depending on the frequency range of interest or the desired depth of sampling. For 0.125 m spacings a small steel ball was used, and a light ball peen hammer was used for 0.25, 0.5, 1 m spacings to produce high frequency vibration which is necessary to sample shallow layers. A heavy sledge hammer (8 kg) and drop weight (approximately 100 kg and height varied between 1 to 2 m) were employed for large spacings to induce a signal with low frequency. To enhance signal quality, i.e., increased signal to noise ratio, the results from five signals were averaged. In order to produce a signal with high coherence in the frequency range of interest, the test was repeated using different sources or impact surfaces, e.g., by employing rubber pads. To detect dipping or inhomogenity in the layer, the test was perform for both forward and reverse configurations.

8.1.2 Construction of the Field Dispersion Curve

The relative phase angle spectra and corresponding coherence function for 0.125, 0.25, 0.5, 1, 2, 4 and 8 m receiver spacings are shown in Fig. 8.1, respectively. The usual procedure for unwrapping was used and the phase velocity and the wavelength was evaluated using Equations 3.4 through 3.6. These calculations were performed in a commercial spread-sheet program (Excel). Data points with low coherence (i.e., less than 0.90) were eliminated. The forward and the reverse tests of the relative phase angle spectra for 16 m spacings (Fig. 8.1) are different from each other. This implies that the layers are not horizontal and hence this spectrum was not included in the analysis.

The SASW test is usually performed for several receiver spacings. Therefore, dispersion data from different spacings are overlapped over wide frequency ranges and for each

frequency several dispersion data were available. These dispersion data were combined to generate the average dispersion curve.

As discussed in Section 4.4.1.2 existing filtering criterion were unable to produce representative dispersion curves and a new filtering criterion was introduced in this study. In the new filtering criterion, the data points at the same frequency but obtained from two different receiver spacings are rejected if they do not match each other. In this manner, inconsistencies in the dispersion curve due to erroneous phase unwrapping are avoided.

The final dispersion curve for this site after combining dispersion points from different spacings and applying the new filtering criterion is shown in Fig. 8.2. The curve shows wavelengths ranging from about 0.03 m to about 14 m while the measured Rayleigh-wave phase velocity varied about from 1400 m/s at surface to 180 m/s at longer wavelengths.

8.1.3 INVERSION OF DISPERSION CURVE

For automated inversion it is necessary to reduce the number of dispersion data points to reduce computation time. The choice of the number of experimental dispersion data points depends on the number of layer parameters in the trial profile. The number of dispersion data points should be greater than the number of unknowns.

Fig. 8.3 shows dispersion curve for the site in which the data points are reduced. As seen in Fig. 8.3, the phase velocity decrease with increase of wavelength up to 2 m and becomes constant after that.

The backcalculated site profile was obtained using forward modeling with the simplex method. The analysis was based on an assumed layered soil model from the Steady-State inversion procedure of Rayleigh wave data as discussed in Chapter 3. The assumed

initial values of shear wave velocities are shown in Table 8.1. The calculation of the initial dispersion curve and iteration of assumed model parameter was carried out until a matching dispersion curve was found. This process was performed using the computer program SASW-INVERT, which was described in Chapter 7. The sum of the least squares criterion was used for evaluating the degree of the match.

The final theoretical and experimental dispersion curves are shown in Fig. 8.4. Table 8.2 and Fig. 8.5 shows the backcalculated shear wave velocity profile for the site.

A crosshole test was performed at this site. Test results were reported by Al-Hunaidi, 1992 (see Fig. 8.5). The shear wave velocities from SASW test varied from about 1240 m/s at the ground surface to about 162 m/s at depth of approximately 0.5 to 6 m. The shear wave velocities from the crosshole test are about 435 m/s at a depth of 0.4 m to 170 m/s at a depth of 2 m. By comparing the result from SASW and the crosshole test, it is obvious that there is good agreement between these results. There are no crosshole results at shallow depths.

8.2 Soil Site, Fraser Farm (Fallowfield of Carleton County)

The site is located in Fallowfield of Carleton County, approximately 30 Km southwest from University of Ottawa, as shown in Fig. 8.6. At the site, there was a foundation failure of a tower silo that was documented and analyzed by Bozozuk (1977), and Haile (1977). The soil profile in the upper 3 m consists of a clayey silt (light brown color) and below 3 m consists of a silty clay. Wells that have been drilled around this area showed the depth of bedrock to be 30 m.

8.2.1 Field Testing Setup and Data Acquisition

The SASW test was performed in November 1994. The CS array geometry was used, and the spacings between receivers were 1, 2, 4, 8, 16, 32, and 50 meters. Two types of

accelerometer transducers were used to pick up the seismic signal, depending on the frequency range of interest. PCB model 303C accelerameters were used for 1, 2, 4, and 8 m spacings. To pick up low frequency signals to profile deeper layers a B&K 8306 accelerometer was employed for 8, 16, 32, and 50 m spacings. The transducers were attached to aluminum spikes using steel studs or double sided tape. The spikes were pushed into ground to ensure a good coupling between transducers and ground. The dynamic signal was generated in the ground using a hand-held hammer (4 kg) and mechanical drop weight (weight is around 220 kg and the drop height, depending on receivers spacing, was varied between 1 to 2 m). A portable dual channel FFT analyzer (ONO SOKKI model CF-350) was utilized for recording and analyzing the data.

8.2.2 Construction of the Field Dispersion Curve (Fraser Farm)

The relative phase angle spectra and corresponding coherence function for 1, 2, 4, 8, 16, 32 and 50 m receiver spacings are shown in Fig. 8.7, respectively.

Calculations were performed following previously stated guidelines in Section 8.1.2. Since phase data for 50 m has low coherence and the number of cycles is not clear, this spectrum was not included in the analysis.

The final dispersion curve for this site, after combining the dispersion curves of all different spacings and applying the new filtering criterion, is shown in Fig. 8.8. The curve shows wavelength ranging from about 0.30 m to approximately 20 m while the measured Rayleigh-wave phase velocity varied from 56 m/s to 130 m/s.

8.2.3 Inversion of Dispersion Curve

Fig. 8.9 shows the dispersion curve in which the number of data points is reduced. Fig. 8.9 shows that the phase velocity increases with increase in wavelength up to 3.0 m,

from 3.0 m to 5.0 m decreases, then remains constant from 6.0 to 16 m and from 16 m to 20 m the phase velocity increases again.

The dispersion curve was divided into several sections and an initial shear wave velocity profiles was calculated using the empirical inversion procedure as described in Section 3.4. The initial profile is given in Table 8.3. The final theoretical dispersion curve obtained using program SASW-INVERT is compared with the experimental curve in Fig. 8.10. Table 8.4 shows the final shear wave velocity for the site.

Unfortunately, no other seismic test was carried out at this site. The only results available for the site are in-situ vane shear tests and cone penetration tests. These results are shown in Fig. 8.11.

It is known that in-situ values of G_{max} depend on void ratio (e_0), overburden stress(σ'_{vo}), and stress history (OCR). Since cone penetration resistance (q_c) also depends on σ'_{vo} and OCR, a moderate association between G_{max} and q_c is possible, despite their incompatible strain levels. For preliminary correlative purpose, a power function relates in-situ G_{max}, and q_c in clay deposits having a wide range in plasticity, stress history, and consistency was defined. Bouckovalas et al. (1989) determined the following empirical relationship

$$G_{max} = 2.8(q_c)^{1.40} \qquad [8.1]$$

where G_{max} and q_c are both in kpa. Also, G_{max} is related to the shear wave velocity using isotropic elastic theory via

$$G_{max} = \rho V_s^2 \qquad [8.2]$$

where $\rho = \gamma / g$ =mass density of soil, γ = total unit weight and g = gravitational acceleration constant = 9.8 m/s^2.

Martin and Seed (1978) also recommended that for clay, the shear modulus at low-strain can be determined by using undrained shear strength

$$G_{max} = 2500 S_u \qquad [8.3]$$

where S_u is the undrained shear strength.

The shear wave velocities were calculated by Equations 8.1, and 8.3 and are shown with the values obtained from SASW tests in Fig. 8.12. Results obtained using the various method do not agree. This is believed to be caused by the different assumptions implied in these methods. The accuracy of SASW results for this site remains unconfirmed.

The results from the SASW test and undrained shear strength show the same trend. But the shear wave velocities calculated by Equation 8.1 are higher than those obtained from the SASW test. The shear wave velocities obtained from cone penetration resistance are higher for the top layer but are smaller at depth in comparison to those obtained from SASW test. The common feature amongst results obtained by the 3 methods is the presence of a stiff crust just below the surface.

8.3 Soil Site, Richmond, Vancouver (British Columbia)

The site is located in the municipality of Richmond near Vancouver B.C. The location can be seen in Fig. 8.13. The soil profiles at the site consists of sand and silty sands. The water level at the site was located near the surface (around 1 m). The site is on the Fraser River delta and is susceptible to liquefaction. Earlier, the Geological Survey of Canada conducted seismic cone penetration tests. The results of these test are given in Fig. 8.14.

8.3.1 Field Testing Setup and Data Acquisition

The SASW test was carried out in November 1995. The CS array geometry was used, and input signal was produced from a vertically oriented seismic source placed on the ground (Fig. 8.15). The spacings between receivers were 1, 2, 4, and 8 m. A B&K 8306 accelerometer was employed to pick up the signal. The transducers were attached to

aluminum spikes using steel studs. A portable dual channel FFT analyzer (HP 35670 A) was utilized for recording and analyzing the data.

8.3.2 Construction of the Field Dispersion Curve

The relative phase angle spectra and corresponding coherence functions for different spacings are shown in Fig. 8.16. Fig. 8.17 shows the dispersion curve for the site produced by processing data according to the guidelines described in Section 3.4. Poor results were obtained at this site for large receiver-to-receiver spacing. This was caused by a high background noise level (the site was located close to a highway) and insufficient impact energy created by the available impact device.

8.3.3 INVERSION OF DISPERSION CURVE (Richmond)

The experimental dispersion curve and the corresponding matching theoretical dispersion curve are shown in Fig. 8.18. Fig. 8.19 shows a plot of shear wave velocity profiles obtained from SCPT and SASW tests. The seismic cone penetration test could not be performed in the top 5 m because the soil was too weak to support even the self weight of the cone and attached rods. The SASW test was able to determine the shear wave velocities in the top layers and also shows the same trend as the SCPT profile at depths where results were obtained by both methods.

8.4 Summary

The results show that the procedures of construction and inversion of the field dispersion curve developed in this study are working well. Further improvements in these processes are required to enhance the rate of matching theoretical dispersion curves to field dispersion curves.

Table 8.1-Initial guess of soil properties for NRC site.

	Shear Wave Velocity (m/s)	Thickness (m)	Damping ratio	Poisson's ratio	Unit Weight (kN/m^3)
Layer 1	1400	0.20	0.05	0.35	22
Layer 2	350	0.3	0.05	0.35	18
Half-space	200	----------	0.05	0.35	17

Table 8.2-Final soil properties for NRC site.

	Shear Wave Velocity (m/s)	Thickness (m)	Damping ratio	Poisson's ratio	Unit Weight (kN/m^3)
Layer 1	1240	0.2	0.05	0.35	22
Layer 2	366	0.3	0.05	0.35	18
Half-space	162	------	0.05	0.35	17

Table 8.3-Initial guess of soil properties for Fraser Farm site.

	Shear Wave Velocity (m/s)	Thickness (m)	Damping ratio	Poisson's ratio	Unit Weight (kN/m^3)
Layer 1	100	1.0	0.05	0.35	20
Layer 2	175	1.0	0.05	0.35	20
Layer 3	145	1.0	0.05	0.35	20
Layer 4	130	1.0	0.05	0.35	20
Layer 5	145	1.0	0.05	0.35	20
Half-space	150	----------	0.05	0.45	20

Table 8.4-Final soil properties for Fraser Farm site.

	Shear Wave Velocity (m/s)	Thickness (m)	Damping ratio	Poisson's ratio	Unit Weight (kN/m^3)
Layer 1	90	1.0	0.05	0.35	20
Layer 2	162	1.0	0.05	0.35	20
Layer 3	108	1.0	0.05	0.35	20
Layer 4	126	1.0	0.05	0.35	20
Layer 5	135	1.0	0.05	0.35	20
Half-space	145	----------	0.05	0.35	20

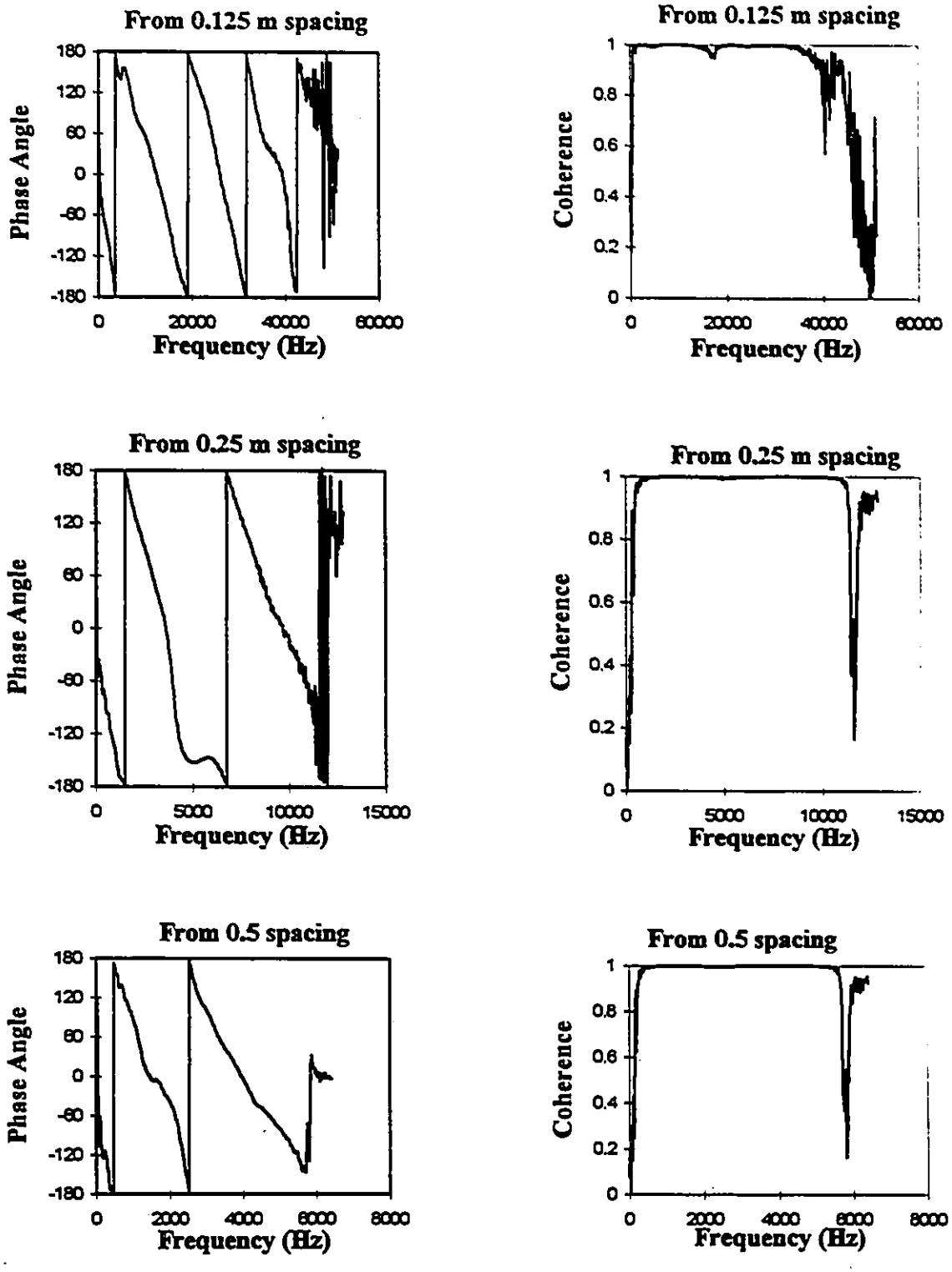

Fig. 8.1-Relative Phase angle spectra and Coherence function for different spacings at NRC.

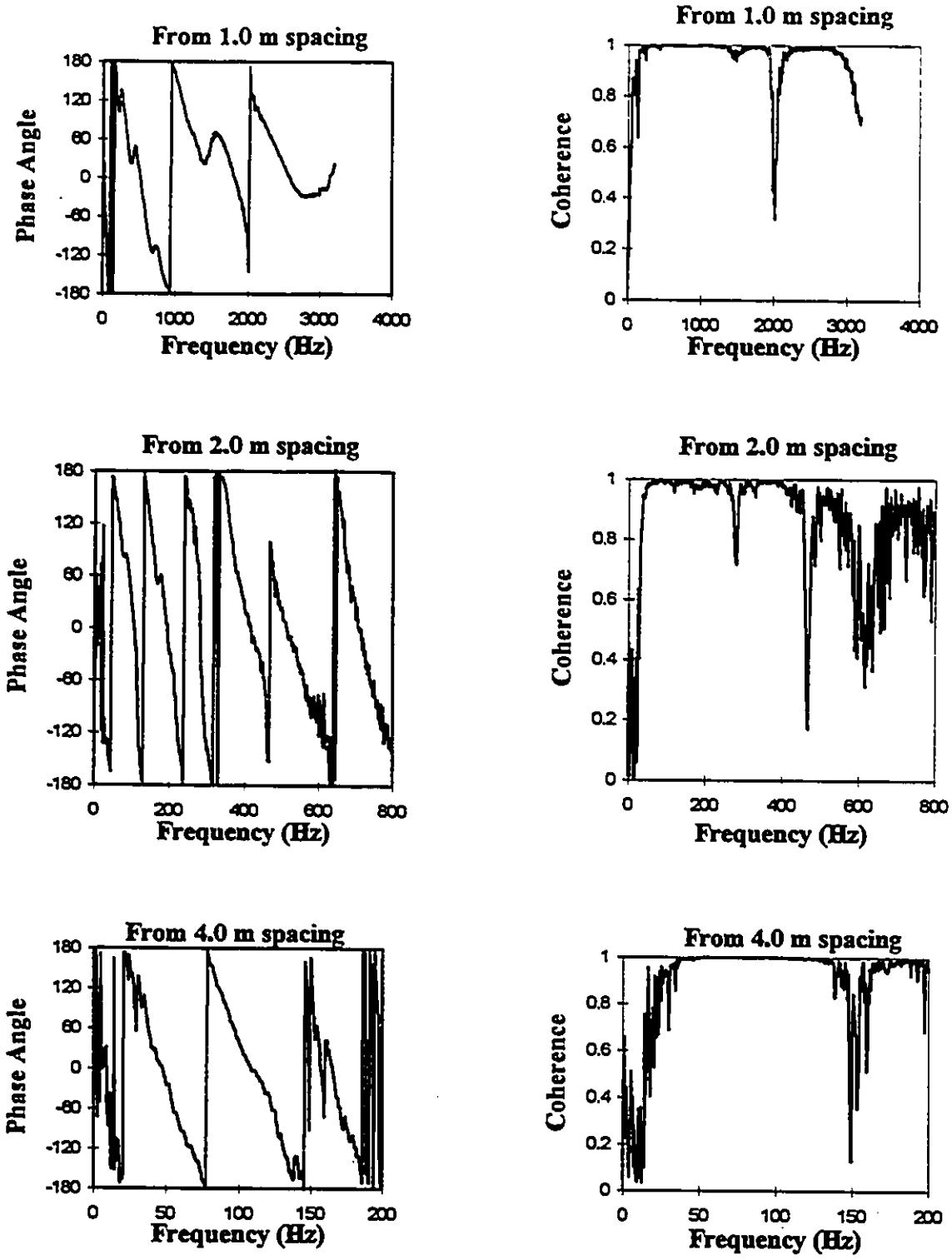

Fig. 8.1-Relative Phase angle spectra and Coherence function for different spacings at NRC (continued).

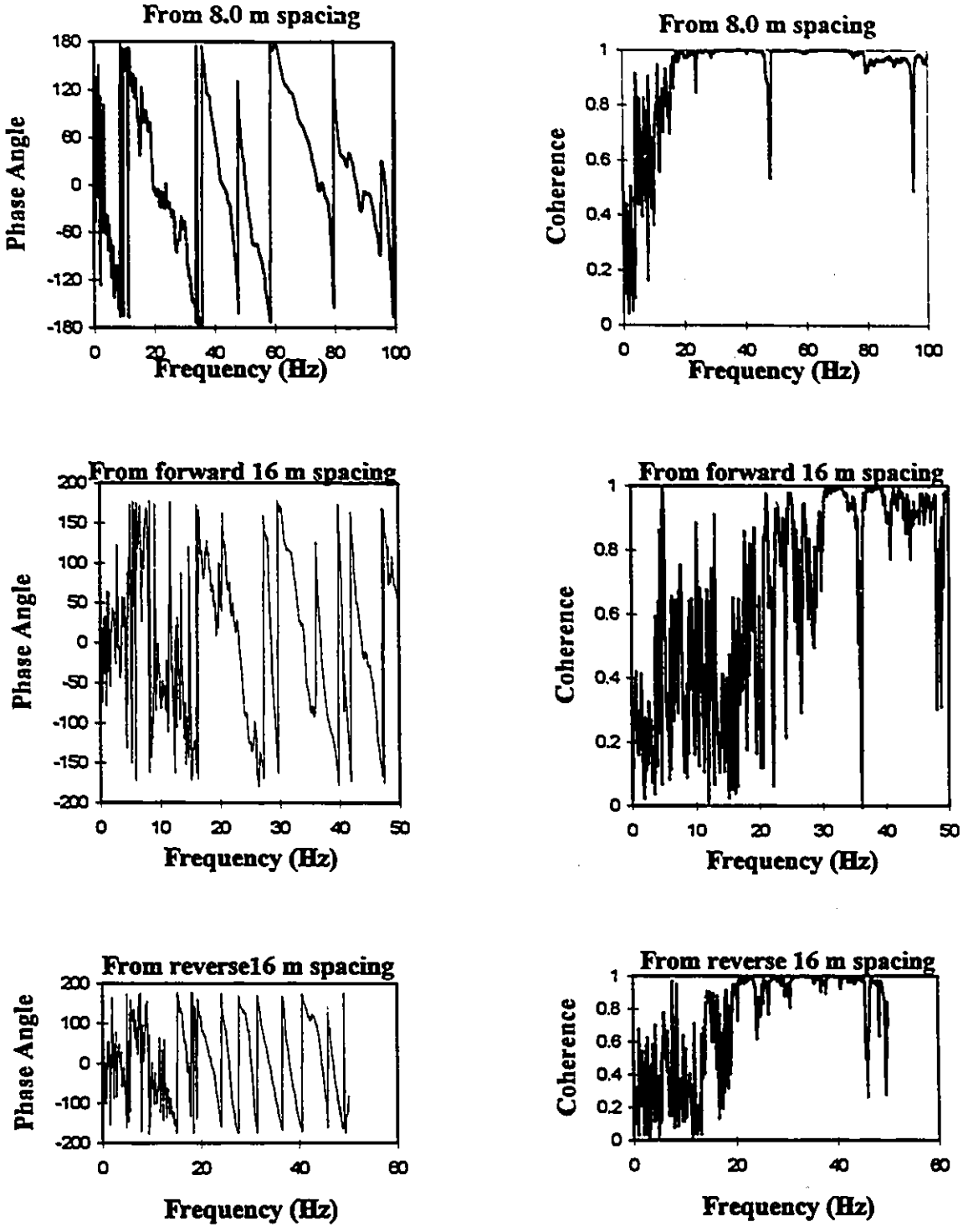

Fig. 8.1-Relative Phase angle spectra and Coherence function for different spacings at NRC (continued).

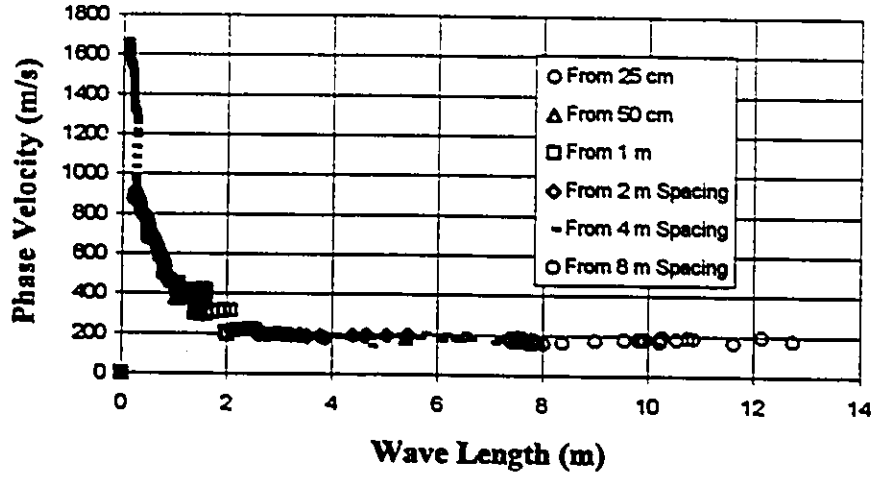

Fig. 8.2- Dispersion curve from proposed filtering criterion.

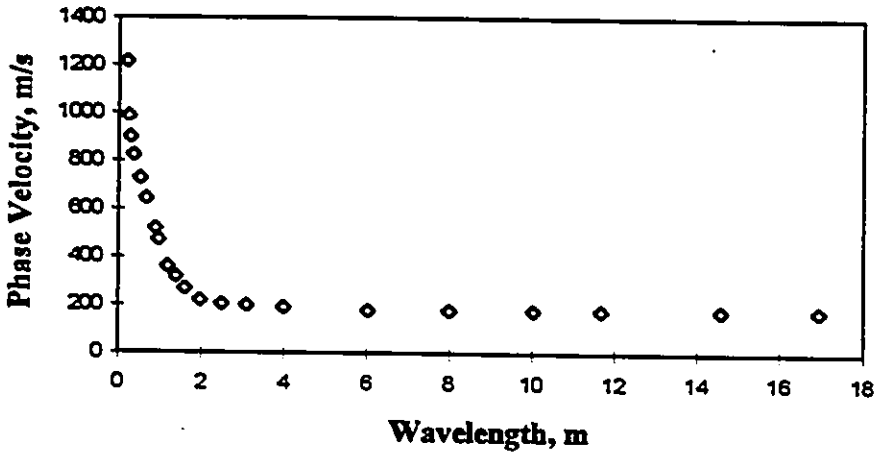

Fig. 8.3-Reduced field Dispersion points.

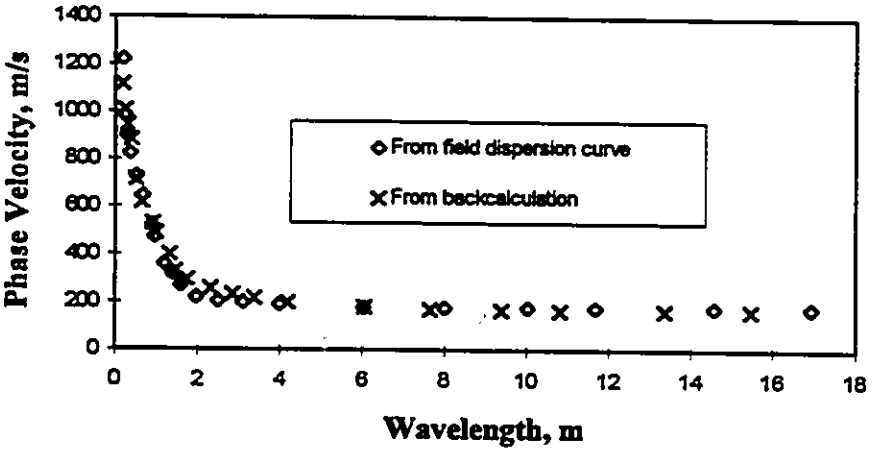

Fig. 8.4-Theoretical and in-situ dispersion curves at NRC site.

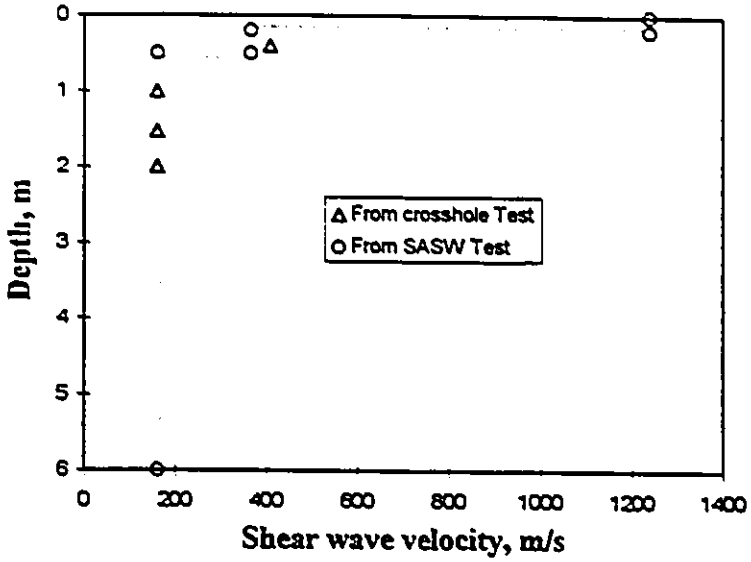

Fig. 8.5-Shear wave velocity profile at NRC site.

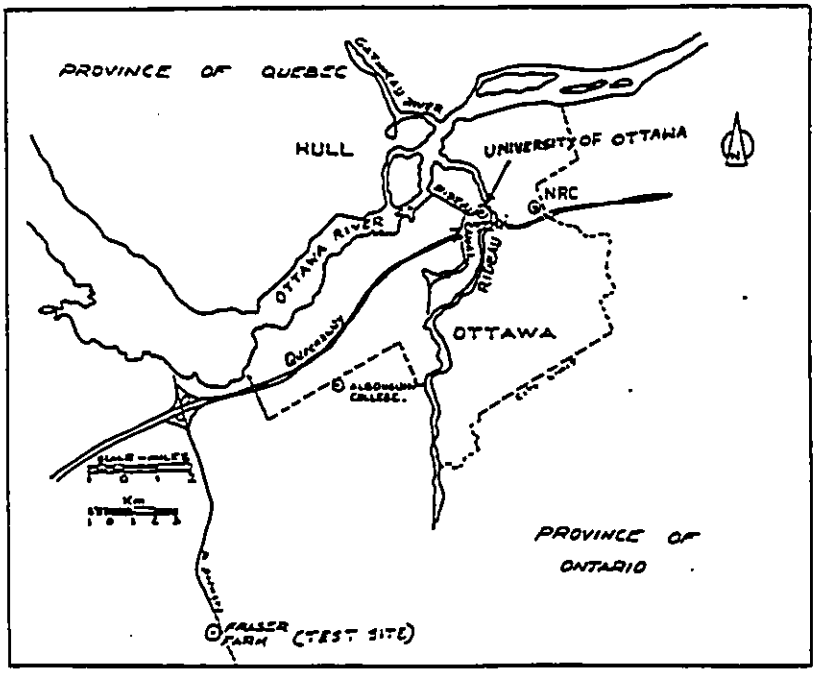

Fig. 8.6-Location of site at Fraser Farm.

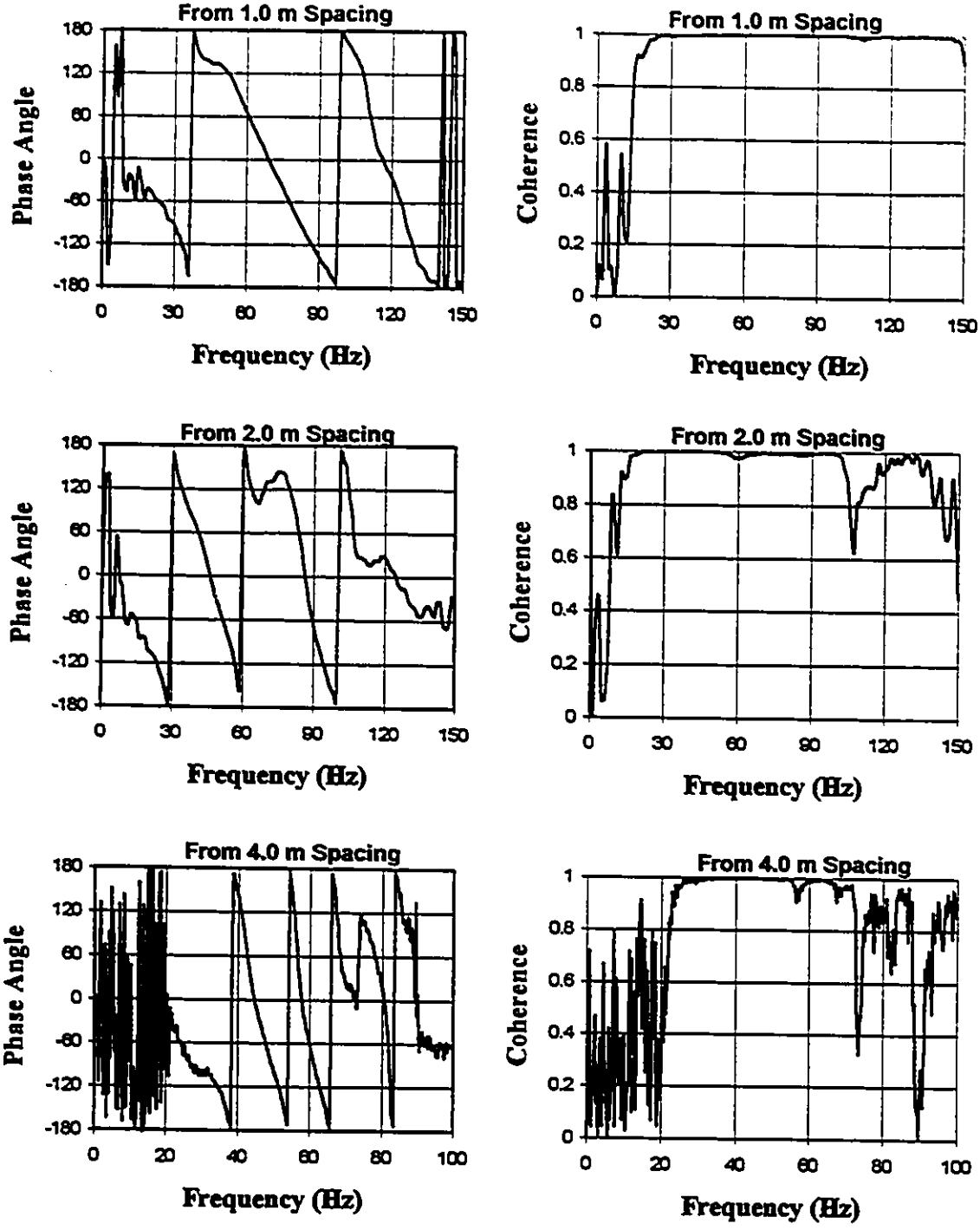

Fig. 8.7-Relative Phase angle spectra and Coherence function for differen spacings at Fraser Farm.

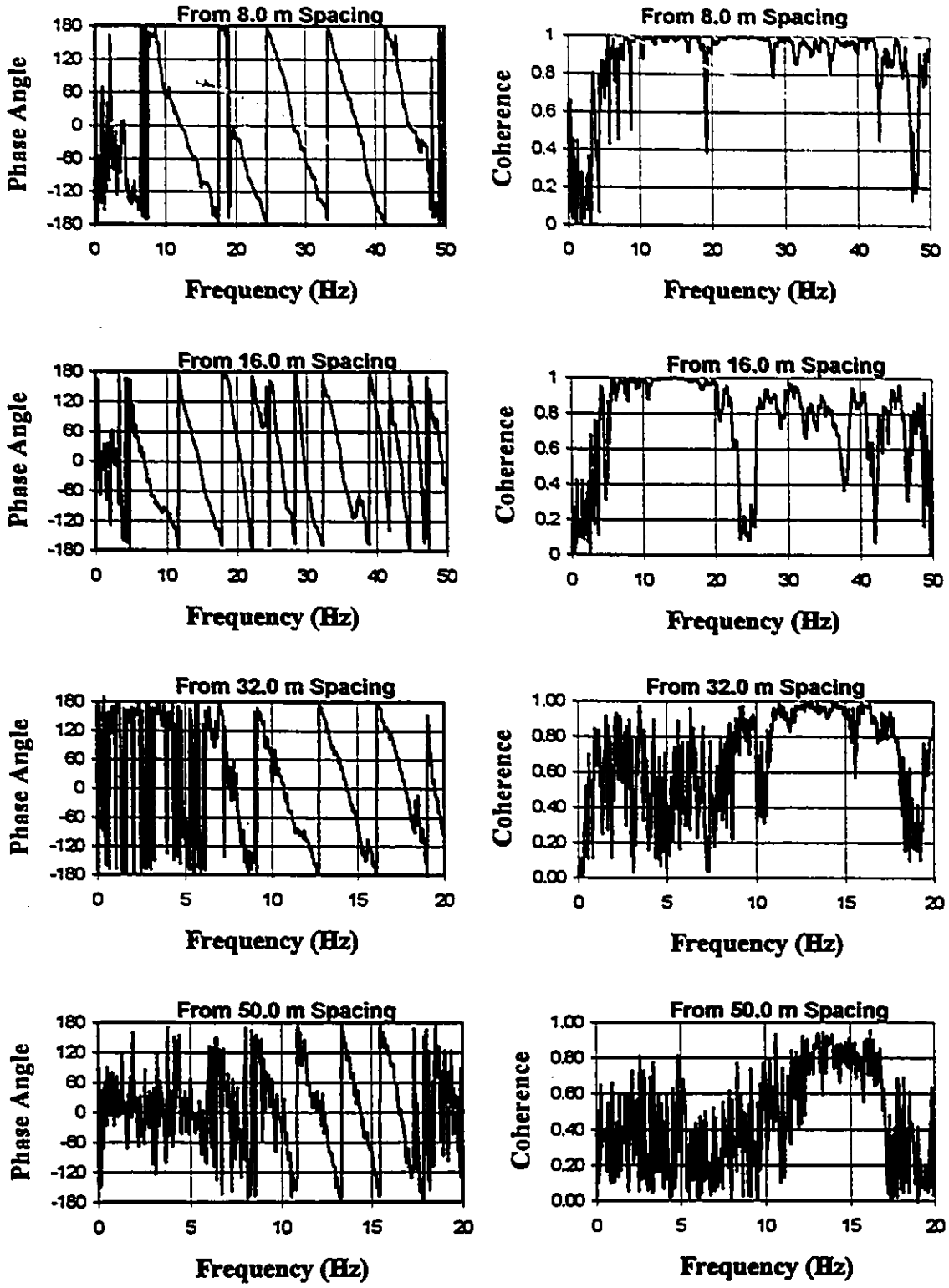

Fig. 8.7-Relative Phase angle spectra and Coherence function for differen spacings at Fraser Farm (continued)

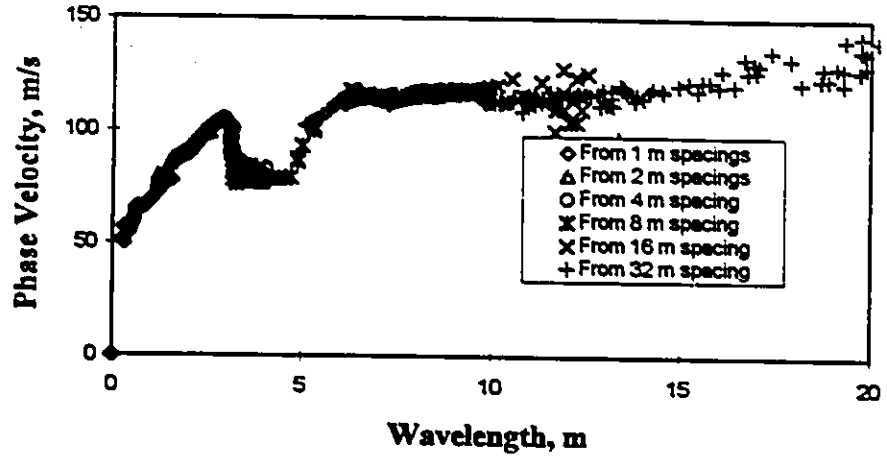

Fig. 8.8-Field dispersion curve from proposed filtering criterion.

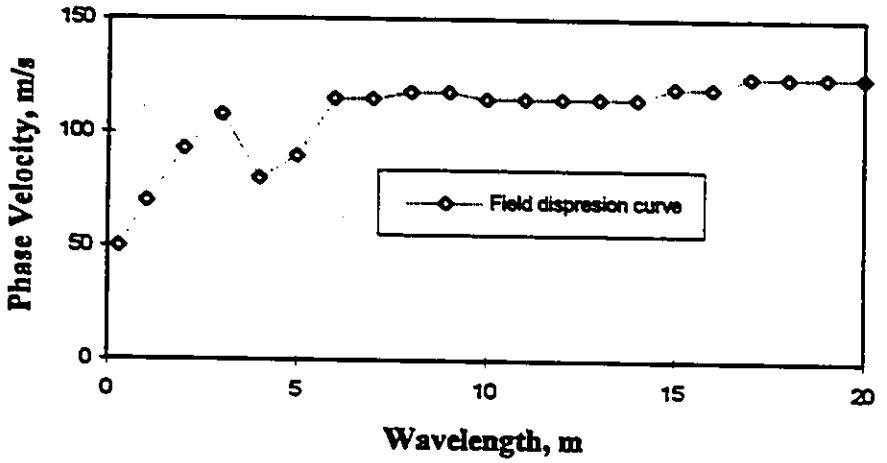

Fig. 8.9-Reduced field dispersion points.

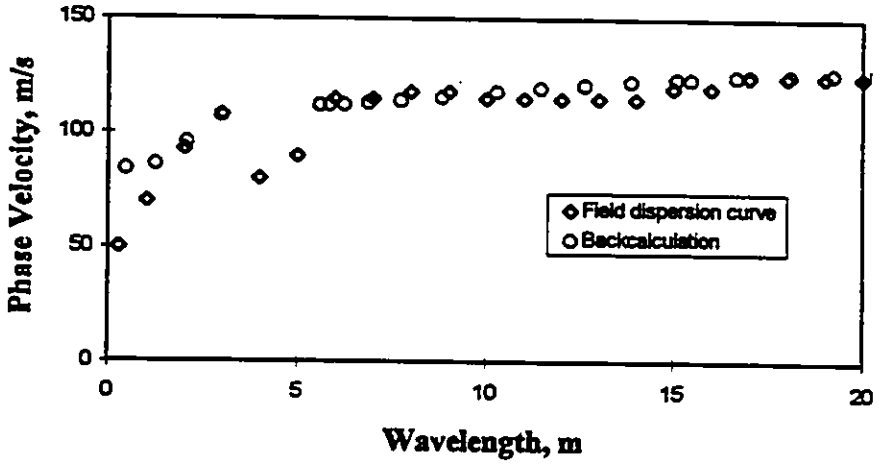

Fig. 8.10-Backcalculated field dispersion curve.

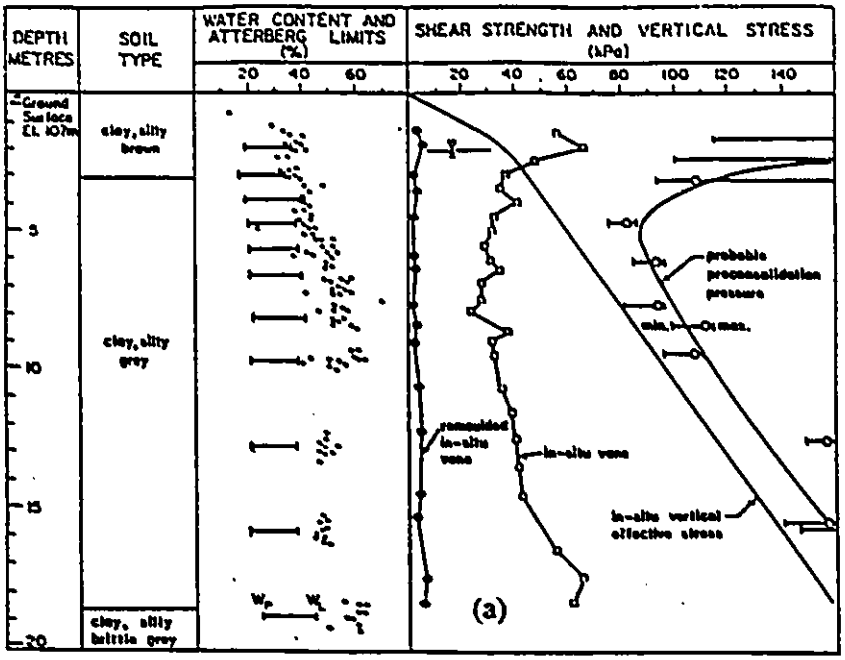

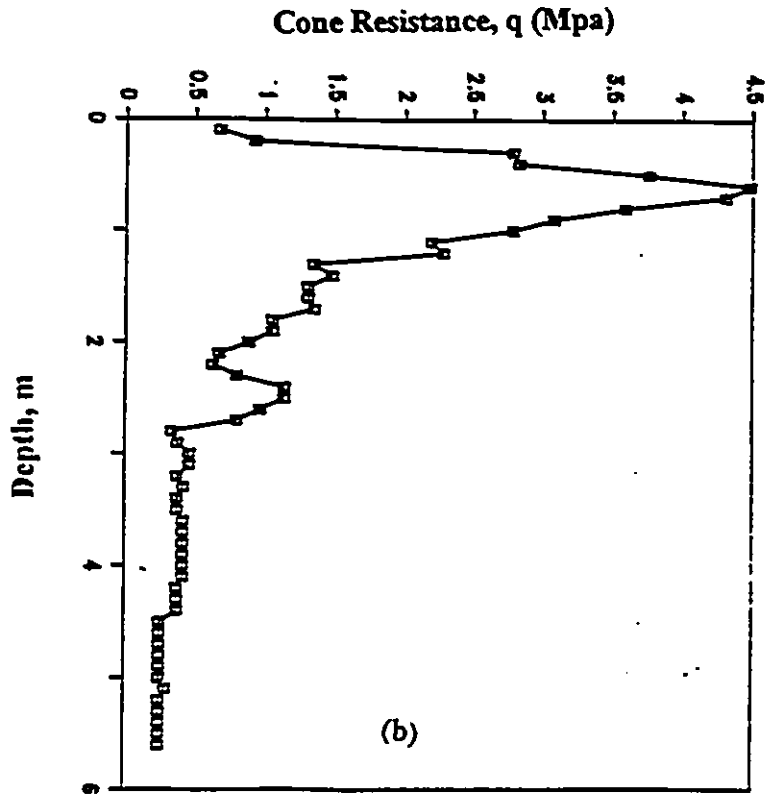

Fig. 8.11- Results of In-situ test at Fraser Farm site,
a) In-situ vane shear strength test,
b) Cone penetration test.

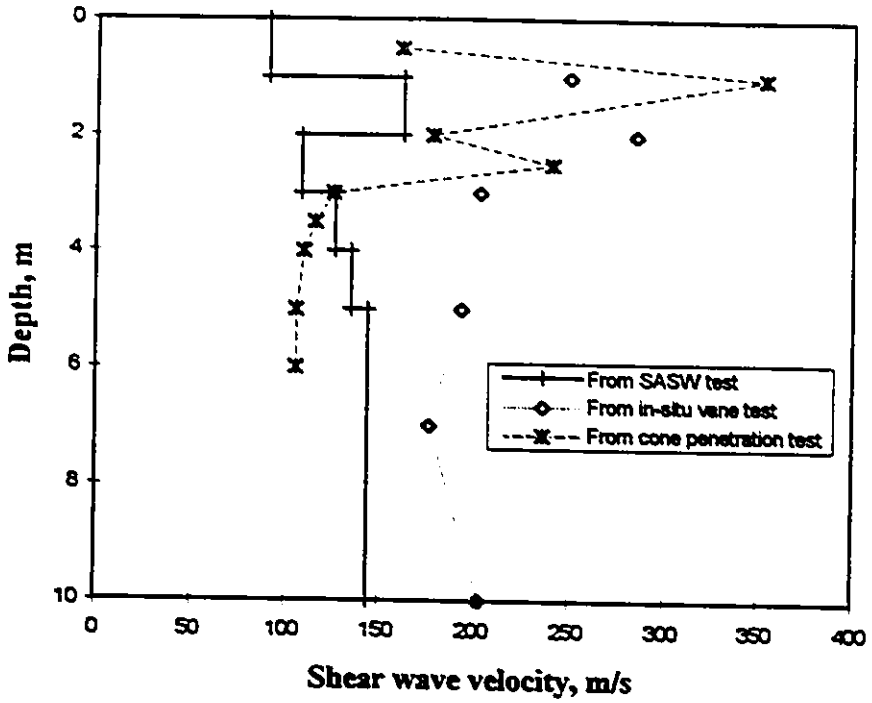

Fig. 8.12-Shear wave velocity profile at Fraser Farm site.

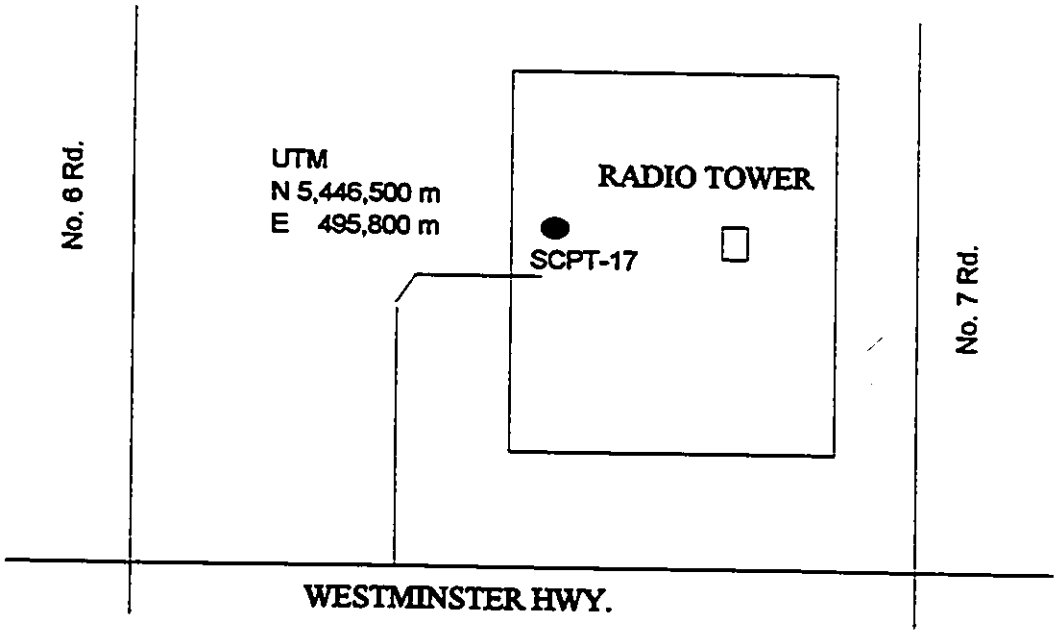

Fig. 8.13-Site location at Richmond, B.C.

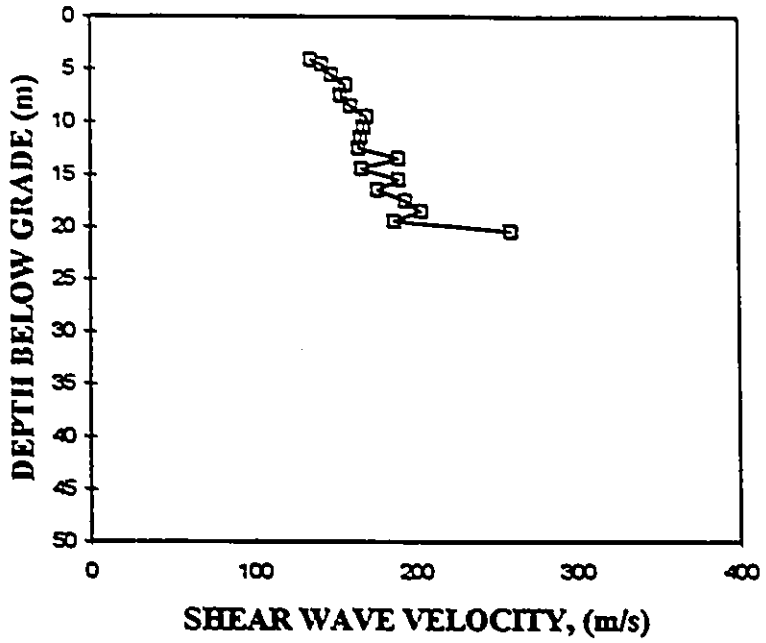

Fig. 8.14-Shear wave velocity Vs. depth for site at Richmond, B.C.

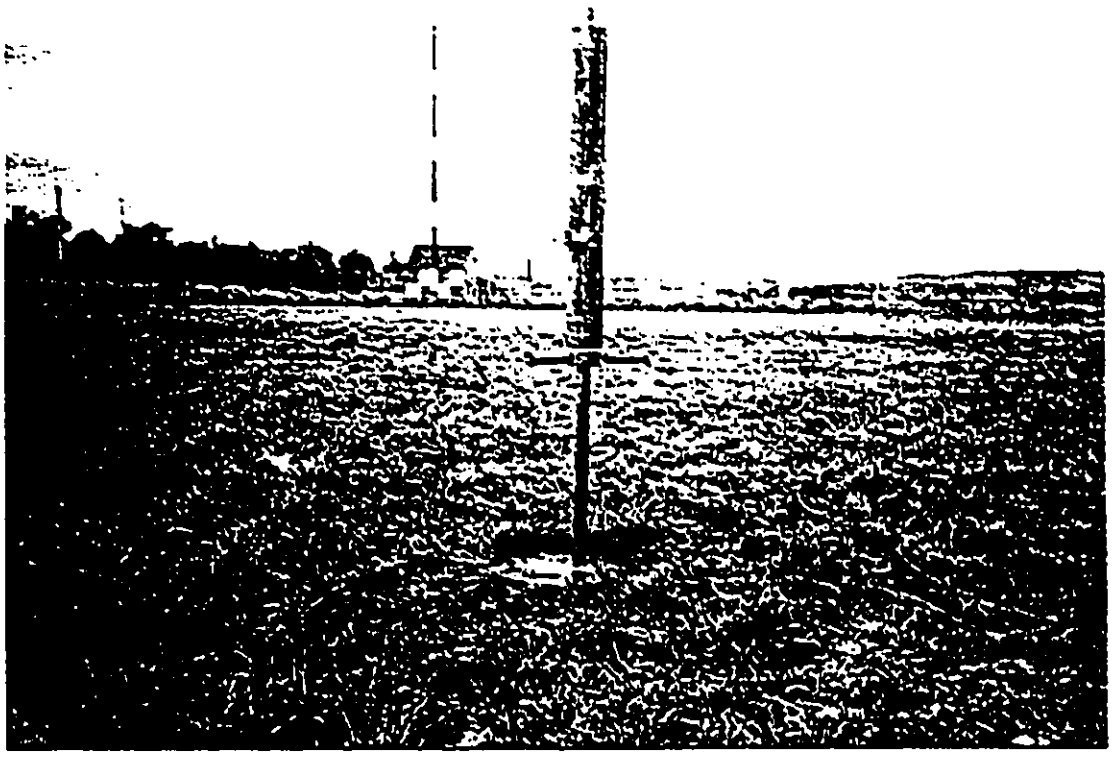

Fig. 8.15-Vertically oriented Seismic Source.

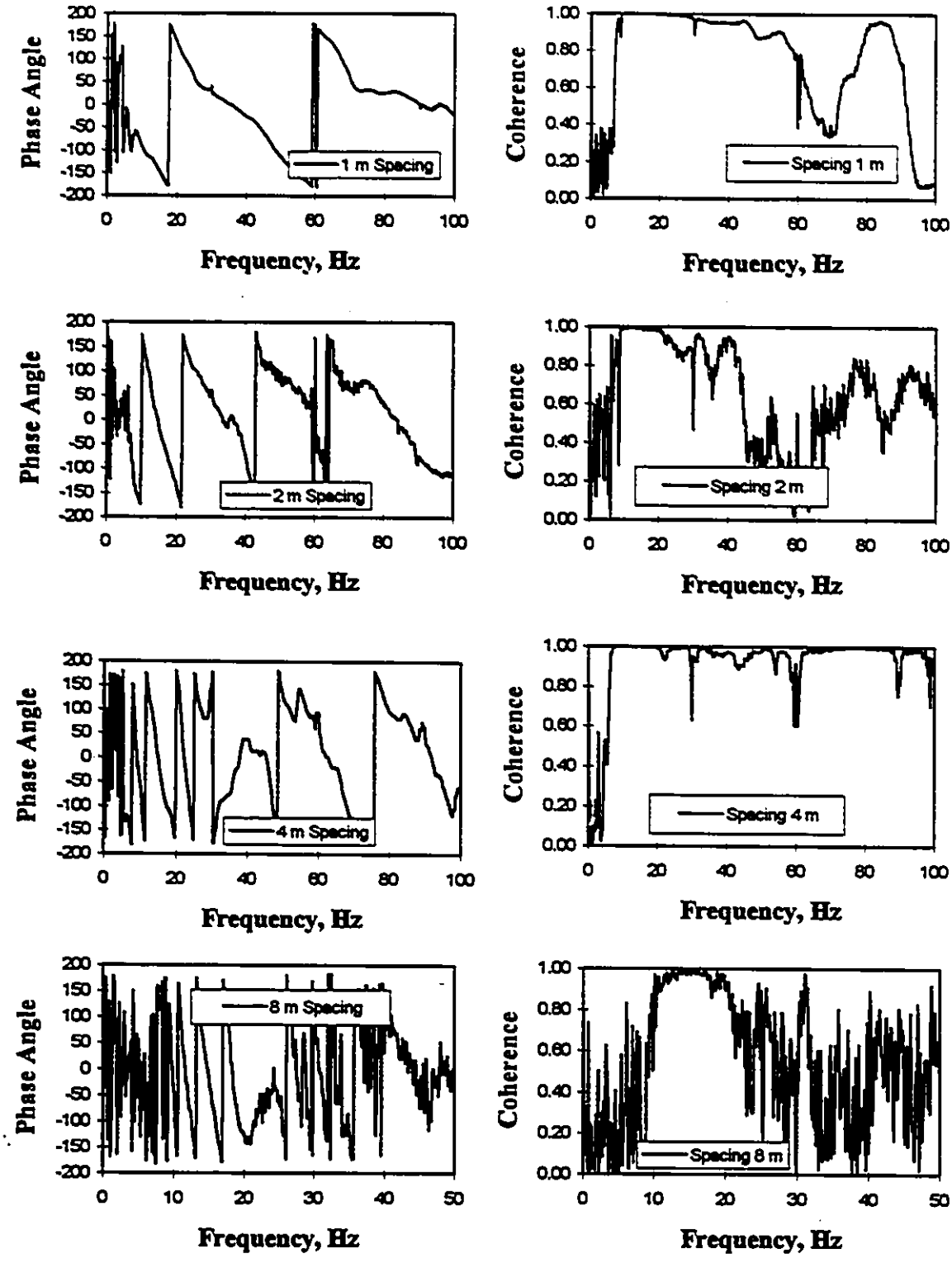

Fig. 8.16-Relative phase angle spectra and Coherence function for different spacings at Richmond.

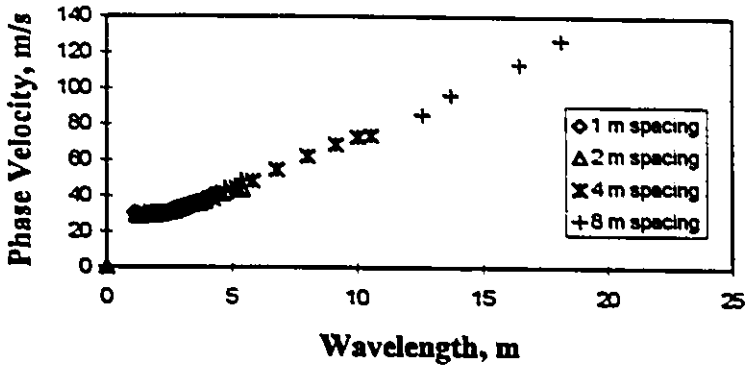

Fig. 8.17-In-situ dispersion curve at Richmond site.

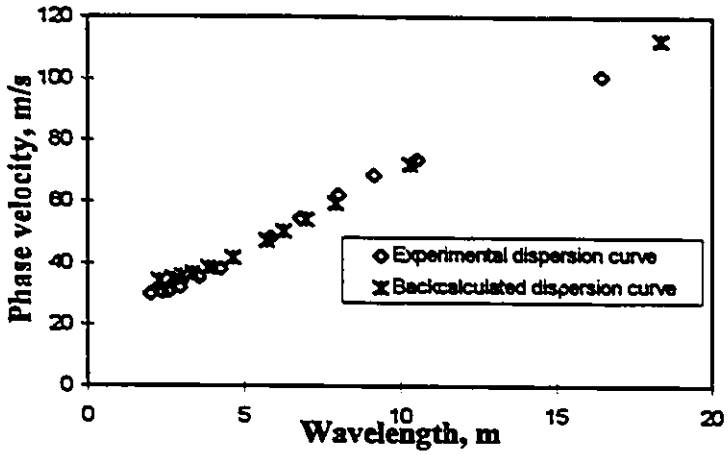

Fig. 8.18-Dispersion curves at Richmond site.

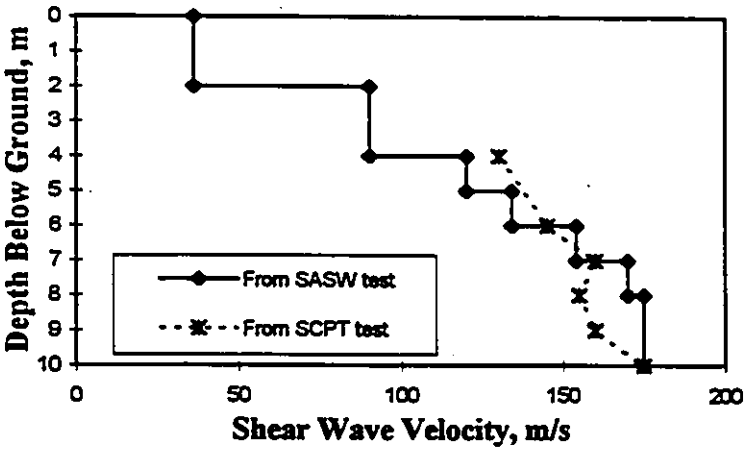

Fig. 8.19-Shear wave velocity Vs. Depth.

CHAPTER 9

CONCLUSIONS AND RECOMMENDATIONS

The objective of this research was to improve the SASW method by developing procedures for incorporating multi-mode propagation in the backcalculation of site profiles. The research work addressed three major issues:

1) difficulties with existing SASW test and analysis procedures,

2) calculation of theoretical multi-mode dispersion curves, and,

3) automation of the backcalculation procedure.

In the first part of the study, a program was developed for calculating Rayleigh wave dispersion curves. Using a case study, it was shown that the fundamental mode is not always the predominant mode of propagation. Also, the contradiction in the filtering criteria, and difficulties with the inversion procedure were shown.

In the second part of the study a new method for calculation of theoretical dispersion curves was developed based on the maximum flexibility coefficient concept. This part also includes the development of three-dimensional numerical simulation of the SASW test, and simulation of the original Steady-State test.

Finally, the new method for calculation of dispersion curves was incorporated with the down-hill simplex method for automatic inversion of SASW data.

9.1 Conclusions

The conclusions that can be drawn from the three previously described parts of this research will be presented separately.

Part 1

1. Higher modes in irregular soil and pavement sites have significant influence on overall wave propagation and in some cases are the dominant ones. Therefore, the inversion of such sites should not by guided solely by theoretical first Rayleigh mode.

2. Available filtering criteria are insufficient to ensure the condition that the measured wave field is composed of one mode. Hence they yield inaccurate dispersion curves when multi-mode propagation occurs.

3. In order to find a reliable dispersion curve a new criterion is introduced. Since the SASW test is usually performed for several receiver spacings, dispersion data from different spacings overlap. Hence, for each frequency several dispersion points may be available. In the new filtering criterion, dispersion points at the same frequency but obtained from two different receiver spacings are rejected if they do not match each other. The new filtering criterion successfully eliminates inconsistencies in the dispersion curve caused by multi-mode propagation.

Part two

1. To evaluate the test and data analysis procedures of the SASW method, a computer program for simulation of actual tests was successfully developed. The implementation and applicability of the computer simulation were verified and demonstrated.

2. To solve the uncertainty caused by unwrapping phase angles in the SASW analysis procedure, a computer program for simulation of the original Steady-State Rayleigh wave was developed.

3. For an assumed profile the vertical flexibility coefficients exhibit sharp peaks at distinct wave numbers. Wave numbers where these peaks occur correspond to the modes of surface waves in the layered system. Using the vertical flexibility coefficient, a new method for calculation of the theoretical dispersion curve was introduced.

4. Theoretical dispersion curves obtained with the maximum flexibility coefficient method are in agreement with those obtained with the root searching technique for regular sites.

5. For irregular soil sites or pavements, the dominant propagation mode may not remain the same for the whole frequency range. It was shown that as frequency increases the predominant mode may shift to higher order modes.

6. It was demonstrated that dispersion curves obtained with simulated SASW tests, and simulated Steady-State tests, are in agreement with those obtained with the maximum vertical flexibility coefficient method for irregular sites.

Part three

1. A computer program was developed for backcalculation of site profiles based on the vertical flexibility coefficient method for calculating theoretical dispersion curves.

2. The backcalculation method was automated using the down-hill simplex optimization method. It was found that:

   i) The automation procedure is sensitive to errant input data and incomplete data.

   ii) If the initial estimate of the shear wave velocity profile is far from the actual (but unknown) solution, the inversion algorithm may never converge to a solution.

3. The new backcalculation procedure was used for obtaining the shear wave velocity profiles from SASW tests at several sites. The SASW results were in agreement with those of other seismic methods.

4. At some sites the transient input motions generated by hammers and drop weights did not provide acceptable results at low frequencies. Vibration amplitude at a particular frequency is a function of the weight of the source, the contact area, the velocity of impact, and the characteristics of the ground surface itself. Therefore, to find a source that generates sufficient amplitudes for the frequencies of interest, it is usually necessary to try different sources. This trial and error testing of various sources significantly increases the time required to perform the SASW test.

In closing, the backcalculation method developed in this study based on the maximum flexibility coefficient is superior to existing methods based on root searching in situations of multi-mode propagation. It should be noted, however, that the success of the new method is limited to situations where only one mode predominates. This could be the first mode or any higher mode. Also, the optimization technique implemented in this procedure may not converge to a global minimum solution as occurs with optimization techniques implemented with existing inversion procedures.

9.2 Recommendations

Determination of shear wave velocities and thickness of soil and pavement layers by inversion of surface wave dispersion curve is very attractive. To improve and promote the use of the SASW method, the following areas require further research.

1. Sources to generate sufficient vibration amplitudes at low frequencies. This may include sources such as air and water guns and explosives.

2. The interpretation of phase spectra (i.e. the process of unwrapping phase) is the most difficult part of the SASW test procedure. The coherence function plays important role in SASW phase spectrum interpretation. More investigation is required regarding the use of the coherence function for processing of the SASW data.

3. Global optimization techniques.

4. The procedure for construction of field dispersion curve needs to be standardized.

REFERENCES

Addo, K.O., and Robertson, P.K. 1992. Shear-wave velocity measurement of soils using Rayleigh waves. Canadian Geotechnical Journal, 29(4): 558-568.

Aki, K. and Richards, P.G. 1980. Quantitative seismology: theory and methods. W.H. Freeman and Company, San Francisco, California, Vol. I and II, 932 pp.

Al-Hunaidi, M.O. 1991. Nondestructive profiling of pavement sites using the surface wave method: A case study. 44th Canadian Geotechincal Conference, September 29, to October 2, Vol. 1, paper No. 12, pp. 1-9.

Al-Hunaidi, M.O. 1992. Difficulties with phase spectrum unwrapping in spectral analysis of surface waves nondestructive testing of pavements. Canadian Geotechnical Journal, 29(3): 506-511.

Al-Hunaidi, M.O. 1992. Computer simulation of nondestructive surface wave testing of pavements. The Canadian Society for Civil Engineering Annual Conference Quebec City, Quebec May, pp. 26-29.

Al-Hunaidi, M.O. 1993. Insights on the SASW nondestructive testing method. Canadian Journal of Civil Engineering, Vol. 20, pp. 940-950.

Al-Hunaidi, M.O. 1994. Analysis of dispersed muti-mode signals of the SASW method using the multiple filter crosscorrelation technique, Soil Dynamics and Earthquake Engineering, Vol. 11, pp. 1-12

Andreasson, B. 1979. Deformation characteristics of soft, high-plastic clays under dynamic loading conditions. Ph.D. Dissertation, Department of Civil Engineering, Chamers University of Technology, Gothenburg, Sweden.

Baladi, G., Bruzzi, D., Superbo, S., Battaglio, M. and Jamiolkowski, M. 1988. Seismic cone in Po River sand. Proceedings of the first International Symposium on Penetration Testing (ISOPT-1), Orlando, Florida, Vol. 2, pp. 643-650.

Ballard (JR), R.F. 1964. Determination of soil shear moduli at depths by in-situ vibratory techniques. United States Army Engineer Waterways Experiment Station, Corps of Engineers, Vicksburg, MS, MP No. 4-691, 9 pp.

Ben-Menahem, A. and Singh, S.J. 1981. Seismic waves and sources, Springer-Verlag, New York, NY, 1108 pp.

Borm, G.W, 1977. Method from exploration seismology: reflection, refraction and borehole prospecting. Dynamical Methods in Soil and Rock Mechanics, Vol. 3, pp. 87-112.

Bouckovalas, G., Kalteziotis, N., Sabatakakis, N., and Zervogiannis, C., 1989. Shear wave velocity in a very soft clay. Proceedings, Twelfth International Conference on Soil Mechanics and Foundation Engineering, Vol. 1, Rio de Janeiro, Balkema, Rotterdam, pp. 191-194.

Bozozuk, M., 1983. Evaluating strength tests from foundation failures. Proceeding Ninth International Conference on Soil Mechanics and Foundation Engineering, Tokyo, Vol. 1, pp. 55-59.

Brigham, E.D. 1988. The fast fourier transform and its applications, Prentice Hall, Englewwod Cliffs, New Jersey, 449 pp.

Burden, R. and Faires, J.D. 1988. Numerical Analysis, Prindle, Weber & Schmidt, Boston, Third Edition, Mass. 676 pp.

Caceci, M. S. and Cacheris, W.P. 1984. Fitting curves to data, the simplex algorithm is the answer, Byte, Vol. 9, No. 5, pp. 340-362.

Chachill, R.V. and Brown, J.W. 1987. Fourier series and boundary value problems, McGraw-Hill Book Company, New York, NY, 339 pp.

Douglas, R.A., Eddy, J.L., and Wahls, H.E. 1989. On transforms and the dispersion computations used for evaluating layer properties, In nondestructive testing of pavements and back-calculation of moduli. Edited by A.J . Bush III and G.Y.Baladi. American Society for Testing and Materials, Special Publication 1026, pp. 612-627.

Douglas, R.A. and Eller, G.L. 1986. Nondestructive pavement testing by wave propagation: Advanced Methods Research Record No. 1070, pp. 53-62.

Dorman, J., and Ewing, M. 1962. Numerical inversion of seismic surface wave dispersion data and Crust-Mantle structure in the New York-Pennsylvania area. Journal Of Geophysical Research, 67: 5227-5241.

Dunkin, J.W. 1965. Computation of Modal solutions in layered, Elastic Media at High Frequencies. Bulletin of Seismological Society of America, 55 (2), 335-358.

Dziewonski,A.M. and Hales A.L. 1972. Numerical analysis of dispersed seismic waves. Methods for Computational Physics, 11: 39-84.

Ewing, W.M., Jardetzky, W.S. and Press, F. 1957. Elastic waves in layered media, McGraw-Hill Book Company, Inc., New York, NY, 298 pp.

Gucunski, N. & Woods, R.D. 1991. Use of Rayleigh modes in interpretation of SASW test, Proceedings of the Second International Conference on Recent Advances in Geotechnical Earthquake Engineering and Soil Dynamics, March 11-15, St. Louis, Missouri, Paper No. 10-10

Gucunski, N. & Woods, R.D. 1991. Inversion of Rayleigh wave dispersion curve for SASW test, Proceedings of the 5th International Conference on Soil Dynamics and Earthquake Engineering , Karlsruhe, Germany, Sep. 23-26, pp. 127-138.

Gucunski, N. & Woods, R.D. 1992. Numerical simulation of the SASW test, Soil Dynamics and Earthquake Engineering, Vol. 11, pp. 213-227.

Gucunski, N., Trefor, P.W. and Vedrana, K. 1995. Surface wave testing inversion by neural networks. Proceedings of the 2nd Congress on Computing in Civil Engineering (New York) Vol. 1 1995. ASCE, New York, NY, USA. pp. 574-581

Haile, G. 1977. Foundation performance of a tower silo M.A.Sc. Thesis, Department of Civil Engineering, University of Ottawa, Canada.

Hardin, B.D. and Drnevich, V.P. 1972. Shear modulus and damping in soils: Measurement and Parameter Effects. Journal Soil Mech. and Found. Div., Proc. ASCE, Vol. 89, No. SM6, pp. 603-624.

Hardin, B.D. and Drnevich, V.P. 1972. Shear modulus and damping in soils: Design Equations and Curves. Journal Soil Mech. and Found. Div., Proc. ASCE, Vol. 89, No. SM7, pp. 667-693.

Haskell, N.A. 1953. The dispersion of surface waves on multi layered media. Bulletin of Seismological Society of America, Vol. 43, pp. 17-34.

Heisey, J.S., Stokoe, K.H. II, Hudson, W.R., and Meyer, A.H. 1982. Determination of in-situ shear wave velocities from spectral analysis of surface waves. Research Report No. 256-2, Center for Transportation Research, The University of Texas at Austin, December, 277 pp.

Heisey, J.S., Stokoe, K.H. II, and Meyer, A.H. 1983. Moduli of pavement systems from spectral analysis of surface waves. Transportation Research Record, No. 852, pp. 22-31.

Hewlett-Packard Company 1985. Digital signal analysis time and frequency domain measurements, Application Note 240-0, Hewlett-Packard, August.

Hiltunen, D.R. and Woods, D. 1989. Influence of source and receiver geometry on the testing of pavements by the surface waves method. Nondestructive Testing of Pavements and Backcalculation of Moduli, STP 1026, A. J. Bush III and G. Y. Baladi (eds), ASTM, Philadelphia, Pa., pp. 502-524.

Hiltunen, D.R. and Woods, D. 1990. Variables affecting the testing of pavements by the surface waves method. Transportation Research Record, No. 1260, pp. 42-52.

Hoar, R.J. and Stokoe, K.H., II, 1978. Generation and measurement of shear waves in-situ, Dynamic Soil and Rock Testing in the Field and Laboratory for Seismic Studies, ASTM STP 654, American Society for Testing and Materials.

Hoar, R.J. 1982. Field measurement of seismic wave velocity and attenuation for dynamic analyses. Ph.D Dissertation, Department of Civil Engineering, University of Texas, Austin, Texas, 478 pp.

Hossian, M.M. and Drnevich, V.P. 1989. Numerical and optimization techniques applied to surface wave for back-calculation of layer moduli,. Nondestructive Testing of

Pavements and Backcalculation of Moduli. Edited by A. J. Bush III and G. Y. Baladi. American Society for Testing and Materials, Special publication 1026, pp. 649-669

Jones, R. 1962. Surface wave technique for measuring the elastic properties and thickness of roads: theoretical developments. British Journal of Applied Physics, 13: 21-29.

Kirkpatrick, S. 1984. Optimization by simulated annealing: Quantitative studies. Journal of statistical physics, vol. 34, pp. 975-986

Kausel, E. & Roesset, J.M. 1981. Stiffness matrices for layered soils, Bulletin of Seismological Society of America, 71(6), pp. 1743-1761.

Kirkpatrick, S. 1984. The annealing algorithm, Journal of Statistical physics, vol. 34, pp. 975-986.

Knopoff, L. 1961. Green's function for eigenvalue problems and the inversion of Love wave dispersion data. Geophysical Journal, 4:161-173.

Knopoff, L. 1964. A matrix method for elastic wave problems. Bulletin of Seismological Society of America, 54(1), 431 -438.

Larsson, R. and Mulabdic, M. 1991. Shear moduli in Scandinavian clays. Swedish Geotechnical Institute, Report No. 40, Linkoping, Sweden, 127pp.

Lysmer, J., and Kuhlemeyer, R.L. 1969. Finite dynamic model for infinite media. Journal of the Engineering Mechanics Division, ASCE, Vol. 95, No. EM4, Proc. Paper 6719, August, 1969, pp. 859-877.

Lysmer, J. 1970. Lumped mass method for Rayleigh waves. Bulletin of Seismological Society of America, 60(1), 89-104.

Lysmer, J. and Waas, G. 1972. Shear waves in plane infinite structures. Journal of the Engineering Mechanics Division, ASCE, Vol. 98 No. EM1, Proc. Paper 6719, February, 1972, pp. 85-105.

Lysmer, J., and Drake, L.A. 1972. A finite element method for seismology. Methods for Computational Physics, 11: 181-216.

Martin, P.P and Seed, H.B. 1978. A computer program for the non-linear analysis of vertically propagating shear waves in horizontally layered deposits, Rpt. UCB/EERC 78/23, Earthquake Eng. Res. Ctr., Univ. of Calif., Berkeley.

Meier, R.W. and Rix, G.J. 1993. An initial study of surface wave inversion using artificial neural networks. Geotechnical Testing Journal, GTJODJ, Vol. 16, No. 4, pp. 425-431.

Miller, G.F. and Pursey, H. 1955. On the partition of energy between elastic waves in a semi-infinite solid, Proceedings Royal Society, London, A, Vol. 233, pp. 55-69.

Mora, p. 1988. Elastic wave field inversion and the adjoint operation for the elastic wave equation. Mathematical Geophysics, Vlaar, N.J., Nolet G., Wortel, M.K.R., Cloetingh, S.A.P.L. (editor), D. Reidel Publishing Company, Dordrecht, Holland, pp. 117-137.

Nazarian, S. and Stokoe, K.H. II, and Hudson, W.R. 1983. Use of spectral analysis of surface waves method for determination of moduli and thicknesses of pavement system. In Transportation Research Record, No. 930, pp. 38-45.

Nazarian, S. 1984. In-situ determination of elastic moduli of soil deposits and pavement systems by spectral-analysis-of-surface-waves method, Ph.D. Dissertation, Civil Engineering Department, University of Texas at Austin.

Nazarian, S. and Stokoe, K.H. II, 1986. Use of surface waves in pavement evaluation. In Transportation Research Record, No. 1070, pp. 132-144.

Nazarian, S. and Desai, M.R. 1993. Automated surface wave method: Inversion Technique. J. Geotech. Engrg., ASCE, Vol . 119, No. 7, pp. 1112-1126..

Nelder, J.A., and Mead, R. 1956. A simplex method for function minimization. Computer Journal, Vol. 7, pp. 308-313.

Press, F., Harkrider, D. and Seafeldt, C.A. 1961. A fast convenient program for computation of surface wave dispersion curves in multi-layered media. Bulletin of Seismological Society of America, Vol. 51, No. 4, pp. 495-502.

Press, W.H., Teukolsky, S.A, Vetterling, W.T., and Flannery, B. P. 1992. Numerical Recipes in Fortran-The Art of Scientific Computing, Second Edition, Cambridge University Press, Cambridge, Mass. 963 pp.

Ramirez, R.W. 1985. The FFT Fundamentals and Concepts, Prentice-Hall, Inc, Englewwod Cliffs, New Jersey, 178 pp.

Richart, F.E., Jr., Woods, R.D., and Hall, J.R., Jr., 1970. Vibration of soils and foundations, Prentice-Hall, Inc., Englewood Cliffs, New Jersey, 414 pp.

Robertson, P.K., Campanella, R.G., Gillespie, D. and Rice, A. 1986. Seismic cone penetration test to measure in-situ shear wave velocity. ASCE Journal of Geotechnical Engineering, Vol. 112, No. 8, pp. 791-803.

Roesset, J.M., Chang, D-W., Stokoe, K.H. II. and Aouad, M. 1990. Modulus and thickness of the pavement surface layer from SASW tests. Transportation Research Record, No. 1260, pp. 53-63.

Roesset, J.M., Chang, D-W., Stokoe, K.H. II. 1991. Comparison of 2-D and 3-D models for analysis of surface wave test. Proceedings of the 5th International Conference on Soil Dynamics and Earthquake Engineering , Karlsruhe, Germany, Sep. 23-26, pp.111-126.

Sanchez-Salinero, I., Roesset, J.M., Shao, K-Y, Stokoe, K.H. II and Rix, G.J. 1987. Analytical evaluation of variables affecting surface wave testing of pavements. Transportation Research Record, No. 1136, pp. 86-95.

Sayyedsadr, M., and Drnevich, V.P. 1989. SASWOPR: A program to operate on spectral analysis of surface wave data. In nondestructive testing of pavements and back-calculation of moduli. Edited by A.J . Bush III and G.Y.Baladi. American Society for Testing and Materials, Special Publication 1026, pp. 670-682.

Schwab, F., and Knopoff, L. (1970). Surface wave dispersion computations. Bulletin of Seismological Society of America, 60(2), 321 -344.

Shannon and Wilson, Inc., and Agbabian Associates, 1976. In-situ impulse test: An Experimental and Analytical Evaluation of Data Interpretation Procedures, Report No. NUREG-0028, Nuclear Regulatory Commission, September 1976, 264 pp.

Sheu, J.C., Stokoe, K.H. II and Roesset, J.M. 1988. Effect of Reflected waves in SASW testing of pavements. Transportation Research Record, No. 1196, pp. 51-61.

Stokoe, K.H. II and Hoar, R.J. 1977. Field measurement of shear wave velocity by crosshole and downhole seismic methods, Proceedings of the Conference on Dynamic Methods in Soil and Rock Mechanics, Karlsruhe, Germany, Vol. 3, pp. 115-137.

Stokoe, K.H. II, Nazrian, S. 1983. Effectiveness of ground improvement from spectral analysis of surface waves. Proceedings, Eight European Conference on Soil Mechanics and Foundation Engineering, Helsinki, Finland, Vol. 1, pp. 91-95.

Stokoe, K.H. II, Nazrian, S., Rix, G.J., Sanchez-Salinero, I., Sheu, J-C., and Mok, Y-J. 1988. In-situ testing of hard-to sample soils by surface waves method. Earthquake engineering and Soil Dynamics II. Recent Advances in Ground- Motion , Proceedings of the Specialty Conference, Park City, UT, June 27-30, ASCE, New York, NY, pp. 264-278.

Szendrei, M.E., and Freeme, C.R. 1970. Road responses to vibration tests. ASCE Journal of the Soil Mechanics and Foundations Division, 86: 2099-2124.

Tanaka, A., Baure, G. and Queiroz De Carvalho, J.B. 1989. Failure and analysis of a concrete silo. 12th International Conference on Soil Mechanics and Foundation Engineering, Rio, de Janeiro, 1:345-348.

Thomson, W.T. 1950. Transmission of elastic waves through a stratified soil media, M.I.T. Research Report R 81-2, Order No. 689, Dept. of Civil Engineering, M.I.T., Cambridge, Mass.

Thrower, E.N. 1965. The computation of the dispersion of elastic waves in layered media. Journal of Sound Vibration, Vol. 2, No. 3, pp. 210-226.

Tokimatsu, K., Kuwayama, S., Tamura, S., and Miyadera, Y. 1991. Vs determination from steady state Rayleigh wave method. Soils and Foundations., 31(2), 153-163.

Tokimatsu, K., Shinzawa, K., and Kuwayama, S. 1992. Use of short-period microtremors for Vs profiling. J. Geotech. Engrg., ASCE, 118(10), 1544-1558.

Tokimatsu, K., Tamura, S., and Kojima, H. 1992. Effects of multiple modes on Rayleigh wave dispersion. J. Geotech. Engrg., ASCE, 118(10), 1529-1543.

Tokimatsu, K., Tamura, S, Kuwayama, S. 1991. Liquefaction potential evaluation based on Rayleigh wave investigation and its comparison with field behavior. Proceedings of the Second International Conference on Recent Advances in Geotechnical Earthquake Engineering and Soil Dynamics, March 11-15, St. Louis, Missouri, Paper No. 3.8, pp. 357-364.

Vrettos, C. and Prange, B. 1990. Evaluation of in-situ effective shear modulus from dispersion measurements, Journal of Geotechnical Engineering, ASCE, Vol. 116, No. 10, pp. 1581-1585.

Waas, G. 1972. Earth vibration effects and abatement for military facilities. Technical Report S-71-114, U.S. Army Engineer Waterways Experiment Station, Vicksburg, Miss.

Watkins, D.J., Lysmer, J., and Monismith, C.L. 1974. Nondestructive pavement evaluation by propagation method. Report TE-74-2, Department of Civil Engineering, Institute of Transportation and Traffic Engineering, University of California, Berkeley, Calif.

Watson, T.H. 1970. A note on fast computation of Rayleigh wave dispersion in the multi-layerd elastic half-space. Bulletin of Seismological Society of America, 60(1),161-166.

Williams, T.P. and Gucunski, N. 1995. Neural networks for backcalculation of moduli from SASW test. Journal of Computing in Civil Engineering, Vol. 9 No. 1, pp. 1-8.

Wolf, J.P. and Darbre, G.R. 1983. Dynamic-stiffness-matrix of surface foundation on layered half-space on stiffness-matrix approach, in Summary Report, UAEA Specialists' Meeting on Gas-Cooled Reactor Seismic Design Problems and Solutions, IAEA IWGGCRUC-77, General Atomic Company, San Diego, Calif., pp. 183-206.

Wolf, J.P. and Obernhuber, P. 1982. Free-field response from inclined SH-waves and Love-waves, Earthquake Engineering and Structural Dynamics, 10, pp. 823-845.

Wolf, J.P. 1985. Dynamic soil-structure interaction, Prentice-Hall, Inc., Englewood Cliffs, NJ, 466 pp.

Yuan, D. and Nazarian, S. 1993. Automated surface wave method: Inversion Technique. J. Geotech. Engrg., ASCE, Vol. 119, No. 7, pp. 1113-1126

APPENDIX

FLOW CHARTS, INPUT AND OUTPUT DATA FILES OF COMPUTER PROGRAMS

A.1 DISU

This program calculates theoretical dispersion curves based on root-searching as described in Section 4.3 for system without damping. Fig. A.1 shows the flow chart of this program. The required input data* is as follows:

1-initial condition of the bottom layer (the program has the capability of considering layered system in three different ways: layered system over half-space or fixed based or free base),

2-number of layers,

3-shear wave velocity (m/s), thickness (m), unit weight (kN/m^3), Poisson's ratio of each layer,

4-frequency range and increment (Hz),

5-increment of phase velocity (m/S), and

6-number of required modes.

The output file contains two columns. The first column shows the frequency (Hz) and the second one shows the phase velocity (m/s).

* Input data is free format.

A.2 DISD

This program calculates theoretical dispersion curves based on root-searching as described in Section 4.3 for system with damping. Fig. A.2 shows the flow chart of this program. The required input data* is as follows:

1-initial condition of the bottom layer (the program has the capability of considering layered system in three different ways: layered system over half-space or fixed based or free base),

2-number of layers,

3-shear wave velocity (m/s), thickness (m), unit weight (kN/m^3), Poisson's ratio, and damping ratio of each layer,

4-frequency range and increment (Hz),

5-increment of phase velocity (m/s), and

6-number of required modes.

The output file contains three columns. The first column shows the frequency (Hz) and the second one shows the phase velocity (m/s) and the third one shows the apparent** velocity (m/s).

* Input data is free format.

** $c_a = \dfrac{\sqrt{\mathrm{Re}(V_{ph})^2 + \mathrm{Im}(V_{ph})^2}}{\mathrm{Re}(V_{ph})}$

Where

c_a = Apparent velocity

$\mathrm{Re}(V_{ph})$ = Real part of phase velocity

$\mathrm{Im}(V_{ph})$ = Imaginary part of phase velocity

A.3 SIM

This program simulates SASW tests, calculates the vertical flexibility coefficients, simulates a steady-state test, and calculates dispersion curves based on the maximum vertical flexibility coefficient method. The required formulation was explained in Chapters 4 through 6. Fig. A.3 shows the flow chart of this program. The required input data* is as follows:

1-initial condition of the bottom layer (the program has the capability of considering layered system in three different ways: layered system over half-space or fixed based or free base),

2-number of layers,

3-shear wave velocity (m/s), thickness (m), unit weight (kN/m^3), Poisson's ratio of each layer,

4-frequency range and increment (Hz),

5- wave number range and increment,

6-radius of loading disk (m),

7-loading of disk (kN),

for simulation of the SASW test

8-number of receiver-to-receiver spacings,

9-receiver-to-receiver distance (m).

for simulation of the Steady-State test

10-surface distance that is interested to simulate the Steady-State test (m),

The output file for simulation of SASW tests contains eight columns as follows:

1-receiver-to-receiver spacing (m),

2-frequency (Hz),

3-real part of transfer function,

4-imaginary part of transfer function,

5-wrapped phase angle of transfer function,

6-unwrapped phase angle of transfer function,

7-wavelength in m,

8-phase velocity in m/s.

The output file for simulation of Steady-State test contains four columns as follows:

1-distance from source (m),

2-real part of vertical surface motion,

3-imaginary part of vertical surface motion,

4-in-phase position of surface motion.

The output file for calculating the vertical flexibility coefficient contains three columns as follows:

1-wave number

2-real part of vertical flexibility coefficient,

3-imaginary part of vertical flexibility coefficient.

The output file for calculating theoretical dispersion curve based on the vertical flexibility coefficient approach contains four columns as follows:

1-frequency (Hz),

2-maximum wave number,

3-phase velocity (m/s),

4-amplitude of vertical flexibility coefficient.

* Input data is free format.

A.4 SASW-INVERT

This program matches the field and the theoretical dispersion data points by the down-hill simplex method as described in Section 7.2. Fig. A.4 shows the flow chart of this program. Input data* is as follows:

1-initial condition of the bottom layer (the program has the capability of considering layered system in three different ways: layered system over half-space or fixed based or free base),

2-number of layers in initial profile,

3-shear wave velocity (m/s), thickness (m), unit weight (kN/m^3), Poisson's ratio and damping ratio of each layer in the initial profile,

4-number of iterations,

5-number of field dispersion data points,

6-values of dispersion data points.

The output file contains initial and final profiles, field and theoretical dispersion data points, and final Least Squares value of difference between field and theoretical dispersion data points.

* Input data is free format.

A.5 SVD-INVERT

This program matches the field and the theoretical dispersion data points by the linearized least-square optimization technique as described in Section 7.4. Fig. A.5 shows the flow chart of this program. Input data* is as follows:

1-initial condition of the bottom layer (the program has the capability of considering layered system in three different ways: layered system over half-space or fixed based or free base),

2-number of layers in initial profile,

3-shear wave velocity (m/s), thickness (m), unit weight (kN/m^3), Poisson's ratio and damping ratio of each layer in the initial profile,

4-number of iterations,

5-number of field dispersion data points,

6-values of dispersion data points.

The output file contains initial and final profile, and field and theoretical dispersion data points, and final least-squares value of difference between field and theoretical dispersion data points.

* Input data is free format.

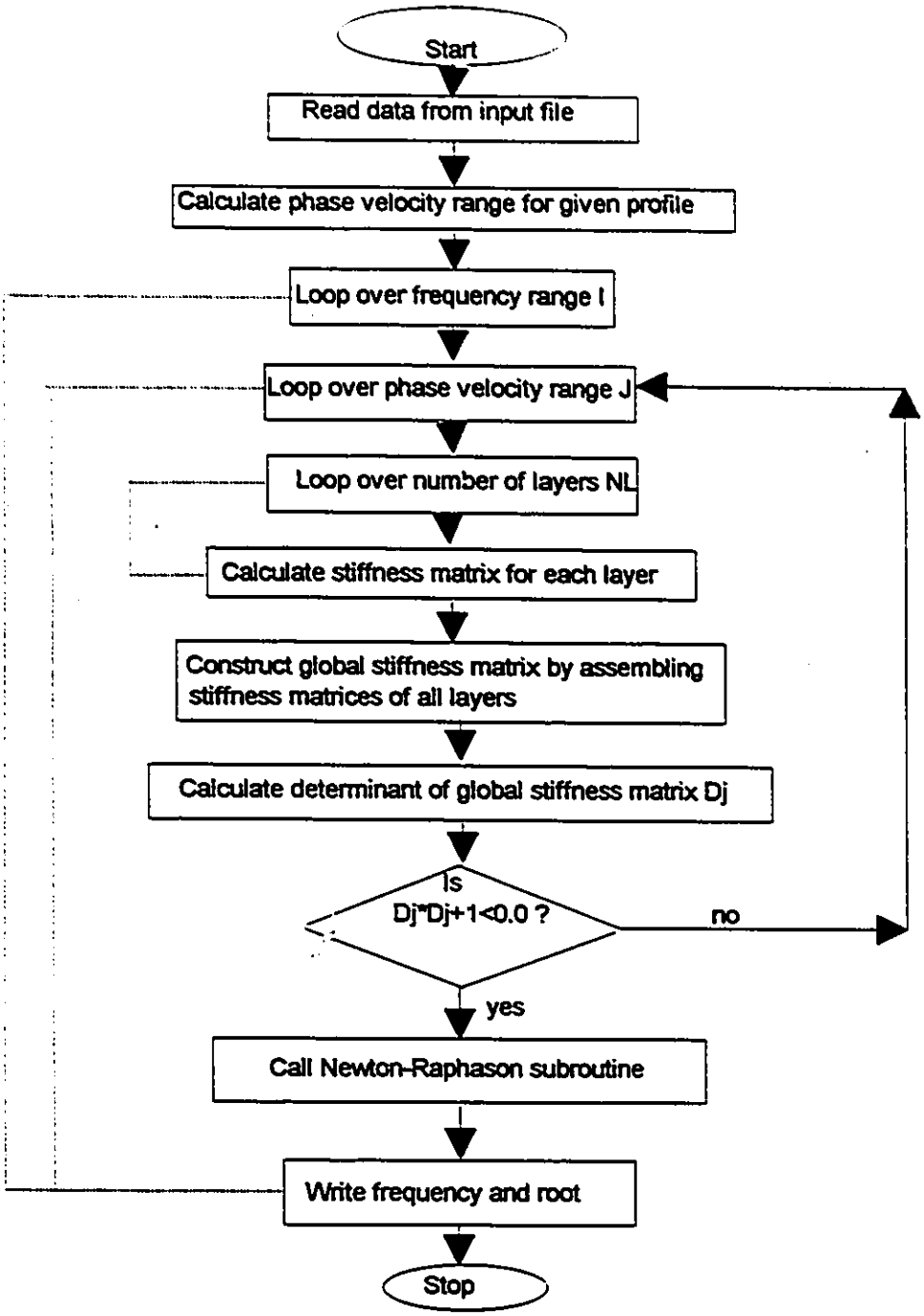

Fig. A.1-Flow chart of DISU: a program to calculate theoretical dispersion curves for system with no damping.

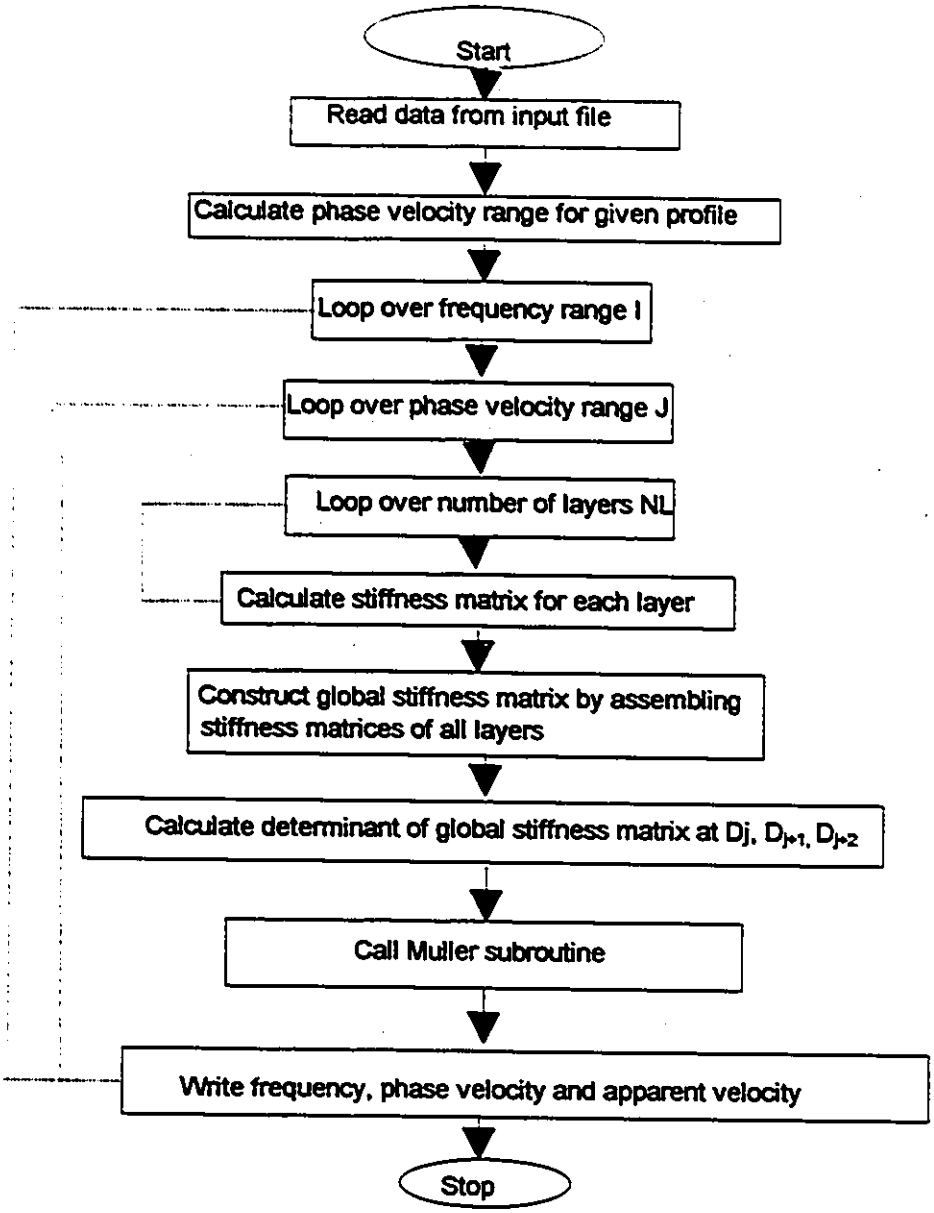

Fig. A.2-Flow chart of DISU: a program to calculate theoretical dispersion curves for system with damping.

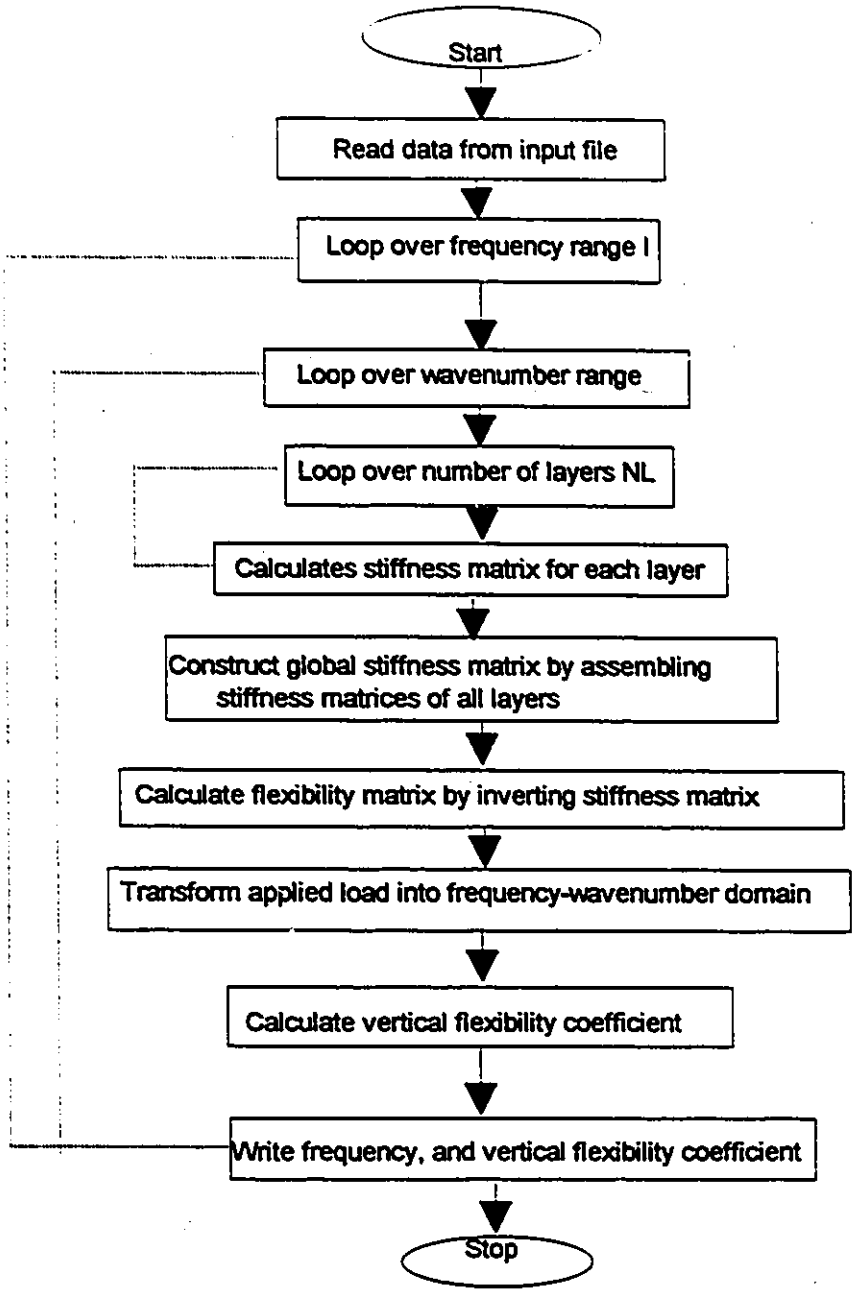

Fig. A.3a-Flow chart of SIM: a program to calculate vertical flexibility coefficient.

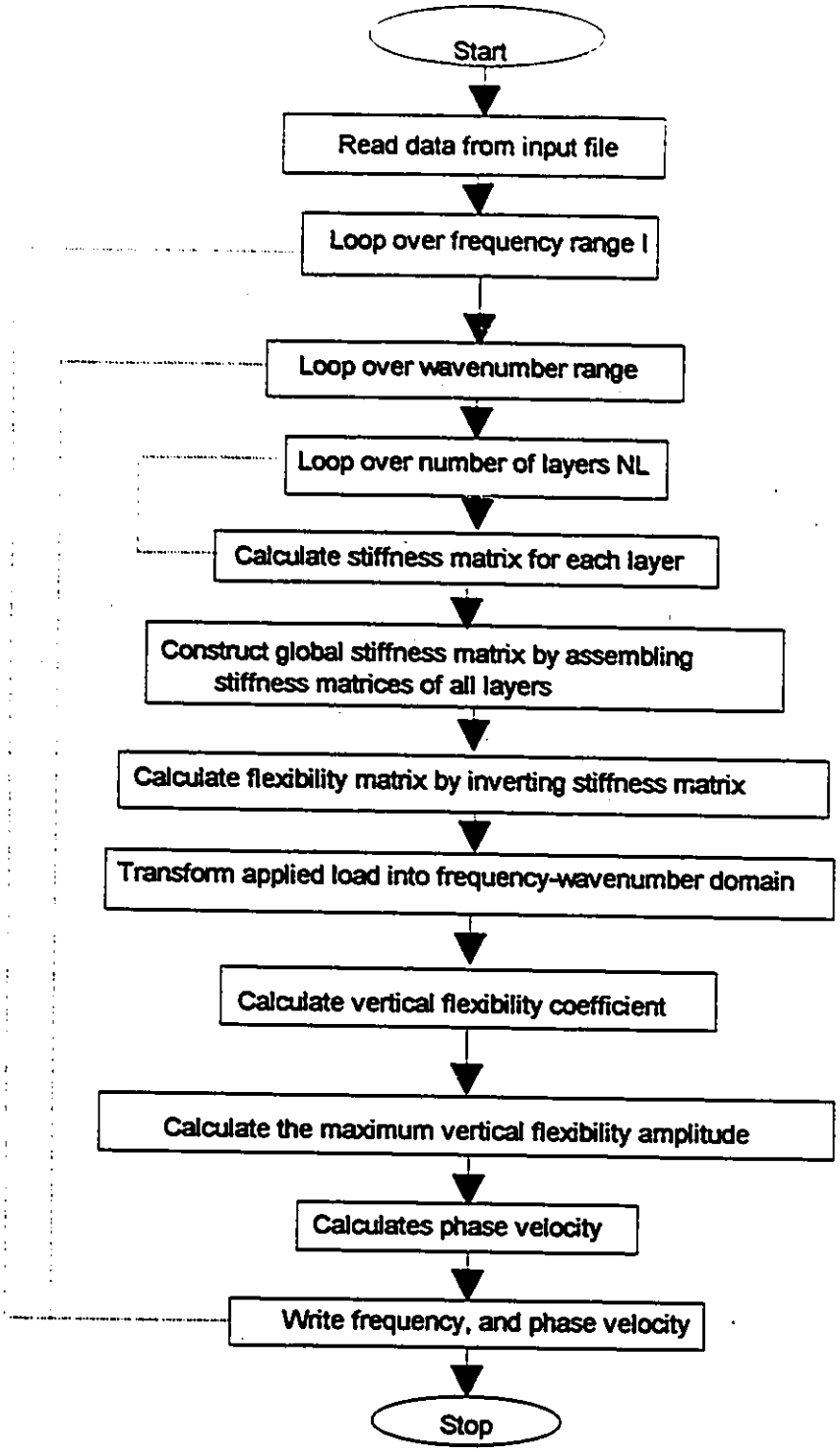

Fig. A.3b-Flow chart of SIM: a program to calculate theoretical dispersion curves.

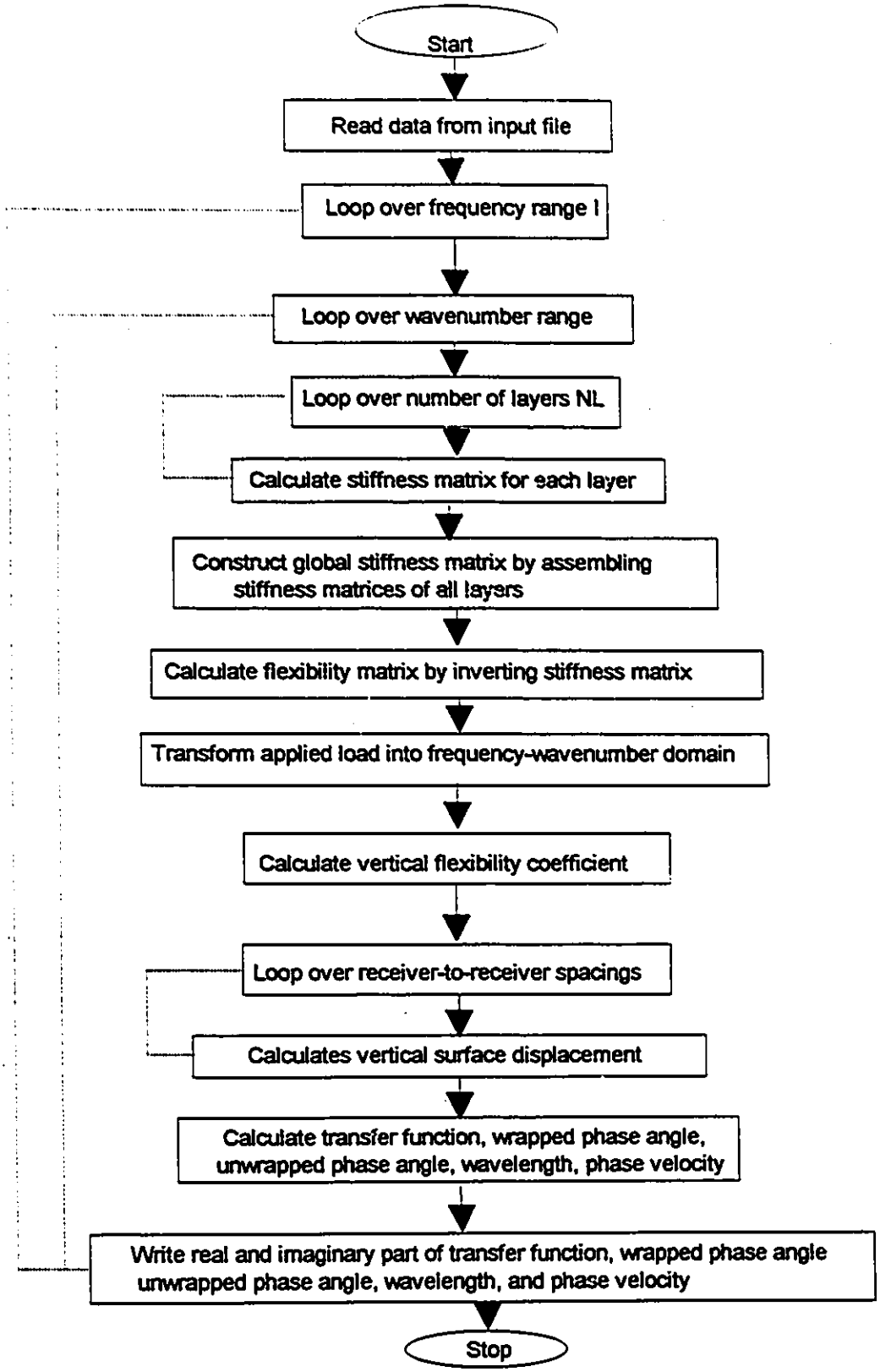

Fig. A.3c-Flow chart of SIM: a program to simulate SASW tests.

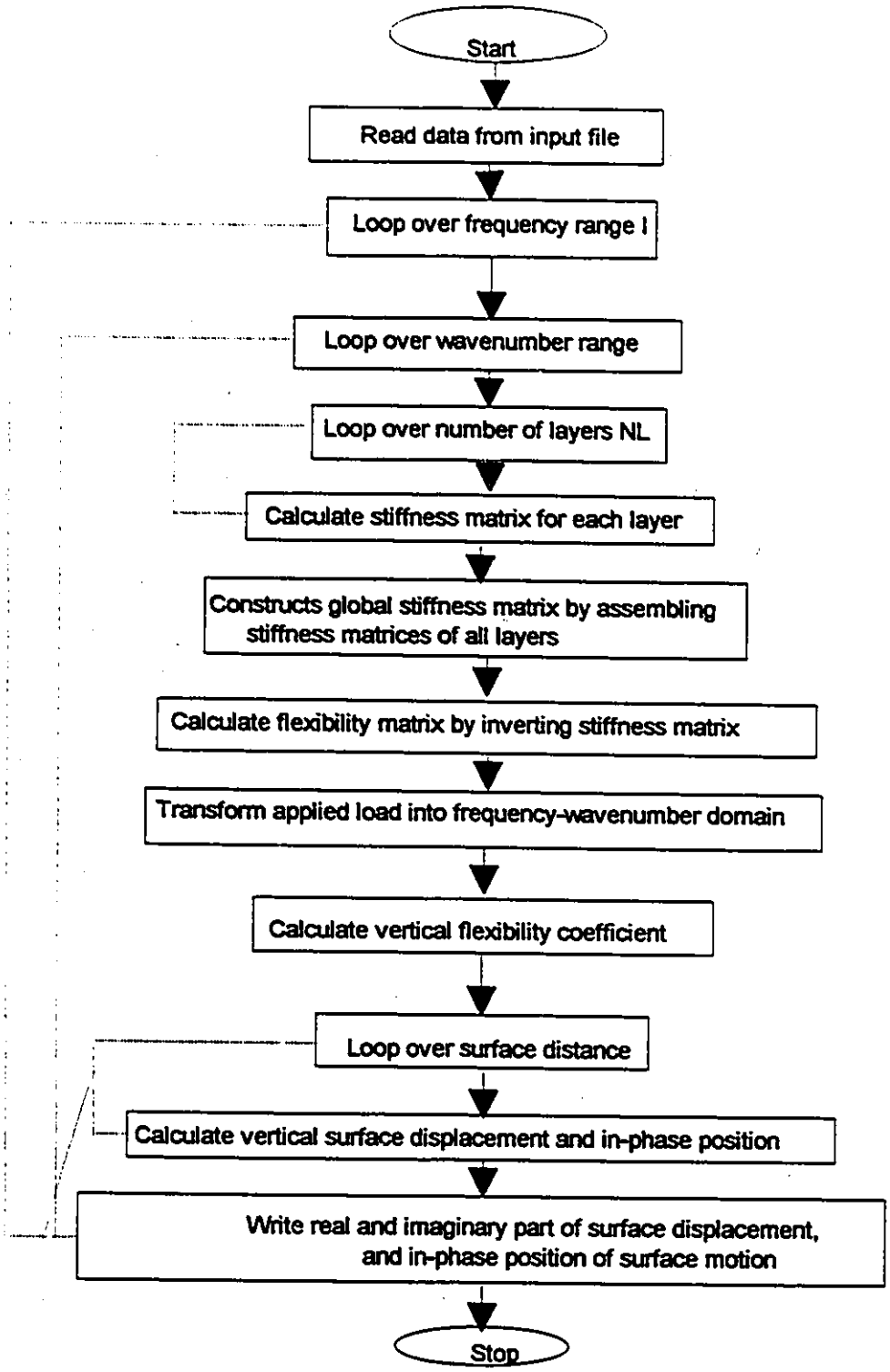

Fig. A.3d-Flow chart of SIM: a program to simulate Steady-State tests.

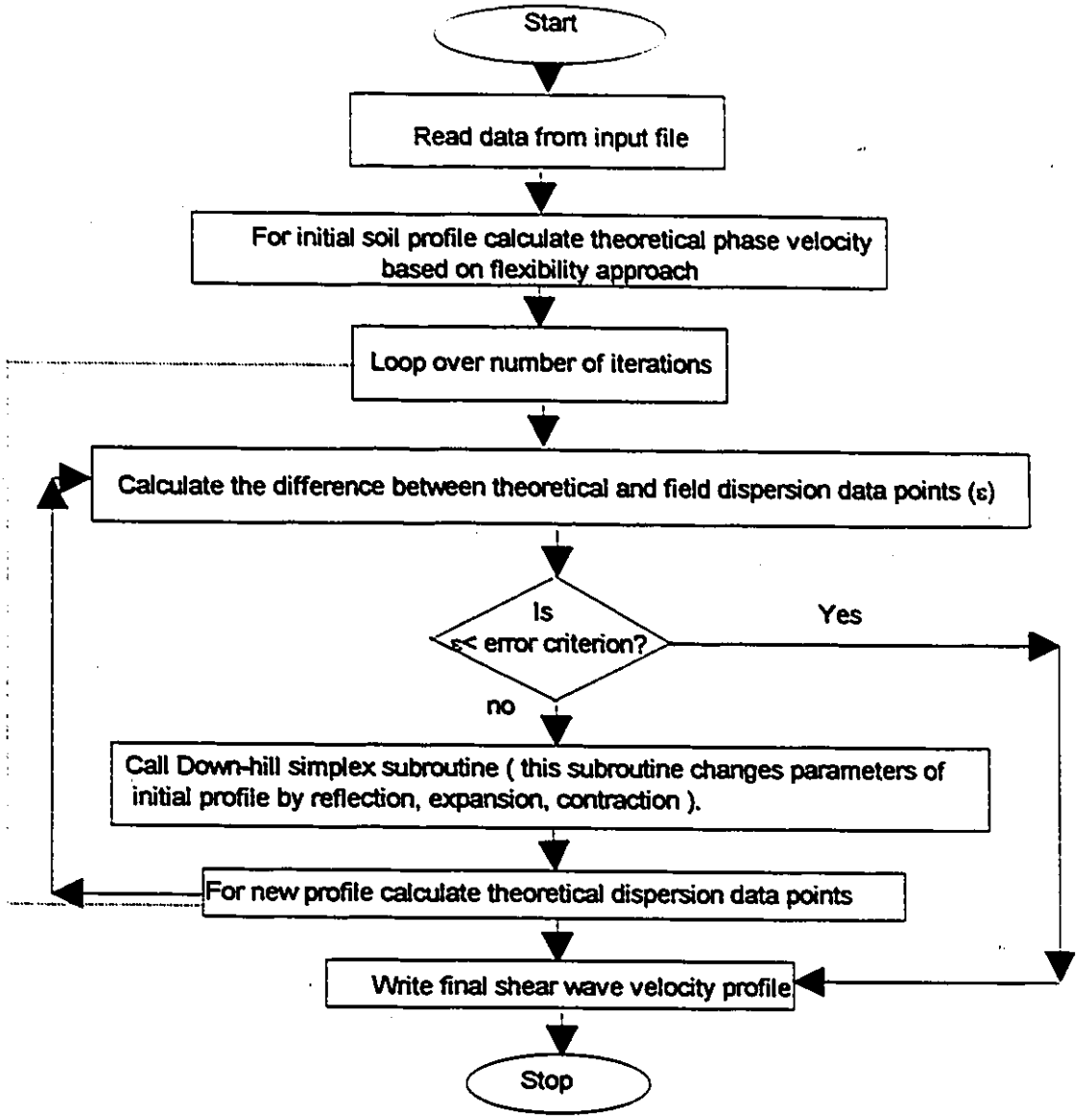

Fig. A.4-Flow chart of SASW-INVERT: a program to backcalculate site profile using simplex method.

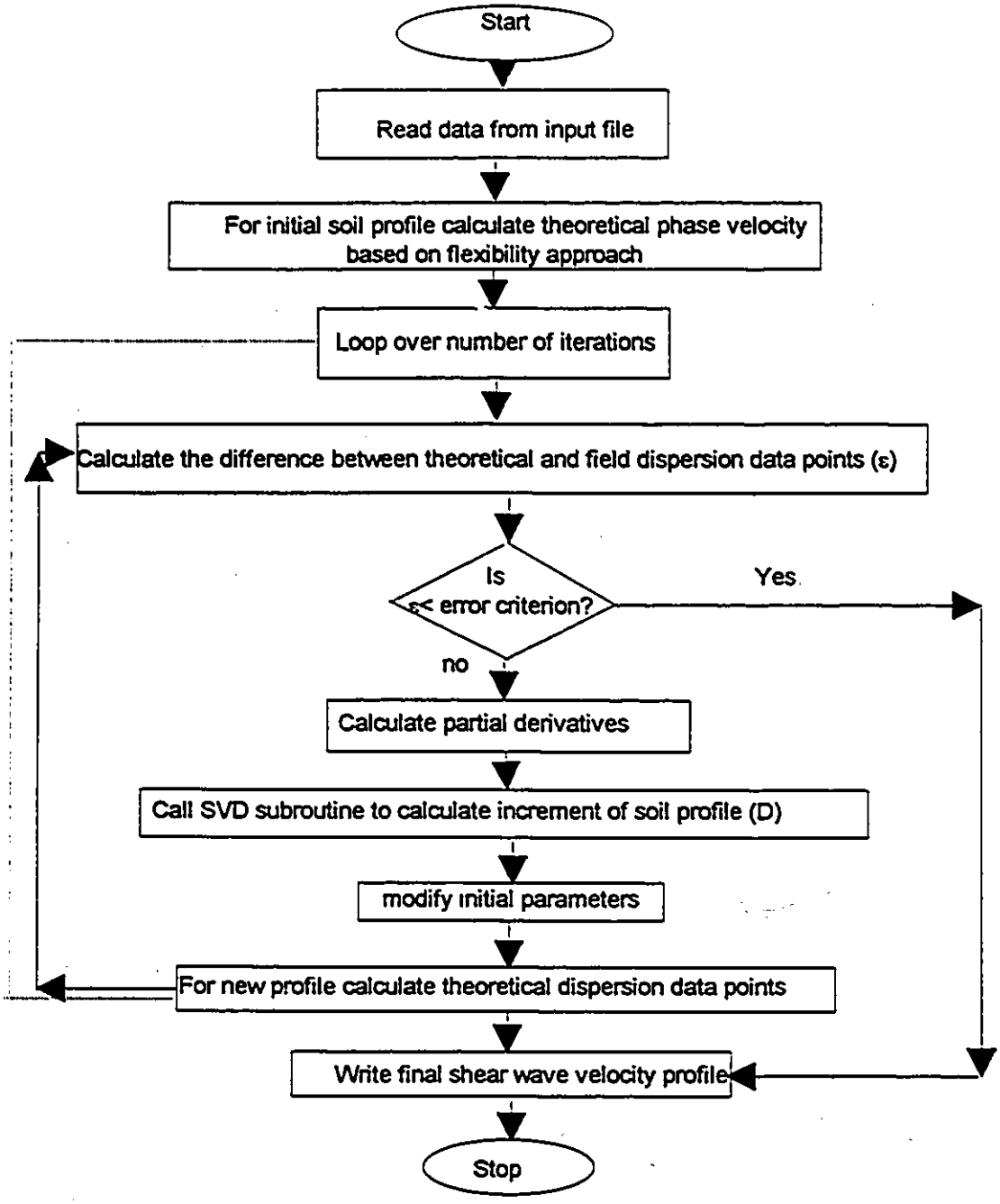

Fig. A.5-Flow chart of SVD-INVERT: a program to backcalculate site profile using linearized least squares method with singular value decomposition.